Contemporary erosion rates in the Kruger National Park, South Africa, inferred from reservoir siltation surveys

Dissertation

(kumulativ)

zur Erlangung des akademischen Grades
Dr. rer. nat. (doctor rerum naturalium)

vorgelegt dem Rat der
Chemisch-Geowissenschaftlichen Fakultät der
Friedrich-Schiller-Universität Jena

von Bastian Reinwarth (M. Sc.)

geboren am 15.11.1985 in Plauen

Gutachter:

1. PD Dr. Jussi Baade (Friedrich-Schiller-Universität Jena)

2. Prof. Dr. Roland Mäusbacher (Friedrich-Schiller-Universität Jena)

3. Prof. Dr. Hans-Rudolf Bork (Christian-Albrechts-Universität Kiel)

Datum der Verteidigung: 18.07.2018

Freigabe zur Veröffentlichung: 15.07.2020

The following manuscripts constituting the chapters 3 to 5 of this thesis were published in or submitted to peer-reviewed journals.

Chapter 3:

Reinwarth, B., Miller, J.K., Glotzbach, C., Rowntree, K.M., Baade, J., 2017. Applying regularized logistic regression (RLR) for the discrimination of sediment facies in reservoirs based on composite fingerprints. *Journal of Soils and Sediments* **17** (6), 1777-1795. DOI: 10.1007/s11368-016-1627-7.

Chapter 4:

Reinwarth, B., Riddell, E.S., Glotzbach, C., Baade, J., 2018. Estimating the sediment trap efficiency of intermittently dry reservoirs: lessons from the Kruger National Park, South Africa. *Earth Surface Processes and Landforms* **43** (2), 463-481. DOI: 10.1002/esp.4263.

Chapter 5:

Reinwarth, B., Petersen, R., Baade, J., submitted. Contemporary sediment yield and erosion rates in the Kruger National Park, South Africa, and related uncertainties. Submitted to: *Geomorphology*[1].

For already published manuscripts, reprint permissions were provided by the publishers (for details, see appendix).

Electronic supplementary material for the chapters 3 and 4 is provided on a compact disc (CD). Manuscripts and supplementary material may be also accessed via the following websites:

https://doi.org/10.1007/s11368-016-1627-7 (Chapter 3)

https://doi.org/10.1002/esp.4263 (Chapter 4)

---

[1] A shortened version of Chapter 5 has been published in *Geomorphology*. The full reference of the article is:

Reinwarth, B., Petersen, R., Baade, J., 2019. Inferring mean rates of sediment yield and catchment erosion from reservoir siltation in the Kruger National Park, South Africa: An uncertainty assessment. *Geomorphology* **324**, 1-13. DOI: 10.1016/j.geomorph.2018.09.007.

Table of contents

Figures

Chapter 6: Discussion and Synthesis

Tables

Acronyms

a	coefficient of the sediment rating curve
A	reservoir catchment size
AI	proportion of impervious surfaces to the total catchment area (parameter of the daily time step Pitman rainfall-runoff model)
APE	mean annual American class A-pan evaporation
A_R	full supply area of the reservoir
A_S	area covered with reservoir deposits at the survey date
ASR	initial area-storage relationship of the reservoir basin
α	elastic-net parameter in RLR analysis
b	exponent of the sediment rating curve
$BareSurf$	area percentage of bare surfaces
β	coefficient vector in RLR analysis (variable)
$\beta_{\alpha,\lambda}$	optimal coefficient vector for a given parameter α and a weighting factor λ in RLR analysis
β_i	ith element of a coefficient vector in RLR analysis
C	water storage capacity (unspecified)
CD	compact disc
CE	conservation estate (i.e., protected and conservation areas)
$Cl95$	two-tailed 95% confidence level
Clay&Silt$_\%$	percentage of the <63 µm fraction
C_M	mean water storage capacity
$Coef$	coefficient
C_R	initial water storage capacity
$C_{R,\,min}$	minimum value for the initial water storage capacity
$C_{R,\,max}$	maximum value for the initial water storage capacity
C_S	water storage capacity at the survey date
CV	coefficient of variation (unspecified)
CV_{dBD}	site-specific coefficient of variation of dBD values
d	index for a specific day
D	dimensionless parameter that may range between 0.0046 and 1
dBD	dry bulk density
DEM	digital elevation model
DFA	discriminant function analysis
DFG	Deutsche Forschungsgemeinschaft (German Research Foundation)
d_i	distance between the particle size of a given sample and the lower and upper bounds of the confidence band of a mean particle size distribution (ith particle size class)
DIP	Hartigan's dip statistic
D_{Lt}	long-term (typically $\geq 10^5$ years) average denudation rates (i.e., chemical weathering and physical erosion)
DOI	digital object identifier
DS	depth sounding
d_{soil}	soil thickness
DTM	digital terrain model
d_{vadose}	thickness of the vadose zone
ΔP_{post}	posterior probability residual
δV_S	absolute uncertainty in the determination of the volume of reservoir deposits

$\delta V_{S,\,boundary}$	absolute uncertainty in the determination of the volume of reservoir deposits arising from the identification of the facies boundary
$\delta V_{S,\,ran}$	absolute random error in the determination of the volume of reservoir deposits
E	catchment-wide average rate of erosion by water
eCov	equal within-group covariance
E_d	evaporation from the reservoir's water surface at a day d
E_{Lt}	long-term (typically $\geq 10^5$ years) average rates of physical erosion
E_{min}	minimum catchment-wide rate of erosion by water
ε_A	relative uncertainty of A value
ε_{dBD}	relative uncertainty of dBD value
ε_E	relative uncertainty of E value
ε_{Emin}	relative uncertainty of E_{min} value
ε_{SDR}	relative uncertainty of SDR value
ε_{SSY}	relative uncertainty of SSY value
ε_{TE}	relative uncertainty of TE value
ε_{TR}	relative uncertainty of T_R value
ε_X	relative uncertainty of value X (unspecified)
f_i	particle size frequency (ith particle size class)
FLA_d	flooded area within the reservoir basin at a day d
F_{soil}	factor accounting for vertical variations in the effective soil porosity
FT	percolation rate at soil moisture equal to ST (parameter of the daily time step Pitman rainfall-runoff model)
$FUC_{A,\,SSY}$	fractional uncertainty contribution of A values with respect to the overall uncertainty inherent in SSY values
$FUC_{dBD,\,SSY}$	fractional uncertainty contribution of dBD values with respect to the overall uncertainty inherent in SSY values
$FUC_{SDR,\,E}$	fractional uncertainty contribution of SDR values with respect to the overall uncertainty inherent in E values
$FUC_{TE,\,SSY}$	fractional uncertainty contribution of TE values with respect to the overall uncertainty inherent in SSY values
$FUC_{TR,\,SSY}$	fractional uncertainty contribution of T_R values with respect to the overall uncertainty inherent in SSY values
$FUC_{VS,\,SSY}$	fractional uncertainty contribution of V_S values with respect to the overall uncertainty inherent in SSY values
$FUC_{X,\,SSY}$	fractional uncertainty contribution of a factor X (unspecified) with respect to the overall uncertainty inherent in SSY values
G	number of groups to be distinguished (in RLR and stepwise DFA analysis)
GDF	Gaussian density function
GL	lag of groundwater discharge (parameter of the daily time step Pitman rainfall-runoff model)
GNSS	global navigation satellite system
HAE	Height above ellipsoid
HSR	initial height-storage relationship of the reservoir basin
i	index (e.g., ith particle size class, ith sample)
j	Index (e.g., jth sediment property)
I	mean annual inflow
I_d	volume of water flowing into the reservoir at a day d
IDEM	(TanDEM-X) Intermediate DEM
k	number for sediment characteristics

<p style="text-align:center">Acronyms</p>

KDE	kernel density estimation
κ_i	ith coefficient for the estimation of the SDR (i.e., κ_1, κ_2, and κ_3)
KNP	Kruger National Park
ℓ	log-likelihood function in RLR analysis
L	over-water distance from the main reservoir inlet to the outlet
L_α	elastic-net penalty function in RLR analysis (for elastic-net parameter α)
LDA	linear discriminant analysis
l_i	lower bound of the 95% confidence band of a mean particle size distribution (ith particle size class)
LMean	mean grain size of the fine sediment (≤2 mm) determined with the logarithmic method of moments
LRP	local reference point
LSort	sorting of the fine sediment (≤2 mm) determined with the logarithmic method of moments
LUM	luminance
λ	non-negative weighting factor in RLR analysis (governs the strength of the constraint)
Λ	Wilks' lambda (in stepwise DFA analysis)
MAE	mean annual Symon's pan evaporation
MAP	mean annual precipitation
MAR	mean annual catchment runoff
ML	maximum likelihood
n	number for sediment samples involved in discriminant analysis
N	number (unspecified)
N_{dBD}	number of dry bulk density measurements
N_{DS}	number of depth soundings
p	significance level (unspecified)
P_β	cumulative probability function and regression model in RLR analysis
P_{CAL}	calcium-lactate leachable phosphorus
P_d	precipitation on the reservoir's water surface at a day d
PI	total size of the interception storage (parameter of the daily time step Pitman rainfall-runoff model)
PI_{BC}	size of the interception storage of grass and litter between the woody plant canopy
PI_C	size of the interception storage of the woody plant canopy
PI_{UC}	size of the interception storage of grass and litter under the woody plant canopy
p_{MW}	significance level derived from Mann-Whitney U test
POR	effective soil porosity
POW	parameter that influences the relationship between soil moisture state and groundwater discharge (parameter of the daily time step Pitman rainfall-runoff model)
P_{post}	posterior probability
PSD	particle size distribution
PSD_{Dist}	particle size deviance
p_{SW}	significance level derived from Shapiro-Wilk test
Q_{best}	best estimate runoff scenario
Q_d	mean catchment runoff at day d
QDR	quaternary drainage region
Q_{high}	high runoff scenario

<h1 style="text-align:center">Acronyms</h1>

Q_{low}	low runoff scenario
Qs	total mass of sediment entering the reservoir
Qs_d	fluvial sediment delivery from the catchment at day d
R	Pearson's correlation coefficient
R	parameter that controls the relationship between actual evaporation, potential evaporation and soil moisture state; parameter ranges between 0 and 1 (parameter of the daily time step Pitman rainfall-runoff model)
RGB	red – green – blue (colour space)
RLR	regularized logistic regression
RMSE	root mean square error
$Roads$	area percentage of roads
RTK GNSS	real-time kinematic global navigation satellite system
RUSLE	Revised Universal Soil Loss Equation
SANParks	South African National Parks
SC_d	mean sediment concentration in water flowing into the reservoir at a day d
S_d	water volume stored in the reservoir basin at a day d
$\hat{S}_d$	storage state of the reservoir (i.e., the stored volume of water and sediment) at a day d
SDR	sediment delivery ratio
$Skeleton_{\%}$	percentage of the >2 mm fraction (calculated relative to the fine sediment mass, i.e., ≤2 mm)
SL	soil moisture content below which no percolation occurs (parameter of the daily time step Pitman rainfall-runoff model)
$Slope$	mean slope inclination of the catchment
SM	total mass of reservoir deposits
$SPILL$	mean annual reservoir spillage
$SPILL_d$	volume of spilled water at a day d
SRTM	Shuttle Radar Topography Mission
SRZ	summer rainfall zone
SSY	area-specific sediment yield
ST	maximum soil storage, i.e., the sum of ST_{soil} and ST_{vadose} (parameter of the daily time step Pitman rainfall-runoff model)
STO	storativity of the vadose zone
ST_{soil}	water storage capacity of the soil
ST_{vadose}	water storage capacity of the vadose zone
SV_d	sediment volume (reservoir deposits) stored in the reservoir basin until a day d
σ	standard deviation (unspecified)
σ_{dBD}	site-specific standard deviation of dBD values
$t_{0.025,\ N-1}$	two-sided t value derived from Student's t distribution with N - 1 degrees of freedom (corresponding to the 95% confidence level)
T_C	year of dam construction
TC	total carbon
TE	sediment trap efficiency (unspecified)
TE_B	mean trap efficiency according to Brown (1944)
$TE_{C,d}$	trap efficiency at a day d calculated according to USACE (1995)
TE_d	adjusted trap efficiency at a day d
TE_H	mean trap efficiency according to Heinemann (1981)
$TE_{H,\ fit}$	mean trap efficiency according to a modification of Heinemann's (1981) equation
TE_{sim}	mean trap efficiency calculated based on the simulated water and sediment flux

TIN	triangular irregular network
TL	lag of surface runoff (parameter of the daily time step Pitman rainfall-runoff model)
TLS	terrestrial laser scanner
TOC	total organic carbon
T_R	observation period (i.e., the operational lifetime of a reservoir during which reservoir deposits were accumulated)
T_S	year of surveying or dam decommissioning
u_i	upper bound of the 95% confidence band of a mean particle size distribution (ith particle size class)
USD	U.S. dollar
UTM	Universal Transverse Mercator
VI	variable importance (unspecified)
VI_j	variable importance of the jth variable
V_{MAP}	volume of mean annual precipitation in the reservoir catchments
VP	vertical sample profile (e.g., VP1 and VP2)
V_S	volume of reservoir deposits that accumulated until the year of surveying
WCOV	mean fractional woody cover of the reservoir catchment
WGS	World Geodetic System
WRB	World Reference Base
WRZ	winter rainfall zone
x_i	vector with sediment properties of the ith sample
y	variable indicating the group affiliation of samples
y_i	group of samples to which the ith sample belongs
YRZ	year-round rainfall zone
ZAR	South African Rand
ZMINN	nominal minimum catchment absorption rate (parameter of the daily time step Pitman rainfall-runoff model)
ZMAXN	nominal maximum catchment absorption rate (parameter of the daily time step Pitman rainfall-runoff model)

Acknowledgements

Abstract

Soil erosion by water is a significant environmental issue that affects about 70% of South Africa's land surface. On-site effects of soil erosion are the loss of fertile topsoil and soil nutrients as well as the reduction of the soil water storage. As a consequence, soil erosion is frequently associated with land degradation. Off-site effects of soil erosion by water encompass an increased water turbidity in aquatic ecosystems, unwanted sedimentation along watercourses, and the silting of reservoirs. Overall costs arising from the on-site and off-site effects of soil erosion in South Africa are in excess of 360 million U.S. dollars per year.

Erosion and sediment transport in rivers represent quasi-natural processes, whose intensity is governed by rainfall and runoff conditions, relief characteristics, soil properties, and vegetation cover, among other natural factors. Human impact, through the transformation of natural landscapes into cultivated land and pasture, expansion of road networks and settlements, and other forms of land use, has led to accelerated soil erosion. Considering the obvious need for soil conservation measures in South Africa, it is important to consider the extent to which erosion can be attributed to natural environmental conditions – that are largely unavoidable – and the degree to which it is intensified by human impact. In this regard, the quantification of contemporary erosion rates that would occur under natural or near-natural environmental conditions is an important step towards the definition of realistic management goals for a sustainable use of soil resources. However, knowledge about contemporary 'natural' erosion rates in South Africa is presently very limited.

In this thesis, mean rates of contemporary erosion and sediment yield are presented for river catchments in the near-natural savanna landscape of the southern Kruger National Park (KNP). The KNP is an about 19 500 km^2 large conservation area located within the *'Lowveld'* geomorphic province in the northeast of South Africa, in between the Great Escarpment to the west and the coastal plains of Mozambique to the east. The southern part of the KNP was set aside for wildlife conservation by the turn of the 19th to 20th century. Even before that the area was largely spared from colonial farming. Archaeological and palynological evidence as well as historic sources suggest, moreover, a rather localized and low-intensity pre-colonial land use. Therefore, the KNP has been previously identified as a potential study area to establish benchmarks for tolerable soil loss in the *Lowveld*.

Abstract

Between 1930 and 1980, more than 50 reservoirs were constructed within the KNP to secure water provision for wildlife during dry periods. Since their establishment, these reservoirs impound intermittent surface runoff and trap sediment that is delivered from the catchments. A pilot study carried out in 2008 revealed that reservoir deposits (i.e., the post-dam facies) can be distinguished from soils and sediments that constitute the pre-dam facies based on colour and grain size. Quantifying the amount of reservoir deposits stored in the reservoir basins makes is possible to assess the mean sediment yield of the reservoir catchments to draw conclusions about catchment-wide average rates of erosion by water.

The overarching goal of this thesis is to establish benchmarks for rates of tolerable soil loss in the *Lowveld* by inferring contemporary rates of erosion by water for reservoir catchments in the southern KNP. For this, 15 small ($\leq 350 \times 10^3 \, \text{m}^3$) intermittently dry reservoirs with operational lifetimes of 30 to 65 years were investigated. The size of the reservoir catchments varies from <1 km^2 to about 100 km^2. High-resolution surveys were carried out in dry reservoir basins using a differential Global Navigation Satellite System (GNSS) and a terrestrial laser scanner (TLS). Reservoir deposits were mapped and spatial variations of the sediment thickness ascertained based on depth soundings with Pürckhauer-type and gouge augers. Samples were taken to ascertain the site-specific mean dry bulk density of the reservoir deposits. By combining these data, the mass of reservoir deposits that was accumulated in the reservoir basins up to the survey date can be quantified.

At selected reservoirs (N = 4), samples were collected from the pre- and post-dam facies to scrutinize criteria that were used for the discrimination of the facies in the field. These samples (N = 250) were analyzed with respect to physical (grain size composition, colour) and chemical (content of calcium-lactate leachable phosphorus) properties. Statistical discriminant analysis was carried out to identify a 'composite fingerprint', i.e., a subset of sediment properties that enables 'optimal' discrimination between the facies. For this, two methodological approaches were tested: stepwise discriminant function analysis (DFA) and regularized logistic regression (RLR). Based on 50% of the samples (i.e., the training set), discriminant functions and regression models were fitted. These were subsequently used to classify samples with respect to their affiliation to either the pre-dam facies or post-dam facies. The performance of both approaches was assessed based on the remaining 50% of the data retained for validation and the field-based assignment of the samples to the facies. The analysis was extended

by means of Monte Carlo simulations and synthetic datasets to quantify uncertainties that might result from a potential non-representative sampling. Both methodological approaches lead to low and nearly identical misclassification rates of ≤3%. Even when a potential sampling bias is taken into account, misclassification rates amount to only about 5%. These results verify the appropriateness of criteria (i.e., colour and texture) that were used for the discrimination of the facies in the field.

Sediment that is delivered to the reservoir inlets is only partly accumulated in the reservoir basins. During high-discharge events, water and sediment are released via uncontrolled overflow spillways when the water storage capacity of the reservoirs is exhausted. The sediment trap efficiency (*TE*) of a reservoir is defined as the proportion of sediment that is eventually deposited in the reservoir basin. Due to absence of records on catchment runoff and fluvial sediment transport, the mean *TE* was estimated by means of modelling. Catchment runoff, water fluctuations in the reservoirs, and the frequency and magnitude of spillage events were simulated with a daily time step rainfall-runoff model. The model was calibrated based on historical water levels in the reservoirs derived from field observations and aerial imagery. Different runoff scenarios were established to cope with various uncertainties. In addition, scenarios for the relationship between water and sediment discharge were created using sediment rating curves. The modelling results indicate that a few ($N \leq 6$) high-discharge events contributed ≥65% to the sediment delivery at all investigated reservoirs. Mean *TE* estimates range from 25% to >90% among the study sites.

The mean area-specific sediment yield (*SSY*) for the reservoir catchments can be calculated from the mass of the reservoir deposits, the operational lifetime and mean trap efficiency of the reservoirs, and the catchment size. In addition, temporary storage of sediment in the catchments needs to be taken into account to draw conclusions about average rates of erosion by water (*E*). For this, the sediment delivery ratio (*SDR*), defined as the ratio of *SSY* and *E*, was estimated from established empirical equations. An analysis of the propagation of uncertainties, consistently expressed at the 95% confidence level, highlights the estimation of *TE* and *SDR* values to be the major source of uncertainty in this study. The *TE* estimation contributes on average 64% to the uncertainty of *SSY* values, while the mean fractional contribution of the *SDR* estimation to uncertainties of *E* values amounts to 79%. By comparison, the uncertainty contribution from field and laboratory measurements is of minor importance amounting to <30% and <6% for *SSY* and *E* values, respectively.

Abstract

SSY values determined in this study range from 5 to 80 t km^{-2} yr^{-1} (N = 15) and are in good agreement with the *SSY* values of 10 to 60 t km^{-2} yr^{-1} (N = 5) ascertained in the pilot study. The results point to a highly significant correlation between *SSY* and mean annual precipitation (*MAP*; R = 0.71; p < 0.01) and a weakly significant correlation with the mean slope inclination (*Slope*; R = 0.45; p < 0.10) of the catchments. *MAP* and *Slope* values are likewise correlated (R = 0.58; p < 0.03). The mean (and median) *SSY* value for all study sites equals 30 ± 10 t km^{-2} yr^{-1} (20 [15, 50] t km^{-2} yr^{-1}). The mean relative uncertainty of *SSY* values amounts to ±21% and is therefore comparatively low. *E* values are subject to a higher mean uncertainty of ±46% due to the uncertain *SDR* estimation. *E* values are typically ≤190 t km^{-2} yr^{-1} except for catchments being affected by gully erosion (N = 3) that show *E* values of up to 360 t km^{-2} yr^{-1}. Whether contemporary gully erosion in the KNP is primarily driven by natural factors or due to human impact is an open question that cannot be conclusively answered with the available data. Comparing *SSY* and *E* values from catchments inside and outside the KNP elucidates that even values ascertained for gullied catchments are still comparatively low.

SSY and *E* values for reservoir catchments located outside conservation estates, for example, at the western boundary of the *Lowveld*, as well as in other regions of South Africa are by an order of magnitude higher than within the KNP. This difference can be clearly attributed to low erosion rates in the near-natural savanna landscape of the southern KNP as compared to other areas where anthropogenic influences such as pastoral farming, crop cultivation, and other forms of land use led to accelerated soil erosion. There is little data currently available to permit a comparison of *SSY* and *E* values from the KNP with corresponding values for catchments in other areas in South Africa also characterized by near-natural conditions.

Rates of soil loss under near-natural conditions ascertained on the plot-scale are comparable to results from this study, if differing environmental conditions and issues of scale (i.e., spatial and temporal) are taken into consideration. At the same time, mean and median *E* values determined in this study are >4 times higher than long-term (typically ≥10^5 years) average denudation rates (D_{Lt}) for the same catchments, that were ascertained from cosmogenic beryllium-10 concentrations in quartz-bearing river sediments. Results from previous studies indicate, moreover, that soil formation rates in South Africa are possibly similar to D_{Lt} values and probably not higher than *E* values of non-gullied catchments within the southern KNP. Interpreting the *E* values of these

catchments as benchmarks for tolerable rates of soil loss in the *Lowveld* leads to a soil conservation management goal of ≤ 190 t km^{-2} yr^{-1}.

Kurzfassung

Bodenerosion durch Wasser ist ein bedeutendes Umweltproblem, von dem etwa 70% der Landoberfläche Südafrikas betroffen sind. *On-site*-Effekte (d.h. vor Ort entstehende Auswirkungen) von Bodenerosion umfassen den Verlust von fruchtbarem Oberboden und Nährstoffen sowie die Verringerung des Bodenwasser-Speichervermögens. Infolgedessen geht Bodenerosion häufig mit Landdegradation einher. *Off-site*-Effekte (d.h. andernorts entstehende Auswirkungen) von Bodenerosion beinhalten eine erhöhte Wassertrübung in aquatischen Ökosystemen, unerwünschte Sedimentablagerungen entlang Fließgewässern und Sedimentation in Stauseen. Im Durchschnitt übersteigen in Südafrika die durch *On-site-* und *Off-site*-Effekte von Bodenerosion durch Wasser entstehenden Gesamtkosten 360 Millionen US-Dollar pro Jahr.

Erosion und Sedimenttransport in Flüssen repräsentieren quasinatürliche Prozesse, deren Intensität durch Niederschlags- und Abflussverhältnisse, Relief- und Bodeneigenschaften, Pflanzenbedeckung sowie andere natürliche Faktoren gesteuert wird. Anthropogene Einflüsse wie der Wandel von Naturlandschaften zu Acker- und Weideland, die Erweiterung von Straßennetzen und Siedlungsgebieten und andere Landnutzungsformen haben weitverbreitet zu beschleunigter Bodenerosion geführt. In Anbetracht der offenkundigen Notwendigkeit von Bodenschutzmaßnahmen in Südafrika ist es eine wichtige Frage, wie viel Erosion auf natürliche Umweltbedingungen zurückzuführen ist und insofern als weitgehend unvermeidbar angesehen werden muss, und in welchem Ausmaß Erosion durch menschliche Einflüsse verstärkt wird. In dieser Hinsicht ist die Quantifizierung rezenter Erosionsraten, wie sie unter naturbelassenen oder naturnahen Umweltbedingungen auftreten würden, ein wichtiger Schritt zur Definition realistischer Managementziele zugunsten einer nachhaltigen Nutzung von Bodenressourcen. Allerdings liegen bislang nur sehr wenige Erkenntnisse zu rezenten „natürlichen" Erosionsraten vor.

In dieser Arbeit werden mittlere rezente Erosions- und Sedimentaustragsraten für Flusseinzugsgebiete in der naturnahen Savannenlandschaft des südlichen *Kruger National Park* (KNP) präsentiert. Der KNP ist ein etwa 19 500 km^2 großes Naturschutzgebiet, das im Nordosten Südafrikas in der als „*Lowveld*" bezeichneten geomorphologischen Region liegt, die sich zwischen der Große Randstufe (engl.: *Great Escarpment*) im Westen und den Küstenebenen Mosambiks im Osten befindet. Der südliche Teil des KNP wurde um die Wende vom 19. zum 20. Jhd. als Natur- und

Wildpark unter Schutz gestellt. Schon davor blieb das Gebiet von kolonialer Landwirtschaft weitgehend unberührt. Archäologische und palynologische Befunde sowie historische Quellen deuten zudem auf eine nur lokale und wenig intensive prä-koloniale Landnutzung hin. Deshalb wurde der KNP bereits in einer vorangegangenen Studie als ein potenzielles Untersuchungsgebiet identifiziert, in dem Richtwerte für einen tolerierbaren Bodenabtrag im *Lowveld* ermittelt werden können.

Zwischen 1930 und 1980 wurden mehr als 50 Stauhaltungen im KNP errichtet, um die Wasserversorgung von Wildtieren während Trockenperioden zu gewährleisten. Seit ihrem Erbau werden die Stauhaltungen durch intermittierenden Oberflächenabfluss gespeist, wobei es in den Staubecken zur Ablagerung von Sedimenten kommt, die aus den Einzugsgebieten herantransportiert werden. Im Zuge einer Pilot-Studie, die 2008 durchgeführt wurde, konnte gezeigt werden, dass Stauseesedimente (die Post-Damm-Fazies) anhand ihrer Farbe und Korngrößenzusammensetzung von Böden und Sedimenten, die der Prä-Damm-Fazies angehören, unterschieden werden können. Durch die Quantifizierung der Stauseesedimente ist es möglich, den Sedimentaustrag aus den Einzugsgebieten zu bestimmen, um Rückschlüsse auf durchschnittliche Raten des Bodenabtrags durch Wasser zu ziehen.

Das übergeordnete Ziel dieser Arbeit ist es, durch die Bestimmung des rezenten durchschnittlichen Bodenabtrags in Stauseeeinzugsgebieten im KNP, Richtwerte für tolerierbare Erosionsraten im *Lowveld* zu ermitteln. Dafür wurden 15 kleine ($\leq 350 \times 10^3$ m^3), episodisch trockenfallende Stauseen mit Bestandszeiten von jeweils 30 bis 65 Jahren untersucht. Die Größe der Stausee-Einzugsgebiete variiert zwischen <1 km^2 und etwa 100 km^2. Die trockengefallenen Staubecken wurden hochauflösend mit einem differentiellen globalen Navigationssatellitensystem (GNSS) und einem terrestrischen Laserscanner (TLS) vermessen. Die Stauseesedimente wurden kartiert und deren räumlich variable Sedimentmächtigkeit durch Tiefensondierungen mit Pürckhauer-Bohrstöcken und Schlitzsonden erfasst. Zusätzlich wurden Proben genommen, um die Trockenlagerungsdichte der Stauseesedimente zu bestimmen. Durch das Zusammenführen dieser Daten kann die Masse der Stauseesedimente quantifiziert werden, die bis zum Tag der Felduntersuchungen abgelagert wurde.

An ausgewählten Stauhaltungen (N = 4) wurden die Prä- und Post-Damm-Fazies beprobt, um Kriterien zu überprüfen, die für die Unterscheidung beider Fazies im Feld herangezogen wurden. Dafür wurden die Proben (N = 250) in Bezug auf physikalische (Korngrößenzusammensetzung, Farbe) und chemische Eigenschaften (Gehalt an

kalziumlaktat-löslichem Phosphor) analysiert. Durch eine statistische Diskriminanzanalyse wurde ein „*composite fingerprint*" bestimmt, also eine Auswahl an Sedimenteigenschaften, die eine bestmögliche Unterscheidung verspricht. Dafür wurden zwei methodische Ansätze getestet: die schrittweise Diskriminanz-funktionsanalyse (DFA) sowie *regularized logistic regression* (RLR; logistische Regression mit Beschränkung der Regressionskoeffizienten). Basierend auf etwa 50% der Proben (Trainingsdatensatz) wurden Diskriminanzfunktionen und Regressionsmodelle optimiert. Diese wurden nachfolgend genutzt, um Proben hinsichtlich ihrer Zugehörigkeit zur Prä- oder Post-Damm-Fazies zu klassifizieren. Die Ergebnisse wurden mit einem aus den verbleibenden 50% der Proben bestehenden Validierungsdatensatz und der feldbasierten Zuordnung der Proben überprüft. Die Analysen wurden anhand von Monte-Carlo-Simulationen und synthetisch erzeugten Daten ausgeweitet, u.a. um Unsicherheiten zu quantifizieren, die aus einer möglicherweise nicht-repräsentativen Probenahme entstehen. Beide methodischen Ansätze führen zu niedrigen und nahezu identischen Fehlklassifikationsraten von ≤3%. Selbst unter Berücksichtigung einer möglicherweise nicht-repräsentativen Probenahme ergeben sich lediglich 5% Fehlklassifikationen. Diese Ergebnisse belegen die Eignung der im Feld verwendeten Kriterien (Farbe und Textur) zur Unterscheidung der Fazies.

Nur ein Teil des in die Stauseen eingetragenen Sediments wird in den Staubecken abgelagert. Im Zuge von Starkabflussereignissen wird Wasser und Sediment unkontrolliert durch Überläufe abgegeben, wenn die Staukapazität der Stauhaltungen erschöpft ist. Das Sedimentrückhaltevermögen (engl.: *sediment trap efficiency*; *TE*) eines Stausees ist definiert als der Anteil des eingetragenen Sediments, der letztendlich im Staubecken verbleibt. Angesichts des Fehlens entsprechender Abfluss- und Sedimentfrachtmessungen wurde die *TE* durch Modellierung abgeschätzt. Abflussraten, Wasserspiegelschwankungen in den Stauseen sowie die Häufigkeit und Magnitude von Überlaufereignissen wurden mit einem Niederschlags-Abfluss-Modell in täglicher Auflösung simuliert. Das Modell wurde anhand von historischen Wasserspiegelständen kalibriert, die entweder im Feld beobachtet oder aus Luftbildern abgeleitet wurden. Verschiedene Abflussszenarien wurden getestet, um diverse Unsicherheiten zu berücksichtigen. Zusätzlich wurden anhand von Eichkurven (engl.: *sediment rating curves*) Szenarien für die Beziehung zwischen Abflussrate und Sedimentfracht generiert.

Die Modellierungsergebnisse deuten an, dass einige wenige ($N \leq 6$) Starkabflussereignisse ≥65% zum Sedimenteintrag in allen untersuchten Stauhaltungen beigetragen haben. Die mittleren *TE*-Schätzwerte variieren zwischen 25% und >90% zwischen den Untersuchungsstandorten.

Der mittlere flächenbezogene Sedimentaustrag (engl.: *area-specific sediment yield; SSY*) aus den Stausee-Einzugsgebieten kann aus der Masse der Stauseesedimente, der Bestandszeit der Dämme und dem Sedimentrückhaltevermögen (*TE*) der Stauseen sowie der Einzugsgebietsgröße berechnet werden. Um Rückschlüsse auf mittlere Raten des Bodenabtrags durch Wasser (*E*) ziehen zu können, muss zusätzlich die temporäre Zwischenspeicherung von Sediment in den Einzugsgebieten berücksichtigt werden. Dafür wurden sogenannte *sediment delivery ratios* (*SDR*), die als das Verhältnis von *SSY* zu *E* definiert sind, mit etablierten Schätzbeziehungen ermittelt.

Eine Analyse zur Fortpflanzung von Unsicherheiten, bezogen auf das 95%-Konfidenzniveau, zeigt auf, dass die Abschätzung der *TE*- und *SDR*-Werte die Hauptunsicherheit in dieser Studie darstellt. Die *TE*-Abschätzung trägt im Mittel 64% zur Gesamtunsicherheit der *SSY*-Werte bei, während der mittlere anteilige Beitrag der *SDR*-Abschätzung zur Unsicherheit von *E*-Werten 79% beträgt. Im Vergleich dazu sind Beiträge von Unsicherheiten, die durch Feld- und Labormessungen entstehen, mit <30% bzgl. *SSY* und <6% bzgl. *E* von geringer Bedeutung.

Die in dieser Studie ermittelten *SSY*-Werte variieren zwischen 5 und 80 t km^{-2} a^{-1} ($N = 15$) und stehen im Einklang mit *SSY*-Werten von 10 bis 60 t km^{-2} a^{-1} ($N = 5$), die in der Pilot-Studie ermittelt wurden. Die *SSY*-Werte korrelieren hochsignifikant mit mittleren Jahresniederschlägen (engl.: *mean annual precipitation*; *MAP*; $R = 0.71$; $p < 0.01$) und schwach signifikant mit der mittleren Hangneigung (*Slope*; $R = 0.45$; $p < 0.10$) in den Einzugsgebieten. *MAP* und *Slope* sind ebenfalls korreliert ($R = 0.58$; $p < 0.03$). Der Mittelwert (und Median) aller ermittelten *SSY*-Werte beträgt 30 ± 10 t km^{-2} a^{-1} (20 [15, 50] t km^{-2} a^{-1}). Die mittlere relative Unsicherheit der *SSY*-Werte beläuft sich auf ±21%. *E*-Werte sind aufgrund der unsicheren *SDR*-Abschätzung durch einen höheren mittleren relativen Fehler von 46% gekennzeichnet. *E*-Werte belaufen sich typischerweise auf ≤190 t km^{-2} a^{-1}, abgesehen von Einzugsgebieten, in denen rezent Gully-Erosion stattfindet ($N = 3$) und die Werte von bis zu 360 t km^{-2} a^{-1} aufweisen. Inwieweit rezente Gully-Erosion primär auf natürliche Faktoren zurückzuführen ist oder eine Folge anthropogener Einflüsse darstellt, ist eine offene Frage, die mit derzeit verfügbaren Daten nicht abschließend beantwortet werden

kann. Ein Vergleich von *SSY*-Werten und *E*-Werten für Einzugsgebiete innerhalb und außerhalb des KNP verdeutlicht, dass selbst die für Einzugsgebiete mit Gully-Systemen bestimmten Werte als vergleichsweise niedrig anzusehen sind.

SSY- und *E*-Werte von Einzugsgebieten, die sich außerhalb von Naturschutzgebieten befinden, zum Beispiel im westlichen Teil des *Lowveld*, aber ebenso in anderen Regionen Südafrikas, sind um eine Größenordnung höher als im KNP. Dieser Unterschied weist auf vergleichsweise niedrige Erosionsraten in der naturnahen Savannenlandschaft des KNP und beschleunigte Bodenerosion in anderen, durch menschliche Einflüsse geprägten Gebieten hin. Gegenwärtig sind kaum Daten verfügbar, die einen Vergleich von *SSY*- und *E*-Werten für Einzugsgebiete im KNP mit entsprechenden Werten für andere Areale in Südafrika gestatten würden, die ebenfalls durch naturnahe Bedingungen gekennzeichnet sind.

Erosionsraten, die in anderen Studien auf kleinräumigen Versuchsflächen mit naturnaher Vegetationsbedeckung ermittelt wurden, sind vergleichbar mit Ergebnissen dieser Studie, wenn abweichende Umweltbedingungen und die Skala der Betrachtung (d.h. räumlich und zeitlich) berücksichtigt werden. Zugleich sind Mittelwert und Median der in dieser Studie ermittelten *E*-Werte mehr als viermal höher als langzeitliche (typischerweise $\geq 10^5$ Jahre) Denudationsraten (D_{Lt}), die für dieselben Einzugsgebiete anhand von Beryllium-10-Gehalten in quarzhaltigen Flusssedimenten bestimmt wurden. Ergebnisse früherer Studien deuten zudem darauf hin, dass Bodenneubildungsraten möglicherweise ähnlich zu D_{Lt}-Werten sind und wahrscheinlich nicht höher als *E*-Werte von Einzugsgebieten im KNP, die nicht von Gully-Erosion betroffen sind. Werden die *E*-Werte dieser Einzugsgebiete als Richtwerte für den Bodenschutz im *Lowveld* herangezogen, so ergibt sich daraus ein tolerierbarer Bodenabtrag von ≤ 190 t km^{-2} a^{-1}.

Chapter 1

Introduction

Author: Bastian Reinwarth

1 Introduction

Soil erosion by water is considered a major environmental problem and the most important cause of land degradation in South Africa (e.g., Garland et al., 2000; Boardman et al., 2012; Manyevere et al., 2016) and some of its neighbouring countries (e.g., Whitlow, 1988; O'Keefe et al., 1991; Mushala et al., 1997; Hochschild et al., 2003). Adverse consequences of soil erosion involve 'on-site' damages that emerge at places from which soil material is eroded, as well as 'off-site' effects that are related to the transport and deposition of material at distant locations (Morgan, 2005). On-site damages resulting from sheet and rill erosion comprise the loss of surface soil, exposure of infertile or indurated subsoil, decline of soil moisture storage and thinning or complete loss of vegetation cover (Boardman et al., 2017). Concentration of overland flow may culminate with the incision of gullies, locally referred to as 'dongas' (King and Fair, 1944) or 'sluits' (Rowntree, 2013), that can be observed across much of southern Africa (Showers, 1996; Felix-Henningsen et al., 1997; Mararakanye and Le Roux, 2012). Off-site effects occur when mobilized material enters watercourses, thereby increasing turbidity and nutrient levels (Flügel et al., 2003) which affect aquatic habitats (Gordon et al., 2015). Sedimentation along watercourses often interferes with the use of infrastructure (Braune and Looser, 1989). Water storage capacity loss due to reservoir siltation is particularly crucial in South Africa, as the population and economy rely heavily on water supply from dams given widespread semi-arid climate conditions (van Vuuren, 2012; Le Roux, in press).

There are considerable environmental and economic costs that arise from on-site and off-site effects of soil erosion by water. Due to limited rainfall, soil properties and other factors, only 11% of South Africa is suitable for crop cultivation (Johnston et al., 2013). In some regions, soil erosion is considered a major factor that impairs economically profitable crop production (Manyevere et al., 2014). Garland et al. (2000) estimated that until the end of the 20th century as much as 70% of South Africa's land surface was degraded to a varying extent due to soil erosion by water. Consequently, this led to a 25% reduction in the total amount of topsoil material across the country (Pretorius, 2006). Based on currency exchange rates using the year 2000 as a reference (Worldbank, 2017), average costs for fertilizers that would have been required to fully compensate the nation-wide erosive loss of soil nutrients (i.e., nitrogen, phosphorus and potassium) might have amounted to about 220 million U.S. dollars per year (Hoffman

and Ashwell, 2001, p. 82) (Tab. 1). Mean annual costs for the replacement of water storage capacity, lost due to reservoir siltation, were likely in the order of 20 to 30 million U.S. dollars (Braune and Looser, 1989; DEAT, 2000, p. 24). Taking into account additional costs for the remediation of infrastructure that is affected by sedimentation along watercourses and expenses for water purification that result from elevated water turbidity (DEAT, 2006, p. 99), the mean costs arising from off-site effects may be in excess of 140 million U.S. dollars per year (Hoffman and Ashwell, 2001). In total, mean annual costs of soil erosion by water therefore likely exceed 360 million U.S. dollars in South Africa, which corresponds to ≥8% of the mean annual net value added in the agricultural sector in 2000 (Worldbank, 2017).

Tab. 1 Overview on estimated mean annual costs that arose from on-site and off-site effects of soil erosion by water in South Africa in 2000.

Effect	Costs [10^6 ZAR]	Costs [10^6 USD]	Source(s)
Loss of major soil nutrients (i.e., nitrogen, phosphorus and potassium	>1500	>220	Hoffmann and Ashwell (2001)
On-site effects - Total	*>1500*	*>220*	
Replacement of water storage capacity lost by reservoir siltation	150 to 200	20 to 30	Braune and Looser (1989) DEAT (2000)
Remediation of infrastructure and expenses for water purification	>850	>120	Hoffman and Ashwell (2001)
Off-site effects - Total	*>1000*	*>140*	
Soil erosion by water –Total	*>2500*	*>360*	

Costs are given in South African Rand (ZAR) and U.S. dollar (USD) based on the official average currency exchange rate for the reference year 2000 (1 USD = 6.94 ZAR; Worldbank, 2017)

Soil erosion is a quasi-natural process (Mortensen, 1955) that is driven by prevailing environmental conditions, but has been accelerated globally due to anthropogenic activities throughout the Holocene (e.g., Borrelli et al., 2017; Vanwalleghem et al., 2017). Major natural factors that influence rates of erosion by water include rainfall characteristics, vegetation cover, relief attributes and soil properties (Wischmeier and Smith, 1965; Le Roux et al., 2008). Considering these factors, large areas within South Africa appear to be predisposed to erosion by water (Garland et al., 2000), whereby many of the most susceptible areas are located in the

eastern part of the country (Meadows and Hoffman, 2002). Anthropogenic factors that led to accelerated soil erosion in South Africa include the transformation of the natural vegetation cover to pasture and cultivated land by pre-colonial (Marker and Evers, 1976; Dean et al., 1995; MacPherson et al., in press) and colonial farmers (e.g., Meadows and Asmal, 1996; Compton et al., 2010; Boardman et al., 2012) as well as extensive land use that was reinforced through the regulation of land ownership in the Apartheid era (e.g., Hoffman and Todd, 2000; Laker, 2000; Watson, 2001). Additional factors include the abandonment of cultivated lands (Kakembo and Rowntree, 2003; Kakembo et al., 2009), expanding road networks (Beckedahl et al., 2001; Seutloali et al., 2016) and settlements (Marker, 1988; Watson, 1996; Gebel et al., 2017) among others (DEAT, 2006, p. 98f.).

Considering the indisputable need for soil and water conservation in South Africa, one of the 'big questions' (Boardman et al. 2010, p. 65) is how much soil erosion is man-made and, thus, avoidable, and to what extent erosion can be attributed to natural environmental conditions (Poesen, 2018). Several authors have argued for a complex interplay of natural and anthropogenic factors in governing soil erosion in South Africa (e.g., Serfontein, 1930; Meadows and Hoffman, 2003; Rowntree et al., 2004; Sonneveld et al., 2005; Boardman et al., 2010). Shedding light on the magnitude of natural erosion is therefore an important step towards the definition of realistic management goals (Murgatroyd, 1979; Montgomery, 2007). Reviews on soil erosion research in South Africa (e.g., Garland et al., 2000; Laker, 2004; Boardman et al., 2012) suggest, however, that knowledge about contemporary erosion rates that would occur under pristine environmental conditions is limited.

The Kruger National Park (KNP) in the northeast of South Africa (Fig. 1) has been identified as a suitable study area to establish benchmarks for contemporary 'natural' erosion rates (Baade et al., 2012). The KNP is a 19 500 km^2 large conservation area (Joubert, 1986) located in the summer rainfall zone (SRZ; >66% precipitation occurs between October and March; Chase and Meadows, 2007) of South Africa (Fig. 1a). The area is characterized by an undulating savanna landscape (Venter et al., 2003) and belongs to the *'Lowveld'* geomorphic province (Partridge et al., 2010) with the Great Escarpment to the west and coastal plains of Mozambique to the east (Fig. 1b). The southern part of the KNP was set aside for wildlife conservation by the
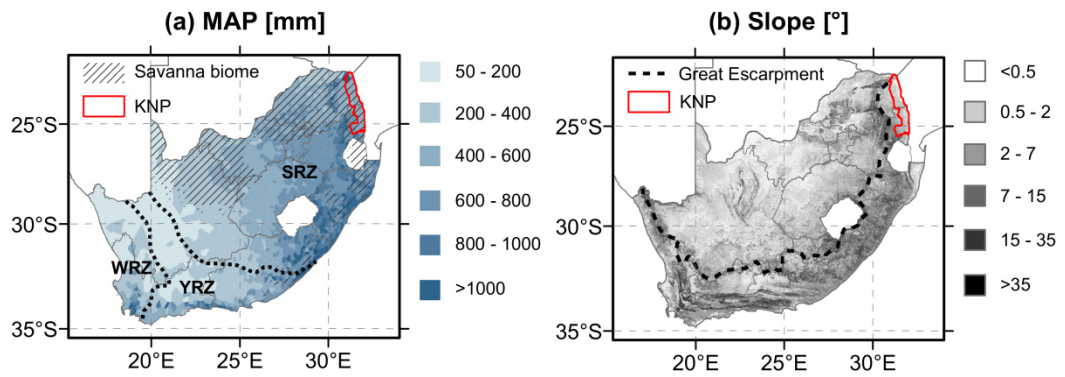
Fig. 1. Rainfall conditions and relief characteristics of South Africa and the location of the Kruger National Park (KNP): (a) mean annual precipitation (MAP; Thiessen polygons based on data provided by Pitman and Bailey, 2015), rainfall zones according to Chase and Meadows (2007), i.e., the winter rainfall zone (WRZ; >66% precipitation occurring between April and September), the summer rainfall zone (SRZ; >66% precipitation occurring between October and March) with the year-round rainfall zone (YRZ) in between, and the spatial extent of the savanna biome according to Mucina and Rutherford (2010); (b) slope inclination (based on Jarvis et al., 2008, and slope inclination classes suggested by Leser and Stäblein, 1975) and the location of the Great Escarpment (Kounov et al., 2013).

turn of the 19th to 20th century (Mabunda et al., 2003). Even before that, the area was largely spared from agricultural activities. In pre-colonial times, the population density may have peaked at about 0.8 person per square kilometre (Freitag-Ronaldson and Foxcroft, 2003), but archaeological evidence (Plug, 1989), pollen records (Ekblom et al., 2011) and historical sources (Pienaar, 1985) suggest a rather localized and low intensity pre-colonial land use. Later, the area was avoided by colonial farmers due to poor soils (Pollard et al., 2003, p. 428) and insect infestations during the rainy season that brought diseases threatening humans (e.g., malaria) and livestock (e.g., nagana) (Carruthers, 1995, p. 41). People who lived in the area were forced to leave after the proclamation of the KNP (Dikeni, 2016).

Today, less than 3% of the area is directly affected by human infrastructure (Freitag-Ronaldson et al., 2003) and large parts of the KNP can be considered 'intact wilderness' (MacFayden, 2010, p. 45) including granite areas with bush and shrub savanna (Fig. 2a) in the western part, and open tree savanna underlain by basalt (Fig. 2b) in the eastern part of the southern KNP. Summarizing these findings, environmental change (MacFayden et al., 2016) and erosion within the KNP appear to be mainly driven by natural factors. This is in clear contrast to nearby areas outside the KNP where extensive land use led to accelerated soil erosion and land degradation (Wessels et al., 2007).

Fig. 2. Intact wilderness in the southern Kruger National Park: (a) bush and shrub savanna with granite 'koppies' (i.e., hills) near Stolznek (25° 17' S; 31° 24' E) at the end of the rainy season in February 2014; (b) view from the Nkumbe outlook south of Tshokwane (24° 51'S; 31° 53' E) on basalt plains with open tree savanna at the end of the dry season in September 2015.

Baade et al. (2012) began to study rates of erosion and fluvial sediment transport in the KNP by assessing reservoir siltation in small intermittently dry reservoirs. These reservoirs were constructed between the 1930s and 1980s to ensure water provision for wildlife during dry periods (Pienaar, 1985). Since their establishment, they impound ephemeral surface runoff and trap sediment that is delivered from the reservoir catchment. By quantifying the mass of reservoir deposits that accumulated in the reservoir basins, conclusions can be drawn about the sediment yield of the catchments for the operational lifetime of the reservoirs (e.g., Langbein and Schumm, 1958). Within the framework of a reconnaissance survey carried out in 2008, Baade et al. (2012) demonstrated that reservoir deposits (i.e., the post-dam facies) can be distinguished from soils and sediments belonging to the pre-dam facies. The mean contemporary sediment yield was assessed for five reservoir catchments located entirely within the KNP.

This thesis is the continuation of the work commenced by Baade et al. (2012). The aim is to establish benchmarks for tolerable rates of erosion by water in the *Lowveld* geomorphic province by quantifying the mean contemporary sediment yield and average rates of erosion by water for reservoir catchments in the near-natural savanna environment of the southern KNP. Within the course of consecutive field campaigns, carried out between 2014 and 2016, 15 small reservoirs were investigated, including four previously studied reservoirs that were re-examined with a significantly enhanced resolution. The mean sediment yield for the operational lifetime of the

reservoirs (i.e., 30 to 65 years) was assessed based on high-resolution surveys of the reservoir basins, and the mapping and characterization of reservoir deposits. Granulometric and geochemical analysis were undertaken to confirm the validity of criteria that were used to differentiate between the pre- and post-dam facies in the field. Rainfall-runoff modelling was conducted to establish scenarios for the frequency and magnitude of spillage events from which the sediment trap efficiency of the reservoirs was estimated. Taking into account the intermediate storage of sediment in the catchments, estimates for catchment-wide rates of erosion by water were established. Uncertainties inherent in field, laboratory, and modelled data were quantified, and the relative importance of various sources of uncertainty assessed. Finally, sediment yield values and rates of erosion by water were compared to previously published data for areas inside and outside the KNP.

The thesis is organized as follows: **chapter 2** provides a brief overview on previous erosion research that has been carried out across southern Africa. Data on contemporary erosion rates in near-natural environments and rates of tolerable soil loss that were previously established for South Africa are presented. Information about long-term denudation rates ($>10^4$ years), derived from cosmogenic nuclides, is provided at the end of the chapter.

Chapter 3 is dedicated to the distinction between the pre- and post-dam facies. Criteria that were used for the facies discrimination in the field are scrutinized based on geochemical and granulometric analysis. The collection of samples and their subsequent physico-chemical characterization is described. Regularized logistic regression (RLR) is introduced as an innovative statistical tool to identify of a set of sediment properties that is particularly useful for the facies discrimination. The performance of RLR is compared to the outcome of stepwise discriminant function analysis (DFA) that has been applied in previous studies dealing with the discrimination of soils and sediments (Miller et al., 2015). The analysis is extended based on Monte Carlo simulations and synthetic datasets in order to quantify uncertainties and to enhance the method comparison. Merits and drawbacks of RLR and stepwise DFA are discussed.

In **chapter 4**, a methodological framework is presented that permits the estimation of the mean sediment trap efficiency for reservoirs in the KNP. This framework takes into account the prevailing semi-arid climate conditions that lead to strong water level fluctuations in the reservoirs and extended periods without spillage. The modelling approach for the simulation of catchment runoff, the reconstruction of

water level fluctuations and the assessment of the frequency and magnitude of spillage events is described. Scenarios for the relationship between water and sediment discharge are established based on sediment rating curves. Trap efficiency estimates are subsequently derived from all scenarios. The modelling results are compared to trap efficiency values that were calculated with equations from Brown (1944) and Heinemann (1981). The latter two approaches have been frequently applied all over the world but were developed mainly based on data from temperate climate regions.

Chapter 5 contains detailed information about the surveying, mapping and characterization of reservoir deposits and the subsequent processing of field data. Mean contemporary sediment yield values are presented and compared to results from Baade et al. (2012). Correlations between mean contemporary sediment yield and catchment properties are explored. Neglecting and taking into account the reservoir trap efficiency and intermediate sediment storage in catchments, minimum and best estimates for catchment-wide rates of erosion by water are calculated, respectively. The relative contribution of different error sources to the overall uncertainty inherent in sediment yield values and erosion rates is quantified. Implications for a reasonable surveying and sampling strategy in the field are discussed.

In **chapter 6**, the results are contextualized based on previously published contemporary sediment yield values and long-term average denudation rates for the *Lowveld*. Furthermore, the results are compared to data that were derived from reservoir siltation studies in other regions of South Africa. Finally, conclusions are drawn regarding tolerable rates of soil loss for the *Lowveld*. Open research questions that might be addressed in the future are highlighted.

References

Baade, J., Franz, S., Reichel, A., 2012. Reservoir siltation and sediment yield in the Kruger National Park, South Africa: a first assessment. Land Degradation and Development 23 (6), 586-600. DOI: 10.1002/ldr.2173.

Beckedahl, H.R., Hill, T.R., Moodley, M., 2001. Soil conservation perspectives of road infrastructure within a development context in South Africa. In: Stott, D.E., Mohtar, R.H., Steinhardt, G.C. (Eds.). Sustaining the global farm. Selected papers from the 10th International Soil Conservation Organization Meeting, May 24-29, 1999, West Lafayette. International Soil Conservation Organization in cooperation with the USDA and Purdue University: West Lafayette, Indiana, USA, pp. 324-328.

Boardman, J., Foster, I., Rowntree, K., Mighall, T., Gates, J., 2010. Environmental stress and landscape recovery in a semi-arid area, the Karoo, South Africa. Scottish Geographical Journal 126 (2), 64-75. DOI: 10.1080/14702541003711038.

Boardman, J., Hoffman, M.T., Holmes, P.J., Wiggs, G.F.S., 2012. Soil erosion and land degradation. In: Holmes, P., Meadows, M. (Eds.). Southern African Geomorphology. Recent Trends and New Directions. Sun Press: Bloemfontein, South Africa, pp. 307-328.

Boardman, J, Foster I.D.L., Rowntree, K.M., Favis-Mortlock, D.T., Mol, L., Suich, H., Gaynor, D., 2017. Long-term studies of land degradation in the Sneeuberg uplands, eastern Karoo, South Africa: a synthesis. Geomorphology 285, 106-120. DOI: 10.1016/j.geomorph.2017.01.024.

Borrelli, P., Robinson, D.A., Fleischer, L.R., Lugato, E., Ballabio, C., Alewell, C., Meusburger, K., Mudugno, S., Schütt, B., Ferro, V., Bagarello, V., Van Oost, K., Montanarella, L., Panagos, P., 2017. An assessment of the global impact of 21st century land use change on soil erosion. Nature Communications 8 (2013), 13 pp. DOI: 10.1038/s41467-017-02142-7.

Braune, E., Looser, U., 1989. Cost impacts of sediments in South African rivers. In: Hadley, R.F., Ongley, E.D. (Eds.). Sediment and the Environment (Proceeding of the Baltimore Symposium, May 1989). IAHS Publication No. 184. IAHS: Wallingford, UK, pp. 131-143.

Brown, C.B., 1944. Discussion of 'Sedimentation in Reservoirs' by B. J. Witzig. Transactions of the American Society of Civil Engineers 109, 1080-1086.

Carruthers, J., 1995. The Kruger National Park. A social and political history. University of KwaZulu-Natal Press: Scottsville, South Africa, 170 pp.

Chase, B.M., Meadows, M.E., 2007. Late Quaternary dynamics of southern Africa's winter rainfall zone. Earth-Science Reviews 84, 103-138. DOI: 10.1016/j.earscirev.2007.06.002.

Compton, J.S., Herbert, C.T., Hoffman, M.T., Schneider, R.R., Stuut, J.B., 2010. A tenfold increase in the Orange River mean Holocene mud flux: implications for soil erosion in South Africa. The Holocene 20 (1), 115-122. DOI: 10.1177/0959683609348860.

Dean, W.R.J., Hoffman, M.T., Meadows, M.E., Milton, S.J., 1995. Desertification in the semi-arid Karoo, South Africa: review and reassessment. Journal of Arid Environments 30 (3), 247-264. DOI: 10.1016/S0140-1963(05)80001-1.

DEAT, 2000. State of the Environment South Africa 1999 – an overview. Department of Environmental Affairs and Tourism (DEAT): Pretoria, South Africa, 46 pp.

DEAT, 2006. South Africa Environment Outlook. A Report on the State of the Environment. Department of Environmental Affairs and Tourism (DEAT): Pretoria, South Africa, 371 pp.

Dikeni, L.M., 2016. Habitat and struggle! The case of the Kruger National Park in South Africa. A study of the outcome of the interface between government, NGOs, managers of

natural resources and local communities. Real African Publishers: Houghton, Johannesburg, South Africa, 216 pp.

Ekblom, A., Gillson, L., Notelid, M., 2011. A historical ecology of the Limpopo and Kruger National Parks and Lower Limpopo Valley. Journal of Archaeology and Ancient History 1, 1-29.

Felix-Henningsen, P., Morgan, R.P.C., Mushala, H.M., Rickson, R.J., Scholten, T., 1997. Soil erosion in Swaziland: a synthesis. Soil Technology 11 (3), 319-329. DOI: 10.1016/S0933-3630(97)00016-0.

Freitag-Ronaldson, S., Foxcroft, L.C., 2003. Anthropogenic influences at the ecosystem level. In: Du Toit, J.T., Rogers, K.H., Biggs, H.C. (Eds.). The Kruger experience. Ecology and management of savanna heterogeneity. Island Press: Washington D.C., USA, pp. 391-421.

Freitag-Ronaldson, S., Kalwa, R.H., Badenhorst, J.C., Erasmus, J.P., Venter, F.J., Nel, F.J., 2003. Wilderness, wilderness quality management, and recreational opportunities zoning within Kruger National Park, South Africa. In: Watson, A., Sproull, J. (Eds.). Science and stewardship to protect and sustain wilderness values. Seventh World Wilderness Congress Symposium 2001, November 2-8, Port Elizabeth, South Africa. USDA Forest Service Proceedings RMRS-P-27. US Department of Agriculture, Forest Service, Rocky Mountain Research Station: Ogden, Utah, USA, pp. 39-49.

Flügel, W.-A., Märker, M., Moretti, S., Rodolfi, G., Sidrochuk, A., 2003. Integrating geographical information systems, remote sensing, ground truthing and modelling approaches for regional erosion classification of semi-arid catchments in South Africa. Hydrological Processes 17, 929-942. DOI: 10.1002/hyp.1171.

Garland, G., Hoffman, T., Todd, S., 2000. Soil degradation in South Africa: an overview. In: Hoffman, T., Todd, S., Ntshona, Z., Turner, S. (Eds.). Land degradation in South Africa. Department of Environmental Affairs: Pretoria, South Africa, pp. 69-107.

Gebel, M., Bürger, S., Wallace, M., Malherbe, H., Vogt, H., Lorz, C., 2017. Simulation of land use impacts on sediment and nutrient transfer in coastal areas of Western Cape, South Africa. Change and Adaptation in Socio-Ecological Systems 3 (1), 1-17. DOI: 10.1515/cass-2017-0001.

Gordon, A.K., Griffin, N.J., Palmer, C.G., 2015. The relationship between concurrently measured SASS (South African Scoring System) and turbidity data archived in the South African River Health Programme's Rivers Database. Water SA 41 (1), 21-25. DOI: 10.4314/wsa.v41i1.4.

Heinemann, H.G., 1981. A new sediment trap efficiency curve for small reservoirs. Journal of the American Water Resources Association 17 (5), 825-830. DOI: 10.1111/j.1752-1688.1981.tb01304.x.

Hochschild, V., Märker, M., Rodolfi, G., Staudenrausch, H., 2003. Delineation of erosion classes in semi-arid southern African grasslands using vegetation indices from optical remote sensing data. Hydrological Processes 17, 917-928. DOI: 10.1002/hyp.1170.

Hoffman, M.T., Todd, S., 2000. A national review of land degradation in South Africa: the influence of biophysical and socio-economic factors. Journal of Southern African Studies 26 (4), 743-758. DOI: 10.1080/03057070020008251.

Hoffman, T., Ashwell, A., 2001. Nature divided. Land degradation in South Africa. University of Cape Town Press: Lansdowne, Cape Town, South Africa, 168 pp.

Jarvis, A., Reuter, H.I., Nelson, A., Guevara, E., 2008. Hole-filled seamless SRTM data V4. International Centre for Tropical Agriculture (CIAT). <http://srtm.csi.cgiar.org> accessed 11 June 2017 (last modified: 19 August 2008).

Johnston, P., Thomas, T.S., Hachigonta, S., Majele Sibanda, L., 2013. South Africa. In: Hachigonta, S., Nelson, G.C., Thomas, T.S., Majele Sibanda, L. (Eds.). South African Agriculture and Climate Change: A Compehensive Analysis. IFRI Research Monograph. International Food Policy Research Institute (IFRI): Washington D.C, USA, pp. 175-212.

Joubert, S.C.J., 1986. The Kruger National Park – an introduction. Koedoe 29 (1), 1-11. DOI: 10.4102/koedoe.v29i1.516.

Kakembo, V., Rowntree, K.M., 2003. The relationship between land use and soil erosion in the communal lands near Peddie Town, Eastern Cape, South Africa. Land Degradation & Development 14, 39-49. DOI: 10.1002/ldr.509.

Kakembo, V., Xanga, W.W., Rowntree, K., 2009. Topographic thresholds in gully development on the hillslopes of communal areas in Ngqushwa Local Municipality, Eastern Cape, South Africa. Geomorphology 110 (3-4), 188-194. DOI: 10.1016/j.geomorph.2009.04.006.

King, L.C., Fair, T.J.D., 1944. Hillslopes and dongas. Transactions of the Geological Society of South Africa 47, 1-4.

Kounov, A., Viola, G., Dunkl, I., Frimmel, H.E., 2013. Southern African perspectives on the long-term morpho-tectonic evolution of cratonic interiors. Tectonophysics 601, 177-191. DOI: 10.1016/j.tecto.2013.05.009.

Laker, M.C., 2000. Soil resources: distribution, utilization, and degradation. In: Fox, R., Rowntree, K. (Eds.). The geography of South Africa in a changing world. Oxford University Press: Oxford, United Kingdom, pp. 326-360.

Laker, M.C., 2004. Advances in soil erosion, soil conservation, land suitability evaluation and land use planning research in South Africa, 1978-2003. South African Journal of Plant and Soil 21 (5), 345-368. DOI: 10.1080/02571862.2004.10635069.

Langbein, W.B., Schumm, S.A., 1958. Yield of sediment in relation to mean annual precipitation. Eos, Transactions American Geophysical Union 39 (6), 1076-1084. DOI: 10.1029/TR039i006p01076.

Le Roux, J.J., in press. Sediment yield potential in South Africa's only large river network without a dam: implications for water resource management. Land Degradation and Development. DOI: 10.1002/ldr.2753.

Le Roux, J.J., Morgenthal, T.L., Malherbe, J., Pretorius, D.J., Sumner, P.D., 2008. Water erosion prediction at a national scale for South Africa. Water SA 34 (3), 305-314.

Leser, H., Stäblein, G., 1975. Geomorphologische Kartierung. Richtlinien zur Herstellung geomorphologischer Karten 1:25 000 (2nd edn.). Arbeitskreis Geomorphologische Karte der Bundesrepublik Deutschland. GMK-Schwerpunktprogramm. Geomorphologische Detailkartierung in der Bundesrepublik Deutschland. Berlin: Institut für Physische Geographie der Freien Universität Berlin, 39 pp.

Mabunda, D., Pienaar, D.J., Verhoef, J., 2003. The Kruger National Park: a century of management and research. In: Du Toit, J.T., Rogers, K.H., Biggs, H.C. (Eds.). The Kruger experience. Ecology and management of savanna heterogeneity. Island Press: Washington D.C., USA, pp. 3-21.

MacFayden, S., 2010. Identifying priority zones within protected areas. A biodiversity sensitivity-value analysis of the Kruger National Park, South Africa. Master thesis. Faculty of Earth and Life Science, Vrije Universiteit Amsterdam: Amsterdam, The Netherlands, 57 pp.

MacFayden, S., Hui, C., Verburg, P.H., Van Teeffelen, A.J.A., 2016. Quantifying spatiotemporal drivers of environmental heterogeneity in Kruger National Park, South Africa. Landscape Ecology 31 (9), 2013-2029. DOI: 10.1007/s10980-016-0378-6.

MacPherson, A.J., Gillson, L., Hoffman, M.T., in press. Climatic buffering and anthropogenic degradation of a Mediterranean-type shrubland refugium at its semi-arid boundary, South Africa. The Holocene. DOI: 10.1177/0959683617735582.

Manyevere, A., Muchaonyerwa, P., Laker, M.C., Mnkeni, P.N.S., 2014. Farmers' perspectives with regard to crop production: an analysis of Nkonkobe Municipality, South Africa. Journal of Agriculture and Rural Development in the Tropics and Subtropics 115 (1), 41-53.

Manyevere, A., Muchaonyerwa, P., Mnkeni, P.N.S., Laker, M.C., 2016. Examination of soil and slope factors as erosion controlling variables under varying climatic conditions. Catena 147, 245-257. DOI: 10.1016/j.catena.2016.06.035.

Mararakanye, N., Le Roux, J.J., 2012. Gully location mapping at a national scale for South Africa. South African Geographical Journal 94 (2), 208-218. DOI: 10.1080/03736245.2012.742786.

Marker, M.E., 1988. Soil erosion in a catchment near Alice, Ciskei, southern Africa. In: Dardis, G.F., Moon, B.P. (Eds.). Geomorphological studies in southern Africa. Balkema: Rotterdam, The Netherlands, pp. 267-276.

Marker, M.E., Evers, T.M., 1976. Iron age settlement and soil erosion in the Eastern Transvaal, South Africa. The South African Archaeological Bulletin 31 (123/124), 153-165. DOI: 10.2307/3887737.

Meadows, M.E., Asmal, O., 1996. Chronology, sedimentology and geochemistry at Verlorenvlei (Western Cape Province, South Africa) as evidence of anthropogenically-induced land degradation. Zeitschrift für Geomorphologie N.F. 107 (Suppl.), 45-62.

Meadows, M.E., Hoffman, M.T., 2002. The nature, extent and causes of land degradation in South Africa: legacy of the past, lessons for the future? Area 34 (4), 428-437. DOI: 10.1111/1475-4762.00100.

Meadows, M.E., Hoffman, T.M., 2003. Land degradation and climate change in South Africa. The Geographical Journal 169 (2), 168-177. DOI: 10.1111/1475-4959.04982.

Miller, J.R., Macklin, G., Orbock Miller, S.M., 2015. Application of geochemical tracers to fluvial sediment. Springer Briefs in Earth Sciences. Springer: Cham, Germany, 142 pp.

Montgomery, D.R., 2007. Soil erosion and agricultural sustainability. Proceedings of the National Academy of Sciences of the United States of America (PNAS) 104 (33), 13268-13272. DOI: 10.1073/pnas.0611508104.

Morgan, R.P.C., 2005. Soil erosion and conservation. 3rd edn. Blackwell: Malden, USA, 304 pp.

Mortensen, H., 1955. Die "quasinatürliche" Oberflächenformung als Forschungsproblem. Wissenschaftliche Zeitschrift der Ernst-Moritz-Arndt-Universität Greifswald, Mathematisch-naturwissenschaftliche Reihe 4 (6-7), 625-628.

Mucina, L., Rutherford, M.C., 2010. The vegetation of South Africa, Lesotho and Swaziland (CD set). Strelitza 19. South African National Biodiversity Institute (SANBI), Pretoria, South Africa.

Murgatroyd, A.L., 1979. Geologically normal and accelerated rates of erosion in Natal. South African Journal of Science 75, 395-396.

Mushala, H.M., Morgan, R.P.C., Scholten, T., Felix-Henningsen, P., Rickson, R.J., 1997. Soil erosion and sedimentation in Swaziland: an introduction. Soil Technology 11, 219-228. DOI: 10.1016/S0933-3630(97)00009-3.

O'Keefe, P, Kirkby, J., Cherrett, I., 1991. Mozambican environmental problems: myths and realities. Public Administration and Development 11, 307-324. DOI: 10.1002/pad.4230110403.

Partridge, T.C., Dollar, E.S.J., Moolman, J., Dollar, L.H., 2010. The geomorphic provinces of South Africa, Lesotho and Swaziland: a physiographic subdivision for earth and environmental scientists. Transactions of the Royal Society of South Africa 65 (1), 1-47. DOI: 10.1080/00359191003652033.

Pienaar, U.d.V., 1985. Indications of progressive desiccation of the Transvaal Lowveld over the past 100 years, and implications for the water stabilization programme in the Kruger National Park. Koedoe 28, 93-165. DOI: 10.4102/koedoe.v28i1.540.

Pitman, B., Bailey, A., 2015. A wealth of new freely downloadable information on the water resources of South Africa, Swaziland and Lesotho. Journal of the South African Institution of Civil Engineers 23 (5), 13-18.

Plug, I., 1989. Aspects of life in the Kruger National Park during the Early Iron Age. South African Archaeological Society Goodwin Series 6, 62-68. DOI: 10.2307/3858133.

Poesen, J., 2018. Soil erosion in the Anthropocene: research needs. Earth Surface Processes and Landforms 43 (1), 64-84. DOI: 10.1002/esp.4250.

Pollard, S., Shackleton, C., Carruthers, J., 2003. Beyond the fence: people and the Lowveld landscape. In: Du Toit, J.T., Rogers, K.H., Biggs, H.C. (Eds.). The Kruger experience. Ecology and management of savanna heterogeneity. Island Press: Washington D.C., USA, pp. 422-446.

Pretorius, D., 2006. South Africa: the implementation of land degradation assessment and rehabilitation programmes – an agricultural perspective. In: King, C., Bigas, H., Adeel, Z., (Eds.). Desertification and the international policy imperative. Proceedings of a joint international conference. Algiers, Algeria. 17-19 December, 2006. UNU Desertification Series 7. United Nations University (UNU): Hamilton, Ontario, Canada, pp. 158-165.

Rowntree, K.M., 2013. The evil of sluits: a re-assessment of soil erosion in the Karoo of South Africa as portrayed in century-old sources. Journal of Environmental Management 130, 98-105. DOI: 10.1016/j.jenvman.2013.08.041.

Rowntree, K., Duma, M., Kakembo, V., Thornes, J., 2004. Debunking the myth of overgrazing and soil erosion. Land Degradation and Development 15 (3), 203-214. DOI: 10.1002/ldr.609.

Serfontein, J.L., 1930. Soil erosion in South Africa. Farming in South Africa 5 (49), 13-14.

Seutloali, K.E., Beckedahl, H.R., Dube, T., Sibanda, M., 2016. An assessment of gully erosion along major armoured roads in south-eastern region of South Africa: a remote sensing and GIS approach. Geocarto International 31 (2), 1-15. DOI: 10.1080/10106049.2015.1047412.

Showers, K.B., 1996. Soil erosion in the Kingdom of Lesotho and development of historical environmental impact assessment. Ecological Applications 6 (2), 653-664. DOI: 10.2307/2269399.

Sonneveld, M.P.W., Everson, T.M., Veldkamp, A., 2005. Multi-scale analysis of soil erosion dynamics in KwaZulu-Natal, South Africa. Land Degradation and Development 16 (3), 287-301. DOI: 10.1002/ldr.653.

van Vuuren, L., 2012. In the footsteps of giants – exploring the history of South Africa's large dams. Water Research Commission Report SP 31/12. Water Research Commission of South Africa: Gezina, Pretoria, South Africa, 334 pp.

Vanwalleghem, T., Gómez, J.A., Infante Amate, J., González de Molina, M., Vanderlinden, K., Guzmán, G., Laguna, A., Giráldez, J.V., 2017. Impact of historical land use and soil management change on soil erosion and agricultural sustainability during the Anthropocene. Anthropocene 17, 13-29. DOI: 10.1016/j.ancene.2017.01.002.

Venter F.J., Scholes, R.J., Eckhardt H.C., 2003. The abiotic template and its associated vegetation pattern. In: Du Toit, J.T., Rogers, K.H., Biggs, H.C. (Eds.). The Kruger experience. Ecology and management of savanna heterogeneity. Island Press: Washington D.C., USA, pp. 83-129.

Watson, H.K., 1996. Short and long term influence on soil erosion of settlement by peasant farmers in KwaZulu Natal. South African Geographical Journal 78 (1), 1-6. DOI: 10.1080/03736245.1996.9713600.

Watson, H.K., 2001. Soil sustainability and land reform in South Africa. In: Conacher, A.J. (Eds.). Land degradation. The GeoJournal Library. Volume 58. Kluwer: Dordrecht, The Netherlands, pp. 153-166.

Wessels, K.J., Price, S.D., Malherbe, J., Small, J., Frost, P.E., VanZyl, D., 2007. Can human-induced land degradation be distinguished from the effects of rainfall variability? A case study in South Africa. Journal of Arid Environments 68, 271-297. DOI: 10.1016/j.jaridenv.2006.05.015.

Whitlow, R., 1988. Potential versus actual erosion in Zimbabwe. Applied Geography 8 (2), 87-100. DOI: 10.1016/0143-6228(88)90026-4.

Wischmeier, W.H., Smith, D.D., 1965. Predicting rainfall-erosion losses from cropland east of the Rocky Mountains. Guide for selection of practices for soil and water conservation. Agriculture Handbook No. 282. Agricultural Research Service, US Department of Agriculture: Washington DC, USA, 47 pp.

Worldbank, 2017. World development indicators. <http://data.worldbank.org/country/south-africa> accessed 03 September 2017 (last modified: 02 August 2017).

Chapter 2

Soil erosion research in South Africa and previously established estimates of tolerable soil loss

Author: Bastian Reinwarth

2 Soil erosion research in South Africa and previously established estimates of tolerable soil loss

2.1 Previous research on contemporary sediment yield and soil erosion rates in southern Africa

In South Africa, on-site and off-site effects of accelerated soil erosion by water have been recognized at least since the late 19th century (e.g., Shaw, 1874; Roe, 1897; cf. Rowntree, 2013). Pioneering soil erosion research dates back to the 1920s (e.g., Jennings, 1923; Haviland, 1929). Between 1930 and 1950, South Africa became internationally known as being frightened by 'a national catastrophe, due to soil erosion' (Jacks and Whyte, 1939, p. 264), that was 'more imminent [...] than in any other country' (ibid.) of the world. Later, such opinions were partially considered 'neo-Malthusian narratives' (Stringer and Reed, 2007, p. 99), but the socio-economical relevance of soil erosion became generally accepted (e.g., Beinart, 1984). A visit of Hugh Bennett, the Chief of the United States Soil Conservation Service, to South Africa in 1944 prompted media attention and boosted the public interest in combating soil erosion (Dodson, 2005). Thereafter, numerous soil erosion studies ensued (Garland, 1982; Laker, 2004).

Aerial images (e.g., Talbot, 1947; Rowntree et al., 1991; Kakembo et al., 2009) and satellite data (e.g., Wentzel, 2002; Wessels et al., 2007; Mararakanye and Le Roux, 2012; Mararakanye and Sumner, 2017) were used to map the extent of erosional features in terms of surface area, partly at varying points in time. Measurements of contemporary erosion rates were carried out with soil wash traps (Haylett, 1960; Le Roux and Roos, 1982; Scott et al., 1998; Dlamini et al., 2011) and erosion pins (Keay-Bright and Boardman, 2009; Boardman et al., 2015). Fallout isotopes (e.g., ^{137}Cs) were mainly studied for the purpose of sediment dating or sediment source tracing (e.g., Foster et al., 2007), while the quantification of erosion rates from soil inventories (cf. Walling et al., 2003) was found to be challenging due to the rather low nuclear fallout on the southern hemisphere (Foster et al., 2017). Erosion models were applied to predict the soil loss and sediment transport at the scale of catchments (e.g., Breetzke et al., 2013; Le Roux, in press), regions (e.g., Schulze, 1979; Flügel et al., 2003) and the entire South Africa (Schulze et al., 2007; Le Roux et al., 2008). Empirically-based large-scale assessments were founded mainly on sediment yield data obtained from reservoir

siltation studies and sediment monitoring in rivers (Midgley, 1952, cit. in Garland et al., 2000; Schwartz and Pullen, 1966; Rooseboom and von M. Harmse, 1979; Rooseboom et al., 1992; Msadala et al., 2012).

A synopsis of previous studies indicates that soil erosion by water tends to be more intense in the eastern part of South Africa than in the west (Fig. 1). Modelling with a modified version of the Revised Universal Soil Loss Equation (RUSLE; Renard et al., 1991) revealed an average actual soil loss of 500 to 1000 t km^{-2} yr^{-1} (Le Roux et al., 2008; Msadala et al., 2012, p. 241) for the North West, Western Cape and Northern Cape Provinces (Fig. 1a). For all other provinces, the predicted average actual soil loss is >1500 t km^{-2} yr^{-1}, with a maximum value of 2200 t km^{-2} yr^{-1} in the Eastern Cape. The nation-wide average soil loss for South Africa amounts to 1260 t km^{-2} yr^{-1} (ibid.). The RUSLE-based approach is capable of predicting soil loss by sheet and rill erosion but does not account for gully erosion (Renard et al., 1991). The spatial distribution and frequency of gullies has been investigated by Mararakanye and Le Roux (2012) based on panchromatic sharpened SPOT 5 satellite imagery, merged to a geometric resolution of 5 m. Accordingly, gullies affect <0.2% of the land surface in the Western Cape, North West and Gauteng Provinces, but show a five times higher abundance in the Eastern Cape and KwaZulu-Natal Provinces (Fig. 1b). In total, gullies affect about 0.5%
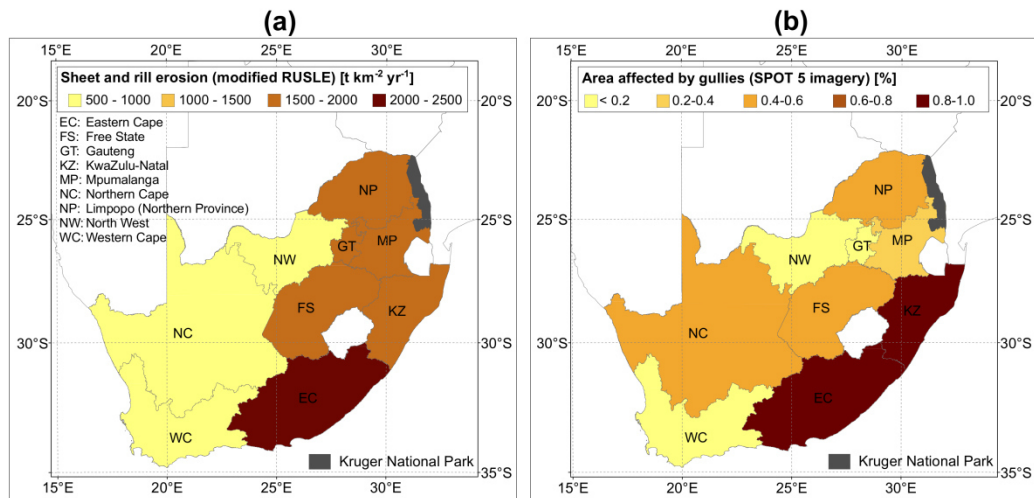
Fig. 1. Soil erosion by water in the nine provinces of South Africa: (a) mean actual sheet and rill erosion predicted based on a modified version of the Revised Universal Soil Loss Equation (RUSLE) (based on data from Le Roux et al., 2008, updated by Msadala et al., 2012); and (b) percentage of area affected by gullies mapped from SPOT 5 satellite imagery acquired between 2005 and 2008 (based on data from Mararakanye and Le Roux, 2012).

of South Africa's land surface. Although these findings might partially reflect the degree to which gully rehabilitation measures were implemented in the respective provinces, they certainly also point to spatial variations in the severity of gully erosion.

Spatial variations in fluvial sediment transport have been demonstrated based on sediment yield data obtained from reservoir siltation surveys and sediment monitoring in rivers (e.g., Msadala et al., 2012). The area-specific sediment yield (*SSY*) is defined as the mass of sediment that passes a (sub-) catchment outlet (e.g., a reservoir inlet or a
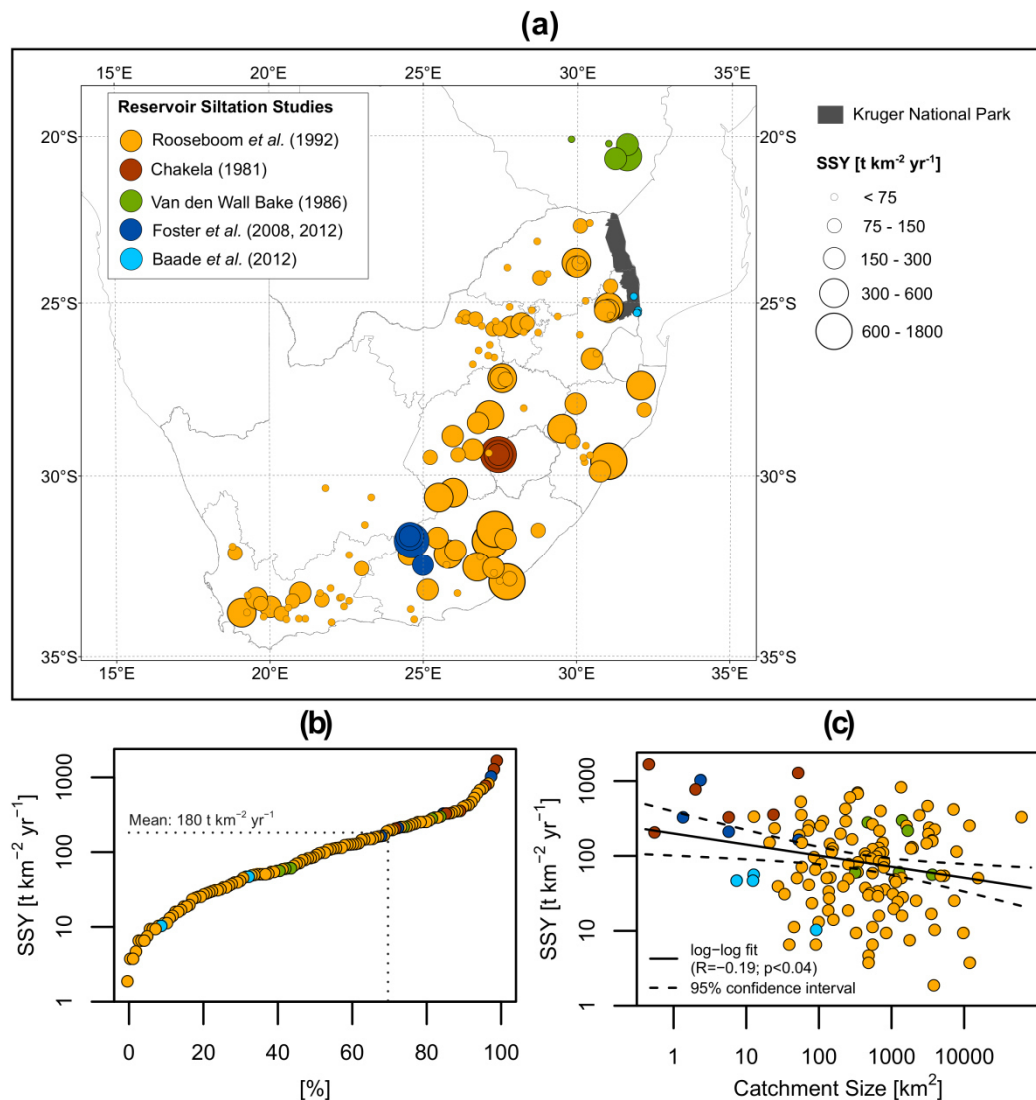
Fig. 2. Mean area-specific sediment yield (SSY) values for observation periods varying from 8 to 100 years derived from reservoir siltation studies in southern Africa (including Lesotho and southern Zimbabwe): (a) overview map with study site locations; (b) cumulative distribution of SSY values; (c) relationship between catchment size and SSY values (based on data from Chakela, 1981; Van den Wall Bake, 1986; Rooseboom et al., 1992; Foster et al., 2008, 2012; Baade et al., 2012).

Tab. 1 Average contemporary area-specific sediment yield values for South Africa (except Kruger National Park, KNP) derived from reservoir siltation studies.

Study	N	T_R [years]	A [km^2]	SSY [t km^{-2} yr^{-1}]
Midgley (1952)[1]	15	na	na	300 ± na
Schwartz and Pullen (1966)	17	20 ± 5	2980	200 ± 125
Rooseboom et al. (1992)	112	30 ± 20	2300	150 ± 30
All reservoir catchments except KNP	116	30 ± 20	2230	150 ± 30

Note: number of investigated reservoirs (N), average time span for which reservoir siltation data is available (T_R; ± 1σ), average catchment size (A), and mean annual area-specific sediment yield (SSY; ± Cl95) obtained from all study sites; 1) cited in Garland et al. (2000).

runoff gauge) per unit of time and catchment size (e.g., Labadz et al., 1991). *SSY* values differ from catchment-wide rates of erosion by water due to the storage and remobilization of sediment in inter-drainage areas and along watercourses (de Vente et al., 2007), but reflect the intensity of off-site effects (Verstraeten et al., 2006). Hence, *SSY* values can be used as 'baseline data' (Trimble and Crosson, 2000, p. 250) to assess the magnitude of catchment-wide rates of erosion by water.

Reservoir siltation studies in southern Africa, particularly the eastern and southern part of South Africa (Rooseboom et al., 1992; Foster et al., 2008, 2012; Msadala et al., 2012; Baade et al., 2012), Lesotho (Chakela, 1981) and southern Zimbabwe (Van den Wall Bake, 1986), revealed *SSY* values ranging from <10 t km^{-2} yr^{-1} to 1800 t km^{-2} yr^{-1} (Fig. 2a) for time intervals (T_R) of 8 to 100 years and catchments varying in size (*A*) from <1 to 68 000 km^2. The distribution of *SSY* values (Fig. 2b) from all study sites (N = 132) is positively skewed which is indicated by a comparatively low median of 90 [60, 130] t km^{-2} yr^{-1} and a higher mean value of 180 ± 50 t km^{-2} yr^{-1} (in the following, uncertainties always correspond to the 95% confidence level, *Cl95*, unless stated otherwise; see Chapter 5 for details). Results from *SSY* assessments carried out for reservoir catchments within the Republic of South Africa only, revealed average *SSY* values in the range of 150 to 300 t km^{-2} yr^{-1} (Tab. 1). The average *SSY* is therefore four to ten times lower than the nation-wide average soil erosion rate (1260 t km^{-2} yr^{-1}) predicted by Le Roux et al. (2008). This points to a considerable net accumulation of recently eroded sediment in the reservoir catchments (de Vente et al., 2007). Sediment storage is relevant especially in large catchments which is indicated by a general trend of decreasing *SSY* with increasing catchment size (Fig. 2c).

2.2 Previously established values of contemporary erosion rates under near-natural conditions and tolerable soil loss in South Africa

Empirical data on contemporary erosion rates under near-natural environmental conditions is unfortunately rather sparse (Tab. 2). Measurements with soil wash traps that were conducted between the 1930s and 1950s on erosion plots next to Pretoria revealed an average soil loss of 25 to 50 t km^{-2} yr^{-1} on near-natural veld, i.e., grass and scrub (Haylett, 1960). This is in accordance to a soil loss of 50 t km^{-2} yr^{-1} for natural veld conditions reported by Mathee (1984, cit. in Hoffman and Ashwell, 2001, p. 85). In

Tab. 2 Overview on contemporary erosion rates measured under near-natural conditions and previously published values on tolerable rates of soil loss in South Africa.

Study	Description	Soil loss [t km^{-2} yr^{-1}]
Contemporary erosion rates under near to natural conditions in South Africa		
Haylett (1960)	average soil loss on experimental plots (length: 27 m) close to Pretoria with near to natural veld (i.e., grass and scrub) and a slope inclination of 4% in the 27yr period from 1931 to 1957	25
Haylett (1960)	average soil loss on experimental plots (length: 27 m) close to Pretoria with near to natural veld (i.e., grass and scrub) and a slope inclination of 7% in the 22yr period from 1936 to 1957	50
Mathee (1984)[1]	average soil loss on experimental plots with near to natural veld conditions (i.e., grass and scrub) and a 5% slope inclination; location and period unknown	50
Venter (1988)	average soil loss on experimental plots with open Acacia savanna (length: 22.13 m; slope inclination: 5 to 11%) in a fenced-off section of the Umfolozi Game Reserve (Hluhluwe-iMfolozi Park, Kwa-Zulu-Natal) with a normal game population (culling operations applied) in a 3 yr monitoring period in the mid-1980s	25
Venter (1988)	average soil loss on experimental plots with open Acacia savanna (length: 22.13 m; slope inclination: 5 to 11%) in sections of the Umfolozi Game Reserve (Hluhluwe-iMfolozi Park, Kwa-Zulu-Natal) with a high game population (no culling operations applied) in a 3 yr monitoring period in the mid-1980s	75
Hoffman and Ashwell (2001)	estimate on natural erosion rates on undisturbed veld and in conservation areas; established from a comprehensive literature review	2 to 75
Estimates on tolerable soil loss in South Africa		
Russell (1983)[2]	average soil loss tolerance for cultivated land in South Africa	1000
Pretorius and Cooks (1989)	soil loss tolerance limits depending on soil thickness (i.e., higher soil loss tolerance with increasing soil thickness)	400 to 2000
Le Roux and Smith (2014)	estimated nation-wide average soil formation rate for South Africa	<500

1) cited in Hoffman and Ashwell (2001, p. 85); 2) cited in Scott et al. (1998, p. 57)

the mid-1980s, Venter (1988) investigated plot scale erosion rates in the Umfolozi Game Reserve (Hluhluwe-iMfolozi Park, KwaZulu-Natal). Average erosion rates in a three years monitoring period amounted to about 25 t km^{-2} yr^{-1} in fenced-off areas where the game population was managed by culling operations, and to 75 t km^{-2} yr^{-1} in non-culling areas with a diminished vegetation cover (ibid.). Based on a comprehensive literature review, Hoffman and Ashwell (2001, p. 85) estimated that erosion rates on natural veld and in conservation areas of South Africa might range between 2 and 75 t km^{-2} yr^{-1}. Mean area-specific sediment yield values (40 to 60 years) established by Baade et al. (2012) for reservoir catchments (8 to 100 km^2; N = 5) in the southern Kruger National Park vary from 10 to 60 t km^{-2} yr^{-1}.

Published values on tolerable rates of soil loss for South Africa are by an order of magnitude higher than empirically derived erosion rates for near-natural conditions (Tab. 2). According to Russell (1983, cit. Scott et al., 1998, p. 57), a soil erosion rate of 1000 t km^{-2} yr^{-1} is tolerable for cultivated land. Pretorius and Cooks (1989) argued that soil erosion rates of 400 t km^{-2} yr^{-1} are acceptable for shallow soils, while a soil loss of up to 2000 t km^{-2} yr^{-1} can be considered tolerable, if soils were sufficiently thick. More recently, Le Roux and Smith (2014) stated that tolerable erosion rates for South Africa are likely <500 t km^{-2} yr^{-1}.

2.3 Long-term average denudation rates in South Africa inferred from cosmogenic nuclides

Long-term average denudation rates (typically for 10^3 to 10^7 years; Darvill, 2013), i.e., the lowering of the landscape by physical erosion and chemical weathering, can been quantified based on in situ-produced cosmogenic nuclides (e.g., ^{10}Be, ^{36}Cl, ^{21}Ne, ^{3}He; Lal, 1991). Primary and secondary cosmic ray particles continuously encounter the Earth surface and trigger spallation processes and muon reactions that lead to the in situ-production of cosmogenic nuclides in minerals (cf. von Blanckenburg, 2006). Since cosmic ray particles quickly loose energy as they penetrate into solid material, production rates are highest on horizontal unshielded surfaces and decrease with increasing depth (Lal, 1991). Comsogenic nuclide concentrations of steadily eroding surfaces rise with exposure time until an equilibrium is reached in which the production and removal of cosmogenic nuclides are balanced (Darvill, 2013). In the absence of

bioturbation and other disturbance, stable nuclides (e.g., ^{21}Ne, ^{3}He) are removed solely by denudation (i.e., physical erosion and chemical weathering), while an additional loss by radioactive decay is to be taken into account for radionuclides (e.g., ^{10}Be, ^{36}Cl).

For surfaces that are steadily lowered by denudation, the surface concentration of cosmogenic nuclides behaves inversely proportional to the denudation rate (Lal, 1991). Assuming steady state erosion, long-term average rates can be established when factors influencing the cosmic ray intensity (e.g., sampling location, shielding effects), properties of the sampled material (e.g., density, absorption coefficient of the host mineral), and characteristics of the investigated nuclides (e.g., decay rate) are taken into account (e.g., Heimsath et al., 2001). Spatially averaged long-term denudation rates for catchments can be determined from cosmogenic nuclide concentrations in river sediment samples (Granger et al., 1996). Here, it must be assumed that sediment mixing leads to an adequate representation of spatially variable denudation rates (von Blanckenburg, 2006). Denudation rates may be overrated when the river sediments contain subsurface material that was mobilized by gully or bank erosion (Glotzbach et al., 2016).

Investigations on cosmogenic nuclide concentrations in South Africa have been carried out along the southern Cape coast (Scharf et al., 2013; Bierman et al., 2014), in the vicinity of the Great Escarpment (Fleming et al., 1999; Kounov et al., 2007; Decker et al., 2011; Keen-Zebert et al., 2016), in the interior of South Africa (Kounov et al., 2007; Dirks et al., 2010, 2016; Decker et al., 2011, 2013; Keen-Zebert et al., 2016) and within the Kruger National Park (Chadwick et al., 2013; Glotzbach et al., 2016). These studies reveal generally low long-term average denudation rates on both sides of the Great Escarpment (Fig. 3a). Excluding samples from erosion scarps and river valleys, the mean value for rock outcrops and topsoils (Fig. 3b) amounts to $(7 \pm 5) \times 10^{-6}$ m yr^{-1} (N = 21). Values of up to 60×10^{-6} m yr^{-1} (Fleming et al., 1999) and 255×10^{-6} m yr^{-1} (Keen-Zebert et al., 2016) were determined for erosion scarps and river valleys, respectively (not shown in Figures 3a and 3b). The mean value of spatially averaged long-term denudation rates obtained from river sediments (Fig. 3c) amounts to $(4.5 \pm 0.4) \times 10^{-6}$ m yr^{-1} (N = 61). About 80% of the sampled rock outcrops and topsoils (excluding erosion scarps and river valleys), and 97% of the river sediment samples reveal a long-term average denudation rate of $\leq 8 \times 10^{-6}$ m yr^{-1}. Assuming a mean rock density of about 2.7 g cm^{-3} (e.g., Decker et al., 2011; Glotzbach et al., 2016), this corresponds to a long-term average denudation rate of ≤ 20 t km^{-2} yr^{-1}. These low rates

point to weathering resistant rocks and tectonic stability in southern Africa throughout the Quaternary (Decker et al., 2013; Scharf et al., 2013).
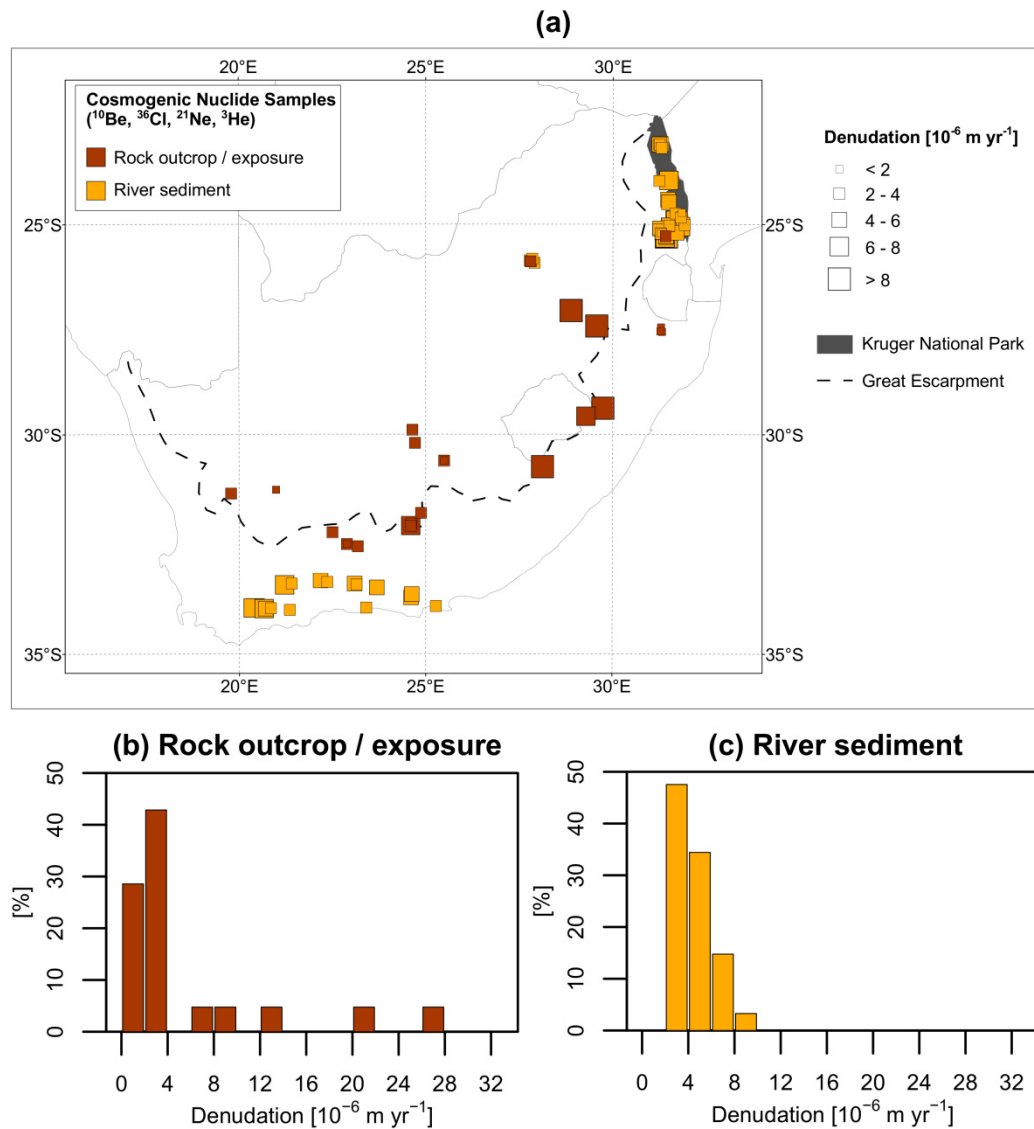
Fig. 3. Long-term average denudation rates (>10^4 years) in South Africa obtained from in situ-produced cosmogenic nuclide concentrations: (a) sampling sites; (b) distribution of long-term average denudation rates obtained from rock outcrops and exposures (N = 21) excluding samples from erosion scarps and river valleys; (c) distribution of long-term average denudation rates obtained from river sediments (N = 61) (based on data from Fleming et al., 1999; Kounov et al., 2007, 2013; Dirks et al., 2010, 2016; Decker et al., 2011; Chadwick et al., 2013; Scharf et al., 2013; Bierman et al., 2014; Glotzbach et al., 2016; Keen-Zebert et al., 2016)

References

Baade, J., Franz, S., Reichel, A., 2012. Reservoir siltation and sediment yield in the Kruger National Park, South Africa: a first assessment. Land Degradation and Development 23 (6), 586-600. DOI: 10.1002/ldr.2173.

Beinart, W., 1984. Soil erosion, conservationism and ideas about development: a southern African exploration, 1900-1960. Journal of Southern African Studies 11 (1), 52-83. DOI: 10.1080/03057078408708088.

Bierman, P.R., Coppersmith, R., Nevelling, J., Portenga, E.W., Rood, D.H., 2014. A cosmogenic view of erosion, relief generation, and the age of faulting in southern Africa. GSA Today 24 (9), 4-11. DOI: 10.1130/GSATG206A.1.

Boardman, J., Favis-Mortlock, D., Foster, I., 2015. A 13-year record of erosion on badland sites in the Karoo, South Africa. Earth Surface Processes and Landforms 40 (14), 1964-1981. DOI: 10.1002/esp.3775.

Breetzke, G.D., Koomen, E., Critchley, W.R.S., 2013. GIS-assisted modelling of soil erosion in a South African catchment. Evaluating the USLE and SLEMSA approach. In: Wurbs, R. (Ed.). Water resources planning, development and management. InTech: Rijeka, Croatia, pp. 53-71. DOI: 10.5772/52314.

Chadwick, O.A., Roering, J.J., Heimsath, A.M., Levick, S.R., Asner, G.P., Khomo, L., 2013. Shaping post-orogenic landscapes by climate and chemical weathering. Geology 41 (11), 1171-1174. DOI: 10.1130/G34721.1.

Chakela, Q.K., 1981. Soil erosion and reservoir sedimentation in Lesotho. Scandinavian Institute of African Studies: Uppsala, Sweden, 150 pp.

Darvill, C.M., 2013. Cosmogenic nuclide analysis (chapter 4.2.10). In: Clarke, L.E., Nield, J.M., (Eds.). Geomorphological Techniques (Online Edition). British Society of Geomorphology: London, United Kingdom, 25 pp. <http://geomorphology.org.uk/geomorph_techniques> accessed 03 October 2017 (last modified: 2013).

Decker, J.E., Niedermann, S., de Wit, M.J., 2011. Soil erosion rates in South Africa compared with cosmogenic ^{3}He-based rates of soil production. South African Journal of Geology 114 (3-4), 475-488. DOI: 10.2113/gssajg.114.3-4.475.

Decker, J.E., Niedermann, S., de Wit, M.J., 2013. Climatically influenced denudation rates of the southern African plateau: clues to solving a geomorphic paradox. Geomorphology 190, 48-60. DOI: 10.1016/j.geomorph.2013.02.007.

de Vente, J., Poesen, J., Arabkhedri, M., Verstraeten, G., 2007. The sediment delivery problem revisited. Progress in Physical Geography 31 (2), 155-178. DOI: 10.1177/0309133307076485.

Dirks, P.H.G.M., Kibii, J.M., Kuhn, B.F., Steininger, C., Churchill, S.E., Kramers, J.D., Pickering, R., Farber, D.L., Mériaux, A.S., Herries, A.I.R., King, G.C.P., Berger, L.R., 2010. Geological setting and age of Australopithecus sediba from Southern Africa. Science 328, 205-208. DOI: 10.1126/science.1184950.

Dirks, P.H.G.M., Placzek, C.J., Fink, D., Dosseto, A., Roberts, E., 2016. Using ^{10}Be cosmogenic isotopes to estimate erosion rates and landscape changes during the Plio-Pleistocene in the Cradle of Humankind, South Africa. Journal of Human Evolution 96, 19-34. DOI: 10.1016/j.jhevol.2016.03.002.

Dlamini, P., Orchard, C., Jewitt, G., Lorentz, S., Titshall, L., Chaplot, V., 2011. Controlling factors of sheet erosion under degraded grasslands in the sloping lands of KwaZulu-Natal, South Africa. Agricultural Water Management 98, 1711-1718. DOI: 10.1016/j.agwat.2010.07.016.

Dodson, B., 2005. A soil conservation safari: Hugh Bennett's 1944 visit to South Africa. Environment and History 11 (1), 35-53. DOI: 10.3197/0967340053306176.

Fleming, A., Summerfield, M.A., Stone, J.O., Fifield, L.K., Cresswell, R.G., 1999. Denudation rates for the southern Drakensberg escarpment, SE Africa, derived from in-situ-produced cosmogenic ^{36}Cl: initial results. Journal of the Geological Society 156, 209-212. DOI: 10.1144/gsjgs.156.2.0209.

Flügel, W.-A., Märker, M., Moretti, S., Rodolfi, G., Sidrochuk, A., 2003. Integrating geographical information systems, remote sensing, ground truthing and modelling approaches for regional erosion classification of semi-arid catchments in South Africa. Hydrological Processes 17 (5), 929-942. DOI: 10.1002/hyp.1171.

Foster, I.D.L., Boardman, J., Keay-Bright, J., 2007. Sediment tracing and environmental history for two small catchments, Karoo Uplands, South Africa. Geomorphology 90 (1-2), 126-143. DOI: 10.1016/j.geomorph.2007.01.011.

Foster, I.D.L., Boardman, J., Gates, J.B., 2008. Reconstructing historical sediment yields from the infilling of farm reservoirs, Eastern Cape, South Africa. In: Schmidt, J., Cochrane, T., Phillips, C., Elliott, S., Davies, T., Basher, L. (Eds.). Sediment Dynamics in Changing Environments (Proceedings of a symposium held in Christchurch, New Zealand, December 2008). IAHS Publications 325. International Association of Hydrological Sciences (IAHS) Press: Wallingford, United Kingdom, pp. 440-447.

Foster, I.D.L., Rowntree, K.M., Boardman, J., Mighall, T.M., 2012. Changing sediment yield and sediment dynamics in the Karoo uplands, South Africa; post-European impacts. Land Degradation and Development 23 (6), 508-522. DOI: 10.1002/ldr.2180.

Foster, I.D.L., Boardman, J., Collins, A.L., Copeland-Phillips, R., Kuhn, N.J., Mighall, T.M., Pulley, S., Rowntree, K.M., 2017. The potential of gamma-emitting radionuclides to contribute to an understanding of erosion processes in South Africa. In: Collins, A., Stone, M., Horowitz, A., Foster, I. (Eds.). Integrating monitoring and modelling for understanding, predicting and managing sediment dynamics. IAHS Publications 375. International Association of Hydrological Sciences (IAHS): Wallingford, United Kingdom, pp. 29-34.

Garland, G., 1982. An appraisal of South African research into runoff erosion. South African Geographical Journal 64 (2), 138-143. DOI: 10.1080/03736245.1982.10559663.

Garland, G., Hoffman, T., Todd, S., 2000. Soil degradation in South Africa: an overview. In: Hoffman, T., Todd, S., Ntshona, Z., Turner, S. (Eds). Land degradation in South Africa. Department of Environmental Affairs (DEA): Pretoria, South Africa, pp. 69-107.

Glotzbach, C., Paape, A., Baade, J., Reinwarth, B., Rowntree, K., Miller, J., 2016. Cenozoic landscape evolution of the Kruger National Park as derived from cosmogenic nuclide analyses. Terra Nova 28 (5), 316-322. DOI: 10.1111/ter.12223.

Granger, D.E., Kirchner, J.W., Finkel, R., 1996. Spatially averaged long-term erosion rates measured from in situ-produced cosmogenic nuclides in alluvial sediment. The Journal of Geology 104 (3), 249-257. DOI: 10.1086/629823.

Haviland, P.H., 1929. Soil erosion. The Rhodesia Agricultural Journal 26 (2), 128-136.

Haylett, D.G., 1960. Run-off and soil erosion studies at Pretoria. South African Journal of Agricultural Science 3 (3), 379-394.

Heimsath, A.M., Chappell, J., Dietrich, W.E., Nishiizumi, K., Finkel, R.C., 2001. Late Quaternary erosion in southeastern Australia: a field example using cosmogenic nuclides. Quaternary International 83-85, 169-185. DOI: 10.1016/S1040-6182(01)00038-6.

Hoffman, T., Ashwell, A., 2001. Nature divided. Land degradation in South Africa. University of Cape Town Press: Lansdowne, Cape Town, South Africa, 168 pp.

Jacks, G.V., Whyte, R.O., 1939. The rape of the earth. A world survey of soil erosion. Faber and Faber Ltd.: London, United Kingdom, 312 pp.

Jennings, A.C., 1923. Soil Washing, or the surface erosion of cultivated land. The Rhodesia Agricultural Journal 20 (6), 647-651.

Kaey-Bright, J., Boardman, J., 2009. Evidence from field-based studies of rates of soil erosion on degraded land in the central Karoo, South Africa. Geomorphology 103, 455-465. DOI: 10.1016/j.geomorph.2008.07.011.

Kakembo, V., Xanga, W.W., Rowntree, K. 2009. Topographic thresholds in gully development on the hillslopes of communal areas in Ngqushwa Local Municipality, Eastern Cape, South Africa. Geomorphology 110 (3-4), 188-194. DOI: 10.1016/j.geomorph.2009.04.006.

Keen-Zebert, A., Tooth, S., Stuart, F.M., 2016. Cosmogenic ^{3}He measurements provide insight into lithologic controls on bedrock incision: examples from the South African interior. The Journal of Geology 124 (3), 423-434. DOI: 10.1086/685506.

Kounov, A., Niedermann, S., de Wit, M.J., Viola, G., Andreoli, M., Erzinger, J., 2007. Present denudation rates at selected sections of the South African escarpment and the elevated continental interior based on cosmogenic ^{3}He and ^{21}Ne. South African Journal of Geology 110 (2-3), 235-248. DOI: 10.2113/gssajg.110.2-3.235.

Kounov, A., Viola, G., Dunkl, I., Frimmel, H.E., 2013. Southern African perspectives on the long-term morpho-tectonic evolution of cratonic interiors. Tectonophysics 601, 177-191. DOI: 10.1016/j.tecto.2013.05.009.

Labadz, J.C., Burt, T.P., Potter, A.W.R., 1991. Sediment yield and delivery in the blanket peat moorlands of the southern Pennines. Earth Surface Processes and Landforms 16, 255-271. DOI: 10.1002/esp.3290160306.

Laker, M.C., 2004. Advances in soil erosion, soil conservation, land suitability evaluation and land use planning research in South Africa, 1978-2003. South African Journal of Plant and Soil 21 (5): 345-368. DOI: 10.1080/02571862.2004.10635069.

Lal, D., 1991. Cosmic ray labeling of erosion surfaces: in situ nuclide production rates and erosion models. Earth and Planetary Science Letters 104 (2-4), 424-439. DOI: 10.1016/0012-821X(91)90220-C.

Le Roux, J.J., in press. Sediment yield potential in South Africa's only large river network without a dam: implications for water resource management. Land Degradation and Development. DOI: 10.1002/ldr.2753.

Le Roux, J.J., Smith, H., 2014. Soil erosion in South Africa – its nature and distribution. <http://www.grainsa.co.za/soil-erosion-in-south-africa---its-nature-and-distribution> accessed 19 August 2017 (last modified: 2014-11-01).

Le Roux, J.J., Morgenthal, T.L., Malherbe, J., Pretorius, D.J., Sumner, P.D., 2008. Water erosion prediction at a national scale for South Africa. Water SA 34 (3), 305-314.

Le Roux, J.S., Roos, Z.N., 1982. Surface wash on a low-angled slope near Bloemfontein. South African Geographical Journal 64 (2), 114-124. DOI: 10.1080/03736245.1982.10559661.

Mararakanye, N., Le Roux, J.J., 2012. Gully location mapping at a national scale for South Africa. South African Geographical Journal 94 (2), 208-218. DOI: 10.1080/03736245.2012.742786.

Mararakanye, N., Sumner, P.D., 2017. Gully erosion: a comparison of contributing factors in two catchments in South Africa. Geomorphology 288, 99-110. DOI: 10.1016/j.geomorph.2017.03.029.

Mathee, J.F. la G., 1984. A primer on soil conservation. National Department of Agriculture: Pretoria, South Africa, 128 pp.

Midgley, D.C., 1952. A preliminary survey of the surface water resources of the Union of South Africa (unpublished PhD thesis). University of Natal: Pietermaritzburg, South Africa.

Msadala, V., Gibson, L., Le Roux, J., Rooseboom, A., Basson, G.R., 2012. Sediment yield prediction for South Africa: 2010 edition. WRC Report No. 1765/1/10. Water Research Commission (WRC): Pretoria, South Africa, 250 pp.

Pretorius, J.R., Cooks, J., 1989. Soil loss tolerance limits: an environmental management tool. GeoJournal 19 (1), 67-75.

Renard, K.G., Foster, G.R., Weesies, G.A., Porter, J.P., 1991. RUSLE. Revised Universal Soil Loss Equation. Journal of Soil and Water Conservation 46 (1), 30-33.

Roe, W., 1897. Fruit culture. Thoughts on Orange culture. Agricultural Journal of the Cape of Good Hope 11 (11), 639-643.

Rooseboom, A., von M. Harmse, H.J., 1979. Changes in the sediment load of the Orange River during the period 1929-1969. In: IAHS (Ed.). The hydrology of areas of low precipitation (Proceedings of the Canberra Symposium, December 1979). IAHS Publications 128. International Association of Hydrological Sciences (IAHS): Wallingford, United Kingdom, pp. 459-470.

Rooseboom, A., Verster, E., Zietsman, H.L., Lotriet, H.H., 1992. The development of the new sediment yield map of southern Africa. WRC Report No. 297/2/92. Water Research Commission (WRC): Pretoria, South Africa, 117 pp.

Rowntree, K.M., 2013. The evil of sluits: a re-assessment of soil erosion in the Karoo of South Africa as portrayed in century-old sources. Journal of Environmental Management 130, 98-105. DOI: 10.1016/j.jenvman.2013.08.041.

Rowntree, K.M., Ntsaba, M.M., van B. Weaver, A., 1991. Changing patterns of erosion in a peri-urban catchment, Maseru, Lesotho. In: Peters, N.E., Walling, D.E. (Eds.). Snow, hydrology and forests in high alpine areas (Proceedings of the Vienna Symposium 1991). IAHS Publications 203. International Association of Hydrological Sciences (IAHS): Wallingford, United Kingdom, pp. 93-102.

Russell, W.B., 1983. Conservation of arable land in the USA: report on service tour, unpublished report. Department of Agriculture and Fisheries, Natal Region: Cedara, South Africa.

Scharf, T.E., Codilean, A.T, de Wit, M., Jansen, J.D., Kubik, P.W., 2013. Strong rock sustain ancient postorogenic topography in southern Africa. Geology 41 (3), 331-334. DOI: 10.1130/G33806.1.

Schulze, R.E., 1979. Soil loss in the key area of the Drakensberg. A regional application of the Soil Loss Estimation Model for Southern Africa (SLEMSA). In: Schulze, R.E. (Ed.). Hydrology and Water Resources of the Drakensberg. Natal Town and Regional Planning Reports 42. Natal Town and Regional Planning Commission: Pietermaritzburg, South Africa, pp. 149-167.

Schulze, R.E., Lorentz, S.A., Horan, M.J.C., Maharaj, M., 2007. Sediment yield. In: Schulze, R.E. (Ed.). South African Atlas of Climatology and Agrohydrology. WRC Report 1489/1/06, Section 21.7. Water Research Commission (WRC): Pretoria, South Africa, 5 pp.

Schwartz, H.I., Pullen, R.A., 1966. A guide to the estimation of sediment yield in South Africa. Transactions of the South African Institution of Civil Engineers 8, 343-346.

Scott, D.F., Versfeld, D.B., Lesch, W., 1998. Erosion and sediment yield in relation to afforestation and fire in the mountains of the Western Cape Province, South Africa. South African Geographical Journal 80 (1): 52-59. DOI: 10.1080/03736245.1998.9713644.

Shaw, J., 1874. On the changes going on in the vegetation of South Africa through the introduction of the Merino sheep. Botanical Journal of the Linnean Society of London 14 (75), 202-208. DOI: 10.1111/j.1095-8339.1874.tb00312.x.

Stringer, L.C., Reed, M.S., 2007. Land degradation assessment in southern Africa: integrating local and scientific knowledge bases. Land Degradation and Development 18 (1), 99-116. DOI: 10.1002/ldr.760.

Talbot, W.J., 1947. Swartland and Sandveld. A survey of land utilization and soil erosion in the western lowland of the Cape Province. Oxford University Press: London, United Kingdom, 79 pp.

Trimble, S.W., Crosson, P., 2000. U.S. Soil erosion rates: myth and reality. Science 289 (5477), 248-250. DOI: 10.1126/science.289.5477.248.

Van den Wall Bake, G.W., 1986. Siltation and soil erosion survey in Zimbabwe. In: Hadley, R.F. (Ed.). Drainage Basin Sediment Delivery, Proceedings of a symposium held at Albuquerque, August 1986. IAHS Publications 159. International Association of Hydrological Sciences (IAHS) Press: Wallingford, United Kingdom, pp. 69-80.

Venter, J., 1988. Soil loss and run-off in Umfolozi Game Reserve and the implications for game reserve management. Volume 1. PhD Thesis. Department of Grassland Science, Faculty of Agriculture, University of Natal: Pietermaritzburg, South Africa, 192 pp.

Verstraeten, G., Bazzoffi, P., Lajczak, A, Rãdoane, M., Rey, F., Poesen, J., de Vente, J., 2006. Reservoir and pond sedimentation in Europe. In: Boardman, J., Poesen, J. (Eds.). Soil erosion in Europe. Wiley & Sons: Chichester, United Kingdom, pp. 757-774. DOI: 10.1002/0470859202.ch54.

von Blanckenburg, F., 2006. The control mechanisms of erosion and weathering at basin scale from cosmogenic nuclides in river sediment. Earth and Planetary Science Letters 242 (3-4), 224-239. DOI: 10.1016/j.epsl.2005.11.017.

Walling, D.E., He, Q., Appleby, P.G., 2003. Conversion models for use in soil-erosion, soil-redistribution and sedimentation investigations. In: Zapata, F. (Ed.). Handbook for the assessment of soil erosion and sedimentation using environmental radionuclides. Kluwer: Dordrecht, The Netherlands, pp. 111-164.

Wentzel, K., 2002. Determination of the overall soil erosion potential in the Nsikazi District (Mpumalanga Province, South Africa) using remote sensing and GIS. Canadian Journal of Remote Sensing 28 (2), 322-327. DOI: 10.5589/m02-013.

Wessels, K.J., Prince, S.D., Malherbe, J., Small, J., Frost, P.E., Van Zyl D., 2007. Can human-induced land degradation be distinguished from the effects of rainfall variability? A case study in South Africa. Journal of Arid Environments 68, 271-297. DOI: 10.1016/j.jaridenv.2006.05.015.

Chapter 3

Applying regularized logistic regression (RLR) for the discrimination of sediment facies in reservoirs based on composite fingerprints

Authors: Bastian Reinwarth • Jordan K. Miller • Christoph Glotzbach •
Kate M. Rowntree • Jussi Baade

Electronic supplementary material may be found in the appendix of this thesis.

CrossMark

SEDIMENTS, SEC 3 • HILLSLOPE AND RIVER BASIN SEDIMENT DYNAMICS • RESEARCH ARTICLE

Applying regularized logistic regression (RLR) for the discrimination of sediment facies in reservoirs based on composite fingerprints

Bastian Reinwarth[1] · Jordan K. Miller[2] · Christoph Glotzbach[3] · Kate M. Rowntree[2] ·
Jussi Baade[1]

Abstract

Purpose Soils and sediments can be distinguished based on "composite fingerprints", i.e., sets of physical and chemical properties that are suitable for discrimination. At present, statistical stepwise variable selection methods are frequently applied to identify composite fingerprints, although they have been seriously criticized. Here, we test regularized logistic regression (RLR) as an alternative approach in the context of a reservoir siltation study where the post-dam facies is to be distinguished from the pre-dam facies.

Materials and methods The pre- and post-dam facies of four reservoirs located in the Kruger National Park were examined with respect to grain size composition, color, and content of calcium-lactate leachable phosphorus (P_{CAL}). A composite fingerprint was identified applying RLR to training data. The fitted regression model was used for the classification of samples not involved in the training dataset. For comparison, variable selection was performed with stepwise discriminant function analysis (DFA) and samples were classified by applying linear discriminant analysis (LDA). Both approaches were validated by comparing field interpretation and classification results. The analysis was extended based on Monte Carlo simulations and synthetic datasets to quantify uncertainties and to enhance the method comparison.

Results and discussion RLR and stepwise DFA identify grain size parameters and P_{CAL} content to be particularly useful for the facies discrimination. Neglecting and taking into account a potential sampling bias, both approaches lead to ≤3 and 5% misclassifications, respectively. RLR outperforms stepwise DFA/LDA in Monte Carlo simulations, although misclassification rates do not significantly differ ($p = 0.84$). RLR uses on average 12% less fingerprint properties. Moreover, RLR-derived probabilities of group membership represent a more reliable measure for classification conclusiveness than probabilities calculated from LDA, which is evident in significantly lower ($p < 0.001$) probability residuals for misclassified samples. Stepwise DFA/LDA reveals lower misclassification rates than RLR when data fulfill multivariate normality in each group and equal within-group covariance matrices.

Conclusions RLR is an innovative tool for the discrimination of sediment facies in reservoirs and, more generally, for studies requiring the discrimination of soils and sediments. Although stepwise procedures will in practice often perform similarly well, we discourage their use for the identification of composite fingerprints due to the risk of suboptimal variable selection involving variables with spurious discriminatory power.

Responsible editor: Hugh Smith

✉ Bastian Reinwarth
 bastian.reinwarth@uni-jena.de

1 Department of Geography, Friedrich Schiller University, Löbdergraben 32, 07743 Jena, Germany

2 Geography Department, Rhodes University, P.O. Box 94, Grahamstown 6140, South Africa

3 Department of Geosciences, University of Tübingen, Wilhelmstraße 63, 72074 Tübingen, Germany

⬤ Springer

1 Introduction

Physical and chemical properties have been used for a long time in combination with multivariate statistical techniques for the discrimination of soils and sediments (Birks 1987). The selection of suitable properties is a crucial step and should involve expert knowledge and rigorous statistical analysis (Kraushaar et al. 2015). Sediment properties that do not significantly differ between investigated soil and sediment types should be eliminated, since they introduce noise into the dataset which may affect classification results (Tibshirani 1996). The remaining properties should constitute a "composite fingerprint" (Collins and Walling 2002), i.e., a subset of sediment properties that enables optimal discrimination between the investigated soil and sediment types (Walling and Woodward 1995). Statistical variable selection methods are commonly employed to identify composite fingerprints and to verify their discriminatory power (Collins and Walling 2002).

Among a variety of available variable selection methods (see Collins et al. 2012), a two-step procedure including a non-parametric pre-test and stepwise discriminant function analysis (DFA) is at present most frequently applied in fingerprinting studies (e.g., Miller et al. 2015; Pulley et al. 2015; Pulley and Rowntree 2016). However, stepwise DFA (Huberty 1989; Thompson 1989, 1995; Whitaker 1997), and stepwise variable selection algorithms in general (e.g., Harrell 2001; Whittingham et al. 2006; Flom and Cassell 2007), have been seriously criticized. Perhaps most importantly, stepwise methods represent so-called "greedy algorithms" (Cormen et al. 2001) that iteratively enhance preliminary solutions based on heuristic principles. Although these algorithms perform satisfactorily in many cases, they often fail to produce "optimal" results as the set of potential solutions in a particular stage is confined by preliminary solutions of previous steps (Huberty 1994). Moreover, stepwise DFA based on Wilks' lambda is founded on the assumption of input data with multivariate normality in each group and equal within-group covariance matrices (Tabachnick and Fidell 2001). Although the method is reasonably robust against "mild" violations (Hastie et al. 1995) of this assumption, strong violations can negatively impact variable selection and classification results. Therefore, several authors have raised the need to explore alternative statistical approaches (e.g., Collins et al. 2012; Walling 2013).

Here, we explore the potential of regularized logistic regression (RLR) for the identification of composite fingerprints in the context of a reservoir siltation study where the post-dam facies (i.e., reservoir deposits) is to be distinguished from the pre-dam facies (i.e., fluvial sediments and soils). RLR belongs to a family of machine learning algorithms referred to as shrinkage methods (Simpson and Birks 2012) and is specifically designed for variable selection (Zou and Hastie 2005). A

further advantage is that RLR does not rely on multivariate normality and equal within-group covariance matrices (Tabachnick and Fidell 2001).

The aim of this study is twofold: (i) the identification of sediment properties that are suitable for the discrimination between the pre- and post-dam facies and (ii) the assessment of the performance of the RLR approach compared to variable selection with stepwise DFA and subsequent classification based on (predictive) linear discriminant analysis (LDA). Both approaches are applied on an empirical dataset acquired from four reservoirs in the Kruger National Park (South Africa). Results are validated by comparing field interpretation and classification results for samples with unambiguous group affiliation. Synthetic datasets resembling the structure of the empirical data are generated and employed within the framework of Monte Carlo simulations to quantify uncertainties in variable selection and classification results arising from a potential sampling bias. Additional synthetic datasets with normally distributed sediment properties in each group and equal within-group covariance matrices are generated to enhance the method comparison. Merits and drawbacks of RLR and stepwise DFA and the potential of the RLR approach for facies discrimination in reservoirs are discussed.

2 Materials and methods

2.1 Study area and site descriptions

The Kruger National Park (KNP) is located in the northeast of the Republic of South Africa (Fig. 1a). It belongs to the tectonically stable "Lowveld" geomorphic province (Partridge et al. 2010) between the Great Escarpment to the west and the coastal plains of Mozambique to the east. Low erosion rates ($<10^{-2}$ mm yr^{-1}) in this region were largely compensated by isostatic uplift throughout the Cenozoic era (Glotzbach et al. 2016). The KNP is characterized by an undulating relief with altitudes ranging from 150 to 840 m asl (MacFayden et al. 2016) and a main drainage direction towards the east. Mean annual precipitation varies between 400 and 700 mm with most of the rainfall and resulting runoff occurring between October and April (Gertenbach 1980). Major geological units strike from north to south (Fig. 1b), with intrusive rocks in the west and volcanic rocks in the east separated by a narrow stretch of sedimentary rocks (Viljoen 2015). The KNP hosts various subtypes of savanna vegetation that largely coincide with lithological and climatic conditions (Venter et al. 2003), including shrubland, bushveld, grassland, and tree savanna (Mucina and Rutherford 2010).

More than 50 small reservoirs were established in the KNP prior to 1975 to ensure water provision for wildlife (Pienaar 1985). In wet years, reservoirs in the KNP are inhabited (e.g., hippopotamus, crocodiles) and regularly frequented by other

Chapter 3

Fig. 1 Location of the Kruger National Park **a** within South Africa and **b** study sites (reservoir catchments) in the southern Kruger National Park. Major geological units are shown according to Petersen (2012), modified after Geological Survey of South Africa (1986a, b)
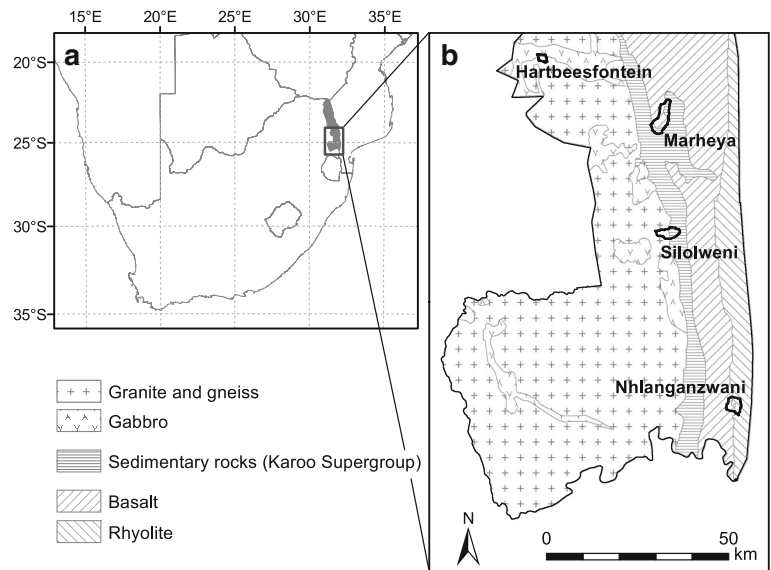
animals (e.g., elephants, buffalos, antelopes, birds), partially inducing eutrophication. The reservoirs impound intermittent surface runoff and trap sediment that is transported along thalwegs. The accumulation of reservoir deposits is restricted to the deepest parts of the reservoir basins (Fig. 2), while bedload from tributaries is deposited in backwater reaches close to tributary inlets. A reconnaissance survey (Baade et al. 2012) demonstrated that the post-dam facies of reservoirs in the KNP typically consist of strongly cracked, blackish fine-grained sediments that can be distinguished from the underlying pre-dam facies exhibiting brighter color and coarser texture.

This study is based on samples from four small reservoirs, the Hartbeesfontein, Marheya, Silolweni, and Nhlanganzwani reservoirs, located in the southern KNP (Fig. 1b). They were established between 1950 and 1970 in thalwegs of intermittent channels (Pienaar 1985). Their surface area ranges from 3 to 16 ha and present-day water storage capacity from 30 to 260×10^3 m³ (Table 1). The four study sites provide a representative cross section through the main geological units of the southern KNP (Fig. 1b). Granite, gneiss, and sedimentary rocks in the Hartbeesfontein, Silolweni, and Marheya reservoir catchments (Table 1) are associated with arenosols (according to FAO 2014); solonetzes are common on footslopes (Venter et al. 2003; van Zijl and Le Roux 2014). The upper part of the Hartbeesfontein reservoir catchment is underlain by gabbro that weathers to vertisols, phaeozems, and leptosols (Venter 1990; Fey et al. 2010). About half of the Marheya and Nhlanganzwani reservoir catchments are characterized by basalt and fine-textured luvisols, nitisols, and phaeozems (Venter 1990; Mills and Fey 2004). Vertisols are frequently found at footslopes and valley bottoms. Weathering-resistant rhyolites and dacites in the eastern part

of the Nhlanganzwani reservoir catchment coincide with leptosols (Venter 1990; Table 1).

2.2 Field surveys and sampling

Field work was carried out in 2014 and 2015 and involved a survey of the (dry) reservoir basins, including volumetric mapping and sampling of reservoir deposits. Sample locations were surveyed using Leica GS 10 GS 15 GNSS receivers in real-time kinematic mode (RTK) as described by Baade and Schmullius (2016). Identification of the pre- and post-dam facies was based on color, structural fabric, and grain size (Tucker 2011). Volumetric mapping was based on 30 to 60 depth soundings along multiple transects ($N \geq 9$ at each site) running approximately parallel to the dam crest using Pürckhauer and gouge augers (length up to 3.4 m).

Post-dam facies samples were acquired along the transects using 100 cm³ core rings at the surface (0–5 cm depth). A sample ring kit and a liner sampler (Eijkelkamp) were used for vertical profiles (up to 265 cm depth), and additional post-dam facies material was collected from augers. Samples of the pre-dam facies were mainly acquired from soils and deposits underlying the post-dam facies. In addition, sediments in riverbeds and soils exposed at river banks upstream and downstream of the reservoirs were examined to further characterize the pre-dam facies. When the affiliation of a sediment sample was not obvious from field observations, it was ascribed to the group "unclear".

The overarching aim of the project under which the sampling was undertaken is the assessment and physical and chemical characterization of reservoir siltation (i.e., the post-dam facies). Thus, more samples were collected from the post-dam facies than from the pre-dam facies (Table 2). The

Chapter 3

Fig. 2 The dried-out Hartbeesfontein reservoir in October 2015. Blackish reservoir deposits representing the post-dam facies are largely restricted to the deepest parts of the reservoir basin and can be easily distinguished from brighter adjacent soils belonging to the pre-dam facies. The width of the reservoir deposits at the dam (*left*) is about 70 m

proportion of subsurface samples (5–265 cm depth) of the total number of samples collected from the post-dam facies ranges from 38% (Marheya reservoir) to 64% (Nhlanganzwani reservoir). Local sandy delta-like deposits clearly distinct from fine-grained blackish reservoir deposits were observed close to tributary inlets. However, taking into account the limited number of samples from these deposits ($N = 8$), and the sensitivity of logistic regression and discriminant analysis to outliers (Tabachnick and Fidell 2001), samples representing delta-like sediments were excluded from the analysis. In total, 49 and 166 samples from the pre- and post-dam facies, respectively, and 35 samples with unclear class affiliation, were collected (total $N = 250$). A kmz file showing the sample locations ($N = 117$) has been included as Electronic Supplementary Material in the online version of this article (Online Resource 1).

2.3 Laboratory analysis

Laboratory analysis focused on properties that differ markedly between the pre- and post-dam facies, i.e., color, phosphorus content, and grain size composition (Baade et al. 2012). A Munsell Soil Color Chart was used to determine the color of moist and rubbed bulk sediment. Munsell colors were converted to RGB color space (Beaudette et al. 2013), and the

luminance (LUM), represented in discrete values ranging from 0 (black) to 255 (white), was calculated according to Russ and Russ (2008). Calcium-lactate leachable phosphorous (P_{CAL}) was extracted from 5 g aliquots following Schüller (1969). P_{CAL} content was quantified with the modified molybdenum blue method (Murphy and Riley 1962), measuring the extinction at 700 nm wavelength with an UV/VIS spectrophotometer (Shimadzu UV-2401 PC).

Particle size distribution (PSD) was determined by sieving (2 and 1 mm meshes) and laser diffraction analysis. Grain size analysis on the ≤1 mm fraction was carried out with a Beckman Coulter LS 13320 following pre-treatment with hydrogen peroxide (H_2O_2; 10 and 30%) to decompose organic matter. Tetrasodium pyrophosphate ($Na_4P_2O_7 \cdot 10\ H_2O$) was added to the suspension to ensure dispersion during the measurement. Sieving and laser particle size data were combined following Dinis and Castilho (2012) to obtain PSDs with 0.5 φ increments. Grain size fractions and texture classes are reported according to the World Reference Base (WRB) classification system (FAO 2014).

The percentage of the <63 μm fraction (subsequently abbreviated Clay&Silt$_\%$) and the percentage of the >2 mm fraction (Skeleton$_\%$) were calculated relative to the fine sediment mass (<2 mm fraction). Mean grain size (LMean) and sorting (LSort) of the fine sediment were determined with the

Table 1 Characteristics of investigated reservoirs and corresponding reservoir catchments

| Data source | Reservoir | | Catchment | | |
	Area (ha) (1)	Capacity (10³ m³) (1)	Area (km²) (2)	Lithology (3)	Predominant soil group(s) (4)
Hartbeesfontein	3.1	30.1	4.3	Granite/gneiss (65%)	Arenosols/solonetzes
				Gabbro (35%)	Phaeozems/vertisols
Marheya	6.8	100.6	27.5	Basaltic rocks (54%)	Luvisols/nitisols/vertisols
				Sandstone (46%)	Arenosols
Silolweni	11.2	141.7	13.2	Ecca group (54%)	Solonetzes
				Granitic rocks (46%)	Arenosols/solonetztes
Nhlanganzwani	16.1	257.0	16.5	Basalt (50%)	Luvisols/nitisols/vertisols
				Rhyolite/dacite (50%)	Leptosols

(1) derived from RTK GNSS surveying; (2) Baade and Schmullius (2015); (3) Geological Survey of South Africa (1986a, b); and (4) according to the World Reference Base soil classification system (FAO 2014) based on Venter (1990), Venter et al. (2003), Mills and Fey (2004), and van Zijl and Le Roux (2014)

Table 2 Number of sample locations and samples from the pre- and post-dam facies of the Hartbeesfontein, Marheya, Silolweni, and Nhlanganzwani reservoirs

	Hart	Marh	Silol	Nhlang	Total
Sample locations	*19*	*28*	*36*	*34*	*117*
Post-dam facies	14	18	20	28	80
Pre-dam facies	4	5	16	4	29
Unclear group affiliation	3	8	11	8	30
Post-dam facies samples	*33*	*29*	*29*	*75*	*166*
Included in the training dataset	15	15	15	15	60
Included in the validation dataset	14	14	14	14	56
Included in the test dataset	4	0	0	46	50
Pre-dam facies samples	*4*	*8*	*32*	*5*	*49*
Included in the training dataset	2	2	2	2	8
Included in the validation dataset	2	2	2	2	8
Included in the test dataset	0	4	28	1	33
Unclear samples	*3*	*12*	*12*	*8*	*35*
Included in the test dataset	3	12	12	8	35
Total number of samples	*40*	*49*	*73*	*88*	*250*

Due to the inclusion of vertical profiles, the number of samples is generally higher than the number of sample locations. Identical numbers of samples from each site were included in the training and validation datasets. Samples with unclear group affiliation and all remaining samples were conflated in a test dataset

logarithmic method of moments and are given in φ units (Krumbein 1936). Hartigan's dip statistic (DIP) was calculated for the sample-specific range of grain size exhibiting positive PSD values to obtain a measure of multimodality in PSDs. DIP increases with growing divergence of an empirical distribution from unimodality (Hartigan and Hartigan 1985). In order to further compare shapes of PSD curves, reservoir-specific mean PSDs with 95% confidence bands were calculated from all samples categorized as post-dam facies. Subsequently, the Euclidean distance from PSDs to these confidence bands, henceforth referred to as "particle size deviance" (PSD_{Dist}), was determined by applying Eq. (1), where N is the total number of 0.5 φ increments, the subscript i belongs to the ith increment, and d_i (in percent) is defined according to Eq. (2) as the distance between the particle size frequency f_i (in percent) of a given sample and the confidence band specified by the upper and lower bounds u_i (in percent) and l_i (in percent), respectively.

$$\mathrm{PSD_{Dist}} = \sqrt{\sum_{i=1}^{N} d_i^2} \qquad (1)$$

$$d_i = \begin{cases} f_i - u_i, & f_i > u_i \\ 0, & u_i \geq f_i \geq l_i \\ l_i - f_i, & f_i < l_i \end{cases} \qquad (2)$$

Hence, the following variables were included in subsequent statistical analysis: LUM, P_{CAL} content, Clay&Silt$_\%$, Skeleton$_\%$, LMean, LSort, DIP, and PSD$_{Dist}$. Mean, minimum, and maximum values of all examined soil and sediment characteristics were calculated from all samples representing the pre- and post-dam facies. Mean values are reported with confidence intervals corresponding to the two-tailed 95% confidence level (Cl95) and were calculated based on Student's t distribution. Prior to subsequent analysis, values of all sediment characteristics were centered and scaled.

2.4 Stratified random sampling

The number of pre- and post-dam facies samples differs greatly among the four study sites (Table 2). For the establishment of a composite fingerprint applicable to all investigated reservoirs, an imbalanced dataset might evoke bias (Zadrozny 2004; Ben-David et al. 2010) due to variable soil and sediment characteristics at the different study sites. Thus, a subset containing equal numbers of samples from each reservoir was created for unbiased training and validation. The dataset was stratified so that each "stratum" contained the samples from a certain reservoir and a certain group (i.e., pre-dam facies, post-dam facies, or unclear group affiliation). Afterwards, samples were randomly drawn from strata representing either the pre- or post-dam facies using the R software package "sampling" (Tillé and Matei 2015; R Core Team 2014). The number of samples had to correspond to the minimum of site-specific numbers of available samples. Hence, 4 and 29 samples from each site representing the pre- and post-dam facies, respectively, were included in the subset. From this, about 50% of the samples from all strata were randomly chosen and included in a training set, while the other samples were retained for validation. The training set contains 60 samples from the pre-dam facies and 8 samples from the post-dam facies, and the validation set consists of 56 samples from the post-dam facies and 8 samples from the pre-dam facies. Differences in the size of the training and validation set result from uneven sample numbers in various strata (Table 2). All samples not included in training and validation sets were merged into a test dataset together with all samples with unclear group affiliation ($N = 35$).

2.5 Generation of synthetic datasets

Synthetic datasets were generated for two purposes: (i) to examine uncertainties in variable selection and classification results arising from the limited number of samples involved in training and validation using a Monte Carlo approach (e.g., Carnes and Slade 1982) and (ii) to enhance the statistical power of the method comparison. Three compilations containing

1000 synthetic datasets with 200 samples each were created. Datasets in the first compilation resemble the statistical distribution of sediment properties that characterize the investigated pre- and post-dam facies. Statistical distributions are represented in kernel density estimates (KDEs) that were derived from empirical data. Expectancy values of KDEs (i.e., expected mean values of sample populations randomly drawn from KDEs) were varied within two-tailed Cl95 intervals to simulate a potential sampling bias.

The second and third compilations contain datasets with differing statistical distributions that meet the criteria of multivariate normality (Gaussian density functions (GDFs)) and equal within-group covariance (eCov) matrices (Mateo-Sanz et al. 2004; Bates and Mächler 2016). While field data are highly unlikely to fulfill the latter criteria (Sheriff et al. 2015), the second and third compilations were created to test the performance of RLR and stepwise DFA/LDA under conditions where the underlying assumptions of stepwise DFA hold. Datasets from the second compilation contain eight synthetic sediment properties for two groups of samples (i.e., the binomial case). Datasets of the third compilation consist of 15 synthetic sediment properties for 5 groups of samples (i.e., the multinomial case). Details on the generation of the compilations and examples of synthetic datasets are provided in the Electronic Supplementary Material (Online Resources 2 and 3).

2.6 Statistical pre-tests

Most recent sediment fingerprinting studies employ a non-parametric test as a precursor step in the identification of composite fingerprints to eliminate variables that do not significantly discriminate between investigated groups of soils and sediments (Miller et al. 2015). Here, the Mann-Whitney U test was applied on datasets containing two groups, while the Kruskal-Wallis H test was used for synthetic datasets with five groups (Laceby et al. 2015). Since the pre-test is involved in variable selection, its application was restricted to the training data to ensure independency of validation results. Variables that revealed no significant differences between groups at the $p = 0.05$ significance level were excluded from subsequent analysis. Normality of population distributions in the empirical dataset was tested individually for samples from the pre- and post-dam facies as suggested by Royston (1983, 1992), with the extended Shapiro-Wilk test for single variables and Royston's H test for multivariate normality (Korkmaz et al. 2014). Since the latter test revealed significant ($p < 0.001$) divergence from multivariate normality for both groups, Box's M test for equal within-group covariance matrices was omitted as the test relies on multivariate normality and is sensitive to violations of this assumption (Manly 2004).

2.7 Regularized logistic regression (RLR)

Composite fingerprints were identified applying RLR with elastic-net penalties (Hastie et al. 2009) using the R software package "glmnet" (Friedman et al. 2010). The procedure fits a logistic regression model, while coefficients of predictor variables are systematically constrained, eliminating the influence of superfluous predictors (Simpson and Birks 2012). Given a training dataset of n sediment samples with k sediment characteristics $x_i = (x_{i1}, ..., x_{ik})$, $i \in \{1, ..., n\}$, belonging to the classes y_i, where $y_i = 1$, if the sample represents the post-dam facies, and $y_i = 0$ otherwise, the binomial RLR method after Friedman et al. (2010) fits a regression model (Eq. (3)) that expresses the probability of a sample x_i to belong to the class $y = 1$ (post-dam facies).

$$P_\beta(y = 1 | x = x_i) = \frac{1}{1 + e^{-(\beta_0 + \beta_1 x_{i1} + ... + \beta_k x_{ik})}} \tag{3}$$

The unknown coefficient vector $\beta = (\beta_0, ..., \beta_k)$ needs to be fitted. This is realized by solving Eq. (4), where $\beta_{\alpha,\lambda}$ is the optimal coefficient vector for a given parameter α with $0 \leq \alpha \leq 1$ and a non-negative weighting factor λ, $\ell(\beta)$ is the log-likelihood function (Eq. (5)) corresponding to the cumulative probability function P_β and the (training) data (x_i, y_i), and $L_\alpha(\beta)$ is the elastic-net penalty function (Eq. (6); for details, see Friedman et al. 2010).

$$\beta_{\alpha,\lambda} = \underset{\beta}{\text{argmax}} \left(\frac{1}{n} \ell(\beta) - \lambda L_\alpha(\beta) \right) \tag{4}$$

$$\ell(\beta) = \sum_{i=1}^{n} \begin{pmatrix} y_i(\beta_0 + \beta_1 x_{i1} + ... + \beta_k x_{ik}) \\ -\log(e^{\beta_0 + \beta_1 x_{i1} + ... + \beta_k x_{ik}} + 1) \end{pmatrix} \tag{5}$$

$$L_\alpha(\beta) = \sum_{j=1}^{k} \left(\frac{1}{2}(1-\alpha)\beta_j^2 + \alpha|\beta_j| \right) \tag{6}$$

The strength of the constraint is governed by the choice of the weighting factor λ in Eq. (4). Increasing λ will likely decrease the penalty function $L_\alpha(\beta_{\alpha,\lambda})$, and consequently, some coefficients in $\beta_{\alpha,\lambda}$ will approach zero, thus eliminating the influence of the corresponding predictor variables. The elastic-net penalty is governed by the parameter α (Eq. 6) and represents a generalization of the ridge regression ($\alpha = 0$) and lasso ($\alpha = 1$) penalties (Zou and Hastie 2005). Setting α close to 0 tends to result in simultaneous shrinkage of coefficients from correlated variables with increasing λ, which will likely result in a rather large number of remaining variables in the resulting composite fingerprint. In contrast, setting α close to 1 typically reduces the number of influential variables (Simpson and Birks 2012).

Since stepwise DFA is designed for the determination of a parsimonious variable selection (Huberty 1989), α was set to 1 to facilitate the method comparison. Alternative values of 0.5 and 0.75 were also tested, but the pre-selection of α was found to have only a small influence on resulting misclassification rates, which amounted to <0.2 and <0.1% on average for synthetic datasets resembling empirical data and those meeting the requirements of stepwise DFA, respectively. The optimal parameter λ was determined based on misclassification rate estimates obtained from tenfold cross validation for a sequence of values λ ranging from 10^{-4} to $>10^{-1}$. Due to the associated random partitioning of the training data, misclassification rates vary when cross validation runs are repeated. Thus, mean misclassification rates and mean standard errors were calculated from 100 cross-validation runs as this number of iterations ensured a sufficient reproducibility of the results. The optimal regression model was identified applying the "one-standard-error rule" suggested by Hastie et al. (2009, p. 244). Accordingly, the optimal model belongs to the set of regression models whose mean (cross validation derived) misclassification rate is within the mean standard error range of the regression model revealing the lowest mean misclassification rate. Within this set, the regression model corresponding to the highest value λ is considered optimal.

Fitted regression models (Eq. (3)) were used to calculate probabilities of group membership. A sample x was classified as a representative of the post-dam facies when the corresponding probability $P_\beta(x)$ exceeded 0.5; otherwise, it was ascribed to the pre-dam facies. The threshold 0.5 is the most intuitive choice and induces identical chance of misclassification for both groups. The variable importance VI_j (in percent) of a sediment property $j \in \{1, ..., k\}$ was calculated based on the absolute values of entries in the optimized coefficient vector $\beta_{\alpha,\lambda} = (\beta_0, ..., \beta_k)$ as shown in Eq. (7), i.e., excluding the intercept β_0.

$$VI_j = 100\% \cdot \frac{\left|\hat{\beta}_j\right|}{\sum_{l=1}^{k} \left|\hat{\beta}_l\right|} \qquad (7)$$

For the application of Eq. (7), input data have to be centered and scaled.

Multinomial RLR is applied when soils and sediments of $G \geq 3$ groups are to be distinguished. In this case, the regression model consists of G equations having the form of Eq. (3) (cf. Friedman et al. 2010). Coefficients of all equations are to be fitted, while the selection of a grouped penalty (referring to the option "type.multinomial = 'grouped'" in the glmnet package) ensures simultaneous shrinkage of coefficients corresponding to the same variable in all G equations. Probabilities of group membership are calculated from the fitted regression model, and samples are ascribed to the group exhibiting the highest probability. Variable importance of sediment characteristics can be assessed based on Euclidean norms of vectors containing the corresponding G fitted coefficients (instead of the absolute values in Eq. (7)) provided that input data are centered and scaled.

2.8 Stepwise DFA and LDA

For comparison, variable selection and classification were conducted applying stepwise DFA and LDA, respectively. Stepwise DFA was performed with the forward selection algorithm implemented in the R software package "klaR" (Weihs et al. 2005). This algorithm repeatedly calculates Wilks' lambda for various variable subsets. In the first step, the variable with the highest discriminatory power as indicated by the lowest Wilks' lambda is selected. Afterwards, variables minimizing Wilks' lambda are iteratively chosen from the remaining variables and added to the model. At each step, an F test is performed to evaluate the significance of the reduction in Wilks' lambda. The variable selection ceases when the p value exceeds a pre-defined threshold (for details, see Tabachnick and Fidell 2001). Following D'Haen et al. (2013), a threshold of $p = 0.2$ was used, which is in accordance with the recommendations from Constanza and Afifi (1979).

Predictive LDA was applied to the classification of samples using the composite fingerprint identified with stepwise DFA. Discriminant functions were set up based on samples from training sets employing the maximum likelihood (ML) discriminant rule and assuming identical prior probabilities. The resulting discriminant function was used for classification. Posterior probabilities were calculated with the "predictive" method suggested by Venables and Ripley (2002, p. 339). Variable importance was calculated from absolute values of coefficients in the discriminant function by applying Eq. (7).

2.9 Monte Carlo simulations, validation, and method comparison

Synthetic datasets resembling the structure of the empirical data were employed in Monte Carlo simulations to investigate uncertainties in classification results taking into account a potential sampling bias (e.g., Carnes and Slade 1982). As above, RLR and stepwise DFA/LDA were applied to synthetic datasets following the statistical pre-test. The resulting regression models and discriminant functions were used for the classification of samples in the empirical dataset. Cases of inconsistency between field interpretation and classification results for samples with unambiguous group affiliation were interpreted as misclassifications. Mean variable importance, mean probabilities of group membership for individual

samples, and mean misclassification rates were calculated from all simulations ($N = 1000$).

Moreover, all synthetic dataset compilations were analyzed to enhance the comparison between RLR and stepwise DFA/LDA. Misclassification rates were calculated separately for the training and validation subsets. While misclassification rates derived from training data might overvalue the performance of classifiers due to potential overfitting, misclassification rate estimates obtained from data not involved in the training of regression models and discriminant functions are expected to reveal a more reliable indication for the evaluation of the methods (Hastie et al. 2009). In addition, both approaches were compared with respect to the number of identified fingerprint properties and posterior probabilities of group membership for misclassified samples. For the latter, the probability residual ΔP_{post} of individual samples x_i belonging to the group y_i was calculated based on the posterior probability of group membership $P_{post}(y_i|x_i)$ as shown in Eq. (8).

$$\Delta P_{post}(x_i, y_i) = 1 - P_{post}(y_i|x_i) \tag{8}$$

The mean probability residual of misclassified samples can range between 0.5 and 1 and was used as an indicator for the cogency of probabilities with respect to the conclusiveness of related classification results. Average values with Cl95 intervals were calculated for misclassification rates, mean probability residuals of misclassified samples, and number of selected fingerprint properties. The significance of differences in results derived with RLR and combined stepwise DFA/LDA was tested with the Mann-Whitney U test.

3 Results and interpretation

3.1 Characteristics of the pre- and post-dam facies

The post-dam facies of all study sites is characterized by silt loams exhibiting a black to brownish black color (2.5Y 2–3/1), resulting in a luminance (LUM) < 75 when the sediment is moist and rubbed. Grain size analysis reveals bimodal site-specific mean PSDs with a maximum in the silt fraction (Fig. 3a). Intra-site variability is rather small as evident in a mean particle size deviance (PSD_{Dist}) < 8 (Fig. 3b). Bimodality is reflected in mean values of Hartigan's dip statistic (DIP) ranging from 0.04 to 0.05. Mean percentage of the <63 μm fraction (Clay&Silt$_\%$) is $87 \pm 2\%$. Skeleton (>2 mm) is nearly absent in the post-dam facies apart from samples taken at marginal positions within reservoir basins. Mean content of calcium-lactate leachable phosphorus (P_{CAL}) is 90 ± 10 ppm.

The characteristics of the pre-dam facies differ markedly from the post-dam facies. In the pre-dam facies, LUM shows high variability and ranges between 40 and 130. Clay&Silt$_\%$ does not exceed 72% (Fig. 4a) and is $38 \pm 5\%$ on average, while mean Skeleton$_\%$ is $6 \pm 2\%$. Mean grain size (LMean) is higher (i.e., a lower value in terms of φ units), and sorting (LSort) tends to be poorer than in the post-dam facies (Fig. 4b). As expected, PSD_{Dist} values are higher and more variable in the pre-dam facies with mean values >15 for all study sites (Fig. 3b). Mean DIP values range between 0.04 and 0.07 and are therefore rather similar to values obtained from the post-dam facies. P_{CAL} content is generally low in the pre-dam facies with a mean value of 17 ± 5 ppm, although higher P_{CAL} content of >50 ppm was found for some soil samples taken at the Marheya reservoir (Fig. 4a).

Notably, the disparity of sediment properties between the pre- and post-dam facies exceeds the inter-site variability within both facies (Fig. 4). This justifies the application of a joint composite fingerprint for all study sites which would have been inadequate otherwise. The Mann-Whitney test reveals significant ($p < 0.05$) differences between the facies for all considered variables except DIP (Table 3). At the same time, the Shapiro-Wilk test indicates significant deviation from normality for six and eight properties characterizing the pre- and post-dam facies, respectively.

3.2 Composite fingerprints and variable importance obtained from empirical data

The fitted RLR model corresponds to the parameter $\lambda = 0.0278$ and reveals a cross validation-derived misclassification rate of $4 \pm 2\%$. Results show that not all input variables provide essential information for the discrimination of the pre- and post-dam facies. While most coefficients decrease with increasing λ (Fig. 5a, b), misclassification rates remain on a low level for $\lambda < 10^{-2}$ (Fig. 5c). Coefficients and variable importance corresponding to the optimized regression model are shown in Table 4. Clay&Silt$_\%$ has the highest variable importance (39%). PSD_{Dist} (26%) and P_{CAL} content (26%) are also important, while Skeleton$_\%$ has only a minor influence (9%). All other variables have no significance for the optimized model. Hence, the RLR-derived composite fingerprint contains the following four variables: Clay&Silt$_\%$, PSD_{Dist}, P_{CAL} content, and Skeleton$_\%$.

Stepwise DFA identifies the same variables to be the most important, although in a slightly different order with Skeleton$_\%$ being already selected in the second step (Table 4). In addition, LMean and LSort are selected, resulting in a composite fingerprint consisting of six sediment properties including all variables passing the Mann-Whitney test except LUM. Wilks' lambda is monotonically decreasing in the course of the selection procedure, indicating improved discriminatory power with the addition of a new variable in
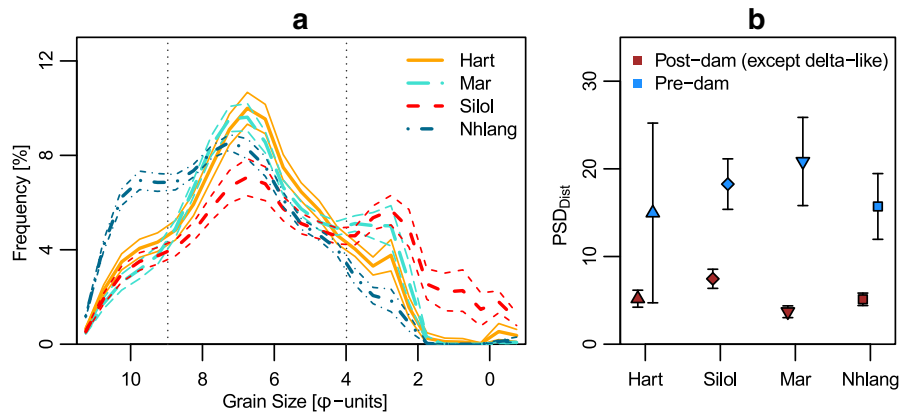
Fig. 3 Variability of mean particle size distributions (PSDs) and derived particle size deviance (PSD_Dist) **a** mean PSDs with 95% confidence bands for the post-dam facies in the Hartbeesfontein, Marheya, Silolweni, and Nhlanganzwani reservoirs. *Vertical dotted lines* indicate the boundaries between the clay, silt, and sand fractions, respectively. **b** Mean PSD_Dist values obtained from samples of the pre- and post-dam facies for all study sites. PSD_Dist values were calculated from particle size frequencies (expressed in percent) according to Eq. (1) and are interpreted as a dimensionless metric. *Error bars* denote 95% confidence intervals

each iteration. The algorithm stops with a Wilks' lambda of 0.23 after which no significant improvement can be achieved.

Coefficients of the discriminant function calculated with LDA based on the composite fingerprint derived from stepwise DFA indicate highest variable importance for Clay&Silt_% (48%) followed by LMean (20%) and LSort (11%), although the latter two variables were selected only in the sixth and fifth steps of the stepwise DFA, respectively. Signs of coefficients in the RLR model and the discriminant function are all in line with expectations (Table 4). For example, P_{CAL} coefficients are positive while coefficients of Skeleton_% are negative, indicating higher probability for a

Fig. 4 Selected sediment properties of samples from all study sites characterizing the pre- and post-dam facies **a** percentage of the <63-μm fraction (Clay&Silt_%) and calcium-lactate leachable phosphorus content (P_{CAL}), **b** mean grain size and sorting of the <2-mm fraction, and **c** Hartigan's dip statistic (used as a measure for multimodality in PSDs) and luminance values
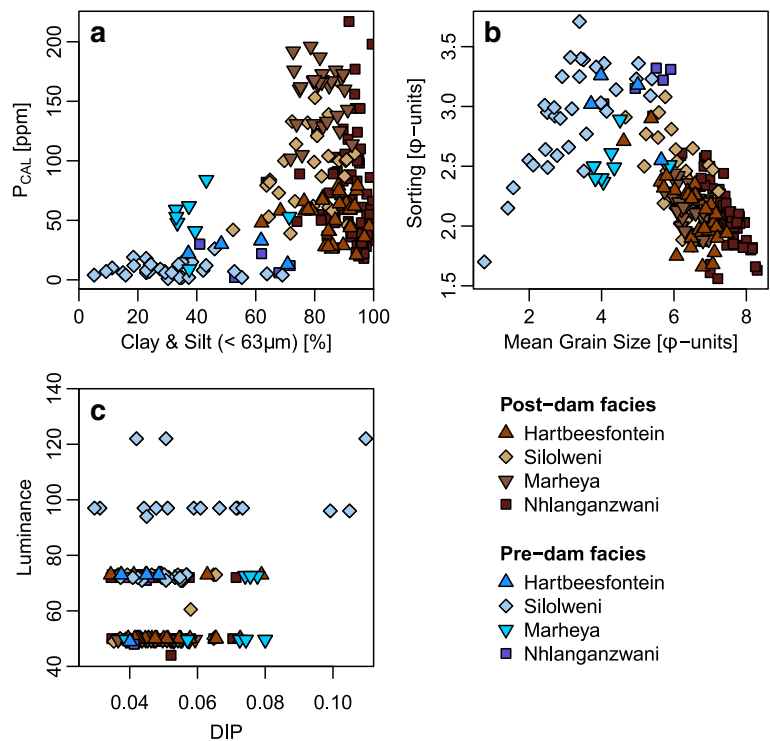
Table 3 Mean values with 95% confidence levels (Cl95) of sediment properties analyzed on samples from the pre- ($N = 49$) and post-dam facies ($N = 166$) of all study sites and p values obtained from the Shapiro-Wilk (p_{SW}) and Mann-Whitney U tests (p_{MW})

Variable	Post-dam facies			Pre-dam facies			p_{MW}
	Mean	Cl95	p_{SW}	Mean	Cl95	p_{SW}	
LUM (0–255)	58	2	*<0.001*	79	5	*<0.001*	*0.017*
P_{CAL} (ppm)	90	10	*<0.001*	17	5	*<0.001*	*<0.001*
Clay&Silt$_\%$ (%)	87	2	0.063	38	5	*<0.001*	*<0.001*
Skeleton$_\%$ (%)	0.7	0.3	*<0.001*	5.8	2.2	*<0.001*	*0.001*
LMean (φ)	6.8	0.1	0.703	3.7	0.3	0.243	*<0.001*
LSort (φ)	2.2	0.1	0.054	2.9	0.1	*0.002*	*<0.001*
DIP	0.05	0.01	*<0.001*	0.06	0.01	*<0.001*	0.402
PSD$_{Dist}$	5.3	0.5	*0.026*	18.2	2.1	*<0.001*	*<0.001*

Significant p_{SW} values indicate deviation from normality, while significant p_{MW} values testify differences between population distributions in the pre- and post-dam facies. Since the Mann-Whitney test represents a precursor step in the identification of composite fingerprints, its application was restricted to samples from the training set. Significant p values (<0.05) are shown italics

sample to belong to the post-dam facies with increasing P_{CAL} content and decreasing Skeleton$_\%$.

3.3 Classification results obtained from empirical data

Comparing results of the RLR approach with field interpretation reveals low misclassification rates of 2, 0, and 5% for samples belonging to the training, validation, and test datasets, respectively (Table 5). Misclassifications with RLR were obtained for five soil samples including one sample in the training set and four samples in the test set. Combining stepwise DFA and LDA performs only slightly poorer with 3, 3, and

4% misclassifications in the training, validation, and test sets, respectively. In total, RLR and stepwise DFA lead to 2 and 3% misclassifications (Table 5). Neglecting a potential sampling bias, these figures represent an estimate for the risk of misclassifying samples with unclear group affiliation.

Figure 6 depicts the probabilities for an affiliation to the post-dam facies as derived from the RLR and LDA approaches for all samples involved in the analysis. With the RLR model, 12% of all samples, including four out of five misclassified samples, fall into the probability range of 0.2 to 0.8 (Fig. 6a). The stepwise DFA/LDA procedure is more decisive in the sense that probabilities are strongly focused towards 0 and 1 (Fig. 6b). Only 2% of all samples show probabilities between 0.2 and 0.8, including none of the misclassified samples. The mean probability residual for misclassified samples is 0.69 ± 0.20 ($N = 5$) for RLR and 0.97 ± 0.03 ($N = 7$) for stepwise DFA/LDA. Samples with unclear field interpretation reveal probabilities of <0.2, 0.2 to 0.8, and >0.8 for 18, 13, and 4 samples based on RLR and for 18, 3, and 14 samples based on LDA approach, respectively. Comparison of results derived from both methods (Fig. 6c) yields 31 (89%) consistent and 4 (11%) inconsistent classifications for samples with unclear class affiliation.

3.4 Mean variable importance and classification results obtained from Monte Carlo simulations

Monte Carlo simulations based on RLR and stepwise DFA/LDA reveal similar results regarding the mean variable importance. Clay&Silt$_\%$ shows the highest mean variable importance (RLR 26%, LDA 23%; Fig. 7) followed by LMean (23, 20%), PSD$_{Dist}$ (22, 19%), and LSort (14, 16%). P_{CAL} content features a mean variable importance of 8 and 10% in RLR and stepwise DFA/LDA, respectively, while Skeleton$_\%$ (4, 6%), LUM (2, 5%), and DIP values (1, 1%) have on average only a minor influence on classification results.
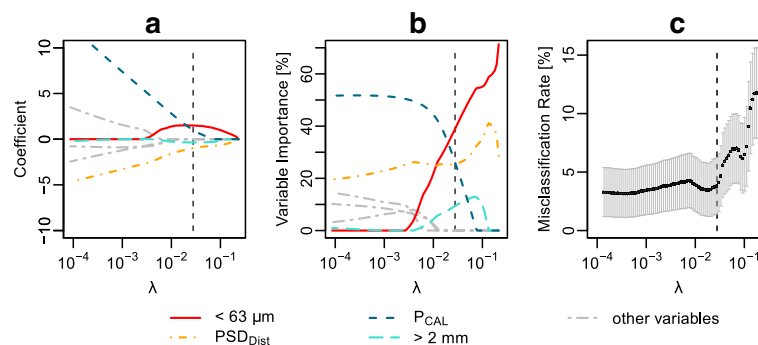
Fig. 5 Results of the variable selection with the RLR method **a** fitted coefficients, **b** variable importance, and **c** average misclassification rates with standard deviations obtained from tenfold cross validation (100 runs) for various values λ. The *vertical dashed line* denotes the optimal value λ based on the "one-standard-error rule" suggested by Hastie et al. (2009). Variables not included in the resulting composite fingerprint are subsumed in the category "other variables"

Table 4 Coefficients (Coef) of the fitted regression model ($\alpha = 1$; $\lambda = 0.0278$) and linear discriminant function obtained from regularized logistic regression (RLR) and linear discriminant analysis (LDA), respectively, indicating variable importance (VI) and the evolution of Wilks' lambda in the course of stepwise discriminant function analysis (DFA)

Variable	RLR			Stepwise DFA		LDA		
	Coef	VI (%)	Rank	Wilks' Λ	Rank	Coef	VI (%)	Rank
(Intercept)	2.21	–	–	–	–	0	–	–
Clay&Silt$_\%$	1.49	39	1	0.46	1	4.74	48	1
Skeleton$_\%$	−0.36	9	4	0.36	2	−1.11	11	3
PSD$_{Dist}$	−0.98	26	2	0.29	3	−0.55	6	5
P_{CAL}	1.00	26	2	0.27	4	0.45	5	6
LSort	0	0	–	0.25	5	1.13	11	3
LMean	0	0	–	0.23	6	−1.96	20	2
LUM	0	0	–	_[a]	_[a]	_[a]	_[a]	_[a]

[a] Variable not selected in the course of the stepwise DFA

Uncertainties in the determination of the mean variable importance (Cl95) are <1%.

Mean probabilities of individual samples obtained from RLR and stepwise DFA/LDA are in a comparable range (Fig. 8), with an absolute mean and maximum deviation of 0.11 ± 0.01 and 0.25 ± 0.02, respectively. The number of misclassifications does not differ significantly ($p = 0.84$). Taking into account classification uncertainties for samples with Cl95 intervals of mean posterior probabilities, including the threshold 0.5, both approaches lead to $5 \pm 1\%$ misclassifications. This figure can be interpreted as a fair estimate for the risk of misclassifying samples with unclear group affiliation, if a sampling bias in the empirical dataset is taken into consideration (Carnes and Slade 1982). Moreover, 83 and 60% of samples that were misclassified with RLR and stepwise DFA/LDA, respectively, fall into the mean probability range between 0.2 and 0.8. This suggests that RLR-derived

mean probabilities especially represent a good indication for classification conclusiveness. Comparison between classification results obtained with RLR and stepwise DFA/LDA for samples with unclear class affiliation yields 33 (94%) consistent and 2 (6%) inconsistent classifications.

3.5 Method comparison based on synthetic dataset compilations

A comparison of the performance of RLR and stepwise DFA/LDA based on synthetic datasets reveals, on average, only minor differences in misclassification rates but substantial disparities in mean probability residuals for misclassified samples and the number of fingerprint properties (Fig. 9). Mean misclassification rates calculated for datasets resembling the structure of empirical data vary between the pre- and post-dam facies (Table 5) but do not significantly differ between RLR

Table 5 Percentage of misclassified samples in the training, validation, and test data subsets of empirical and synthetic data obtained with RLR and combined stepwise DFA/LDA, respectively

			Empirical dataset ($N = 1$)			Synthetic datasets ($N = 1000$)		
			Post-dam	Pre-dam	Total	Post-dam	Pre-dam	Total
RLR		Training	0	13	2	0.3 ± 0.1	0.7 ± 0.1	0.4 ± 0.1
		Validation	0	0	0	1.0 ± 0.2	2.4 ± 0.2	1.4 ± 0.1
		Test[a]	0	12	5	–	–	–
		All[a]	0	10	2	0.7 ± 0.1	1.5 ± 0.2	0.9 ± 0.1
Stepwise DFA/LDA		Training	2	13	3	0.1 ± 0.1	1.2 ± 0.1	0.7 ± 0.1
		Validation	4	0	3	0.2 ± 0.1	2.3 ± 0.2	1.2 ± 0.1
		Test[a]	0	9	4	–	–	–
		All[a]	2	8	3	0.1 ± 0.1	1.8 ± 0.1	0.9 ± 0.1

Misclassification rates of synthetic datasets correspond to mean values with 95% confidence intervals and were derived from a compilation of 1000 datasets resembling the structure of the empirical dataset

[a] Samples ascribed to the group "unclear" based on field interpretation are precluded
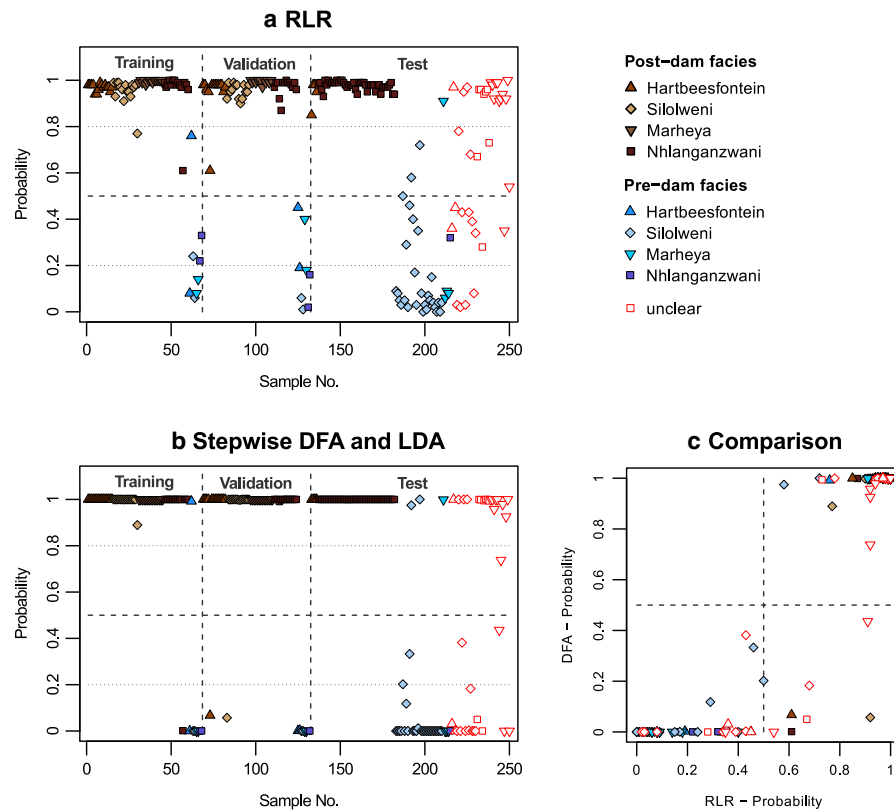
Fig. 6 Probabilities that samples from the training, validation, and test subsets of the emprical dataset belong to the post-dam facies: **a** probabilities of group membership obtained from regularized logistic regression (RLR), **b** posterior probabilities calculated from linear

discriminant analysis (LDA) based on the composite fingerprint identified with stepwise discriminant function analysis (DFA), and **c** comparison of probabilities calculated with the aforementioned methods

and stepwise DFA/LDA for samples in the validation set ($p = 0.09$). Notably, mean misclassification rates are <1.5% (Fig. 9a), which is about 3.5% less than mean misclassification rates compiled with Monte Carlo simulations for samples of the empirical dataset. This is in line with expectations as

sediment characteristics in training and validation data of synthetic datasets were drawn from identical KDEs. Mean probability residuals of misclassified samples are on average <0.67 for RLR and >0.75 for stepwise DFA/LDA (Fig. 9b), which is a highly significant deviation ($p < 0.001$). In addition, the
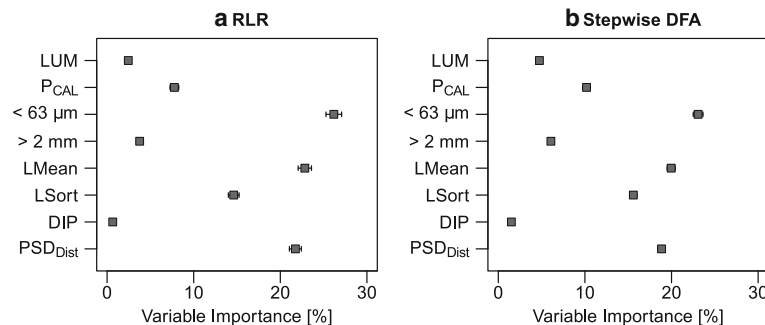
Fig. 7 Mean variable importance of investigated sediment characteristics for the discrimination between the pre- and post-dam facies as derived from a Monte Carlo approach with **a** binomial RLR and **b** stepwise DFA

based on 1000 synthetic datasets resembling the structure of the empirical dataset. *Error bars* correspond to 95% confidence intervals

1789

Fig. 8 Mean probabilities that samples from the study sites belong to the post-dam facies as derived from Monte Carlo simulations based on 1000 synthetic datasets: **a** mean probabilities of group membership obtained from regularized logistic regression (RLR), **b** mean posterior probabilities calculated from linear discriminant analysis (LDA) based on the composite fingerprint identified with stepwise discriminant function analysis (DFA), and **c** comparison of mean probabilities calculated with the aforementioned methods. *Error bars* denote 95% confidence intervals
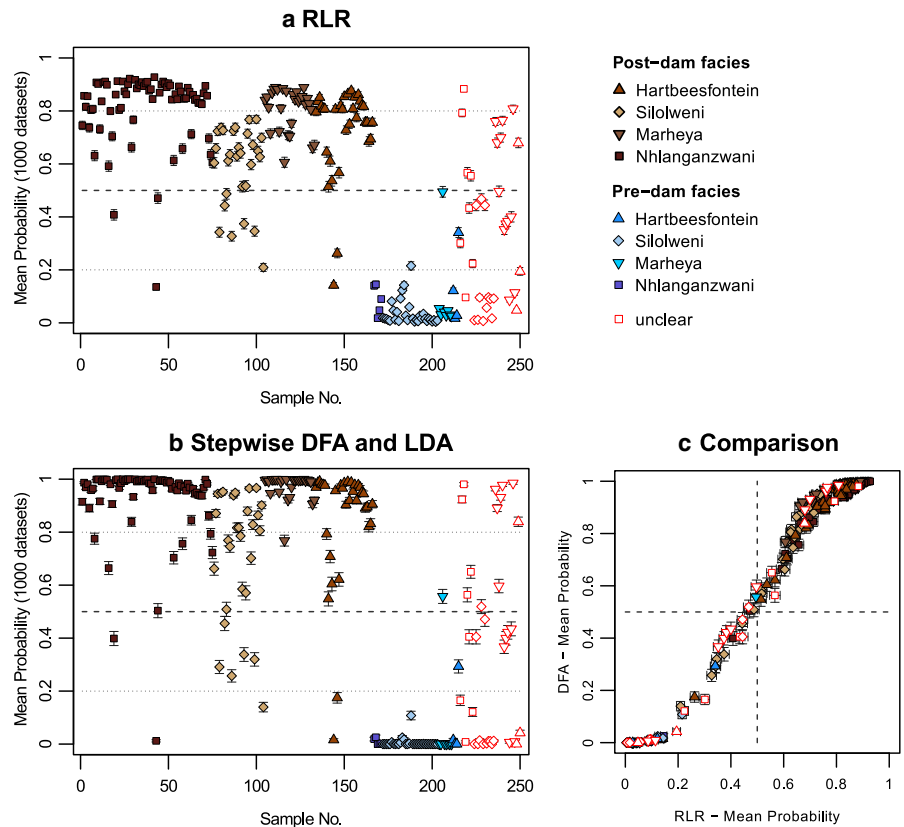
mean number of fingerprint properties differs significantly ($p < 0.001$) and amounts to 5.5 ± 0.1 and 6.2 ± 0.1 for RLR and stepwise DFA, respectively (Fig. 9c).

The compilation of binomial synthetic datasets meeting the criteria of stepwise DFA is more heterogeneous than the compilation of datasets resembling empirical data, which results in two to three times higher uncertainties of mean misclassification rates (Fig. 9d). The difference of misclassification rates derived from RLR and stepwise DFA is not significant ($p = 0.46$) for training sets. For samples in validation sets, RLR and stepwise DFA/LDA result in mean misclassification rates of 1.0 ± 0.2 and $0.8 \pm 0.2\%$, respectively. This difference is significant ($p < 0.001$) despite overlapping confidence intervals. Mean probability residuals of misclassified samples are <0.65 for RLR and >0.71 for stepwise DFA (Fig. 9e), while the mean number of variables included in composite fingerprints is only 2.3 ± 0.1 for RLR and 4.8 ± 0.1 for stepwise DFA (Fig. 9f). Therefore, the mean number of fingerprint properties selected with RLR is $52 \pm 3\%$ lower than for stepwise DFA, while $97 \pm 3\%$ of the variables selected via RLR are also included in the composite fingerprint identified with stepwise DFA. Differences in mean probability residuals of misclassified samples and mean number of composite fingerprint properties are highly significant ($p < 0.001$).

These findings indicate that discrimination of the pre- and post-dam facies based on RLR and stepwise DFA/LDA results in an approximately equal number of misclassifications in the current study, although composite fingerprints identified with RLR contain on average $12 \pm 1\%$ less sediment properties. Stepwise DFA/LDA leads to significantly lower mean misclassification rates than RLR when underlying assumptions apply. However, classification with LDA is based on about twice as many sediment properties and the absolute difference in mean misclassification rates is only $0.2 \pm 0.3\%$. Moreover, probabilities of group membership obtained from RLR represent a better indication for the conclusiveness of classification results, even if analyzed datasets meet the underlying assumption of stepwise DFA. Similar results were obtained for multinomial synthetic datasets where mean misclassification rates for validation sets derived from RLR and stepwise DFA are 0.2 ± 0.1 and $0.1 \pm 0.1\%$, while mean probability residuals are <0.70 and >0.78 and the mean number of selected variables amounts to 8.3 ± 0.2 and 14.2 ± 0.1, respectively. Again, differences in misclassification rates, mean probability residuals, and the number of selected variables are significant with p values <0.001. Hence, it appears that results obtained for the binomial case can be extrapolated to the multinomial case. However, further analyses on datasets with varying numbers
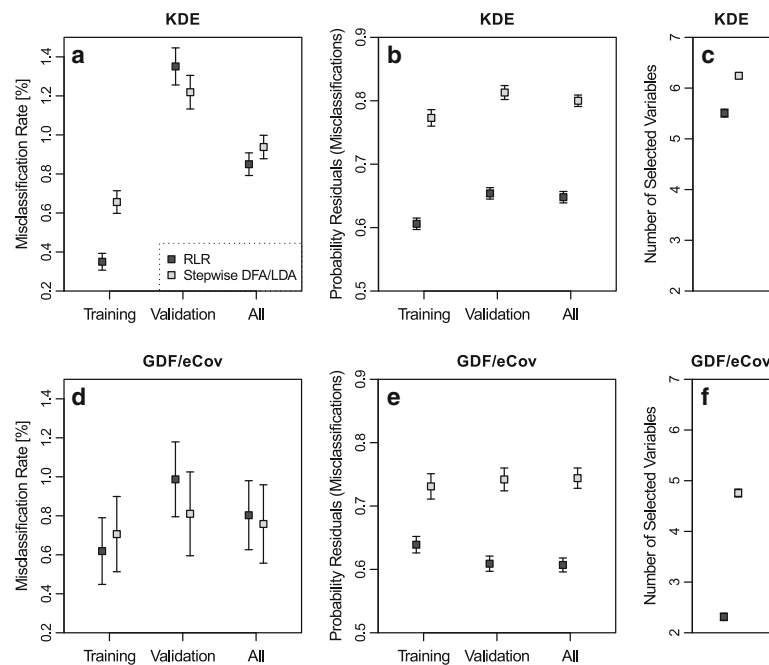
Fig. 9 Performance of binomial RLR (*dark symbols*) and stepwise DFA/LDA (*light symbols*) on synthetically generated datasets in terms of mean misclassification rates (**a**, **d**), mean probability residuals for misclassified samples (**b**, **e**), and mean number of variables involved in the resulting composite fingerprints (**c**, **f**). Synthetic datasets (*N* = 1000) resembling the structure of empirical data acquired from the pre- and post-dam facies of investigated reservoirs were generated based on kernel density estimates (KDE; **a**–**c**). Another compilation of synthetic datasets (*N* = 1000) was created using randomly generated Gaussian density functions (GDFs) and correlation matrices ensuring normally distributed values in each group and equal within-group covariance (eCov), respectively (**d**–**f**). *Error bars* of mean values correspond to 95% confidence intervals

of sediment properties, groups, and samples are required to test this hypothesis.

4 Discussion

4.1 Merits and drawbacks of RLR and stepwise DFA/LDA

In this study, RLR performs slightly better for facies discrimination than combining stepwise DFA and LDA, although misclassifications derived from Monte Carlo simulations do not significantly differ ($p = 0.84$). RLR uses $12 \pm 1\%$ less predictors on average (Fig. 9). Moreover, RLR results in significantly ($p < 0.001$) lower mean probability residuals for misclassified samples. This implies a higher cogency of RLR-derived probabilities of group membership concerning classification conclusiveness compared to posterior probabilities calculated with LDA. This is consistent with findings of other studies that attested a superior performance of regression shrinkage methods when compared to stepwise variable selection (Hastie et al. 2009; Makalic and Schmidt 2010). With respect to the low number of misclassifications, stepwise DFA and LDA still perform reasonably well. This implies that

deviation from multivariate within-group normality (Table 3) does not severely impact the performance of stepwise DFA/LDA in this study.

Although stepwise forward and backward selection will in practice often perform just as well as other variable selection techniques (Murtaugh 2009), we discourage their use for the identification of composite fingerprints. A major disadvantage of stepwise forward (and backward) selection is the disregard of the fact that a combination of several variables not yet included in (excluded from) the variable subset might have a greater discriminatory power than the single variable entering (leaving) the model (Thompson 1989). In each step, the selection of variables is conditional as it relies on the subset of variables previously selected (Makalic and Schmidt 2010). As a consequence, the discriminatory power of the ultimately identified variable subset is often suboptimal (Huberty 1989).

Furthermore, the conditional selection of variables in stepwise DFA leads to biases in Wilks' lambda (Rencher and Larson 1980), F-statistics, and p values (Thompson 1995). Although alternative stopping rules are available, significance levels obtained from F tests remain the most commonly employed termination criterion in stepwise DFA (Munita et al. 2006). If p values are not appropriately adjusted, this

can lead to the inclusion of too many variables in the composite fingerprint, potentially involving variables with spurious discriminatory power (Rencher and Larson 1980). This study provides a good example since RLR results obtained from the empirical dataset indicate that variables selected in the fifth and sixth steps of the stepwise DFA (Table 4) are not essential for discrimination and classification. Notably, the mean number of composite fingerprint properties identified with stepwise DFA is significantly higher ($p < 0.001$) than for RLR for all analyzed dataset compilations.

Results of this study indicate that stepwise DFA/LDA leads to significantly ($p < 0.001$) lower mean misclassification rates than RLR when data are normally distributed in all groups and show equal within-group covariance matrices (Fig. 9d). This is in accordance with previous studies that showed classification based on discriminant functions to be slightly superior to regression models, when underlying assumptions applied (Harrell and Lee 1985). In such cases, "tabu search" algorithms (Stąpor 2015) might be used for variable selection rather than stepwise forward and backward procedures. Otherwise, the application of regression models is preferable (Press and Wilson 1978). Empirical data are, however, highly unlikely to satisfy the assumptions of stepwise DFA (Sheriff et al. 2015), particularly concerning the covariance structure. Moreover, the mean difference to RLR-derived misclassification rates by means of absolute values is very small in this study (0.2 ± 0.3%).

Regression shrinkage with the elastic-net penalty is a reasonable alternative for the identification of composite fingerprints, in particular when requirements of stepwise DFA are not fulfilled. RLR is applicable for high-dimensional datasets (Oswald and Putka 2015), where the so-called "best subset" approaches (e.g., McCabe 1975) become impractical due to their high computational costs (Jović et al. 2015). RLR can handle datasets with many correlated variables (Härdle and Simar 2015) and is comparatively robust against overfitting due to the constraint imposed on coefficients of the regression model (Harrell 2001). Unlike stepwise and best subset procedures, RLR represents a "soft-thresholding" method (Hastie et al. 2009), revealing a nuanced composite fingerprint involving information on variable importance.

RLR appears to be an attractive tool for sediment source tracing studies, where variable selection is employed as a prelude to the application of sediment unmixing models (Collins and Walling 2002). In this framework, the subdivision of the dataset into training and validation subsets is not required unless the predictive power of the model is to be assessed independently from training data. Whether composite fingerprints in sediment source tracing studies should be favorably parsimonious or involve a larger number of sediment properties is subject to an ongoing debate (e.g., Palazón et al. 2015; Sheriff et al. 2015; Manjoro et al. 2016). RLR is a suitable

method to test the influence of the number of fingerprinting properties on unmixing results, since criteria for the choice of α and λ in the optimization of the regression model can be considered as an analogy to the selection of the stopping rule and significance level in stepwise DFA.

Collins and Walling (2002), for example, suggested to stop variable selection with stepwise DFA as soon as all samples are classified correctly (given that 100% correct classifications are achieved). This can be similarly realized with RLR by setting $\alpha = 1$ and selecting the maximum value λ that leads to 100% correct classifications. Likewise, the impact of the number of fingerprint properties on sediment unmixing results may be tested (Laceby et al. 2015) by systematically decreasing α from 1 towards 0, which likely increases the number of selected variables in fitted regression models (Simpson and Birks 2012). Although α was found to have only a minor influence (0.2 ± 0.1%) on misclassification rates in the current study, it might be worthwhile to involve α in the optimization process (Friedman et al. 2010), when the number of variables constituting the composite fingerprint is of no importance.

Sample size requirements for RLR and stepwise DFA can be considered as roughly similar. As a minimum criterion for stepwise DFA, it has been suggested to ensure at least one sample per variable in each group, while the total number of samples involved in the training of the discriminant function should be about 10 times the number of variables (Brown and Tinsley 1983). RLR was successfully applied in genetic studies on datasets with >2000 variables containing <70 training samples and a minimum of only 8 observations per group (Wu 2006). However, fitting the regression model including the optimization of λ via cross validation becomes more uncertain with decreasing sample size, and the glmnet algorithm (Friedman et al. 2010) returns a warning message if the cross validation-based estimation of misclassification rates is founded on <8 observations in any group.

It might be considered a disadvantage that RLR results vary slightly when analysis is repeated due to the randomness involved in the cross validation-based optimization of λ. This problem can be overcome by averaging multiple cross-validation runs (see Sect. 2.7). Coefficient shrinkage and changes in variable importance with increasing λ (Fig. 5a, b) are not affected by randomness and give appreciable insights into the discriminatory power of single variables and variable combinations. Testing the performance of RLR based on empirical datasets involving a higher number of tracers and groups is required for a more complete assessment of the potential of the method. Algorithms for binomial and multinomial RLR (for two and more groups) are implemented in statistics software such as SPSS ("CATREG"; IBM 2013) and SAS ("GLMSELECT"; SAS Institute Inc. 2010). R scripts for binomial and multinomial RLR analysis with the software package glmnet (Friedman et al. 2010) are provided as

Chapter 3

Electronic Supplementary Material with the online version of this article (Online Resources 4–8).

4.2 Potential of the RLR approach for facies discrimination in reservoirs

Soils and sediments from the pre- and post-dam facies of the investigated reservoirs can be distinguished in the field based on color, structural fabric, texture, and other sedimentary features. This is in accordance with many previous reservoir siltation studies (e.g., Small et al. 2003; Haregeweyn et al. 2006; Tamene et al. 2006; Baade et al. 2012). However, the exact allocation of the base of reservoir deposits can be complicated if the underlying material shows similar color and texture characteristics (Rausch and Heinemann 1984). In these cases, a more detailed examination by means of laboratory analysis is useful to scrutinize and substantiate field interpretation (Foster et al. 2007; Schmengler and Vlek 2015).

The approach presented here can assist with the distinction. Validation of classification results indicates that 2 and $5 \pm 1\%$ misclassifications are to be expected for samples initially categorized as unclear when neglecting and taking into account a potential sampling bias, respectively. Posterior probabilities obtained from misclassified samples suggest that classification based on RLR-derived probabilities <0.2 and >0.8 can be regarded conclusive with a reasonable small probability of fallacy. Into this range fall 63 and $46 \pm 4\%$ of the samples with unclear group affiliation based on analysis on the empirical dataset and 1000 Monte Carlo simulations, respectively. Collection of replicate sampling and sampling of sediment sequences improves the chance of conclusive classification results. Hence, this approach is particularly powerful when combined with an adjusted sampling strategy.

Grain size composition turns out to be a valuable indicator for the discrimination of the pre- and post-dam facies, which is evident in a mean variable importance >10% for Clay&Silt$_\%$, PSD$_{Dist}$, LMean, and LSort, respectively (Fig. 7). Sediment entering the reservoir has a grain size composition that is already distinct from catchment soils due to various processes involved in fluvial sediment transport (McLaren and Bowles 1985). Particle size-dependent settling velocities and diminished transport energy within reservoir basins lead to further sorting and grain size distributions of reservoir deposits usually differing from fluvial sediments (Morris and Fan 1998). Hence, grain size composition appears to be a robust indicator for the discrimination of the pre- and post-dam facies.

P_{CAL} content is also a useful parameter which is indicated by a variable importance of $8 \pm 1\%$. Enrichment by calcium-lactate leachable phosphorus (P_{CAL}), occasionally found in the post-dam facies, has been attributed to an elevated P_{CAL} content in allochthonous sediment originating from topsoils (Walter et al. 2012; Schmengler and Vlek 2015) but may be

also influenced by the exchange of phosphorus between water and sediment (Søndergaard et al. 2003). In this study, a five-fold higher P_{CAL} content in the post-dam facies than in the pre-dam facies was found. Walter et al. (2012) found only a twofold P_{CAL} enrichment in the post-dam facies of a reservoir in northwest Peru. Similarly, Schmengler and Vlek (2015) report a twofold P_{CAL} enrichment in the post-dam facies of two reservoirs in the semi-arid Burkina Faso plains. Thus, the applicability of P_{CAL} content for facies discrimination in reservoirs outside the KNP merits further investigation.

Sediment color is useful for the facies discrimination in reservoirs (Haregeweyn et al. 2006) when varying chemical and physical sediment properties are reflected in distinct color characteristics. The rather low variable importance of LUM ($2 \pm 1\%$) in this study is somewhat surprising, taking into account that field evidence suggests clear color differences between the pre- and post-dam facies (Baade et al. 2012; Fig. 2). This result might be partially attributable to soil samples from the pre-dam facies with color characteristics similar to the post-dam facies but distinct grain size composition and P_{CAL} content (Fig. 4). Since the addition of LUM to a composite fingerprint containing grain size parameters and P_{CAL} content does not (significantly) improve classification results of the remaining samples, LUM is unlikely to be selected in the variable selection process. Moreover, it is conceivable that color differences between the facies are not fully expressed in LUM. Therefore, it might be worthwhile to test alternative color signatures in the future (Pulley and Rowntree 2016).

To some degree, all aforementioned sediment characteristics may be subject to post-sedimentary alteration. By comparison, grain size parameters are expected to be rather conservative as weathering is assumed to exert only a minor influence on the particle size of modern (<65 years old) reservoir deposits. Phosphorus cycling is likely intensified in reservoirs of the KNP due to the presence of wildlife (Masango et al. 2010) and may trigger the uptake (and release) of mobile phosphorus forms into (from) reservoir deposits (Søndergaard et al. 2003). Sediment color can be altered with changing redox conditions (Prokoph and Patterson 2004). However, pre-examinations on a 2 m long vertical sampling profile recovered from the Silolweni reservoir in 2008 (Baade et al. 2012) indicated a six times higher P_{CAL} content in the post-dam facies as compared to the underlying pre-dam facies, while less than 10% of the P_{CAL} fraction were found to be readily water soluble. Moreover, field observations revealed a rather uniform color of the post-dam facies and little evidence for color change apart from hydromorphic oxidation stains that were also found in the pre-dam facies. Thus, non-conservatism is not assumed to severely affect the usefulness of the investigated sediment properties in the current study. Summarizing these findings, the presented approach can be most probably successfully applied for the discrimination of facies in other reservoirs of the KNP.

5 Conclusions

This study highlights the potential of regression shrinkage methods for the discrimination of sedimentary facies in reservoirs and, more generally, for studies dealing with the discrimination and classification of soils and sediments. Within a set of sediment properties measurable with comparatively low expenditure, RLR identifies grain size parameters (Clay&Silt$_\%$, LMean, PSD$_{Dist}$, and LSort) and P_{CAL} content to be suitable sediment properties for the discrimination of the pre- and post-dam facies (Table 4 and Fig. 7) for all investigated reservoirs. A thorough validation of the RLR approach neglecting and taking into account a potential sampling bias reveals misclassification rates of 2 and $5 \pm 1\%$, respectively. Misclassification rates resulting from variable selection via stepwise DFA and subsequent classification with (predictive) LDA amount to 3 and $5 \pm 1\%$, respectively, and are therefore not significantly different ($p = 0.84$). This is remarkable, since classification with RLR is based on a 12% lower mean number of fingerprint properties. Since catchments of the investigated reservoirs mirror the heterogeneity of geological and pedological conditions in the southern KNP, the approach presented here most probably can be successfully applied for facies discrimination in other reservoirs.

Extending the method comparison to synthetic datasets violating and fulfilling the requirements of stepwise DFA (i.e., multivariate normality in each group and equal within-group covariance matrices) leads to approximately equal and slightly lower misclassification rates with stepwise DFA/LDA. Although the latter difference is significant ($p < 0.001$), it amounts only to $0.2 \pm 0.3\%$ by means of absolute values. At the same time, RLR results in a 52% lower mean number of fingerprint properties. Moreover, RLR-derived probabilities of group membership are a more reliable indicator for classification conclusiveness than posterior probabilities obtained from LDA, which is evident in significantly ($p < 0.001$) lower mean probability residuals of misclassified samples. Given the risk of suboptimal variable selection with stepwise DFA involving variables with spurious discriminatory power, we discourage its use for the identification of composite fingerprints. RLR appears to represent a reasonable alternative, especially when the requirements of stepwise DFA are not fulfilled. Testing RLR on empirical datasets with a higher number of tracers and groups would help to further elucidate the potential of the method.

References

Baade J, Schmullius C (2015) Catchment properties in the Kruger National Park derived from the new TanDEM-X intermediate digital elevation model (IDEM). Int Arch Photogramm Remote Sens Spat Inf Sci XL-7/W3:293–300

Baade J, Schmullius C (2016) TanDEM-X IDEM precision and accuracy based on a large assembly of differential GNSS measurements in Kruger National Park, South Africa. ISPRS J Photogramm 119: 496–508

Baade J, Franz S, Reichel A (2012) Reservoir siltation and sediment yield in the Kruger National Park, South Africa: a first assessment. Land Degrad Dev 23:586–600

Bates D, Mächler M (2016) Matrix: sparse and dense matrix classes and methods. R package version 1.2–6. http://cran.r-project.org/package=Matrix. Accessed 21 July 2016

Beaudette DE, Roudier P, O'Geen AT (2013) Algorithms for quantitative pedology: a toolkit for soil scientists. Comput Geosci 52:258–268

Ben-David S, Blitzer J, Crammer K, Kulesza A, Pereira F, Vaughan JW (2010) A theory of learning from different domains. Mach Learn 79: 151–175

Birks HJB (1987) Multivariate analysis in geology and geochemistry: an introduction. Chemometr Intell Lab 2:15–28

Brown MT, Tinsley HEA (1983) Discriminant analysis. J Leisure Res 15: 290–310

Carnes BA, Slade NA (1982) Some comments on niche analysis in canonical space. Ecology 63:888–893

Collins AL, Walling DE (2002) Selecting fingerprint properties for discriminating potential suspended sediment sources in river basins. J Hydrol 261:218–244

Collins AL, Zhang Y, McChesney D, Walling DE, Haley SM, Smith P (2012) Sediment source tracing in a lowland agricultural catchment in southern England using a modified procedure combining statistical analysis and numerical modelling. Sci Total Environ 414:301–317

Constanza MC, Afifi AA (1979) Comparison of stopping rules in forward stepwise discriminant analysis. J Am Stat Assoc 74:777–785

Cormen TH, Leiserson CE, Rivest RL, Stein C (2001) Introduction to algorithms, 2nd edn. The MIT Press, Cambridge, Massachusetts, p. 1191

D'Haen K, Verstraeten G, Dusar B, Degryse P, Haex J, Waelkens M (2013) Unravelling changing sediment sources in a Mediterranean mountain catchment: a Bayesian fingerprinting approach. Hydrol Process 27:896–910

Dinis P, Castilho A (2012) Integrating sieving and laser data to obtain bulk grain-size distributions. J Sediment Res 82:747–754

FAO (Food and Agriculture Organization of the United Nations) (2014) World reference base for soil resources 2014. International soil classification system for naming soils and creating legends for soil maps. World soil resources reports 106. FAO, Rome, p. 181

Fey M, Hughes J, Lambrechts J, Dohse T (2010) The soil groups: distribution, properties, classification, genesis and use. In: Fey M (ed) Soils of South Africa. Their distribution, properties, classification, genesis, use and environmental significance. Cambridge University Press, Cambridge, pp. 17–147

Flom PL, Cassell DL (2007) Stopping stepwise: why stepwise and similar selection methods are bad, and what you should use. NorthEast SAS Users Group (NESUG) Inc. 20th Annual Conference: 11-14th November 2007. NESUG, Baltimore, p 7

Foster IDL, Boardman J, Keay-Bright J (2007) Sediment tracing and environmental history for two small catchments, Karoo uplands, South Africa. Geomorphology 90:126–143

Friedman J, Hastie T, Tibshirani R (2010) Regularization paths for generalized linear models via coordinate descent. J Stat Softw 33:1–22

Geological Survey of South Africa (1986a) Geological series 1:250,000. Sheet 2430 Pilgrim's Rest. Government Printer, Pretoria, RSA

Geological Survey of South Africa (1986b) Geological series 1:250,000. Sheet 2530 Barberton. Government Printer, Pretoria, RSA

Gertenbach WPD (1980) Rainfall patterns in the Kruger National Park. Koedoe 23:35–43

Glotzbach C, Paape A, Baade J, Reinwarth B, Rowntree K, Miller J (2016) Cenozoic landscape evolution of the Kruger National Park as derived from cosmogenic nuclide analyses. Terra Nov. 28:316–322

Härdle WK, Simar L (2015) Applied multivariate statistical analysis, 4th edn. Springer, Berlin, p. 580. doi:10.1007/978-3-642-17229-8

Haregeweyn N, Poesen J, Nyssen J, de Wit J, Haile M, Govers G, Deckers S (2006) Reservoirs in Tigray (northern Ethiopia): characteristics and sediment deposition problems. Land Degrad Dev 17:211–230

Harrell FE (2001) Regression modeling strategies. With applications to linear models, logistic regression and survival analysis. Springer, New York, p. 568

Harrell FE, Lee KJ (1985) A comparison of the discrimination of discriminant analysis and logistic regression under multivariate normality. In: Sen PK (ed) Biostatistics: statistics in biomedical, public health, and environmental sciences. Elsevier, Amsterdam, pp. 333–343

Hartigan JA, Hartigan PM (1985) The dip test of unimodality. Ann Stat 13:70–84

Hastie T, Buja A, Tibshirani R (1995) Penalized discriminant analysis. Ann Stat 23:73–102

Hastie T, Tibshirani R, Friedman J (2009) The elements of statistical learning. Data mining, inference, and prediction, 2nd edn. Springer, New York, p. 745

Huberty CJ (1989) Problems with stepwise methods-better alternatives. In: Thompson B (ed) Advances in social science methodology, vol 1. JAI Press, Greenwich, pp. 43–70

Huberty CJ (1994) Applied discriminant analysis. Wiley & Sons, New York, p. 466

IBM (2013) IBM SPSS Statistics v22.0.0 documentation. http://www-01.ibm.com/support/knowledgecenter/SSLVMB_22.0.0/com.ibm.spss.statistics_22.kc.doc/pv_welcome.html. Accessed 25 January 2016

Jović A, Brkić K, Bogunović N (2015) A review of feature selection methods with applications. In: Biljanovic P, Butkovic Z, Skala K, Mikac B, Cicin-Sain M, Sruk V, Ribaric S, Gros S, Vrdoljak B, Mauher M, Sokolic A (eds) Proceedings of the 38th international convention on information on communication technology, electronics and microelectronics (MIPRO), May 25–29, 2015, Opatija, Croatia. IEEE, Rijeka, pp. 1200–1205

Korkmaz S, Goksuluk D, Zararsiz G (2014) MVN: an R package for assessing multivariate normality. The R Journal 6:151–162

Kraushaar S, Schumann T, Ollesch G, Schubert M, Vogel H-J, Siebert C (2015) Sediment fingerprinting in northern Jordan: element-correction factors in a carbonatic setting. J Soils Sediments 15:2155–2173

Krumbein WC (1936) Application of logarithmic moments to size frequency distributions of sediments. J Sediment Petrol 6:35–47

Laceby JP, McMahon J, Evrard O, Olley J (2015) A comparison of geological and statistical approaches to element selection for sediment fingerprinting. J Soils Sediments 15:2117–2131

MacFayden S, Hui C, Verburg PH, Van Teeffelen AJA (2016) Quantifying spatiotemporal drivers of environmental heterogeneity in Kruger National Park, South Africa. Landscape Ecol 31:2013–2029

Makalic E, Schmidt DF (2010) Review of modern logistic regression methods with application to small and medium sample size problems. In: Li Y (ed) AI 2010: advances in artificial intelligence. 23rd Australasian joint conference Adelaide, Australia, December 2010 proceedings. Springer, Berlin, pp. 213–222

Manjoro M, Rowntree K, Kakembo V, Foster I, Collins AL (2016) Use of sediment source fingerprinting to assess the role of subsurface erosion in the supply of fine sediment in a degraded catchment in the Eastern Cape, South Africa. J Environ Manag. doi:10.1016/j.jenvman.2016.07.019

Manly BFJ (2004) Multivariate statistical methods. A primer, 3rd edn. Chapman & Hall, Boca Raton, p. 224

Masango MG, Myburgh JG, Labuschagne L, Govender D, Bengis RG, Naicker D (2010) Assessment of microcystis bloom toxicity associated with wildlife mortality in the Kruger National Park, South Africa. J Wildlife Dis 46:95–102

Mateo-Sanz JM, Martínez-Balleste A, Domingo-Ferrer J (2004) Fast generation of accurate synthetic microdata. In: Domingo-Ferrer J, Torra V (eds) Privacy in statistical databases. Proceedings of the CASC project final conference, PSD 2004, Barcelona, Spain, June 9–11, 2004. Lecture notes in computer science 3050. Springer, Berlin, pp. 298–306

McCabe GP (1975) Computations for variable selection in discriminant analysis. Technometrics 17:103–109

McLaren P, Bowles D (1985) The effects of sediment transport on grain size distributions. J Sediment Petrol 55:457–470

Miller JR, Macklin G, Orbock Miller SM (2015) Application of geochemical tracers to fluvial sediment. Springer briefs in earth sciences. Springer, Cham, p. 142

Mills AJ, Fey MV (2004) Frequent fires intensify soil crusting: physicochemical feedback in the pedoderm of long-term burn experiments in South Africa. Geoderma 121:45–64

Morris GL, Fan J (1998) Reservoir sedimentation handbook. Design and management of dams, reservoirs, and watersheds for sustainable use. McGraw-Hill Book Co., New York, p. 810

Mucina L, Rutherford MC (2010) The vegetation of South Africa, Lesotho and Swaziland (CD set). Strelitzia 19. South African National Biodiversity Institute, Pretoria

Munita CS, Barroso LP, Oliveira PMS (2006) Stopping rule for variable selection using stepwise discriminant analysis. J Radioanal Nucl Ch 269:335–338

Murphy J, Riley JP (1962) A modified single solution method for the determination of phosphate in natural waters. Anal Chim Acta 27:31–36

Murtaugh PA (2009) Performance of several variable-selection methods applied to real ecological data. Ecol Lett 12:1061–1068

Oswald FL, Putka DJ (2015) Statistical methods for big data. A scenic tour. In: Tonidandel S, King EB, Cortina JM (eds) Big data at work. Data science revolution and organizational psychology. Routledge, New York. doi:10.13140/2.1.1907.2800

Palazón L, Latorre B, Gaspar L, Blake WH, Smith HG, Navas A (2015) Comparing catchment sediment fingerprinting procedures using an auto-evaluation approach with virtual sample mixtures. Sci Total Envrion 532:456–466

Partridge TC, Dollar ESJ, Moolman J, Dollar LH (2010) The geomorphic provinces of South Africa. Lesotho and Swaziland: a physiographic subdivision for earth and environmental scientists. T Roy Soc S Afr 65:1–47

Petersen R (2012) A conceptual understanding of groundwater recharge processes and surface- water/groundwater interactions in the Kruger NP. MSc Thesis, University of the Western Cape, Bellville, Cape Town, South Africa

Pienaar UDV (1985) Indications of progressive desiccation of the Transvaal Lowveld over the past 100 years, and implications for the water stabilization programme in the Kruger National Park. Koedoe 28:93–165

Press SJ, Wilson S (1978) Choosing between logistic regression and discriminant analysis. J Am Stat Assoc 73:699–705

Prokoph A, Patterson RT (2004) From depth scale to time scale: transforming sediment image color data into a high-resolution time series. In: Francus P (ed) Image analysis, sediments and paleoenvironments. Developments in Paleoenvironmental research 7. Kluwer Academic Publishing, Dordrecht, pp. 143–164

Pulley S, Rowntree K (2016) The use of an ordinary colour scanner to fingerprint sediment sources in the South African Karoo. J Environ Manag 165:253–262

Pulley S, Foster I, Antunes P (2015) The application of sediment fingerprinting to floodplain and lake sediment cores: assumptions and uncertainties evaluated through case studies in the Nene Basin, UK. J Soils Sediments 15:2132–2154

R Core Team (2014) R: a language and environment for statistical computing. R foundation for statistical computing. Vienna, Austria. http://www.R-project.org. Accessed 18 June 2014

Rausch DL, Heinemann HG (1984) Measurement of reservoir sedimentation. In: Hadley RF, Walling DE (eds) Erosion and sediment yield. Some methods of measurement and modelling. Geobooks, Norwich, pp. 179–200

Rencher AC, Larson SF (1980) Bias in Wilks' Λ in stepwise discriminant analysis. Technometrics 22:349–356

Royston JP (1983) Some techniques for assessing multivariate normality based on the Shapiro-Wilk W. J Roy Stat Soc C-App 32:121–133

Royston P (1992) Approximating the Shapiro-Wilk W-test for non-normality. Stat Comput 2:117–119

Russ JC, Russ JC (2008) Introduction to image processing and analysis. CRC Press, Boca Raton, p. 355

SAS Institute Inc. (2010) SAS/STAT® 9.22 user's guide. SAS Institute Inc., Cary, p. 8444

Schmengler AC, Vlek PLG (2015) Assessment of accumulation rates in small reservoirs by core analysis, ^{137}Cs measurements and bathymetric mapping in Burkina Faso. Earth Surf Proc Landf 40:1951–1963

Schüller H (1969) Die CAL-Methode, eine neue Methode zur Bestimmung des pflanzenverfügbaren Phosphates in Böden. Z Pflanz Bodenkunde 123:48–63

Sheriff SC, Franks SW, Rowan JS, Fenton O, Ó'hUallacháin D (2015) Uncertainty-based assessment of tracer selection, tracer non-conservativeness and multiple solutions in sediment fingerprinting using synthetic and field data. J Soils Sediments 15:2101–2116

Simpson GL, Birks HJB (2012) Statistical learning in palaeolimnology. In: Birks HJB, Lotter AF, Juggins S, Smol JP (eds) Tracking environmental change using lake sediments. Developments in paleoenvironmental research 5. Springer, Dordrecht, pp. 249–327

Small IF, Rowan JS, Duck RW (2003) Long-term sediment yield in Crombie reservoir catchment, Angus; and its regional significance within the Midland Valley of Scotland. Hydrolog Sci J 48:619–635

Søndergaard M, Jensen JP, Jeppesen E (2003) Role of sediment and internal loading of phosphorus in shallow lakes. Hydrobiologia 506-509:135–145

Stapor K (2015) Better alternatives for stepwise discriminant analysis. Acta Universitatis Lodziensis. Folia Oeconomica 311:9–15

Tabachnick BG, Fidell LS (2001) Using multivariate statistics, 4th edn. Allyn & Bacon, Needham Heights, p. 966

Tamene L, Park SJ, Dikau R, Vlek PLG (2006) Reservoir siltation in the semi-arid highlands of northern Ethiopia: sediment yield-catchment area relationship and a semi-quantitative approach for predicting sediment yield. Earth Surf Proc Landf 31:1364–1383

Thompson B (1989) Why won't stepwise methods die? Meas Eval Couns Dev 21:146–148

Thompson B (1995) Stepwise regression and stepwise discriminant analysis need not apply here: a guidelines editorial. Educ Psychol Meas 55:525–534

Tibshirani R (1996) Regression shrinkage and selection via the lasso. J Roy Stat Soc B 58:385–395

Tillé Y, Matei A (2015) Sampling: survey sampling. R package version 2.7. http://CRAN.R-project.org/package=sampling. Accessed on 20 May 2015

Tucker ME (2011) Sedimentary rocks in the field. A practical guide. The geological field guide series, 4th edn. John Wiley & Sons, Chichester, p. 275

van Zijl G, Le Roux P (2014) Creating a conceptual hydrological soil response map for the Stevenson Hamilton research supersite, Kruger National Park, South Africa. Water SA 40:331–336

Venables WN, Ripley BD (2002) Modern applied statistics with S, 4th edn. Springer, New York, p. 495

Venter FJ (1990) A classification of land for management planning in the Kruger National Park. PhD thesis, University of South Africa, Pretoria, p 392

Venter FJ, Scholes RJ, Eckhardt HC (2003) The abiotic template and its associated vegetation pattern. In: Du Toit JT, Rogers KH, Biggs HC (eds) The Kruger experience. Ecology and Management of Savanna Heterogeneity. Island Press, Washington, pp. 83–129

Viljoen M (2015) The Kruger National Park: geology and geomorphology of the wilderness. In: Grab S, Knight J (eds) Landscapes and landforms of South Africa. Springer, Heidelberg, pp. 111–120

Walling DE (2013) The evolution of sediment source fingerprinting investigations in fluvial systems. J Soils Sediments 13:1658–1675

Walling DE, Woodward JC (1995) Tracing sources of suspended sediment in river basins: a case study of the River Culm, Devon, UK. Mar Freshw Res 46:327–336

Walter K, Gunkel G, Gamboa N (2012) An assessment of reservoir reuse for sediment management of Gallito Ciego reservoir, Peru. Lakes and Reservoirs: Research and Management 17:301–314

Weihs C, Ligges U, Luebke K, Raabe N (2005) klaR analyzing German business cycles. In: Baier D, Decker R, Schmidt-Thieme L (eds) Data analysis and decision support. Springer, Berlin, pp. 335–343

Whitaker JS (1997) Use of stepwise methodology in discriminant analysis. Paper presented at the Annual Meeting of the Southwest Educational Research Association, Austin, TX, January, 1997. http://ericae.net/ft/tamu/STEPWIS.htm. Accessed 17 December 2015

Whittingham MJ, Stephens PA, Bradbury RB, Freckleton RP (2006) Why do we still use stepwise modelling in ecology and behaviour? J Anim Ecol 75:1182–1189

Wu B (2006) Differential gene expression detection and sample classification using penalized linear regression models. Bioinformatics 22:472–776

Zadrozny B (2004) Learning and evaluating classifiers under sample selection bias. In: Brodley CE (ed) Proceedings of the 21st international conference on machine learning, Banff, Canada, July 2004. ACM, New York, pp. 114–121

Zou H, Hastie T (2005) Regularization and variable selection via the elastic net. J Roy Stat Soc B 67:301–320

Chapter 4

Estimating the sediment trap efficiency of intermittently dry reservoirs: lessons from the Kruger National Park, South Africa

Authors: Bastian Reinwarth • Edward S. Riddell •
Christoph Glotzbach • Jussi Baade

Electronic supplementary material may be found in the appendix of this thesis.

Estimating the sediment trap efficiency of intermittently dry reservoirs: lessons from the Kruger National Park, South Africa

Bastian Reinwarth,[1]* [iD] Edward S. Riddell,[2,3] Christoph Glotzbach[4] [iD] and Jussi Baade[1] [iD]
[1] Department of Geography, Friedrich Schiller University, Jena, Germany
[2] Centre for Water Resources Research, University of KwaZulu-Natal, Scottsville, Pietermaritzburg, South Africa
[3] Conservation Management, South African National Parks, Skukuza, South Africa
[4] Department of Geosciences, University of Tübingen, Tübingen, Germany

*Correspondence to: Bastian Reinwarth, Department of Geography, Friedrich Schiller University, Löbdergraben 32, 07743 Jena, Germany. E-mail: bastian.reinwarth@uni-jena.de

Earth Surface Processes and Landforms

ABSTRACT: The assessment of sediment yield from reservoir siltation requires knowledge of the reservoir's sediment trap efficiency (TE). Widely used approaches for the estimation of the long-term mean TE rely on the ratio of the reservoir's storage capacity (C) to its catchment size (A) or mean annual inflow (I). These approaches have been developed from a limited number of reservoirs ($N \leq 40$), most of them located in temperate climate regions. Their general applicability to reservoirs receiving highly variable runoff such as in semi-arid areas has been questioned. Here, we examine the effect of ephemeral inflow on the TE of 10 small ($\leq 280 \times 10^3$ m^3), intermittently dry reservoirs located in the Kruger National Park. Fieldwork was conducted to determine the storage capacity of the reservoir basins. The frequency and magnitude of spillage events was simulated with the daily time step Pitman rainfall–runoff model. Different runoff scenarios were established to cope with uncertainties arising from the lack of runoff records and imperfect input data. Scenarios for the relationship between water and sediment discharge were created based on sediment rating curves. Taking into account uncertainties in hydrological modelling, uncertainties of mean TE estimates, calculated from all scenarios ($N = 9$), are moderate, ranging from ±6 to ±11% at the 95% confidence level. By comparison, estimating TE from the storage capacity to catchment area (C/A) ratio induces high uncertainty (ranges of 35 to 65%), but this uncertainty can be confined (15 to 33%) when the latter approach is combined with hydrological modelling. Established methods relying on the storage capacity to mean annual inflow (C/I) ratio most probably lead to an overestimation of the TE for the investigated reservoirs. The approach presented here may be used instead to estimate the TE of small, intermittently dry reservoirs in semi-arid climate regions. Copyright © 2017 John Wiley & Sons, Ltd.

KEYWORDS: reservoir siltation; sediment retention; episodic spillage; Pitman model; sediment rating curve

Introduction

Accounting for the sediment trap efficiency (TE) is fundamental to reservoir siltation studies targeting an assessment of contemporary sediment yield (e.g. Trimble and Bube, 1990; Verstraeten and Poesen, 2000; Baade *et al.,* 2012). TE is defined as the proportion of sediment delivered to a reservoir that is eventually deposited in the reservoir basin (Brown, 1944). Disregarding sediment that is transported across and discharged downstream may lead to a substantial underrating of the total sediment flux. Data for field-based TE determination is often not available. Thus, TE needs to be estimated from empirically derived equations or physically-based models (Trimble and Wilson, 2012). TE is controlled by the hydraulic retention time and net settling velocity of suspended sediment particles in the reservoir basin (Stabel, 1987). Therefore, it is subject to a variety of factors including runoff conditions, sediment dynamics, basin geometry, position and configuration of reservoir inlets and outlets, size and shape of sediment particles,

flocculation, sediment and water density, mixing of the water column, currents and turbulence, among others (e.g. Heinemann, 1984; Haan *et al.,* 1994). While physically-based models have been employed for the determination of the TE of small (≤ 1 ha) flood detention ponds (e.g. Wilson and Barfield, 1985; Verstraeten and Poesen, 2001; Takamatsu *et al.,* 2010), the long-term mean TE of larger reservoirs (> 1 ha) is usually predicted with empirical approaches due to the complexity of processes involved.

Several equations are available to assess the TE of 'normally ponded' (Brune, 1953) reservoirs where no provision of sediment sluicing or flushing is made (Sloff, 1991). Brown (1944) suggested TE prediction from the ratio of the reservoir's water storage capacity (C) to its catchment size (A) (see Table I for acronyms used in this study). This method is attractive, because of low data requirements (Butcher *et al.,* 1992), but induces high uncertainty for reservoirs with low C/A ratio, if no further information on runoff dynamics and sediment characteristics is available (Verstraeten and Poesen,

Chapter 4

Table I.   Alphabetical list of acronyms used in this study

Acronym	Description
a	coefficient of the sediment rating curve (Equation (8))
A	reservoir catchment size
APE	mean annual American class A-pan evaporation
A_R	full supply area of the reservoir
ASR	initial area–storage relationship of the reservoir basin
b	exponent of the sediment rating curve (Equation (8))
C	water storage capacity (unspecified)
Cl95	two-tailed 95% confidence level
C_M	mean water storage capacity
C_R	initial water storage capacity
d	index for a specific day
D	dimensionless parameter used in Equation (13) that may range between 0.0046 and 1
d_{soil}	soil thickness
d_{vadose}	thickness of the vadose zone
DTM	digital terrain model
E_d	evaporation from the reservoir's water surface at a day d
FLA_d	flooded area within the reservoir basin at a day d
F_{soil}	factor accounting for vertical variations in the effective soil porosity
GNSS	global navigation satellite system
HSR	initial height–storage relationship of the reservoir basin
I	mean annual inflow
I_d	volume of water flowing into the reservoir at a day d
KNP	Kruger National Park
L	over-water distance from the main reservoir inlet to the outlet
LRP	local reference point
MAE	mean annual Symon's pan evaporation
MAP	mean annual precipitation
MAR	mean annual catchment runoff
P_d	precipitation on the reservoir's water surface at a day d
PI	total size of the interception storage
PI_{BC}	size of the interception storage of grass and litter between the woody plant canopy
PI_C	size of the interception storage of the woody plant canopy
PI_{UC}	size of the interception storage of grass and litter under the woody plant canopy
POR	effective soil porosity
Q_{best}	best estimate runoff scenario
Q_d	mean catchment runoff at day d
QDR	quaternary drainage region
Q_{high}	high runoff scenario
Q_{low}	low runoff scenario
Qs	total mass of sediment entering the reservoir
Qs_d	fluvial sediment delivery from the catchment at day d
RMSE	root mean square error
RTK	real-time kinematic
SANParks	South African National Parks
SC_d	mean sediment concentration in water flowing into the reservoir at a day d
S_d	water volume stored in the reservoir basin at a day d
$\hat{S}_d$	storage state of the reservoir (i.e. the stored volume of water and sediment) at a day d
SM	total mass of reservoir deposits
SPILL	mean annual reservoir spillage
$SPILL_d$	volume of spilled water at a day d
ST	maximum soil storage, i.e. the sum of ST_{soil} and ST_{vadose}
STO	storativity of the vadose zone
ST_{soil}	water storage capacity of the soil
ST_{vadose}	water storage capacity of the vadose zone
SV_d	sediment volume (reservoir deposits) stored in the reservoir basin until a day d
T_C	year of dam construction
TE	sediment trap efficiency (unspecified)
TE_B	mean trap efficiency according to Equation (13) from Brown (1944)
$TE_{C,d}$	trap efficiency at a day d calculated with Equation (10) from US Army Corps of Engineers (1995)
TE_d	adjusted trap efficiency at a day d calculated with Equation (11)
TE_H	mean trap efficiency according to Equation (14) from Heinemann (1981)
$TE_{H,\,fit}$	mean trap efficiency according to Equation (15), i.e. a modification of Heinemann's (1981) equation
TE_{sim}	mean trap efficiency calculated with Equation (12) based on the simulated water and sediment flux
TIN	triangular irregular network
TLS	terrestrial laser scanner
T_S	year of surveying or dam decommissioning
V_S	volume of reservoir deposits that accumulated until the year of surveying
WCOV	mean fractional woody cover of the reservoir catchment

Note: Please refer to Table VI for an overview on parameters of the daily time step Pitman model.

2000). Presuming the availability of runoff data, Brune (1953) proposed an alternative method based on the ratio of the water storage capacity to the mean annual inflow (I). Later, Brune's method was revised by Heinemann (1981) for the application to small reservoirs ($< 4000 \times 10^3 \, \text{m}^3$). Churchill (1948) suggested TE prediction from a sedimentation index, which was calculated from the water storage capacity, inflow rate and mean flow velocity through the reservoir.

All aforementioned methods were developed from a limited number of reservoirs ($N \leq 40$), most of them located in temperate climate regions of the eastern United States. Their general applicability to reservoirs in semi-arid regions receiving seasonally variable runoff has been questioned (Lewis et al., 2009). Depending on their design and operation, high net evaporation loss and intermittent inflow may lead to prolonged periods without outflow (Haregeweyn et al., 2006), while storm events might result in spillage significantly contributing to the overall sediment discharge (Faithful and Griffiths, 2000). Lewis et al. (2013) demonstrated that the TE of the large Burdekin Falls Dam (storage capacity: $1.9 \times 10^9 \, \text{m}^3$), located in the tropical summer rainfall zone of northeast Australia, was overestimated by the standard Brune and Churchill equations and that estimates could be improved by considering daily discharge rather than annual or long-term mean inflow. So far, little effort has been made to investigate the appropriateness of established empirical approaches to estimate the TE of small reservoirs with variable and peaked hydrographs (Lloyd et al., 1998).

Here, we examine the effect of variable inflow on the TE of small intermittently dry reservoirs with ungauged catchments located in the southern Kruger National Park (KNP) (South Africa). The aim of this study is to establish a methodological approach for the estimation of the long-term mean TE of small reservoirs with ephemeral spillage. Within the framework of an ongoing study on contemporary and millennial scale erosion rates in the KNP (Baade and Schmullius, 2015, 2016; Glotzbach et al., 2016; Reinwarth et al., 2017), we surveyed intermittently dry reservoirs in order to quantify reservoir

siltation and average sediment yield throughout the past 30 to 80 years. For selected reservoirs ($N = 10$), the frequency and magnitude of spillage events, associated sediment discharge and the long-term mean TE of the investigated reservoirs are assessed for various scenarios based on results from fieldwork and hydrological modelling. Resulting TE estimates are then compared with TE values that were determined with the approaches of Brown (1944) and Heinemann (1981). The paper is organized as follows: the section on materials and methods starts with a description of the study area and investigated reservoirs. Then, methods involved in fieldwork, pre-processing of input data, the structure and calibration of the hydrological model and the set-up of scenarios are described. Afterwards, the methodological framework for TE estimation based on daily inflow and outflow data is presented. Modelling results and trap efficiency estimates are reported and associated uncertainties are discussed.

Materials and Methods

Study area and site descriptions

The KNP covers approximately $19\,500 \, \text{km}^2$ of undulating Lowveld savanna set aside for wildlife conservation just over a century ago (Joubert, 1986). It is located in the northeast of the Republic of South Africa (Figure 1a) between the Great Escarpment to the west and the coastal plains of Mozambique to the east. The climate in the study area is semi-arid with $>85\%$ of rainfall occurring between October and April (Venter et al., 2003). Mean annual precipitation (MAP) ranges from $500 \, \text{mm}$ in the north and east to $800 \, \text{mm}$ in the southwest (Figure 1b). Evaporation rates are recorded with Symon's pans and American class A-pans (Table II). In this study, evaporation always refers to Symon's pan evaporation, unless stated otherwise. Average daily evaporation varies from $2 \, \text{mm} \, \text{d}^{-1}$ in June/July to $6 \, \text{mm} \, \text{d}^{-1}$ in December/January (Department of
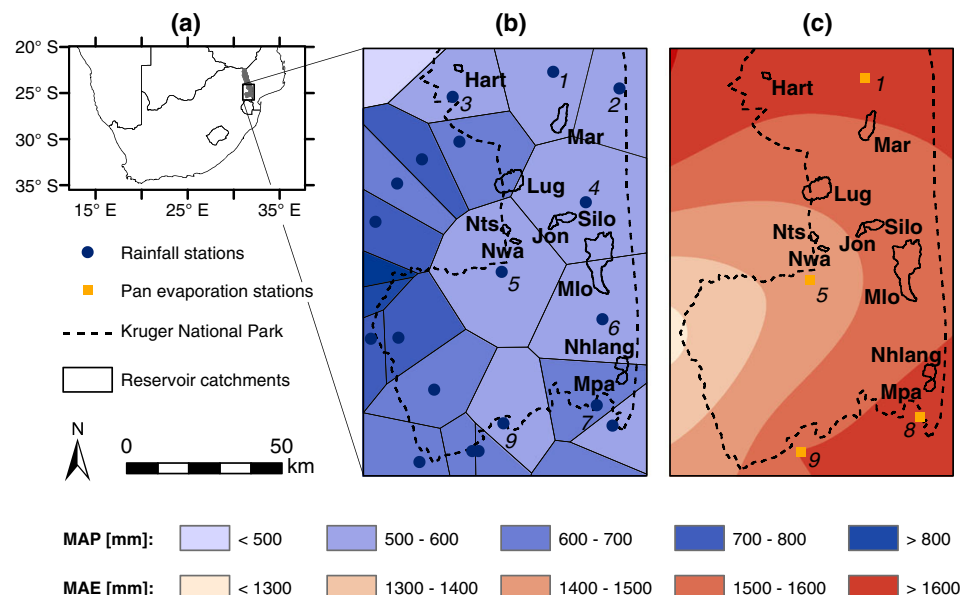
Figure 1. Catchments of investigated reservoirs ($N = 10$) within the southern Kruger National Park (KNP) and meteorological conditions in the study area: (a) the location of the KNP within southern Africa; (b) rainfall stations in the vicinity of the southern KNP and corresponding Thiessen polygons depicting mean annual precipitation (MAP); (c) meteorological stations recording pan evaporation (Symon's pan or A-pan) and interpolated mean annual Symon's pan evaporation (MAE). Meteorological stations from which data were used in the hydrological modelling are numbered (see Table II). Reservoir catchments (see Table III) are shown according to Baade and Schmullius (2015). Rainfall and evaporation data were taken from Department of Water Affairs (2008). [Colour figure can be viewed at wileyonlinelibrary.com]

Table II. Mean annual precipitation (MAP) and mean annual Symon's pan evaporation (MAE) recorded at meteorological stations in the vicinity of the Kruger National Park, measurement periods, and percentage of data gaps

ID	Station	Code	Precipitation			Evaporation			
			Period	MAP (mm)	Gaps (%)	Period	Type	MAE (mm)	Gaps (%)
1	Satara	SAT	1932–2016	530 ± 40	6	1961–1993	S	1640 ± 40	34
2	Nwanetsi	NWA	1966–2016	520 ± 60	1	—	—	—	—
3	Kingfisherspruit	KFI	1956–2016	560 ± 50	1	—	—	—	—
4	Tshokwane	TSH	1944–2016	550 ± 40	1	—	—	—	—
5	Skukuza	SKZ	1911–2016	550 ± 40	6	1960–2009	A/S	1420 ± 30	12
6	Lower Sabie	OSA	1968–2016	590 ± 70	17	—	—	—	—
7	Crocodile Bridge	KRO	1938–2016	610 ± 40	1	—	—	—	—
8	Tenbosch	TEN	NA	NA	NA	1968–1980	A	1650 ± 90	40
9	Mhlati	MHL	1968–1988	560 ± 130	26	1968–1998	S	1610 ± 30	36

Note: Daily rainfall data were provided by SANParks Scientific Services, Skukuza. Monthly evaporation data were taken from Department of Water Affairs (2008). Mean annual evaporation rates that were recorded with American class A-pans (i.e. Type A) were converted to mean annual Symon's pan (i.e. Type S) evaporation rates after Bosman (1990). Uncertainties of MAP and MAE correspond to the two-tailed 95% confidence level. NA, not available.

Water Affairs, 2008). Mean annual evaporation (MAE) ranges from 1300 mm in the southwest to 1700 mm in the north and southeast (Figure 1c). Actual mean annual evapotranspiration is in the order of 450 mm to 700 mm (Ramoelo *et al.,* 2014; van Eekelen *et al.,* 2015). Climatic conditions are reflected in the flow regimes of the rivers within the region. A few major streams with headwaters in the Great Escarpment exhibit perennial flow, but tributaries emanating from areas within the KNP are characterized by ephemeral runoff (O'Keeffe and Rogers, 2003). Hydrological connectivity within catchments varies temporarily depending on antecedent soil moisture conditions, whilst groundwater interactions can have a distinct local influence on the flow duration of ephemeral streams (Riddell *et al.,* 2014). Overland flow and run-off generation is typically caused by isolated rainfall events (Cullum and Rogers, 2011) or recurrent rain associated with tropical low-pressure systems (Dyson and van Heerden, 2001). Major regional flood events occurred in February 1977 (Pienaar, 1985), February 2000 (Christie and Hanlon, 2001; Heritage *et al.,* 2001; Smithers *et al.,* 2001) and January 2012 (Heritage *et al.,* 2014; Fitchett *et al.,* 2016) in the study area. Minor regional floods were observed in January 2013 and March 2014.

More than 50 small reservoirs were established in the KNP prior to 1975 to ensure water supply for wildlife during the dry season (Pienaar, 1985). Uncontrolled overflow spillways with trapezoidal or rectangular cross-sections and a width of ≥10 m permit the release of infrequent storm discharge. These spillways represent the only outlets, so that discharge to downstream reaches is restricted to spillage events, when reservoir storage capacity is exceeded. High evaporation rates lead to strong water level fluctuations and occasional drying up of the reservoirs (Figure 2). Black silt loams (according to the Food and Agriculture Organization for the United Nations, 2014) have accumulated in the deepest parts of the reservoir basins (Reinwarth *et al.,* 2017) where up to 60 cm deep footprints of large mammals (e.g. elephants and hippopotamus) provide evidence for strong bioturbation. Bedload from tributaries is deposited in backwater reaches and close to tributary inlets.

This study is based on the Hartbeesfontein, Marheya, Lugmag, N'tswiriri, Jones-Se, Silolweni, N'wanetsana, Mlondozi, Nhlanganzwani and Mpanamana reservoirs that were established between 1950 and 1970 with initial storage capacities ranging from 5 to 280×10^3 m³. With the exception of the Mlondozi reservoir that has an up to 4 m high concrete wall, all reservoirs are impounded by earth dams. The Nhlanganzwani, Silolweni, Lugmag, and N'wanetsana, reservoirs were decommissioned in 2007, 2008, 2012 and 2014, respectively. All other reservoirs are still in use. Two dam failures occurred at the Mpanamana reservoir prior to 1971 when the dam was finally repaired (Baade *et al.,* 2012) and the Lugmag dam was damaged during a flood in 2012 and not repaired. No dam failures are known for the other investigated reservoirs. The catchments vary in size from 3.2 to 104.2 km² and are characterized by different geological conditions as shown in Table III. Granite, gneiss, rhyolite and sedimentary rocks promote rather dense bush and shrub savanna, while basalt and gabbro support open tree savanna and grassland (Venter, 1990). The mean fractional woody cover of the catchments varies from 16 to 41% (Bucini *et al.,* 2010). Unfortunately, runoff data is not available for any of the catchments.

Surveying and sediment mapping in reservoir basins

Fieldwork was carried out in dried out reservoir basins and involved surveying of the reservoir basins and volumetric mapping of reservoir deposits. High-resolution surveying was conducted along transects with a real-time kinematic (RTK) global navigation satellite system (GNSS) using a LEICA GS10 base station and a GS15 rover (Baade and Schmullius, 2016). The survey point density was enhanced at the spillways and at transition points in the terrain (e.g. the dam, shoreline notches, banks of tributaries). Local reference points (LRPs) were established to ensure accurate merging of survey data

Figure 2. Water level fluctuations in the Mlondozi Reservoir. The reservoir is close to full stage in (a) February 2014. The maximum water depth is about 1.8 m and the width of the water surface in the foreground is about 150 m. The water level is considerably lower in (b) September 2015. Black reservoir deposits are exposed in (c) early March 2016 when the reservoir basin is dry. [Colour figure can be viewed at wileyonlinelibrary.com]

Table III. Catchment characteristics of investigated reservoirs

ID	Reservoir	QDR	Catchment area	Rainfall station	MAE	Woody cover	Lithology
			(km^2)		(mm)		
Hart	Hartbeesfontein	B73F	4.3 ± 0.3	KFI (100%)	1640 ± 110	0.41	Granite/Gneiss (65%) Gabbro (35%)
Mar	Marheya	X40B	27.5 ± 0.3	SAT (100%)	1600 ± 90	0.23	Basalt (54%) Sandstone (46%)
Lug	Lugmag	X40C	47.4 ± 0.2	TSH (85%) SKZ (15%)	1540 ± 110	0.40	Granite/Gneiss (100%)
Nts	N′tswiriri	X32J	5.5 ± 0.1	SKZ (100%)	1510 ± 100	0.36	Granite/Gneiss (100%)
Jon	Jones-Se	X33A	6.2 ± 0.1	TSH (100%)	1500 ± 110	0.41	Granite/Gneiss (100%)
Silo	Silolweni	X40D	13.2 ± 0.7	TSH (100%)	1510 ± 110	0.50	Ecca group (54%) Granite/Gneiss (46%)
Nwa	N′wanetsana	X32J	3.2 ± 0.1	SKZ (100%)	1500 ± 90	0.40	Granite/Gneiss (100%)
Mlo	Mlondozi	X33C	104.2 ± 0.8	TSH (59%) OSA (41%)	1550 ± 120	0.16	Basaltic rocks (88%) Rhyolite/Granophyre (12%)
Nhlang	Nhlanganzwani	X33D	16.5 ± 0.8	KRO (58%) OSA (42%)	1580 ± 90	0.30	Basaltic rocks (50%) Rhyolite/Dacite (50%)
Mpa	Mpanamana	X24H	10.0 ± 0.8	KRO (100%)	1580 ± 100	0.30	Rhyolite/Dacite (54%) Basaltic rocks (46%)

Note: quaternary drainage region (QDR; Pitman and Bailey, 2015); catchment area (±2σ uncertainty; Baade and Schmullius, 2015), closest rainfall station (for station codes, see Table II) with areal percentage of the corresponding Thiessen polygon on the reservoir catchment; mean annual Symon's pan evaporation (MAE ± standard prediction error) obtained from interpolation between meteorological stations (Department of Water Affairs, 2008) via ordinary kriging; mean fractional woody cover (Bucini *et al.*, 2010); and catchment lithology (Geological Survey of South Africa, 1986a, 1986b).

acquired on different days. Post-processing of GNSS data was conducted with the software LEICA Geo Office (version 8.4; LEICA Geosystems, 2014). The Hartbeesfontein, N′tswiriri, Jones-Se, Mlondozi and Mpanamana reservoirs were surveyed with a terrestrial laser scanner (TLS; Riegl VZ-1000). Panorama scans with a range of 450 m and an angular resolution of 0.040° in vertical and horizontal dimension were conducted from several positions to minimize data gaps from occlusion. Absolute geo-referencing was based on tie points surveyed with the RTK GNSS. Point clouds were merged and processed with the software RiScan Pro 2.3 (Riegl, 2016) which involved the removal of non-surface points (e.g. vegetation) through the application of the RiScan Pro 2.3 terrain filter. Mean position errors (1σ) of GNSS and TLS survey points amount to ≤2 cm (Baade and Schmullius, 2016).

The initial surface of the reservoir basins was reconstructed based on up to 60 depth soundings per reservoir from which the thickness of the reservoir deposits was determined. They were carried out with a Pürckhauer type soil auger (1.5 m; $\varnothing$: 18 mm) and with a gouge auger (3.4 m; $\varnothing$: 12 mm). The depth soundings were performed along profiles running parallel to the dam and their position was recorded using RTK GNSS measurements. The boundary between the pre- and post-dam facies was identified based on variations in colour and grain size (Baade *et al.*, 2012). The validity of this visual identification of the boundary has been verified based on statistical analysis of 250 samples and their physiochemical properties (Reinwarth *et al.*, 2017).

Digital terrain models (DTMs) and characterization of reservoir basins

Two digital terrain models (DTMs) were compiled for each reservoir using the software ArcGIS 10.2 (Environmental Systems Research Institute, 2013). The first DTM was generated based on the RTK GNSS readings and represents the present sediment surface of the reservoir basin. The second DTM

shows a reconstruction of the initial surface before the accumulation of reservoir deposits commenced, and was created by combining data from the RTK GNSS survey and depth soundings, i.e. by subtracting the thickness of the reservoir deposits from the altitude of the present sediment surface. Both DTMs were derived by triangular irregular network (TIN) interpolation between survey points. Along-profile and along-thalweg breaklines were used to enhance the resulting DTMs that were converted to raster grids with a cell size of 0.5 m × 0.5 m. The flooded area at full stage (A_R), the initial water storage capacity (C_R) in the year of dam construction (T_C) as well as the storage capacity in the year of surveying (T_S) were determined assuming a height accuracy of ±2.5 cm for the elevation of the overflow spillway, and a mean random error of ±2.5 cm in the determination of the sediment thickness for the area covered with reservoir deposits. The volume of reservoir deposits (V_S) that accumulated until the survey date was calculated from the difference of the initial and present-day storage capacity. The raster cells within the full supply area were extracted to obtain functions that describe the relationship between the flooded area, the water level and the storage state of the reservoir. These functions were compiled with the 'raster' package (Hijmans, 2014) of the software R (version 3.1.1; R Core Team, 2014) and are subsequently referred to as area–storage relationships (ASR) and height–storage relationships (HSR).

The over-water distance (L) from the inlet of the main tributary to the reservoir outlet was determined with the Cost Distance tool of the Spatial Analyst extension in ArcGIS 10.2. This tool calculates distances along paths over a cost raster based on the weighted quasi-Euclidean chamfer metric that is defined for a neighbourhood of 3 × 3 raster pixels (cf. Verwer, 1991). Distances of paths are weighted according to pixel values of the cost raster. Values of 1 and 10 000 were assigned to pixels being located within and outside the full supply area of the reservoir, respectively. The value of 10 000 is arbitrary, but sufficiently high to avoid distance determination along

paths crossing the shoreline. Since the utilized chamfer metric slightly overestimates the true (Euclidean) distance (de Smith, 2004), all chamfer distances were multiplied with the scaling factor 0.95 which yields unbiased distances with a 2σ error of 6% (Vossepoel, 1988). Characteristics of the investigated reservoir basins are summarized in Table IV.

Parameterization of the daily time step Pitman rainfall–runoff model

Rainfall–runoff modelling was conducted with the daily time step Pitman rainfall–runoff model (Pitman, 1976) which is a conceptual hydrological model involving 11 parameters for calibration. It is a further development of an earlier monthly time step model with a very similar model structure (Pitman, 1973, cited in Hughes, 2013a). The monthly Pitman model is employed within water resource assessments for South Africa, Lesotho and Swaziland that are carried out on the scale of quaternary drainage regions (QDRs; originally defined by Midgley and Pitman, 1969, cited in Pitman, 2011), i.e. principal water management units $>50\,km^2$ (Hughes, 2004). Within the framework of these assessments parameter sets have been regionalized and were applied to ungauged catchments (Kapangaziwiri, 2011; Hughes, 2013b). The nearly identical model structure allows for the transfer of selected parameter

values from the calibrated monthly model to the daily version of the Pitman model (Bailey, 2015).

The daily Pitman model incorporates interception, soil moisture and groundwater storages and calculates daily runoff from mean monthly Symon's pan evaporation, daily and monthly rainfall time series and catchment area (Figure 3). For each day of rainfall, the model assumes an S-shaped cumulative rainfall distribution and a linear relationship between the duration of the rainfall event and the total daily rainfall depth. The size of the interception storage is defined by the parameter PI. Surface runoff is generated from impervious surfaces and from infiltration excess. The proportion of impervious surfaces to the total catchment area is described by the parameter AI. Spatial variability of the infiltration capacity on non-impervious surfaces is represented by a symmetrical triangular distribution function where the parameters ZMINN and ZMAXN denote the nominal minimum and maximum catchment absorption rate, respectively (for details see Pitman, 1976). The infiltration capacity is adjusted depending on the ratio of the simulated instantaneous soil moisture state to the maximum soil storage (ST). The relationship between actual evaporation, potential evaporation and soil moisture state is controlled by the parameter R that may range between 0 and 1; whereby catchment evaporation is assumed to equal potential evaporation rates, when the soil moisture deficit is zero. In addition,

Table IV. Characteristics of the investigated reservoirs

Reservoir	T_C	T_S	Survey	C_R	V_S	A_R	L
				$(\times 10^3\,m^3)$	$(\times 10^3\,m^3)$	(ha)	(m)
Hartbeesfontein	1950	2015	TLS/GNSS	39.9 ± 0.8	9.76 ± 0.37	3.04 ± 0.06	270 ± 20
Marheya	1970	2014	GNSS	106.9 ± 1.9	6.33 ± 0.73	6.76 ± 0.07	660 ± 40
Lugmag	1957	2012[a]	GNSS	156.7 ± 3.1	13.78 ± 0.74	11.97 ± 0.13	880 ± 50
N'tswiriri	1960	2016	TLS/GNSS	11.6 ± 0.2	1.70 ± 0.06	0.95 ± 0.02	260 ± 20
Jones-se	1957	2015	TLS/GNSS	27.5 ± 0.7	3.12 ± 0.34	2.35 ± 0.07	290 ± 20
Silolweni	1969	2008[a]	GNSS	162.3 ± 3.1	17.37 ± 1.38	11.19 ± 0.12	840 ± 50
N'wanetsana	1960	2014[a]	GNSS	5.1 ± 0.2	1.33 ± 0.08	0.56 ± 0.01	110 ± 10
Mlondozi	1951	2016	TLS/GNSS	140.3 ± 2.2	33.88 ± 1.33	9.77 ± 0.16	1040 ± 60
Nhlanganzwani	1956	2007[a]	GNSS	279.4 ± 4.1	22.89 ± 0.97	15.98 ± 0.26	820 ± 50
Mpanamana	1957/1971[b]	2016	TLS/GNSS	101.2 ± 2.1	28.48 ± 0.74	7.95 ± 0.18	390 ± 20

Note: year of dam completion (T_C), year of survey or decommissioning (T_S), survey type (Survey), initial storage capacity (C_R), i.e. in the year of dam completion, volume of reservoir deposits (V_S) that accumulated until in the year of survey or decommissioning, full supply area (A_R) and over water-distance (L) from the main reservoir inlet to the outlet. Uncertainties of C_R, V_S and A_R correspond to the 95% confidence level. For L, the 2σ error is reported. T_C is given according to Pienaar (1985) and Kloppers and Bornman (2005).
[a]The year of decommissioning is indicated.
[b]The Mpanamana Dam was initially constructed in 1957 and finally repaired in 1971 after two dam failures.
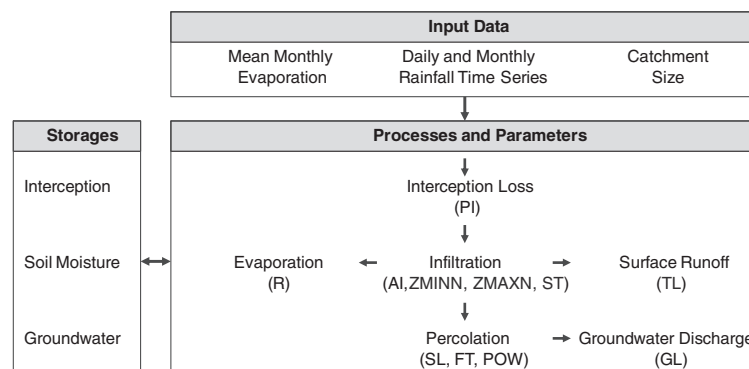
Figure 3. Scheme of the daily time step Pitman rainfall–runoff model. Abbreviations in brackets denote parameters that may be adjusted for model calibration (after Pitman, 1976).

groundwater discharge may contribute to the simulated runoff. A power relationship between the soil moisture state and groundwater recharge is supposed, which depends on the maximum soil storage (ST) that includes the storage capacity in the vadose zone (Kapangaziwiri, 2011), a threshold SL defining the soil moisture content below which no percolation occurs, the parameter FT representing the percolation rate at soil moisture equal to ST, and an exponent POW (Pitman, 1976). The lag of surface runoff and groundwater discharge is controlled by the parameters TL and GL, respectively (Pitman *et al.,* 2015).

Description of the reservoir water balance model

The occurrence and magnitude of spillage events was simulated with a modified version of the reservoir water balance model by Hughes (1992) (Figure 4). Volumetric changes in the reservoir water storage governed by inflow, precipitation and evaporation were calculated with daily resolution by applying Equation (1). Potential groundwater supply, seepage and water abstraction by animals were neglected.

$$S_{d+1} = S_d + I_d + P_d - E_d - SPILL_d \qquad (1)$$

S_d (in m^3) is the water volume stored in the reservoir basin at a day d; I_d (in m^3) refers to the daily inflow that is calculated with the Pitman model; P_d (in m^3) and E_d (in m^3) correspond to rainfall and evaporation on and from the water surface, respectively; and $SPILL_d$ (in m^3) represents uncontrolled spillage that occurs only, if S_d exceeds the water storage capacity of the reservoir. Thus, P_d and E_d depend on the extent of the flooded area (FLA$_d$ in m^2) in the reservoir basin. FLA$_d$, P_d and E_d equal zero, if the reservoir is dried-out at the beginning of the day d (i.e. $S_d = 0$). Otherwise, FLA$_d$ is calculated with the reservoir-specific area–storage function ASR (Equation (2)) based on the current storage state ($\hat{S}_d$ in m^3) that is defined as the sum of the stored water (S_d in m^3) and the sediment volume (SV$_d$ in m^3).

$$FLA_d = ASR\left(\hat{S}_d\right) = ASR(S_d + SV_d) \qquad (2)$$

The accumulation of sediment throughout the lifetime of the reservoir is approximated by assuming a proportional increase of the cumulative volume of sediment and inflowing water. This approach is related to the 'double mass' concept (Rooseboom and Annandale, 1981) that presumes a linear relationship between cumulative river discharge and cumulative sediment delivery on decadal or longer timescales for stationary climate and catchment conditions (Walling and Fang,

2003). The cumulative sediment volume was scaled with respect to the mapped sediment volume (Table IV). Sediment compaction is neglected since studied reservoir deposits show little variation in dry bulk density with increasing sediment depth (Baade *et al.,* 2012, and unpublished data from this study).

Meteorological input data for hydrological modelling

Daily rainfall time series from meteorological stations within the KNP were provided by the South African National Parks (SANParks) Scientific Services, Skukuza. From this data, rainfall time series for the reservoir catchments were interpolated based on Thiessen polygons (Figure 1b). Gaps in the time series (Table II) were filled with data from the rainfall station being closest to the respective reservoir catchment among all stations providing records for the corresponding time period. Mean monthly evaporation was compiled from monthly evaporation time-series available for four stations (Department of Water Affairs, 2008; Figure 1c). For stations providing American class A-pan evaporation values, mean annual A-pan evaporation (APE in mm) was converted to mean annual Symon's pan evaporation (MAE in mm) with Equation (3) after Bosman (1990).

$$MAE = \frac{APE - 26.3622}{1.0786} \qquad (3)$$

The MAE for the reservoir catchments was interpolated by ordinary kriging using a spherical semivariogram model that was optimized via leave-one-out cross-validation. Finally, the fractional contribution of individual months to the mean annual evaporation, recorded at the nearest meteorological station, was multiplied with the interpolated MAE to obtain mean monthly Symon's pan evaporation rates for the reservoir catchments.

Assessment of historical storage states

In the absence of runoff data, the coupled Pitman rainfall–runoff and reservoir water balance model was calibrated against reservoir storage state observations. These observations include direct observations on the days of fieldwork, when the reservoirs were usually completely dry. Further information was derived from aerial photographs of the National Geospatial Information (NGI) database (NGI, 2016) operated by the Department of Rural Development and Land Reform, South Africa, and high-resolution satellite images (Quickbird-2, GeoEye-1, Worldview-2 and Pléiades 1A) available from Google Earth® (Table V). Aerial photographs and satellite
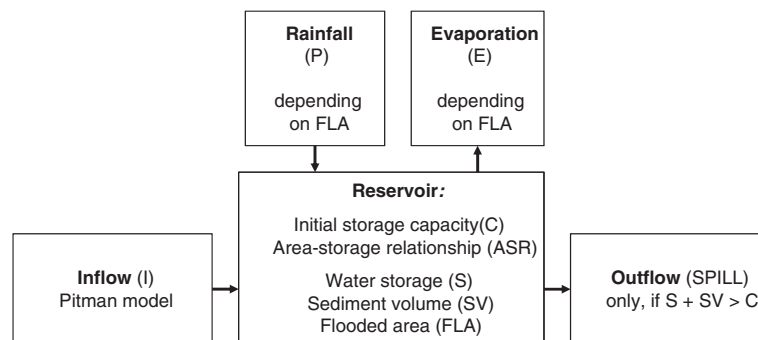
Figure 4. Scheme of the reservoir water balance model (after Hughes, 1992, modified).

images were co-registered on orthorectified aerial images (scale: 1:10 000) acquired between 2008 and 2010. Water levels (in metres above sea level) were determined by digitizing the extent of water surfaces and comparing them with the DTM representing the reservoir basin in the year of dam completion. Water levels were converted to storage states ($\hat{S}_d$) by means of the height–storage relationship (HSR). The entire procedure was repeated three times for each image and mean values of $\hat{S}_d$ with uncertainty bounds were determined. Uncertainty bounds correspond to the two-tailed 95% confidence level (CI95) and were calculated based on Student's *t*-distribution.

Calibration of the hydrological model based on empirically derived storage states and catchment characteristics

Most parameters of the hydrological model (Table VI) were set by taking into account catchment characteristics and results of recent water resource assessments (Pitman and Bailey, 2015; Sami, 2015). Parameter values of AI, SL, *R* and POW were taken

from parameter sets provided by Pitman and Bailey (2015) for the corresponding quaternary drainage regions. The parameter FT was set to the minimum value of 0.01 mm d^{-1}, which is recommended for ephemeral rivers (Pitman, 1976). The parameter TL that governs the lag of surface runoff was set to zero days, since peak river discharge most probably occurs within less than four hours after heavy rainfall events given the rather small size of the reservoir catchments (Schmidt and Schulze, 1984). Different scenarios were adopted for the parameter GL that controls the lag of groundwater discharge. Diminishing the GL value leads to an increase in simulated maximum daily flows associated with runoff events, but has very little influence on simulated total runoff volumes and water level fluctuations. Modelling results from Pitman (1976) suggest that GL typically ranges from one to six days with a median value of three days, while hydrological studies within the KNP (Riddell *et al.,* 2014) point to GL values varying between one and three days. Thus, different scenarios with GL values varying between one and three days were tested.

The parameter PI was estimated with Equation (4) after Yu and D'Odorico (2014) where WCOV denotes the mean fractional woody cover of the reservoir catchments (Table III; Bucini *et al.,* 2010), PI$_C$ (in millimetres) is the size of the interception storage of the woody plant canopy, and PI$_{UC}$

Table V. Overview on the number of aerial images, satellite images and field observations available to this study to determine historical storage states of investigated reservoirs

Type	Aerial image		Satellite image				Field observation		Total
Sensor	Zeiss RMK	Leica DMC	Quickbird-2	GeoEye-1	Worldview-2	Pléiades 1A			
Geometric resolution	<3 m	0.5 m	2.4 m	1.8 m	1.8 m	0.5 m			
Period	1974–1977	2008–2010	2002–2005	2009	2011	2013–2016	2008	2014–2016	
Source	(1)	(1)	(2)	(2)	(2)	(3)	(4)	(5)	
Number of observations									
Hartbeesfontein	1	1	1	—	—	1	—	1	5
Marheya	1	1	1	—	—	2	—	1	6
Lugmag	1	1	1	—	—	—[a]	—	—[a]	3
N'tswiriri	—	1	1	—	—	2	—	1	5
Jones-se	1	1	—	—	—	2	—	1	5
Silolweni	1	—[a]	1	—	—	—[a]	—[a]	—[a]	2
N'wanetsana	—	1	1	—	—	2	—	—[a]	4
Mlondozi	—	1	1	1	1	2	1	1	8
Nhlanganzwani	1	—[a]	1	—	—[a]	—[a]	—[a]	—[a]	2
Mpanamana	1	1	1	—	1	1	1	1	7

Sources: (1) NGI (2016); (2) Google Earth/DigitalGlobe; (3) Google Earth/CNES/Astrium; (4) Baade *et al.* (2012); (5) this study.
[a]The reservoir was already decommissioned at the date of image acquisition or date of survey.

Table VI. Overview on parameters of the daily time step Pitman model (Pitman, 1976)

Parameter	Description	Unit
PI	size of the interception storage	mm
AI	proportion of impervious surfaces to the total catchment area	—
ZMINN	nominal minimum catchment absorption rate	mm h^{-1}
ZMAXN	nominal maximum catchment absorption rate	mm h^{-1}
ST	maximum soil storage, i.e. the sum of the storage capacity in the vadose zone and the soil storage capacity	mm
R	controls the relationship between actual evaporation, potential evaporation and soil moisture state; parameter ranges between 0 and 1	—
SL	soil moisture content below which no percolation occurs	mm
FT	percolation rate at soil moisture equal to ST	mm d^{-1}
POW	influences the relationship between soil moisture state and groundwater discharge	—
TL	lag of surface runoff	d
GL	lag of groundwater discharge	d

(in millimetres) and PI_{BC} represent the size of the interception storage of grass and litter under (subscript 'UC') and between (subscript 'BC') the woody plant canopy, respectively.

$$PI = WCOV \cdot (PI_C + PI_{UC}) + (1 - WCOV) \cdot PI_{BC} \quad (4)$$

Following Yu and D'Odorico (2014), PI_C was assumed to equal 2 mm, while PI_{UC} and PI_{BC} were set to 1 mm, respectively which is comparable to interception losses reported for woody plant canopy (de Villiers, 1982; Scholes and Walker, 1993) and grass (Tsiko et al., 2012) in savannas of southern Africa.

The parameter ST was estimated with a procedure suggested by Kapangaziwiri and Hughes (2008). Accordingly, ST (in millimetres) is the sum of the storage capacity of the vadose zone (ST_{vadose} in millimetres) that is mainly composed of unconsolidated weathered material above hard rock within the KNP (Riddell et al., 2014) and the soil storage capacity (ST_{soil} in millimetres) (Equation (5)).

$$ST = ST_{vadose} + ST_{soil} \quad (5)$$

ST_{vadose} depends on the thickness (d_{vadose} in millimetres) of the vadose zone, its storativity (STO) and a dimensionless factor (F_{vadose}) that reflects the extent to which percolating water is subject to lateral flow (Kapangaziwiri, 2011) (Equation (6)). ST_{soil} is a function of the soil depth (d_{soil} in millimetres), the effective soil porosity (POR in $cm^3 cm^{-3}$) and a factor (F_{soil}) that accounts for vertical variations in the effective soil porosity (Equation (7)).

$$ST_{vadose} = d_{vadose} \cdot STO \cdot F_{vadose} \quad (6)$$

$$ST_{soil} = d_{soil} \cdot POR \cdot F_{soil} \quad (7)$$

The evaluation of groundwater levels in boreholes ($N > 1000$) showed that d_{vadose} is generally <50 m within the KNP (Du Toit, 1998, cited in Riddell et al., 2014). According to Sami (2015), STO ranges from 1.8 to 2.8×10^{-3} for the quaternary catchments in which the investigated reservoirs are located. The value of F_{vadose} may vary between zero and one (for details, see Kapangaziwiri, 2011). Venter (1990) provides ranges of typical soil depths for various land types in the KNP whose spatial distribution is closely related to lithology (Table VII). POR depends on soil texture and may range between 0.32 and 0.49 (Rawls et al., 1982) and the factor F_{soil} typically varies between 0.7 and 0.9 (Kapangaziwiri, 2010). Based on these data and Equations (5)–(7), plausible ranges of ST values were calculated for each lithology. The mean of minimum and maximum values for specific lithologies was adopted and mean ST values for the reservoir catchments

were calculated based on weighted averages depending on the respective proportion of lithological units within the catchment area (Table III).

The parameters ZMINN and ZMAXN were calibrated targeting the minimization of the root mean square error (RMSE) in the prediction of historical storage states. In order to facilitate comparison between different reservoirs, the RMSE was expressed as a percentage of the initial storage capacity. Taking into account the limited availability of information about historical storage states (Table V), identical ZMINN and ZMAXN were adopted for all reservoirs. The calibration of ZMINN and ZMAXN was based on a training set including the Hartbeesfontein, Marheya, Jones-Se, Mlondozi, and Mpanamana reservoirs for which ≥5 calibration points were available. Data on historical storage states of the Lugmag, N'tswiriri, Silolweni, N'wanetsana and Nhlanganzwani reservoirs were reserved for validation. The start of rainfall–runoff simulations was set at least five years prior to the dam construction to ascertain realistic initial catchment conditions. Simulations of water-level fluctuations started on 1 October in the year of dam construction and ended in the year of dam decommissioning (if applicable) or with the survey date. For the Mpanamana reservoir, simulations were started in 1971 when the dam was finally repaired. The RMSE for historical storage states ranges from 16 to 36% (mean ± CI95: 22 ± 10%) of the initial storage capacity in the training set and from 9 to 28% (18 ± 9%) in the validation set (Table VIII).

Set up of runoff scenarios

The lack of runoff records and the limited availability of information about historical storage states induce uncertainty in the calibration of the hydrological model. Additional uncertainty arises from imperfect input data. Hydrological catchment response partially depends on short-term rainfall intensities (Riddell et al., 2014) which might not be well represented by daily rainfall data. Nearest rainfall stations are 10 to 30 km away from the reservoir catchments (Figure 1b). Storm cells that bring heavy rain to the KNP typically have elliptical footprints extending about 15 and 70 km along the minor and major axis, respectively (Dixon, 1977, cited in Venter et al., 2003). It is therefore unclear how well interpolated rainfall time series represent actual rainfall over the reservoir catchments. Although errors might be partially averaged out over longer time-spans, errors in predicted storage states may accumulate over time, affect model calibration and, thus, the simulated frequency and magnitude of spillage events. Fortunately, errors in simulated water levels are reset to zero each time the drying up or spilling of a reservoir is correctly predicted by the model.

Table VII. Estimation of the parameter ST for various lithologies based on typical soil depths in associated land types in the southern KNP as reported by Venter (1990)

Lithology	Land type	Soil depth (m)	ST (mm)		
			Minimum	Maximum	Mean
Granite/Gneiss	Nhlanguleni	0.3–1.0	70	580	330
Gabbro	Orpen	0.3–1.0	70	580	330
Ecca Shale/Mudstone	Vutome	0.3–1.0	70	580	330
Sandstone	Vutome	1.0–2.0	220	1010	620
Basalt	Satara	0.3–1.5	70	800	440
Granophyre/Rhyolite	Sabiepoort	0.0–1.0	0	580	290

Note: The range of ST values was calculated with Equations (5)–(7) from Kapangaziwri and Hughes (2008). Mean ST estimates represent the mean of minimum and maximum ST values and were used to calculate the parameter ST for the reservoir catchments.

Earth Surf. Process. Landforms, Vol. **43**, 463–481 (2018)

60

Table VIII. Calibrated parameter sets and root mean square errors (RMSEs) obtained from the comparison of empirically derived and simulated historical storage states (resulting from the Q_{best} scenario)

Reservoir	PI	AI	ZMINN	ZMAXN	ST	R	SL	FT	POW	TL	GL[a]	RMSE
	(mm)		(mm h^{-1})	(mm h^{-1})	(mm)		(mm)	(mm d^{-1})		(d)	(d)	(%)
Training set												
Hartbeesfontein	1.8	0	4.75	15.0	330	0.5	0	0.01	3	0	1–3	16
Marheya	1.5	0	4.75	15.0	520	0.5	0	0.01	3	0	1–3	36
Jones-Se	1.8	0	4.75	15.0	330	0.5	0	0.01	3	0	1–3	22
Mlondozi	1.3	0	4.75	15.0	420	0.5	0	0.01	3	0	1–3	18
Mpanamana	1.6	0	4.75	15.0	360	0.5	0	0.01	3	0	1–3	17
Validation set												
Lugmag	1.8	0	4.75	15.0	330	0.5	0	0.01	3	0	1–3	28
N'twsiriri	1.7	0	4.75	15.0	330	0.5	0	0.01	3	0	1–3	9
Silolweni	2.0	0	4.75	15.0	330	0.5	0	0.01	3	0	1–3	15
N'wanetsana	1.8	0	4.75	15.0	330	0.5	0	0.01	3	0	1–3	21
Nhlanganzwani	1.6	0	4.75	15.0	370	0.5	0	0.01	3	0	1–3	17

Note: In order to facilitate comparison between the reservoirs, the RMSE is expressed as a percentage of the initial storage capacity.
[a]GL values of 2, 3 and 1 were adopted in the Q_{best}, Q_{low} and Q_{high} scenarios, respectively.

In order to cope with the uncertainty, three different runoff scenarios were set up for each parameter set. The first scenario was obtained by running the calibrated Pitman model with the parameter GL set to two and the interpolated meteorological time-series for the reservoir catchments. This scenario can be considered a best estimate and is subsequently called the Q_{best} scenario. The second and third scenarios represent low (Q_{low}) and high runoff (Q_{high}) scenarios that were created by running the calibrated model with GL values of three and one, lower and higher rainfall, higher and lower evaporation, and using minimum and maximum 2σ uncertainty bounds for the catchment area, respectively. Time series with lower (and higher) rainfall were generated by multiplying daily rainfall amounts from the Q_{best} scenario with the ratio between the lower (upper) uncertainty bounds (95% confidence level) and the mean value of the MAP that resulted from interpolation with Thiessen polygons. Time series of higher (lower) S-pan evaporation were generated in the same manner by using daily evaporation values from the Q_{best} scenario and upper (lower) bounds of the standard prediction errors that were obtained from interpolation via ordinary kriging.

The resulting Q_{low} and Q_{high} scenarios were used to calculate envelope curves for storage states that were predicted based on the Q_{best} scenario. Lower (and upper) envelope curves correspond to low (high) rainfall and high (low) evaporation and the Q_{low} (Q_{high}) runoff scenarios, respectively. Since the Q_{low} and Q_{high} scenarios were simulated with almost identical parameter sets as the Q_{best} scenario (the parameter GL has little influence on simulated water levels), the Q_{low} and Q_{high} scenarios usually lead to an underestimation and overestimation of empirically derived storage states, respectively. Moreover, the magnitude of flood events is much higher (lower) in the Q_{high} (Q_{low}) scenario than in the Q_{best} scenario. This set-up takes into account that errors in the calibration of the hydrological model and in the simulation of the frequency and magnitude of spillage events that may arise from uncertain input data are difficult to quantify.

Trap efficiency estimation from daily inflow and outflow data

The TE can be estimated from daily inflow and outflow data when the following assumptions are made: (i) during periods without reservoir spillage, TE equals 100% (Brune, 1953); (ii) TE can be estimated on a daily basis applying Churchill's

method for periods when spillage occurs (Lewis *et al.*, 2013); (iii) considering daily time steps, flow retardation during spillage events is negligible when the reservoir is at full stage at the beginning of the day (Dendy, 1974); (iv) the relationship between daily catchment runoff and sediment load can be described with a sediment rating curve (e.g. Asselman, 2000) where the daily mean sediment concentration (SC_d in kg m^{-3}) in the inflowing water at day d is a function of the mean daily catchment runoff Q_d (in m^3 s^{-1}), a coefficient a and an exponent b (Equation (8)).

$$SC_d = a \cdot Q_d{}^b \qquad (8)$$

Then, the daily sediment delivery Qs_d (in kg d^{-1}) from the catchment can be calculated with Equation (9) where the factor 86400 (= $24 \times 60 \times 60$) results from the unit conversion from seconds to days.

$$Qs_d = 86400 \cdot SC_d \cdot Q_d = 86400 \cdot a \cdot Q_d{}^{b+1} \qquad (9)$$

Borland (1971) recommended the application of Churchill's (1948) TE estimation approach for intermittently dry reservoirs. According to Lewis *et al.* (2013), the trap efficiency $TE_{C,d}$ (in percent) after Churchill (1948) can be calculated for single days on which the reservoir spills by applying Equation (10) from the US Army Corps of Engineers (1995).

$$TE_{C,d} = 112 - 800 \cdot \left(0.3048 \cdot \frac{C_d{}^2}{Q_d{}^2 \cdot L} \right)^{-0.2} \qquad (10)$$

C_d denotes the water storage capacity (in m^3) which decreases over time due to reservoir siltation, and L is the over-water distance (in metres) from the inlet of the main tributary to the overflow spillway. Equation (10) is based on an approximation of Churchill's sedimentation index where the mean flow velocity is calculated by dividing the flow rate Q_d through the C_d/L ratio (i.e. the mean cross-sectional area; Borland, 1971). $TE_{C,d}$ is set to 100% when the evaluation of Equation (10) results in a value >100%, which may arise from low daily inflow rates corresponding to long retention times of the suspended sediment in the reservoir basin.

Depending on the storage state of the reservoir at the beginning of the first day of a spillage event, a substantial amount of inflowing water and sediment may be retained in the reservoir basin, before spilling commences. Thus, $TE_{C,d}$

most probably underestimates the TE for these days, since Equation (10) assumes continuous spillage during the considered period of time (Dendy, 1974). In order to account for this effect, the daily TE is adjusted with Equation (11) where I_d (in m^3) and SPILL$_d$ (in m^3) denote the daily volume of inflowing and spilled water, respectively.

$$TE_d = 100\% \cdot \left(1 - \frac{SPILL_d}{I_d}\right) + TE_{C,d} \cdot \frac{SPILL_d}{I_d} \quad (11)$$

Equation (11) assumes a TE of 100% before the water level reaches the height of the overflow, and a trap efficiency equal to TE$_{C,d}$ as soon as water is spilled. For days without inflow for which Equation (10) is not defined, the adjusted daily sediment trap efficiency TE$_d$ (in percent) is set to 100%. TE$_d$ is usually higher than TE$_{C,d}$ at the first day of a spillage event, when SPILL$_d$ is smaller than I_d, and approximately equal afterwards. Rainfall onto the reservoir can result in SPILL$_d$ exceeding I_d. In this case, TE$_d$ is slightly lower than TE$_{C,d}$ which is in accordance with elevated outflow rates.

The mass of delivered sediment that is eventually deposited in the reservoir basin can be calculated for each single day by multiplying TE$_d$ and Qs$_d$. The total mass of sediment Qs (in kg) entering the reservoir in a certain time interval and the corresponding mass of accumulated reservoir deposits SM (in kg) equal the sum of the daily values. Hence, the long-term mean trap efficiency (TE$_{sim}$ in percent) can be calculated with Equation (12):

$$TE_{sim} = \frac{SM}{Qs} = \frac{\sum\limits_d (TE_d \cdot Qs_d)}{\sum\limits_d Qs_d} = \frac{\sum\limits_d \left(TE_d \cdot Q_d{}^{b+1}\right)}{\sum\limits_d Q_d{}^{b+1}} \quad (12)$$

The subscript 'sim' indicates that the sediment flux is simulated based on the water storage capacity that is diminished over time due to reservoir siltation, the effective flow length through the reservoir and daily inflow and outflow rates. The exponent b, introduced with Equation (8), determines the extent to which the sediment load of inflowing water increases with increasing water discharge. In the absence of an established sediment rating curve, assumptions are to be made. According to Syvitski *et al.* (2000), b typically ranges between 0.5 and 1.5. Thus, three scenarios were adopted in this study: $b = 0.5$, 1 and 1.5. Combining the three runoff scenarios (Q$_{best}$, Q$_{low}$ and Q$_{high}$) with the three scenarios for the relationship between daily catchment runoff and sediment load ($b = 0.5$, 1 and 1.5) leads to nine scenarios in total. For each scenario, the TE$_{sim}$ value was calculated. Mean TE$_{sim}$ values were calculated from all nine scenarios and are reported with uncertainties at the 95% confidence level (CI95). In addition, the mean annual runoff (MAR) depth, and the ratio of the volume of spilled water to the volume of inflowing water, henceforth referred to as spillage to inflow ratio (SPILL/I), were determined.

Trap efficiency estimates after Brown and Heinemann

TE$_{sim}$ values were compared with trap efficiency estimates according to Brown (1944; TE$_B$ in percent) and Heinemann (1981; TE$_H$ in percent). Equation (13) from Brown (1944) is based on the initial storage capacity (C_R in m^3), the catchment area (A in km^2), and a dimensionless parameter D that equals 0.1 in the 'average' case (Brown, 1944), but may range between 0.046 and 1.

$$TE_B = 100\% \cdot \left(1 - \frac{1}{1 + 0.0021 \cdot D \cdot \frac{C_R}{A}}\right) \quad (13)$$

Minimum (and maximum) TE$_B$ values were calculated based on a D value of 0.046 (and 1) and using maximum (minimum) 2σ uncertainty bounds for the catchment area. In addition, the parameter D was systematically varied, following a suggestion of Verstraeten and Poesen (2000), to test which value resulted in the lowest mean deviation from mean TE$_{sim}$ estimates. The TE$_H$ after Heinemann (1981) was calculated with Equation (14) based on the mean storage capacity (C_M in m^3), i.e. the mean of the storage capacity in the year of dam completion and at the survey date, and the simulated mean annual inflow (I in m^3).

$$TE_H = -22 + \frac{119.6 \cdot \frac{C_M}{I}}{0.012 + 1.02 \cdot \frac{C_M}{I}} \quad (14)$$

Minimum (and maximum) TE$_H$ values were calculated from the storage capacity at the survey date (in the year of dam completion) and the Q$_{high}$ (Q$_{low}$) runoff scenarios. Differences in TE estimates are always reported by means of absolute values.

Results and Interpretation

Catchment runoff, water level fluctuations and spillage events

Modelling results are in agreement with the ephemeral character of surface runoff that was observed in all investigated reservoir catchments. The simulations reveal low mean annual runoff (MAR) depths in the Q$_{best}$ scenario ranging from 3.3 to 16.3 mm (Table IX). The maximum MAR depth among all scenarios amounts to 30.1 mm, implying a runoff coefficient of <5% which is consistent to findings from Riddell *et al.* (2014). MAR depths for the corresponding quaternary drainage regions (QDRs) that were derived with the monthly time-step Pitman model (Pitman and Bailey, 2015) fall in between MAR depths obtained from Q$_{low}$ and Q$_{high}$ scenarios for 8 out of 10 reservoir catchments. Lower simulated MAR depths for the Lugmag reservoir catchment than for the corresponding QDR X40C might be explained by the location of the reservoir in the eastern part of the QDR and increasing rainfall towards the Great Escarpment in the west. Lower simulated MAR depths for the Marheya reservoir catchment than for the corresponding QDR X40B are attributable to the widespread occurrence of sandstone areas in the Marheya reservoir catchment for which a rather high infiltration and soil water storage is assumed (Table VII).

As an example, Figure 5 shows simulated water level fluctuations and spillage events for the Hartbeesfontein reservoir. [Additional figures for all other reservoirs are provided as Supporting Information to this article.] The results highlight that water levels in the investigated reservoirs are governed by catchment runoff, rainfall and evaporation. Water levels decrease during periods without inflow, since mean annual evaporation loss from the water surface is two to three times higher than MAP. As a result, all investigated reservoirs dry out occasionally. When inflow occurs, the water level rises rapidly sometimes leading to spillage. Although spilling events are seldom, 76 to 93% of the inflowing water is spilled according to the Q$_{best}$ scenario. The Q$_{low}$ and Q$_{high}$ scenarios result in lower and higher SPILL/I ratios of 39 to 90% and 81 to 96%, respectively.

Earth Surf. Process. Landforms, Vol. **43**, 463–481 (2018)

62

Table IX. Simulated mean annual runoff (MAR) depth and spillage to mean annual inflow ratios (SPILL/*I*) for reservoir catchments according to the Q_{best}, Q_{low}, and Q_{high} scenarios, and simulated MAR depths for the corresponding quaternary drainage regions (QDRs) that were derived with the monthly time-step Pitman model in the WR2012 study (Pitman and Bailey, 2015)

Reservoir	QDR	Period	MAR depth (mm)				SPILL/*I* (%)		
			WR2012[a]	Q_{best}	Q_{low}	Q_{high}	Q_{best}	Q_{low}	Q_{high}
Hartbeesfontein	B73F	1950–2015	13.7	11.0	5.5	21.4	82	78	87
Marheya	X40B	1970–2014	10.1	3.3	0.8	8.6	77	39	88
Lugmag	X40C	1957–2012	22.5	8.9	4.5	18.0	89	87	93
N'tswiriri	X32J	1960–2016	15.3	9.0	4.0	18.2	92	88	95
Jones-Se	X33A	1957–2015	8.6	12.6	6.2	24.2	89	84	94
Silolweni	X40D	1969–2008	10.3	11.4	5.1	24.2	78	69	84
N'wanetsana	X32J	1960–2014	15.3	9.4	4.3	18.9	93	90	96
Mlondozi	X33C	1951–2016	5.4	5.5	2.1	14.6	92	86	96
Nhlanganzwani	X33D	1956–2007	5.7	7.2	3.6	15.5	76	69	81
Mpanamana	X24H	1971–2016	12.7	16.3	9.1	30.1	84	79	91

[a]Hydrological simulations of the WR2012 study end in September 2010.
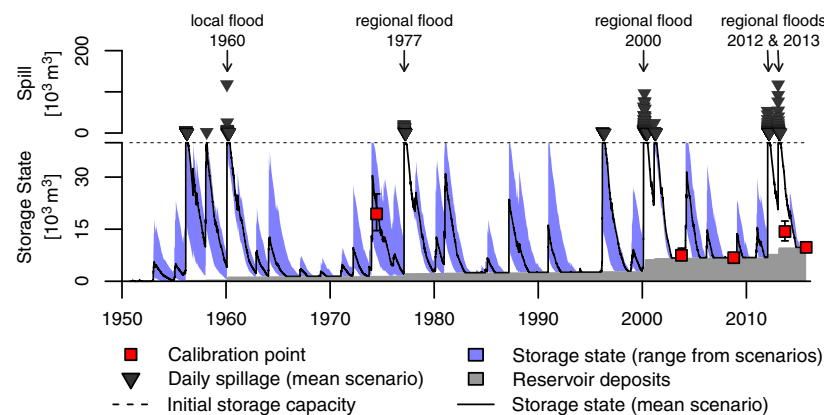
Figure 5. Simulated water level fluctuations for the Hartbeesfontein reservoir and volume of spilled water at days when overflow occurred derived from the Q_{best} scenario. Lower and upper envelope curves for water level fluctuations correspond to the Q_{low} and Q_{high} runoff scenarios, respectively. Major local and regional floods are marked with arrows. Error bars of calibration points depict the uncertainty of empirically derived historical storage states at the 95% confidence level. [Colour figure can be viewed at wileyonlinelibrary.com]

Prominent simulated spillage events coincide with regional floods in the study area. The regional flood event in February 1977 led to the overflowing of all investigated reservoirs except for the N'tswiriri and N'wanetsana reservoirs. The exceptional flood in February 2000 (Smithers *et al.*, 2001) caused spilling of all reservoirs, while subsequent rainfall and high antecedent soil moisture likely triggered further spillage until early April 2000. In January 2012, all non-decommissioned reservoirs spilled in the Q_{best} scenario except for the Marheya reservoir. Subsequent spillage occurred partially as a consequence of minor floods in January 2013 and March 2014. In addition, the simulations provide evidence for local floods affecting only single (or a few) reservoirs, like the strong local flood at Hartbeesfontein in February 1960 (Figure 5).

Simulated sediment flux and long-term trap efficiency estimates

Based on the sediment rating curve approach, the simulations indicate that sediment delivery occurred mainly during major local and regional flood events in 1960, 1977, 2000, 2012, 2013 and 2014, as exemplified for the Hartbeesfontein reservoir in Figure 6. [Figures for all other studied reservoirs are provided as Supporting Information.] In the Q_{best} scenarios,

the sediment delivery during major local and regional floods accounts for ≥72%, ≥ 82% and ≥88% of the total sediment flux at all study sites, if the sediment rating curve exponent *b* is set to 0.5, 1 and 1.5, respectively. High-discharge events cause spilling of the reservoirs. Thus, the delivered sediment is only partially deposited in the reservoir basin. Taking into account simulated TE values, the Q_{best} scenarios with values *b* of 0.5, 1 and 1.5 indicate that ≥64%, ≥ 75% and ≥83% of the reservoir deposits were delivered to the reservoirs during major local and regional floods.

The contribution of small runoff events, i.e. other than the earlier mentioned, varies with the value of *b*. For *b*=0.5, small events still contribute a relevant amount of sediment (≤ 28%), with *b*=1 they are less important (≤ 18%) and with *b*=1.5 they are unimportant (≤ 12%). Sediment that is delivered during small runoff events is effectively trapped due to low transport energy and since spilling rarely occurs. Therefore, TE_{sim} estimates are on average 12% higher in the *b*=0.5 scenarios than in the *b*=1.5 scenarios, when identical runoff scenarios are considered (Table X). Comparing TE_{sim} estimates for different runoff scenarios but identical values *b* results on average in 24% higher TE_{sim} values for the Q_{low} scenario than for the Q_{high} scenario which is clearly attributable to the differing frequency and magnitude of spillage events in the runoff scenarios.

Mean TE_{sim} values tend to increase with increasing ratios of initial storage capacity to catchment area (C_R/A) and mean

Copyright © 2017 John Wiley & Sons, Ltd.

Earth Surf. Process. Landforms, Vol. **43**, 463–481 (2018)

63
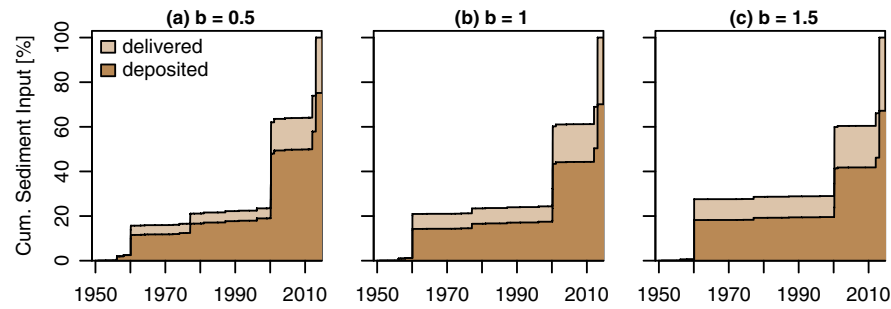
Figure 6. Cumulative volume of sediment that was delivered to and deposited in the Hartbeesfontein reservoir according to the Q_{best} runoff scenario and different relationships between daily runoff and sediment load, i.e. (a) $b = 0.5$, (b) $b = 1$ and (c) $b = 1.5$. The cumulative sediment volume is expressed as a percentage of the total sediment volume delivered to the reservoir until the survey date. The percentage of deposited sediment at the survey date equals the long-term mean trap efficiency (TE_{sim}) of the reservoir according to the Q_{best} scenario. [Colour figure can be viewed at wileyonlinelibrary.com]

Table X. Long-term mean trap efficiency (TE_{sim}) estimates obtained from hydrological modelling, initial storage capacity to catchment size ratios (C_R/A) and mean storage capacity to mean annual inflow ratios (C_M/I) for all investigated reservoirs

Reservoir	TE_{sim} (%)										C_R/A (10^{-3} m)	C_M/I		
	$b = 0.5$			$b = 1.0$			$b = 1.5$			Mean				
	Q_{best}	Q_{low}	Q_{high}	Q_{best}	Q_{low}	Q_{high}	Q_{best}	Q_{low}	Q_{high}	($N=9$)		Q_{best}	Q_{low}	Q_{high}
Hartbeesfontein	75	84	65	70	81	58	67	79	53	70 ± 8	9.3 ± 0.6	0.8	1.5	0.4
Marheya	76	86	65	70	82	60	67	79	56	71 ± 8	3.9 ± 0.1	1.1	4.7	0.4
Lugmag	51	60	37	42	54	24	37	50	17	41 ± 11	3.3 ± 0.1	0.4	0.9	0.2
N'tswiriri	58	68	43	49	61	32	44	55	24	48 ± 11	2.1 ± 0.1	0.2	0.5	0.1
Jones-Se	64	71	55	55	65	44	50	63	36	56 ± 9	4.4 ± 0.1	0.3	0.7	0.2
Silolweni	80	82	71	73	78	64	68	75	59	72 ± 6	12.3 ± 0.7	1.1	2.4	0.5
N'wanetsana	59	69	45	51	61	34	46	55	26	50 ± 10	1.6 ± 0.1	0.1	0.3	0.1
Mlondozi	34	48	24	23	40	13	16	35	8	27 ± 10	1.4 ± 0.1	0.2	0.6	0.1
Nhlanganzwani	86	94	76	84	93	70	82	93	66	83 ± 8	16.9 ± 0.9	2.3	4.6	1.1
Mpanamana	76	84	64	70	81	54	65	78	46	69 ± 10	10.1 ± 0.8	0.5	1.0	0.3

Note: TE_{sim} estimates and C_M/I ratios were calculated separately for the Q_{best}, Q_{low} and Q_{high} runoff scenarios. Moreover, TE_{sim} was determined for different scenarios representing relationships between runoff and sediment load, i.e. $b = 0.5$, 1 and 1.5. Mean TE_{sim} values with 95% confidence (CI95) intervals were calculated from all scenario combinations ($N=9$). Uncertainties of C_R/A ratios were calculated based on CI95 intervals for C_R and 2σ errors for A (according to Baade and Schmullius, 2015).
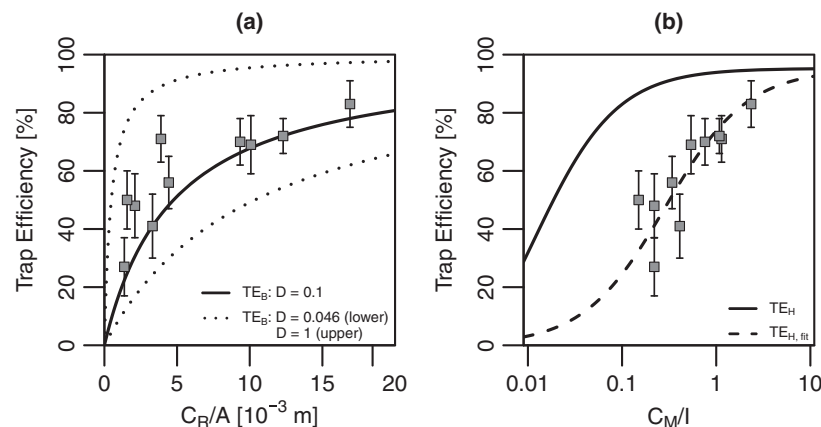
Figure 7. Relationship between mean trap efficiency estimates (TE_{sim}) derived from modelling and (a) the initial water storage capacity (C_R) to catchment size (A) ratio and (b) the mean water storage capacity (C_M) to mean annual inflow (I) ratio for all investigated reservoirs ($N=10$). The relationship between C_R/A ratios and TE_B values (with envelope curves) according to Brown (1944), and the relationship between C_M/I ratios and TE_H values according to Heinemann (1981) as well as the fitted curve $TE_{H, fit}$ represented by Equation (15) are indicated. I was calculated based on the Q_{best} scenario. Error bars of mean TE_{sim} values correspond to the 95% confidence level.

Earth Surf. Process. Landforms, Vol. **43**, 463–481 (2018)

64

storage capacity to mean annual inflow (C_M/I) (Figure 7). Mean TE_{sim} values of the Hartbeesfontein ($70 \pm 8\%$), Marheya ($71 \pm 8\%$), Silolweni ($72 \pm 6\%$), Nhlanganzwani ($83 \pm 6\%$) and Mpanamana reservoirs ($69 \pm 10\%$) are >60%. Therefore, C_R/A and C_M/I ratios of these reservoirs, the latter obtained from the Q_{best} scenario, are $>3.9 \times 10^{-3}$ m and >0.5, respectively (Table X). Mean TE_{sim} values <60% were calculated for the Lugmag ($41 \pm 11\%$), N'tswiriri ($48 \pm 11\%$), Jones-Se ($56 \pm 9\%$), N'wanetsana ($50 \pm 10\%$) and Mlondozi reservoirs ($27 \pm 10\%$) that are characterized by low C_R/A and C_M/I ratios of $<4.4 \times 10^{-3}$ m and <0.4, respectively.

Comparison with trap efficiency estimates after Brown and Heinemann

TE_B estimates after Brown (1944) are consistent with TE_{sim} values obtained from hydrological modelling, since ranges of TE_B values for D values between 0.046 and 1 overlap with Cl95 intervals of all mean TE_{sim} values (Figure 8). However, the estimation based on Brown's method involves high uncertainty due to low C_R/A ratios ranging from 1.4 to 16.9×10^{-3} m (Table X). On average, TE_B values are $55 \pm 8\%$ lower for $D = 0.046$ than for $D = 1$, while the difference for individual reservoirs ranges from 35% (Nhlanganzwani reservoir) to 65% (N'tswiriri reservoir). A more detailed inspection shows that mean TE_B estimates, i.e. $D = 0.1$, are 0% (Lugmag reservoir) to 26% (Marheya

reservoir) lower than mean TE_{sim} values with a mean difference of $9 \pm 7\%$. The lowest mean absolute deviation between mean TE_{sim} and TE_B values is achieved by setting D to 0.14 and amounts to $7 \pm 5\%$. All mean TE_{sim} estimates fall into the TE_B range represented by D values of ≥ 0.1 and ≤ 0.4 (Table XI). These boundaries correspond to TE_B ranges varying between 15% (Nhlanganzwani reservoir) and 33% (N'tswiriri reservoir) with a mean value of $27 \pm 5\%$.

The method from Heinemann (1981) reveals, in general, high TE_H estimates of 80 to 95%. This can be attributed to high C_M/I ratios ranging from 0.1 to 2.3 according to the Q_{best} scenario (Table X), suggesting a long retention time of inflowing water and sediment in the reservoirs. TE_H values that were derived from Q_{best} scenarios are roughly identical ($\pm 3\%$) to maximum TE_B estimates (i.e. $D = 1$) for the Hartbeesfontein, Jones-Se, Silolweni, Nhlanganzwani and Mpanamana reservoirs, but 5 to 16% higher than maximum TE_B estimates for the Marheya, Lugmag, N'tswiriri, N'wanetsana and Mlondozi reservoirs. Furthermore, the Q_{best} scenario reveals TE_H estimates that are 12% (Nhlanganzwani reservoir) to 63% (Mlondozi reservoir) higher than mean TE_{sim} values and do not overlap with the corresponding Cl95 intervals. This methodological comparison suggests that Heinemann's (1981) approach overestimates the TE of reservoirs in the southern KNP. Equation (15) represents a modification of Heinemann's (1981) equation that results from fitting the relationship between mean TE_{sim} estimates and C_M/I ratios derived from the Q_{best} scenario (Figure 7b).
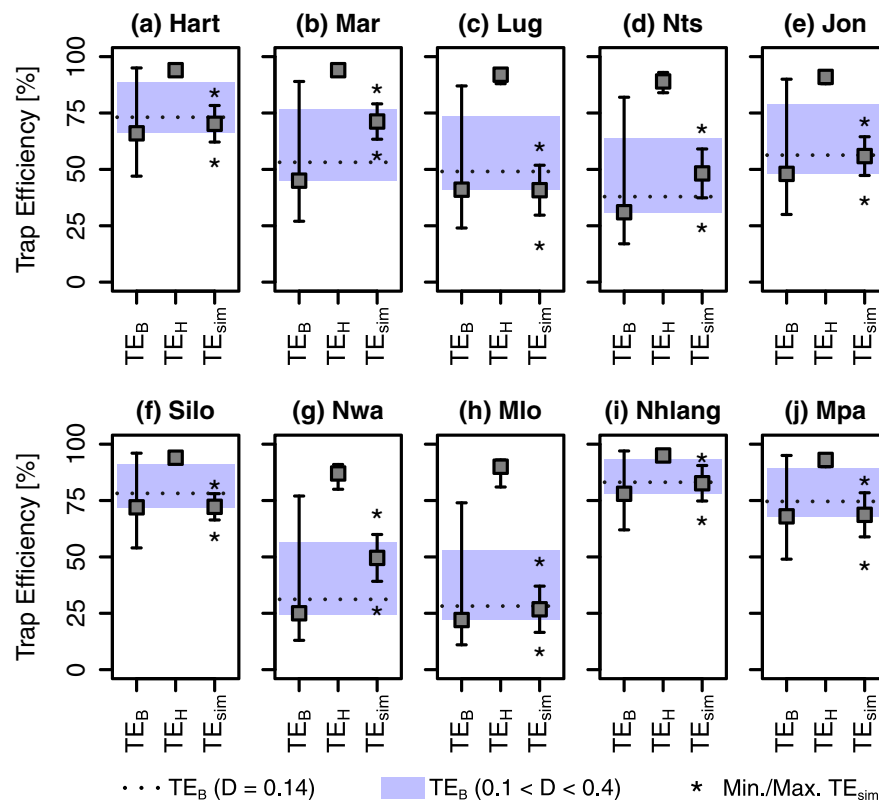
Figure 8. Comparison between trap efficiency estimates obtained from the methods of Brown (1944; TE_B) and Heinemann (1981; TE_H) with mean TE_{sim} values for all investigated reservoirs ($N = 10$). TE_B estimates were calculated by setting D to 0.1 in Equation (13), while the lower and upper ends of the error bars correspond to D values of 0.046 and 1, respectively. The TE_B values corresponding to a D value of 0.14 and intervals of TE_B values corresponding to D values of >0.1 and <0.4 are highlighted. Lower and upper bounds for TE_H estimates correspond to the Q_{high} and Q_{low} runoff scenarios, respectively, but TE_H values show very little variation between the scenarios (see Table XI). The mean TE_{sim} estimate was calculated based on all scenario combinations ($N = 9$) and is shown with uncertainties at the 95% confidence level. [Colour figure can be viewed at wileyonlinelibrary. com]

Table XI.   Trap efficiency estimates for the investigated reservoirs based on the methods from Brown (1944; TE$_B$) and Heinemann (1981; TE$_H$) and mean TE$_{sim}$ estimates obtained from modelling

	TE$_B$ (%)			TE$_H$ (%)			TE$_{sim}$ (%)
	$D = 0.14$	$D = 0.10$	$D = 0.40$	Mean	Minimum	Maximum	Mean ± Cl95
Hartbeesfontein	73	66	89	94	92	94	70 ± 8
Marheya	53	45	77	94	92	95	71 ± 8
Lugmag	49	41	74	92	88	93	41 ± 11
N'tswiriri	38	31	64	89	84	93	48 ± 11
Jones-Se	57	48	79	91	88	93	56 ± 9
Silolweni	78	72	91	94	92	95	72 ± 6
N'wanetsana	31	25	57	87	80	91	50 ± 10
Mlondozi	28	22	53	90	81	93	27 ± 10
Nhlanganzwani	83	78	93	95	94	95	83 ± 8
Mpanamana	75	68	89	93	90	94	69 ± 10

Note: TE$_B$ estimates are shown for D values (see Equation (13)) of 0.14, 0.10 and 0.40. The value of $D = 0.14$ results in the lowest mean deviation between TE$_B$ and TE$_{sim}$ values, while D values of 0.10 and 0.40 are interpreted as lower and upper uncertainty bounds, respectively. Mean, minimum and maximum values of TE$_H$ estimates were determined from all investigated scenarios. Uncertainties of mean TE$_{sim}$ estimates correspond to the 95% confidence level (Cl95).

$$TE_{H,\,fit} = \frac{97.928 \cdot \frac{C_M}{I}}{0.296 + 1.031 \cdot \frac{C_M}{I}} \qquad (15)$$

The mean absolute deviation between TE$_{H,\,fit}$ values (in percent) and mean TE$_{sim}$ values is 8 ± 4% and therefore nearly identical to the mean absolute deviation between TE$_B$ and mean TE$_{sim}$ values (7 ± 5%), if D is set to 0.14.

Discussion

The relevance of the hydrological regime for the TE of reservoirs has been previously highlighted (e.g. Heinemann, 1984; Haan *et al.,* 1994) and is corroborated by results of this study. The simulations indicate that the long-term (40 to 65 years) mean TE of all investigated reservoirs is strongly influenced by a few ($N \leq 6$) high-discharge events. According to the Q$_{best}$ scenarios, these events account for ≥72% of the sediment delivery and ≥64% of the sediment volume that was accumulated in the reservoir basin until the survey date. This is in accordance with other studies on the siltation of reservoirs with ephemeral inflow. Bussi *et al.* (2013) showed that four flood events contributed 65 to 70% to the sediment volume that was accumulated within a 20 year period in a small reservoir in eastern Spain. Likewise, Fischhendler *et al.* (2003, p. 29) attributed 70% of the sediment volume that was accumulated within 40 years in a large reservoir (7.3 × 10^6 m^3) in western Israel to 'a small number of very large floods'.

Given the erratic occurrence of high-discharge events, MAR is a rather poor indicator for the prediction of sediment flux in ephemeral streams. Brune (1953) already noticed that his TE estimation approach that relies on MAR values might lead to an overestimation of the TE for intermittently dry reservoirs. Later, several authors have cautioned that the methods from Brune (1953) and Heinemann (1981) might be inadequate for reservoirs with ephemeral inflow (e.g. Borland, 1971; Lloyd *et al.,* 1998; Verstraeten and Poesen, 2000). This is supported by the modelling results, since TE$_H$ values often exceed TE$_{sim}$ and TE$_B$ estimates without overlapping uncertainty bounds (Figure 8). By comparison, the method of Brown (1944) appears to be more reliable. Indeed, Brown's method was applied in many reservoir siltation studies taking place in semi-arid and arid environments (e.g. Haregeweyn *et al.,* 2006; Tamene *et al.,* 2006; Baade *et al.,* 2012; Alahiane *et al.,* 2016). For reservoirs with low *C/A* ratios, the selection of an adequate value D is crucial to achieve reliable TE estimates with a

reasonable uncertainty (Verstraeten and Poesen, 2000). Without confining the range of D values, this study reveals differences of 35 to 65% between minimum and maximum TE$_B$ estimates. Compared to mean TE$_{sim}$ estimates, the 'average' D value of 0.1 (Brown, 1944) leads to slightly lower TE$_B$ values with a mean difference of 9 ± 7%.

The approach presented here can most probably reduce uncertainties in the TE estimation for intermittently dry reservoirs as the frequency and magnitude of spillage events are explicitly taken into account. An important assumption is that the method of Churchill (1948) is appropriate for the daily TE estimation during spillage periods. Borland (1971) recommended Churchill's method for intermittently dry reservoirs. More recent studies indicate that Churchill's method is preferable especially when the long-term mean TE is estimated based on daily time steps. Butcher *et al.* (1992) compared TE estimates for single high-discharge events with empirical TE determinations for two small reservoirs (140 and 360 × 10^3 m^3) in the southern Pennines (United Kingdom). Although the TE of single events was variable and difficult to predict, Butcher *et al.* (1992) found that Churchill's method resulted in TE estimates close to empirical values when results of the entire measurement period were totalled. Similarly, Lewis *et al.* (2013) derived TE estimates for the large Burdekin Falls Dam (1.9 × 10^9 m^3) in northeast Australia by applying Churchill's method on a daily basis. The resulting TE estimates fell within Cl95 intervals of empirical TE determinations for four out of five years in the monitoring period.

The suitability of Churchill's method partially depends on the particle size of the delivered sediment that is not considered in Equation (10). Coarse and flocculated sediment is subject to higher settling velocities and therefore more efficiently trapped than fine and dispersed sediment (Heinemann, 1984). Chen (1975) investigated the TE for quiescent and turbulent flow conditions and showed that Churchill's method reveals reliable TE values for sediments with a grain size between 6 and 8 φ-units. Grain size data for suspended sediment is currently not available, but reservoir deposits in the KNP are characterized by a mean grain size (logarithmic methods of moments; Krumbein, 1936) of about 6.8 φ-units with rather small variations between different reservoirs (Reinwarth *et al.,* 2017). Taking into account these considerations, Churchill's method is a plausible choice with respect to reservoirs in the KNP.

The presented approach also relies on the assumption that the relationship between streamflow and sediment discharge can be described with a sediment rating curve. Previous work

Copyright © 2017 John Wiley & Sons, Ltd.

Earth Surf. Process. Landforms, Vol. **43**, 463–481 (2018)

66

has shown that this relationship is likely to vary on different timescales owing to changing sediment availability along drainage lines and variable sediment delivery from inter-drainage areas (e.g. Walling, 1977; Grenfell and Ellery, 2009). However, the different scenarios corresponding to values for the exponent *b* of 0.5, 1 and 1.5 represent a range of possible relationships that likely includes a scenario that can be considered realistic (Syvitski *et al.,* 2000). The mean absolute difference for TE_{sim} estimates obtained from *b* values of 0.5 and 1.5 is 12%. This indicates that the potential impact of variable relationships between streamflow and sediment discharge on mean TE_{sim} estimates is reasonably low in this study.

Sediment load measurements and data from repeated reservoir siltation surveys in the southern KNP against which the simulations could be tested are unfortunately missing. The staff gauge at the Mlondozi dam shows that the thickness of reservoir deposits increased by 1.2 ft (= 0.37 m) between September 2008 and March 2016 (Figure 9). Based on the HSR of the initial reservoir basin, this indicates that about 31% of the total volume of reservoir deposits in the Mlondozi reservoir were accumulated between these two dates. This compares to simulated values ranging from 19% (*b* = 0.5) to 28% (*b* = 1.5) in the Q_{best} scenario. The difference between empirically-derived and simulated values can be explained by inaccuracies in the determination of the sediment volume from observations at a single point (Ramos-Diez *et al.,* 2016). Alternatively, the deviation may reflect uncertainties in the simulation of the frequency and magnitude of spillage events.

In this study, uncertainties in hydrological modelling are mainly due to the lack of runoff records and water level readings. Comparison between mean RMSEs in the prediction of historical storage states, obtained from reservoirs included

in the training (22 ± 10%) and validation sets (18 ± 9%), indicates that the calibration of the hydrological model is rather robust, but imperfect input data may induce uncertainty which is indicated by differing MAR depths and SPILL/*I* ratios among the runoff scenarios (Table IX). Although uncertainties in hydrological modelling must be taken into account, the impact on TE_{sim} estimates is moderate. The mean absolute difference between TE_{sim} values obtained from Q_{low} and Q_{high} scenarios for identical values *b* is 24%, which leads to acceptable uncertainties, if mean TE_{sim} values are adopted. Furthermore, errors that result from imperfect input data and model calibration are random. Mean TE_{sim} values that were derived from all scenarios are therefore highly unlikely to systematically overestimate or underestimate the actual TE of the reservoirs. Modelling uncertainties could be diminished, if water and sediment levels in the reservoirs were regularly monitored. Moreover, recent studies suggest that uncertainties could be further reduced, if data on catchment runoff (Riddell *et al.,* 2014) and a more detailed geo-hydrological characterization of the catchments (Dippenaar and van Rooy, 2014; van Zijl and Le Roux, 2014; van Zijl *et al.,* 2016) should become available.

The modelling results are strengthened through the comparison with TE_B estimates after Brown (1944). The simulations indicate that the calibration and regionalization of the parameter *D* in Brown's method that was suggested by Verstraeten and Poesen (2000) is feasible for reservoirs in the southern KNP. Setting *D* to 0.14 results in the lowest mean absolute deviation of 7 ± 5% between mean TE_{sim} and TE_B values. TE_B values corresponding to *D* values of 0.1 and 0.4 can be interpreted as lower and upper uncertainty bounds, respectively, which leads to ranges in TE_B values varying from 15 to 33%. This is in accordance with considerations from Brown (1944) who expected *D* values >0.1 for reservoirs
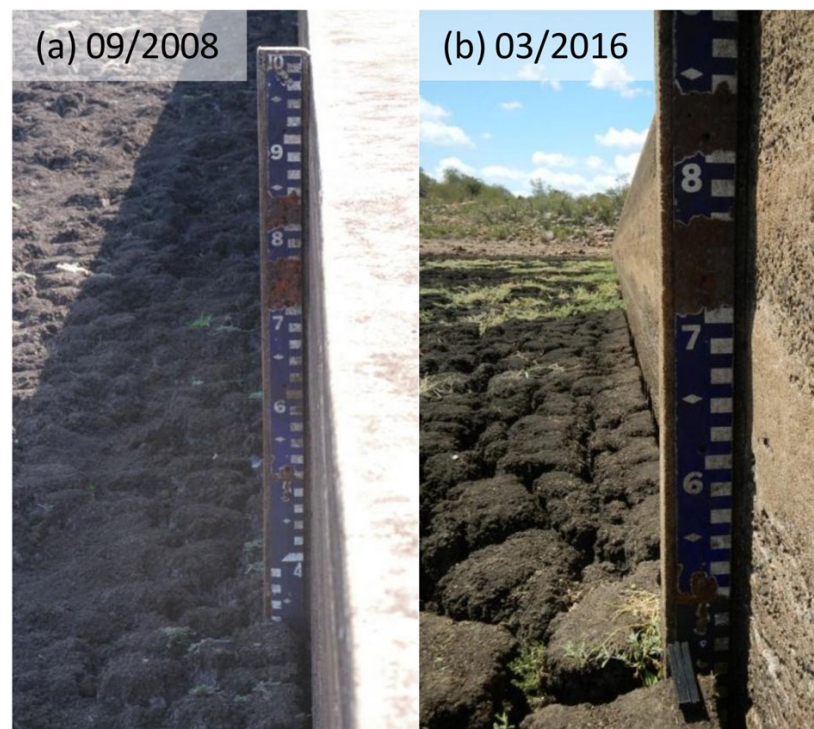
Figure 9. Staff gauge at the concrete wall of the Mlondozi dam. Photographs from (a) September 2008 and (b) March 2016 indicate an increase in the thickness of reservoir deposits of about 1.2 ft (= 0.37 m) within 7.5 years. [Colour figure can be viewed at wileyonlinelibrary.com]

receiving small and variable runoff. The appropriateness of the established D values for management purposes in areas outside the KNP or neighbouring game reserves remains to be studied, since differing catchment characteristics (e.g. land use) may alter the hydrological catchment response as well as the relationship between TE values and C_R/A ratios (e.g. Brune, 1953).

Conclusions

This study underscores the importance of the frequency and magnitude of rainfall and runoff events for the estimation of the long-term mean TE of small, intermittently dry reservoirs. Combining results from hydrological modelling with a sediment rating curve approach indicates that a few high discharge events ($N \leq 6$) within the lifetime of the investigated reservoirs (40 to 65 years) had a strong influence on their long-term mean TE. According to the Q_{best} scenarios, these events contributed ≥ 72 and $\geq 64\%$ to the delivered and deposited sediment, respectively. Although uncertainties in hydrological modelling must be taken into account due to the lack of runoff records and imperfect input data, the uncertainty of mean TE_{sim} estimates is moderate, ranging from ± 6 to $\pm 11\%$ at the 95% confidence level. The results corroborate that the method from Heinemann (1981) tends to overestimate the TE of small, intermittently dry reservoirs in semi-arid climate regions. The approach from Brown (1944) appears to be more reliable, but leads to large differences between minimum and maximum TE_B estimates ranging from 46 to 63%, if the parameter D in Equation (13) is not confined. For the southern part of KNP, $D = 0.14$ provides the smallest deviation compared to the more sophisticated modelling approach used in this paper. Thus, the proposed methodological framework can contribute to a reduction of uncertainties, since the frequency and magnitude of spillage events is explicitly taken into account. The approach has the potential to be applied to other reservoirs in semi-arid regions with similar characteristics.

References

Alahiane N, Elmouden A, Aitlhaj A, Boutaleb S. 2016. Small dam reservoir siltation in the Atlas Mountains of Central Morocco: analysis of factors impacting sediment yield. *Environmental Earth Sciences* **75**: 1035. https://doi.org/10.1007/s12665-016-5795-y.

Asselman NEM. 2000. Fitting and interpretation of sediment rating curves. *Journal of Hydrology* **234**(3–4): 228–248. https://doi.org/10.1016/S0022-1694(00)00253-5.

Baade J, Franz S, Reichel A. 2012. Reservoir siltation and sediment yield in the Kruger National Park, South Africa: a first assessment. *Land Degradation & Development* **23**: 586–600. https://doi.org/10.1002/ldr.2173.

Baade J, Schmullius C. 2015. Catchment properties in the Kruger National Park derived from the new TanDEM-X Intermediate Digital Elevation Model (IDEM). *The International Archives of the Photogrammetry, Remote Sensing and Spatial Information Sciences* **XL-7/W3**: 293–300. https://doi.org/10.5194/isprsarchives-XL-7-W3-293-2015.

Baade J, Schmullius C. 2016. TanDEM-X IDEM precision and accuracy assessment based on a large assembly of differential GNSS measurements in the Kruger National Park, South Africa. *ISPRS Journal of Photogrammetry and Remote Sensing* **119**: 496–508. https://doi.org/10.1016/j.isprsjprs.2016.05.005.

Bailey AK. 2015. *WRSM2000/Pitman Water Resources Simulation Model for Windows. Theory*, WRC Report K5/2143/1. Water Research Commission (WRC): Gezina, Pretoria.

Borland WM. 1971. River sedimentation. In *River mechanics*, Shen HW (ed), Vol. **II**. HW Shen: Fort Collins, CO; 29:1–29:38.

Bosman HH. 1990. Methods to convert American Class A-pan and Symon's tank evaporation to that of a representative environment. *Water SA* **16**(4): 227–236.

Brown CB. 1944. Discussion of 'Sedimentation in Reservoirs' by B. J. Witzig. *Transactions of the American Society of Civil Engineers* **109**: 1080–1086.

Brune GM. 1953. Trap efficiency of reservoirs. *Transactions of the American Geophysical Union* **34**(3): 407–418. https://doi.org/10.1029/TR034i003p00407.

Bucini G, Hanan BP, Boone RB, Smit IPJ, Saatchi SS, Lefsky MA, Asner GP. 2010. Woody fractional cover in Kruger National Park, South Africa: remote sensing-based maps and ecological insights. In *Ecosystem Function in Savannas. Measurement and Modeling at Landscape to Global Scales*, Hill MJ, Hanan NP (eds). CRC Press: Boca Raton, FL; 219–238. https://doi.org/10.1201/b10275-15.

Bussi G, Rodríguez-Lloveras X, Francés F, Benito G, Sánchez-Moya Y, Sopeña A. 2013. Sediment yield model implementation based on check dam infill stratigraphy in a semiarid Mediterranean catchment. *Hydrology and Earth System Sciences* **17**: 3339–3354. https://doi.org/10.5194/hess-17-3339-2013.

Butcher DP, Claydon J, Labadz JC, Pattinson VA, Potter AWR, White P. 1992. Reservoir sedimentation and colour problems in southern Pennine reservoirs. *Journal of the Institute of Water and Environmental Management* **6**(5): 418–431. https://doi.org/10.1111/j.1747-6593.1992.tb00771.x.

Chen CN. 1975. Design of sediment retention basins. In *Proceedings of the National Symposium on Urban Hydrology and Sediment Control*, July 28–31, 1975 (No. UKY BU109). Parsons, Brinckerhoff, Quade & Douglas Inc.: New York; 285–298.

Christie F, Hanlon J. 2001. *Mozambique and the Great Flood 2000*. Indiana University Press: Bloomington, IN.

Churchill MA. 1948. Discussion of 'Analysis and use of reservoir sedimentation data' by L. C. Gottschalk. In *Proceedings of the Federal Inter-agency Sedimentation Conference*, US Bureau of Reclamation (ed). US Department of the Interior: Washington DC; 139–140.

Cullum C, Rogers K. 2011. *A Framework for the Classification of Drainage Networks in Savanna Landscapes*, WRC Report No. TT 498/11. Water Research Commission: Gezina, Pretoria.

de Smith MJ. 2004. Distance transforms as a new tool in spatial analysis, urban planning, and GIS. *Environment and Planning. B, Planning & Design* **31**: 85–104. https://doi.org/10.1068/b29123.

de Villiers GDT. 1982. Predictive models for estimating net rainfall and interception losses in savanna vegetation. *Water SA* **8**(4): 208–212.

Dendy FE. 1974. Sediment trap efficiency of small reservoirs. *Transactions of the American Society of Agricultural Engineers* **17**(5): 898–908. https://doi.org/10.13031/2013.36994.

Department of Water Affairs. 2008. Hydrological Services – Surface Water (Data, Dams, Floods, Flows). https://www.dwa.gov.za/hydrology/ [accessed 4 March 2016].

Dippenaar MA, van Rooy JL. 2014. Review of engineering, hydrogeological and vadose zone hydrological aspects of the Lanseria Gneiss, Goudplaats-Hout River Gneiss and Nelspruit Suite Granite (South Africa). *Journal of African Earth Sciences* **91**: 12–31. https://doi.org/10.1016/j.jafrearsci.2013.11.019.

Dixon MJ. 1977. *Proposed Mathematical Model for the Estimation of the Aerial Properties of High-intensity, Short Duration Storms*, Report TR 78. Department of Water Affairs: Pretoria.

Du Toit WH. 1998. *Geohidrologie van die Nasionale Krugerwildtuin gabaseer op die evaluerung van bestaande boorgatinligting,* Vol. **1** (Teks, DWAF Directorate Geohydrology Internal Report GH 3798. Department of Water Affairs and Forestry (DWAF): Pretoria.

Dyson LL, van Heerden J. 2001. The heavy rainfall and floods over the northeastern interior of South Africa during February 2000. *South African Journal of Science* **97**: 80–86.

Environmental Systems Research Institute. 2013. *ArcGIS Desktop: Release 10.2.* ESRI: Redlands, CA.

Faithful JW, Griffiths DJ. 2000. Turbid flow through a tropical reservoir (Lake Dalrymple, Queensland, Australia): responses to a summer storm event. *Lakes & Reservoirs: Research and Management* **5**: 231–247. https://doi.org/10.1046/j.1440-1770.2000.00123.x.

Fischhendler I, Enzel Y, Gvirtzman H. 2003. Estimation of sedimentation rates under Mediterranean conditions deduced from the Mishmar Ayyalon Reservoir, Israel. *Israel Journal of Earth Sciences* **52**: 21–29.

Fitchett JM, Hoogendoorn G, Swemmer AM. 2016. Economic costs of the 2012 floods on tourism in the Mopani District Municipality, South Africa. *Transactions of the Royal Society of South Africa* **71**: 187–194. https://doi.org/10.1080/0035919X.2016.1167788.

Food and Agriculture Organization of the United Nations. 2014. *World Reference Base for Soil Resources 2014. International Soil Classification System for Naming Soils and Creating Legends for Soil Maps,* World Soil Resources Reports 106. FAO: Rome.

Geological Survey of South Africa. 1986a. *Geological Series 1:250 000. Sheet 2530 Barberton.* Government Printer: Pretoria.

Geological Survey of South Africa. 1986b. *Geological Series 1:250 000. Sheet 2430 Pilgrim's Rest.* Government Printer: Pretoria.

Glotzbach C, Paape A, Baade J, Reinwarth B, Rowntree K, Miller J. 2016. Cenozoic landscape evolution of the Kruger National Park as derived from cosmogenic nuclide analyses. *Terra Nova* **28**(5): 316–322. https://doi.org/10.1111/ter.12223.

Grenfell SE, Ellery WN. 2009. Hydrology, sediment transport dynamics and geomorphology of a variable flow river: the Mfolozi River, South Africa. *Water SA* **35**: 271–282.

Haan CT, Barfield BJ, Hayes JC. 1994. *Design Hydrology and Sedimentology for Small Catchments.* Academic Press: San Diego, CA.

Haregeweyn N, Poesen J, Nyssen J, de Wit J, Haile M, Govers G, Deckers S. 2006. Reservoirs in Tigray (northern Ethiopia): characteristics and sediment deposition problems. *Land Degradation & Development* **17**: 211–230. https://doi.org/10.1002/ldr.698.

Heinemann HG. 1981. A new sediment trap efficiency curve for small reservoirs. *Journal of the American Water Resources Association* **17**(5): 825–830. https://doi.org/10.1111/j.1752-1688.1981.tb01304.x.

Heinemann HG. 1984. Reservoir trap efficiency. In *Erosion And Sediment Yield: Some Methods of Measurement and Modelling,* Hadley RF, Walling DE (eds). Geo Books: Norwich.

Heritage G, Tooth S, Entwistle N, Milan D. 2014. Long-term flood controls on semi-arid river form: evidence from the Sabie and Olifants rivers, eastern South Africa. In *Sediment Dynamics from the Summit to the Sea. ICCE 2014, International Symposium on Sediment Dynamics,* New Orleans, USA, 11–14 December 2014, Jun Xu Y, Allison MA, Bentley SJ, Collins AL, Erskine WD, Golosov V, Horowitz AJ, Stone M (eds), IAHS Publications 367. IAHS Press: Wallingford; 141–146. https://doi.org/10.5194/piahs-367-141-2015.

Heritage GL, Moon BP, Jewitt GP, Large ARG, Rountree M. 2001. The February 2000 floods on the Sabie River, South Africa: an examination of their magnitude and frequency. *Koedoe* **44**: 37–44. https://doi.org/10.4102/koedoe.v44i1.184.

Hijmans RJ. 2014. raster: Geographic data analysis and modeling. R package version 2.5–8. http://CRAN.R-project.org/package=raster [accessed 29 June 2016].

Hughes DA. 1992. A monthly time-step, multiple reservoir water balance simulation model. *Water SA* **18**(4): 279–286.

Hughes DA. 2004. Problems of estimating hydrological characteristics for small catchments based on information from the South African national surface water resource database. *Water SA* **30**(3): 1–6. https://doi.org/10.4314/wsa.v30i3.5088.

Hughes DA. 2013a. A review of 40 years of hydrological science and practice in Southern Africa using the Pitman rainfall–runoff model. *Journal of Hydrology* **501**: 111–124. https://doi.org/10.1016/j.jhydrol.2013.07.043.

Hughes DA. 2013b. Seasonal flow prediction with uncertainty in South Africa and Lesotho. In *Runoff Prediction in Ungauged Basins. Synthesis Across Processes and Scales,* Blöschl G, Sivapalan M, Wagener T, Viglione A, Savenije H (eds). Cambridge University Press: New York; 289–293.

Joubert SCJ. 1986. The Kruger National Park – an introduction. *Koedoe* **29**(1): 1–11. https://doi.org/10.4102/koedoe.v29i1.516.

Kapangaziwiri E. 2010. Regional Application of the Pitman Monthly Rainfall–Runoff Model in Southern Africa Incorporating Uncertainty, PhD Thesis. Rhodes University, Grahamstown.

Kapangaziwiri E. 2011. *Physically Based Parameter Estimation Methods for Hydrological Models. Revised Calibration and Application Procedures for the Pitman Monthly Rainfall–Runoff Model in Southern African Basins.* Saarbrücken: Lambert Academic Publishing.

Kapangaziwiri E, Hughes DA. 2008. Towards revised physically based parameter estimation methods for the Pitman monthly rainfall–runoff model. *Water SA* **34**(2): 183–192.

Kloppers JJ, Bornman H. 2005. *A Dictionary of Kruger National Park Place Names.* SA Country Life: Barberton.

Krumbein WC. 1936. Application of logarithmic moments to size frequency distributions of sediments. *Journal of Sedimentary Petrology* **6**: 35–47. https://doi.org/10.1306/D4268F59-2B26-11D7-8648000102C1865D.

LEICA Geosystems. 2014. *LEICA Geo Office Version 8.4.* LEICA: Heerbrugg.

Lewis SE, Bainbridge ZT, Kuhnert PM, Sherman BS, Henderson B, Dougall C, Cooper M, Brodie JE. 2013. Calculating sediment trapping efficiencies for reservoirs in tropical settings: a case study from the Burdekin Falls Dam, NE Australia. *Water Resources Research* **49**(2): 1017–1029. https://doi.org/10.1002/wrcr.20117.

Lewis SE, Sherman BS, Bainbridge ZT, Brodie JE, Cooper M. 2009. Modelling and monitoring the sediment trapping efficiency and sediment dynamics of the Burdekin Falls Dam, Queensland, Australia. In *Proceedings of the 18th World IMACS Congress and MODSIM09 International Congress on Modelling and Simulation. Modelling and Simulation Society of Australia and New Zealand and International Association for Mathematics and Computers in Simulation, Cairns,* Anderssen RS, Braddock RD, Newham LTH (eds); 4022–4028. ISBN: 978-0-9758400-7-8. http://www.mssanz.org.au/modsim09/I14/lewis.pdf [accessed 11 April 2016].

Lloyd SD, Bishop P, Reinefelds I. 1998. Shoreline erosion: a cautionary note in using small farm dams to determine catchment erosion rates. *Earth Surface Processes and Landforms* **23**: 905–912. http://doi.org/10.1002/(SICI)1096-9837(199810)23:10<905::AID-ESP910>3.0.CO;2-E.

Midgley DC, Pitman WV. 1969. *Surface Water Resources of South Africa,* Hydrological Research Unit Report No. 2/69. University of Witwatersrand: Johannesburg.

National Geospatial Information (NGI). 2016. ITIS Portal. http://itis.ngi.gov.za/itisportalinternet [accessed 29 June 2016].

O'Keeffe J, Rogers KH. 2003. Heterogeneity and management of the Lowveld rivers. In *The Kruger Experience. Ecology and Management of Savanna Heterogeneity,* Du Toit JT, Rogers KH, Biggs HC (eds). Island Press: Washington, DC; 447–468.

Pienaar UDV. 1985. Indications of progressive desiccation of the Transvaal Lowveld over the past 100 years, and implications for the water stabilization programme in the Kruger National Park. *Koedoe* **28**: 93–165. https://doi.org/10.4102/koedoe.v28i1.540.

Pitman B, Bailey A. 2015. A wealth of new freely downloadable information on the water resources of South Africa, Swaziland and Lesotho. *Journal of the South African Institution of Civil Engineers* **23**(5): 13–18.

Pitman WV. 1973. *A Mathematical Model for Generating Monthly River Flows from Meteorological Data in South Africa,* Hydrological Research Unit Report No. 2/73. University of Witwatersrand: Johannesburg.

Pitman WV. 1976. *A Mathematical Model for Generating Daily River Flows from Meteorological Data in South Africa,* Hydrological Research Unit Report No. 2/76. University of Witwatersrand: Johannesburg.

Pitman WV. 2011. Overview of water resource assessment in South Africa: current state and future challenges. *Water SA* **37**(5): 659–664. https://doi.org/10.4314/wsa.v37i5.3.

Pitman WV, Kakebeeke JP, Bailey AK. 2015. *WRSM/Pitman Water Resources Simulation Model for Windows. Simulation of the*

Movement of Water through an Interlinked System of Catchments, River Reaches, Reservoirs, Irrigation Areas and Mines, User's Manual. Water Research Commission: Gezina, Pretoria.

R Core Team. 2014. *R: A Language and Environment for Statistical Computing. R Foundation for Statistical Computing.* R Core Team: Vienna. http://www.R-project.org [accessed 18 June 2014].

Ramoelo A, Majozi N, Mathieu R, Jovanovic N, Nickless A, Dzikiti S. 2014. Validation of global evapotranspiration product (MOD16) using flux tower data in the African savanna, South Africa. *Remote Sensing* **6**: 7406–7423. https://doi.org/10.3390/rs6087406.

Ramos-Diez I, Navarro-Hevia J, San Martín Fernández R, Díaz-Gutiér-rez V, Mongil-Manso J. 2016. Geometric models for measuring sediment wedge volume in retention check dams. *Water Environment Journal* **30**(1–2): 119–127. https://doi.org/10.1111/wej.12165.

Rawls WJ, Brakensiek DL, Saxton KE. 1982. Estimation of soil water properties. *Transactions of the American Society of Agricultural Engineers* **25**(5): 1316–1328. https://doi.org/10.13031/2013.33720.

Reinwarth B, Miller JK, Glotzbach C, Rowntree KM, Baade J. 2017. Applying regularized logistic regression (RLR) for the discrimination of sediment facies in reservoirs based on composite fingerprints. *Journal of Soils and Sediments* **17**(6): 1777–1795. https://doi.org/10.1007/s11368-016-1627-7.

Riddell ES, Nel J, Fundisi D, Jumbi F, van Niekerk A, Lorentz SA. 2014. *Ephemeral Hydrological Processes in Savannas*, WRC Report No. TT 619/14. Water Research Commission: Gezina, Pretoria.

Riegl. 2016. *RiScan Pro 2.3 Operating and Processing Software. Riegl Laser Measurement Systems*: Horn, Austria.

Rooseboom A, Annandale GW. 1981. *Techniques Applied in Determining Sediment Loads in South African Rivers. Erosion and Sediment Transport Measurement* (Proceedings of the Florence Symposium, June 1981, IAHS Publication 133. IAHS Press: Wallingford; 219–224.

Sami K. 2015. *Water Resources of South Africa, 2012 Study (WR2012). WR2012 SAMI Groundwater Module: Verification Studies, Default Parameters and Calibration Guide*, Report to the Water Research Commission by Royal HaskoningDHV (Pty) Ltd. Water Research Commission: Gezina, Pretoria.

Schmidt EJ, Schulze RE. 1984. *Improved Estimates of Peak Flow Rates using Modified SCS Lag Equations*, Agricultural Catchments Research Unit Report 17. Department of Agricultural Engineering, University of Natal: Pietermaritzburg.

Scholes RJ, Walker BH. 1993. *An African Savanna. Synthesis of the Nylsvley Study*. Cambridge University Press: Cambridge. https://doi.org/10.1017/CBO9780511565472.

Sloff CJ. 1991. *Reservoir Sedimentation: A Literature Survey. Communications on Hydraulic and Geotechnical Engineering*, Report No. 91-2. Delft University of Technology: Delft.

Smithers JC, Schulze RE, Pike A, Jewitt GPW. 2001. A hydrological perspective of the February 2000 floods: a case study in the Sabie River catchment. *Water SA* **27**: 325–332. https://doi.org/10.4314/wsa.v27i3.4975.

Stabel HH. 1987. Settling velocity and residence time of particles in Lake Constance. *Swiss Journal of Hydrology* **49**(3): 274–293. https://doi.org/10.1007/BF02538289.

Syvitski JP, Morehead MD, Bahr DB, Mulder T. 2000. Estimating fluvial sediment transport: the rating parameters. *Water Resources Research* **36**(9): 2747–2760. https://doi.org/10.1029/2000WR900133.

Takamatsu M, Barrett M, Charbeneau RJ. 2010. Hydraulic model for sedimentation in storm-water detention ponds. *Journal of Environmental Engineering* **136**(5): 527–534. https://doi.org/10.1061/(ASCE)EE.1943-7870.0000175.

Tamene L, Park SJ, Dikau R, Vlek PLG. 2006. Reservoir siltation in the semi-arid highlands of northern Ethiopia: sediment yield-catchment area relationship and a semi-quantitative approach for predicting sediment yield. *Earth Surface Processes and Landforms* **31**: 1364–1383. https://doi.org/10.1002/esp.1338.

Trimble SW, Bube KP. 1990. Improved reservoir trap efficiency prediction. *The Environmental Professional* **12**: 255–272.

Trimble SW, Wilson B. 2012. Reservoir and lake trap efficiency. In *Encyclopedia of Lakes and Reservoirs*, Bengtsson L, Herschy RW, Fairbridge RW (eds). Encyclopedia of Earth Science Series Springer: Dordrecht; 619–626. https://doi.org/10.1007/978-1-4020-4410-6_146.

Tsiko CT, Makurira H, Gerrits AMJ, Savenije HHG. 2012. Measuring forest floor and canopy interception in a savannah ecosystem. *Physics and Chemistry of the Earth* **47–48**: 122–127. https://doi.org/10.1016/j.pce.2011.06.009.

US Army Corps of Engineers. 1995. *Engineering and Design: Sedimentation Investigations in Rivers and Reservoirs*. USACE: Washington, DC.

van Eekelen BWGM, Jarmain C, Jackson B, Ferreira F, van der Zaag P, Saraiva Okello A, Bosch J, Dye P, Bastidas-Obando E, Dost RJJ, Luxemburg WMJ. 2015. A novel approach to estimate direct and indirect water withdrawals from satellite measurements: a case study from the Incomati basin. *Agriculture, Ecosystems and Environment* **200**: 126–142. https://doi.org/10.1016/j.agee.2014.10.023.

van Zijl GM, Le Roux P. 2014. Creating a conceptual hydrological soil response map for the Stevenson Hamilton Research Supersite, Kruger National Park, South Africa. *Water SA* **40**(2): 331–336. https://doi.org/10.4314/wsa.v40i2.15.

van Zijl GM, van Tol JJ, Riddell ES. 2016. Digital soil mapping for hydrological modelling. In *Digital Soil Mapping Across Paradigms, Scales and Boundaries*, Zhang GL, Brus D, Liu F, Song XD, Lagacherie P (eds). Springer Environmental Science and Engineering: Singapore; 115–129. https://doi.org/10.1007/978-981-10-0415-5_10.

Venter FJ. 1990. A Classification of Land for Management Planning in the Kruger National Park, PhD Thesis. University of South Africa, Pretoria.

Venter FJ, Scholes RJ, Eckhardt HC. 2003. The abiotic template and its associated vegetation pattern. In *The Kruger Experience. Ecology and Management of Savanna Heterogeneity*, Du Toit JT, Rogers KH, Biggs HC (eds). Island Press: Washington, DC; 83–129.

Verstraeten G, Poesen J. 2000. Estimating trap efficiency of small reservoirs and ponds: methods and implications for the assessment of sediment yield. *Progress in Physical Geography* **24**(2): 219–251. https://doi.org/10.1177/030913330002400204.

Verstraeten G, Poesen J. 2001. Modelling the long-term trap efficiency of small ponds. *Hydrological Processes* **15**: 2797–2819. https://doi.org/10.1002/hyp.269.

Verwer BJH. 1991. Local distances for distance transformations in two and three dimensions. *Pattern Recognition Letters* **12**: 671–682. https://doi.org/10.1016/0167-8655(91)90004-6.

Vossepoel AM. 1988. A note on 'Distance transformations in digital images'. *Computer Vision, Graphics, and Image Processing* **43**: 88–97. https://doi.org/10.1016/0734-189X(88)90045-X.

Walling DE. 1977. Limitations of the rating curve technique for estimating suspended sediment loads, with particular reference to British rivers. In *Proceedings of the Symposium on Erosion and Solid Matter Transport in Inland Waters*, Paris, July 1977, IAHS Publication 122. IAHS Press: Wallingford; 34–48.

Walling DE, Fang D. 2003. Recent trends in the suspended loads of the world's rivers. *Global and Planetary Change* **39**(1–2): 111–126. https://doi.org/10.1016/S0921-8181(03)00020-1.

Wilson BN, Barfield BJ. 1985. Modeling sediment detention ponds using reactor theory and advection-diffusion concepts. *Water Resources Research* **21**(4): 523–532. https://doi.org/10.1029/WR021i004p00523.

Yu K, D'Odorico P. 2014. An ecohydrological framework for grass displacement by woody plants in savannas. *Journal of Geophysical Research – Biogeosciences* **119**: 192–206. https://doi.org/10.1002/2013JG002577.

Supporting Information

Additional Supporting Information may be found online in the supporting information tab for this article.

Earth Surf. Process. Landforms, Vol. **43**, 463–481 (2018)

70

Chapter 5

Contemporary sediment yield and erosion rates in the Kruger National Park, South Africa, and related uncertainties

Authors: Bastian Reinwarth • Robin Petersen • Jussi Baade

1   **Contemporary sediment yield and erosion rates in the**

2   **Kruger National Park, South Africa, and related uncertainties**

3   Bastian Reinwarth[1,*], Robin Petersen[2], Jussi Baade[1]

4   1   Department of Geography, Friedrich Schiller University, Löbdergraben 32, 07743 Jena, Germany

5   2   Conservation Management, South African National Parks, Private Bag X402, Skukuza 1350,
6   South Africa

7   *   Corresponding author; Tel.: + 49 (0) 3641 9 48810; Fax: +49 (0) 3641 9 48812
8   E-mail: bastian.reinwarth@uni-jena.de

9

10   **Abstract**

11   Reservoir siltation surveys facilitate the quantification of the mean area-specific

12   sediment yield (*SSY*) of catchments for decadal and longer time spans. This requires

13   information on the volume (V_S) and dry bulk density (*dBD*) of reservoir deposits, the

14   period of time (T_R) during which they were accumulated, the reservoir sediment trap

15   efficiency (*TE*) and the catchment area (*A*). For the calculation of the catchment-wide

16   average rate of erosion by water (*E*), the sediment delivery ratio (*SDR*) of the catchment

17   needs to be estimated. Each step in this workflow represents a potential source of

18   uncertainty. The fractional contribution of individual error sources to uncertainties in

19   *SSY* and *E* values has been rarely systematically assessed. Here, we infer mean *SSY* and

20   *E* values for small to medium-sized catchments ($\leq$100 km^2) of 15 small ($\leq$350 $\times$ 10^3 m^3)

21   intermittently dry reservoirs located in the southern Kruger National Park and

22   observation periods of 30 to 65 years. We explore the relative importance of related

23   uncertainties expressed at the 95% confidence level. The resulting *SSY* values range

24   from 5 to 80 t km^{-2} yr^{-1} with a mean (and median) of 30 $\pm$ 10 t km^{-2} yr^{-1}

25   (20 [15, 50] t km^{-2} yr^{-1}) and correlate significantly with mean annual precipitation

26   (R = 0.71; p < 0.01). The mean (and median) *E* value is 85 $\pm$ 30 t km^{-2} yr^{-1}

27   (70 [45, 115] t km^{-2} yr^{-1}) when catchments being affected by gully erosion (N = 3) are

28   excluded. For gullied catchments, higher E values (up to $360\,\mathrm{t\,km^{-2}\,yr^{-1}}$) were

29   determined. Mean relative uncertainties for SSY and E values amount to $\pm21\%$ and

30    $\pm46\%$, respectively. Uncertainties in SSY values arise mainly from the TE estimation

31   (mean fractional uncertainty contribution of 64%), while the SDR estimation is the

32   major cause (79%) for uncertain E values. Uncertainties in the determination of V_S and

33   dBD values are rather unimportant, contributing together <30% and <6% to the

34   uncertainty of SSY and E values on average, respectively. Conclusions are drawn

35   regarding a reasonable surveying and sampling strategy.

36

37   **Keywords**   reservoir deposits, reservoir siltation survey, sediment mapping,

38   uncertainty propagation

39

40   ## 1. Introduction

41   Reservoir siltation surveys provide an excellent opportunity to assess the sediment yield

42   of catchments (e.g., Langbein and Schumm, 1958; Foster and Walling, 1994; Baade et

43   al., 2012). The accumulation of reservoir deposits represents an off-site effect of soil

44   erosion by water (Verstraeten et al., 2006) and is, thus, a valuable indicator for soil

45   erosion monitoring (e.g., Van Rompaey et al., 2003; Brazier, 2004; Msadala et al.,

46   2012). Interrelations between erosion, sediment yield and reservoir siltation have been

47   recently reviewed by Dutta (2016). Reservoir siltation surveys can be realized within a

48   few days and permit the quantification of the average sediment yield for decadal or

49   longer time spans (Rausch and Heinemann, 1984). Hence, the approach is particularly

50   useful for regions with inter-annually variable erosion where long-term records on

51   fluvial sediment transport are lacking (Vanmaercke et al., 2014).

52   The workflow suggested by Jolly (1982) involves the determination of the

53   volume (V_S) and dry bulk density (dBD) of reservoir deposits that accumulated

54   throughout a specific period of time (T_R). The proportion of the sediment load being

55   delivered to the reservoir that is eventually deposited in the reservoir basin defines the

56   reservoir sediment trap efficiency (TE) (Brown, 1944). In the absence of empirical data,

57   the long-term mean TE can be estimated with appropriate equations or models (e.g.,

58   Heinemann, 1981; Haan et al., 1994; Reinwarth et al., 2018). For this, the water storage

59   capacity (C) of the reservoir needs to be ascertained. Provided that the size of the

60   reservoir catchment (A) is known, the area-specific sediment yield (SSY) can be

61   calculated with Eq. (1) (e.g., Bussi et al., 2013).

62

$$SSY = \frac{V_S \cdot dBD}{T_R \cdot TE \cdot A} \tag{1}$$

63

64   Linking sediment yield and catchment erosion is not straightforward due to the

65   storage and remobilization of sediment in inter-drainage areas and along watercourses

66   upstream the reservoir (e.g., Brown et al., 2009). The sediment delivery ratio (SDR)

67   describes the interrelationship between erosion by water and fluvial sediment delivery

68   and is defined as the ratio of SSY to the catchment-wide average gross erosion rate (E)

69   (Glymph, 1954; Roehl, 1962). Hence, E can be quantified with Eq. (2) (e.g., after

70   Walling, 1983).

71

$$E = \frac{SSY}{SDR} \tag{2}$$

72

73   Errors in the quantification of *SSY* and *E* may arise from an inaccurate

74   determination of V_S (Evans and Church, 2000; Díaz et al., 2014; Ramos-Diez et al.,

75   2017), *dBD* (Verstraeten and Poesen, 2001), *A* (Oksanen and Sarjakoski, 2005) or

76   uncertainties regarding T_R. Further substantial errors may be introduced by the *TE*

77   (Rowan et al., 1995) and *SDR* estimation (USDA-SCS, 1983). Albeit some notable

78   exceptions exist (e.g., Evans and Church, 2000; Verstraeten and Poesen, 2002; Baade et

79   al., 2012), resulting uncertainties in sediment yield and catchment erosion data were

80   rarely systematically assessed and reported.

81   Here, we quantify the relative contribution of individual error sources to the total

82   uncertainty inherent in *SSY* and *E* values that were inferred from high-resolution

83   reservoir siltation surveys. The study is a contribution to a project that aims at the

84   assessment of contemporary ($<10^2$ years) and long-term ($>10^4$ years) erosion rates in the

85   southern Kruger National Park and we report contemporary mean *SSY* and *E* values for

86   small to medium-sized catchments (≤ 100 km^2) of 15 intermittently dry reservoirs. The

87   structure of the paper is as follows: the section on materials and methods starts with a

88   description of the study area and study sites. Then, the field-based determination of *C*,

89   V_S and *dBD* values is described in detail. Uncertainties regarding T_R, the estimation of

90   *TE*, the determination of *A* and the calculation of *SDR* are outlined, and the procedure

91   for the assessment of the uncertainty propagation is presented. Thereafter, the results are

92   shown, *SSY* values, *E* values and associated uncertainties are reported and the

93   correlation between *SSY* values and catchment properties is explored. In the discussion

94   section, the findings are compared to results from an earlier reconnaissance survey

95   (Baade et al., 2012) that was carried out with a distinctively lower resolution. Finally,

96   conclusions are drawn concerning an opportune survey and sampling strategy.

97

2. Materials and methods

98

2.1. Study area and study site descriptions

99

100 The Kruger National Park (KNP) is a 19,500 km^2 large conservation area located in the

101 northeast of South Africa (Fig. 1a). The area belongs to the tectonically stable

102 "Lowveld" geomorphic province (Partridge et al., 2010) with the Great Escarpment to

103 the west and the coastal plains of Mozambique to the east (Venter et al., 2003). The

104 southern KNP is characterized by an undulating relief (Fig. 1b) with altitudes ranging

105 from 150 to 840 m asl. (MacFayden et al., 2016). The entire region was subject to low

106 denudation rates (<10 m Myr^{-1}) throughout the Quaternary (Chadwick et al., 2013;

107 Glotzbach et al., 2016). The climate is semi-arid with >85% of rainfall occurring

108 between October and April (Venter et al., 2003) and monthly average temperatures

109 ranging from 17 °C in June to 27 °C in January (Zambatis, 2006). These conditions

110 support various subtypes of savanna vegetation. Major geological units

111
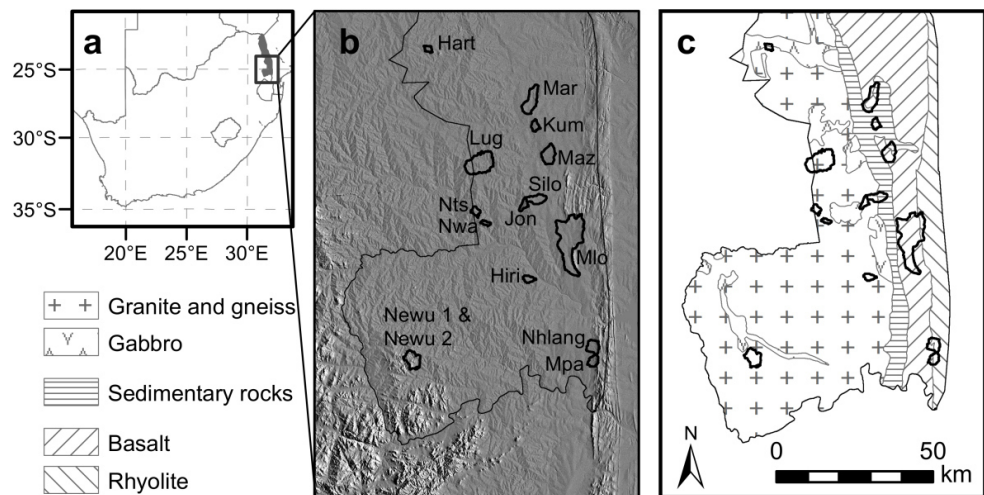
112

113 **Fig. 1.** Location of the study area and investigated reservoir catchments (N = 15): (a) the Kruger
114 National Park (KNP) within South Africa; (b) relief map of the southern KNP with catchments of
115 the surveyed reservoirs (see Table 1); (c) major lithological units in the southern KNP. The
116 hillshade representation of the relief was derived from the SRTMGL1 digital elevation model
117 (USGS EROS, 2015). Lithological units are shown according to Petersen (2012), modified after
118 Geological Survey of South Africa (1986a, b).

119   strike from north to south (Fig. 1c), with intrusive rocks (i.e., granite, gneiss and

120   gabbro) in the west, volcanic rocks (i.e., basalt, rhyolite and granophyre) in the east, and

121   a narrow stretch of sedimentary rocks (i.e., shales of the Ecca Group and sandstones) in

122   between (Geological Survey of South Africa, 1986a, 1986b). Footslopes of granite areas

123   are prone to the formation of solonetzes (Van Tol et al., 2015). Some of these sodic

124   patches are nearly bare of vegetation and were identified as potential erosion hotspots

125   partially supporting gully formation (Khomo and Rogers, 2005). Less than 3% of the

126   KNP is directly disturbed by human infrastructure (Freitag-Ronaldson et al., 2003).

127   Thus, large parts of the KNP can be considered intact wilderness (MacFayden, 2010).

128   About 50 small reservoirs with earth and concrete dams were established in the

129   KNP prior to 1975 to secure water provision for wildlife (Pienaar, 1985). They impound

130   intermittent surface runoff and trap sediment. Water levels fall during extended

131   droughts and rise rapidly within the course of runoff events (Reinwarth et al., 2018).

132   Uncontrolled overflow spillways permit the release of water and suspended sediment

133   when the water storage capacity is exhausted. Reservoir deposits are accumulated in the

134   lowest parts of the reservoir basins (Fig. 2) and can be characterized as black silt loams

135

136

137   **Fig. 2.** The dried-out Jones-Se reservoir in September 2015. Black silt loams in the lower part of
138   the reservoir basin can be easily distinguished from bright adjacent soils and sediments. Close
139   to the dam (in the foreground), the width of the reservoir deposits is about 50 m. The Leica
140   GS10 base station on the dam crest to the left marks the local reference point (LRP) that was
141   established for high-resolution surveying with the real-time kinematic global navigation
142   satellite system (RTK GNSS).
143

144 (Reinwarth et al., 2017), referring to the texture nomenclature of the FAO (2014). They

145 overlie soils and fluvial sediments that are typically brighter in colour and coarser in

146 grain size (Baade et al., 2012). Surfaces of dry reservoir deposits exhibit prominent

147 desiccation cracks, while footprints of large mammals (e.g., elephants and

148 hippopotamus) point to intensive bioturbation. Bedload from tributaries is deposited

149 close to the reservoir inlets and further upstream and consists mainly of sand and gravel.

150 Here, reservoir siltation was assessed in nine reservoirs that dried-out

151 temporarily between 2014 and 2016 (i.e., the Hartbeesfontein, Marheya, Mazithi,

152 N'tswiriri, Jones-Se, Mlondozi, Mpanamana, Kumana and N'watimhiri reservoirs) and

153 six reservoirs that were decommissioned between 2004 and 2015 (i.e., Lugmag,

154 Silolweni, N'wanetsana, Newu 1, Newu 2 and Nhlanganzwani reservoirs). Dam failures

155 occurred at the Mpanamana reservoir in 1968 and 1971 after which the dam was soon

156 repaired (Baade et al., 2012). The dam of the Newu 1 reservoir broke during a major

157 flood in 2000, was repaired, but eventually decommissioned in 2004. Thereafter, the

158 free-flowing stream cut into the reservoir deposits, thereby eroding a significant

159 proportion of the accumulated sediment. Prior to 2004, the Newu 1 and Newu 2

160 reservoirs were impounded by the same dam, but fed by different tributaries. Both

161 reservoirs became connected during flood events, but show clearly separated areas of

162 sediment deposition. Thus, the Newu 1 and Newu 2 reservoirs are considered separately

163 in this study. The Lugmag dam was damaged during a flood in 2012 and not repaired,

164 but there was no indication for a substantial loss of reservoir deposits until the survey

165 date. No dam failures have been reported for the other study sites.

166 The reservoir catchments (Fig 1b) vary in size from 0.6 to 104 km^2 and represent

167 the diversity of environmental conditions in the southern KNP (Table 1). The mean

168 slope inclination (*Slope*), derived from the Shuttle Radar Topographic Mission (SRTM)

169   1 arc-second (~30 m) digital elevation model (SRTMGL1, USGS EROS, 2015), ranges

170   from 1.0° to 6.3° (Fig. 3a). The mean annual precipitation (*MAP*), interpolated from

171   data of rainfall stations by means of Thiessen polygons (Reinwarth et al., 2018), varies

172   between 530 and 670 mm (Fig. 3b). According to the fractional woody cover (*WCOV*)

173   map by Bucini et al. (2010), mean *WCOV* values are 16% to 30% (i.e., grassland and

174   open tree savanna) for catchments that are primarily underlain by

175

176   **Table 1** Catchment properties of the investigated reservoirs: catchment size (A); mean slope
177   inclination (Slope; based on SRTMGL1, USGS EROS, 2015), mean annual precipitation (MAP;
178   based on rainfall data from meteorological stations provided by SANParks Scientific Services,
179   Skukuza, and interpolation with Thiessen polygons), mean fractional woody cover (WCOV;
180   Bucini et al., 2010), area percentage of bare surfaces (BareSurf) and roads (based on aerial
181   images; NGI, 2016) and catchment lithology (Geological Survey of South Africa, 1986a, 1986b).

ID	Reservoir	A [km^2]	Slope [°]	MAP [mm]	WCOV [%]	BareSurf [%]	Roads [%]	Lithology
Hart	Hartbeesfontein	4.2	2.4	560	41	3.3	0.3	Granite/Gneiss (65%) Gabbro (35%)
Mar	Marheya	27.4	2.2	530	23	0.1	0.3	Basalt (54%) Sandstone (46%)
Lug	Lugmag	47.4	1.9	550	40	0.3	0.6	Granite/Gneiss (100%)
Maz	Mazithi	19.9	1.0	550	25	<0.1	0.1	Sandstone (99%) Basaltic rocks (1%)
Nts	N'tswiriri	5.5	2.4	550	36	<0.1	0.7	Granite/Gneiss (100%)
Jon	Jones-Se	6.2	2.5	550	41	<0.1	0.2	Granite/Gneiss (100%)
Silo	Silolweni	13.3	1.4	550	50	1.5	0.2	Ecca Group (54%) Granite/Gneiss (46%)
Nwa	N'wanetsana	3.3	5.4	550	40	<0.1	0.0	Granite/Gneiss (100%)
Mlo	Mlondozi	104.2	1.8	580	16	0.1	0.3	Basaltic rocks (88%) Rhyolite/Granophyre (12%)
Newu 1	Newu 1	20.4	6.3	670	37	0.2	0.2	Granite/Gneiss (89%) Gabbro (11%)
Newu 2	Newu 2	0.6	3.2	670	33	0.4	0.0	Granite/Gneiss (100%)
Nhlang	Nhlanganzwani	16.5	3.0	580	30	0.6	0.2	Basaltic rocks (50%) Rhyolte/Dacite (50%)
Mpa	Mpanamana	10.0	3.5	610	30	0.5	0.4	Rhyolite/Dacite (54%) Basaltic rocks (46%)
Kum	Kumana	6.6	2.1	550	40	0.2	0.3	Sandstone (96%) Ecca Group (4%)
Hiri	N'watimhiri	6.3	2.7	560	41	0.7	<0.1	Granite/Gneiss (100%)

182

183
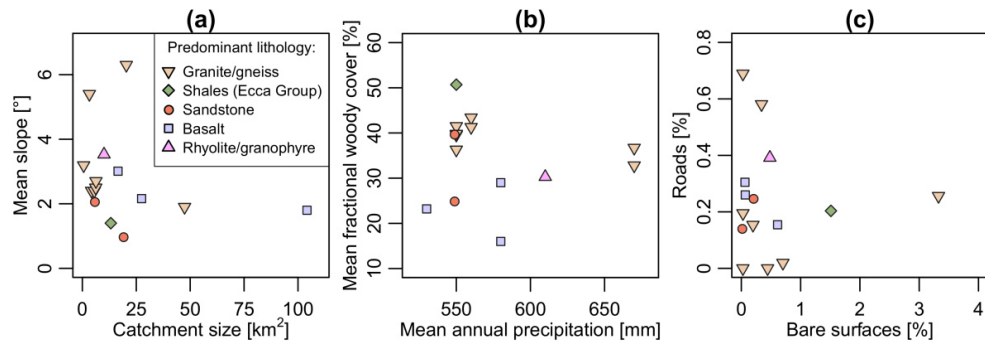
Fig. 3. Overview on catchment properties of the investigated reservoirs: (a) catchment size and
mean slope inclination (based on SRTMGL1, USGS EROS, 2015); (b) mean annual precipitation
(based on rainfall data from meteorological stations provided by SANParks Scientific Services,
Skukuza and Thiessen polygons); and mean fractional woody cover (Bucini et al., 2010);
(c) area percentage of bare surfaces (excluding roads and rock exposures) and roads (NGI,
2016). The predominant lithology of the catchments was derived from 1:250,000 geological
maps (Geological Survey of South Africa, 1986a, 1986b).

volcanic rocks, and 30% to 50% (i.e., bush and shrub savanna) for catchments being

characterized by intrusive and sedimentary rocks. The only exception is the Mazithi

catchment that is dominated by sandstone, but shows a low *WCOV* value of 25%.

Several catchments encompass areas that are nearly bare of vegetation. Mapping the

area percentage of bare surfaces (*BareSurf*) from aerial images acquired between 2008

and 2010 (NGI, 2016) and excluding roads and erosion-resistant rock outcrops reveals

BareSurf values >1% for the Hartbeesfontein (3.3%) and Silolweni catchments (1.5%)

and values <1% for all other sites (Fig. 3c). Gully systems were detected in the

Hartbeesfontein, Silolweni and Newu 1 catchments. The area percentage of roads

(*Roads*) on the reservoir catchments, as derived from aerial images (NGI, 2016), ranges

from 0.0% to 0.7%.

205 **2.2. Survey of the current reservoir basin topography**

206 The reservoir basins were surveyed using the Global Navigation Satellite System

207 (GNSS). At each reservoir, a Local Reference Point (LRP) was established with

208 reference to the South African network of continuously operating GNSS stations

209 (TrigNet). High temporal resolution GNSS data (1 s) spanning 6 to 8 hours per day

210 were collected using a Leica GS10 base station. Post-processing of TrigNet and LRP

211 records to determine LRP coordinates was conducted with the software Leica Geo

212 Office (vers. 8.4; Leica Geosystems, 2014). A real-time kinematic (RTK) GNSS survey

213 of the basin topography was carried out along transects as exemplified in Fig. 4 for the

214

215
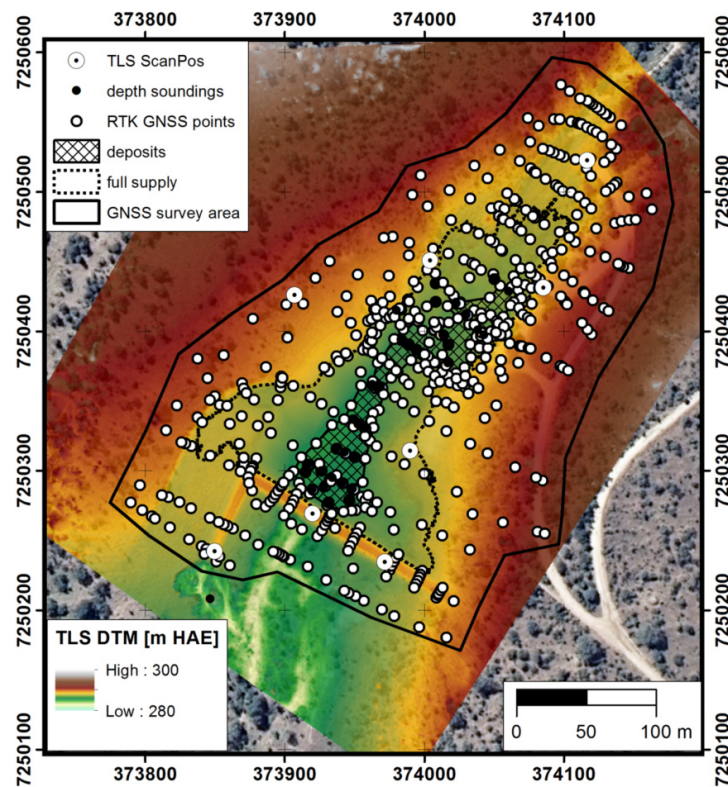
216 **Fig. 4.** TIN representation of the Digital Terrain Model (DTM) for the present-day Jones-Se
217 reservoir basin obtained from Terrestrial Laser Scanning (TLS), scan positions (TLS ScanPos),
218 position of RTK GNSS survey points and location of depth soundings. Coordinates (in meters)
219 refer to the UTM projection, Zone 36, WGS 84 Datum. Heights are shown in meters above the
220 ellipsoid (HAE) of WGS 84.

221

222   Jones-se reservoir and included a survey of the reservoir deposits boundary. The survey

223   point density was enhanced along terrain breaks (e.g., the dam, shoreline notches and

224   banks). Each point was determined with reference to the LRPs using a Leica GS15

225   rover operated in RTK mode with a measurement period of 10 s. The total number of

226   RTK GNSS points for the ten reservoirs surveyed solely using RTK GNSS varied from

227   300 to >1000 which corresponds to an average posting of 10 to 20 m (Table 2).

228

229   **Table 2** Spatial resolution of the RTK GNSS and TLS surveys and sediment mapping based on
230   depth soundings (DS) with soil augers.

Reservoir	Survey area [ha]			Number of points			Posting [m]		
	RTK GNSS	TLS	DS	RTK GNSS	TLS[1]	DS	RTK GNSS	TLS[1]	DS
Hartbeesfontein	11.7	13.1	1.2	802	1.2×10^6	45	12.1	0.25	16.6
Marheya	22.2	n.a.	2.4	943	n.a.	39	15.3	n.a.	24.9
Lugmag	38.5	n.a.	2.6	1075	n.a.	63	18.9	n.a.	20.2
Mazithi	n.a.	27.2	1.2	n.a.	1.5×10^6	26	n.a.	0.25	21.8
N'tswiriri	n.a.	5.2	0.3	n.a.	3.4×10^6	32	n.a.	0.10	8.9
Jones-Se	9.3	17.9	0.6	574	2.0×10^6	36	12.7	0.25	12.7
Silolweni	46.7	n.a.	4.2	1087	n.a.	59	20.7	n.a.	26.6
N'wanetsana	8.4	n.a.	0.3	682	n.a.	35	11.1	n.a.	9.1
Mlondozi	20.3	26.5	5.1	435	3.5×10^6	65	21.6	0.20	28.0
Newu 1	26.2	n.a.	4.2	1291	n.a.	72	14.3	n.a.	24.2
Newu 2	7.9	n.a.	0.2	301	n.a.	18	16.2	n.a.	11.6
Nhlanganzwani	35.4	n.a.	3.7	854	n.a.	56	20.3	n.a.	25.7
Mpanamana	n.a.	19.6	2.9	n.a.	1.4×10^6	56	n.a.	0.25	22.6
Kumana	n.a.	32.3	1.1	n.a.	2.6×10^6	34	n.a.	0.25	18.2
N'watimhiri	n.a.	7.5	0.4	n.a.	0.7×10^6	34	n.a.	0.25	11.0
Mean	*22.7*	*18.7*	*2.0*	*804*	*2.0×10^6*	*45*	*16.3*	*0.23*	*18.8*

231   1) For the ease of data processing, the posting of TLS data was reduced to 0.10 to 0.25 m.
232

233   At eight reservoirs, the basin topography was surveyed with a Riegl VZ-1000

234   Terrestrial Laser Scanner in 300 kHz acquisition mode providing a maximum range of

235   about 450 m. Panorama scans with an angular resolution of 0.04° were conducted from

236   several positions around the reservoir (Fig. 4) to minimize data gaps from occlusion.

237   The point clouds were co-registered using RTK GNSS tie points and the Multi-Station

238   Adjustment (MSA) tool implemented in RiScan Pro 2.5 (Riegl, 2017), where needed.

239   Processing of the point cloud involved the limitation to single and last targets and the

240   removal of non-terrain points (e.g., vegetation) with the terrain filter implemented in

241   RiScan Pro. The total number of terrain points obtained from laser scanning varies from

242   41 to 100×10^6. However, for the ease of data processing, the original point clouds were

243   reduced to data sets with 0.01 m vertical and 0.1 to 0.25 m horizontal resolution

244   (Table 2).

245   Accordingly, TLS data provide a very detailed representation of the basin

246   topography which is evident in a >40 times higher average resolution for TLS than for

247   RTK GNSS surveys. RTK GNSS and TLS surveys were carried out jointly in

248   Hartbeesfontein, Jones-Se and Mlondozi reservoirs which permits a method

249   comparison. Mean position errors (1σ) of TLS and GNSS survey points were <0.02 m

250   with reference to established LRPs (Baade and Schmullius, 2016) and are therefore

251   negligible (Balzter et al., 2016).

252

253   **2.3. Mapping of reservoir deposits**

254   The thickness of the reservoir deposits was mapped based on depth soundings with a

255   Pürckhauer-type soil auger (1.5 m; Ø: 18 mm) and a gouge auger (3.4 m; Ø: 12 mm).

256   Between 18 and 72 depth soundings were performed per reservoir along up to 14

257   transects running perpendicular to the former thalweg. This corresponds to a posting

258   ranging from 9 to 30 m for areas being currently covered with reservoir deposits

259   (Table 2). For each depth sounding, the boundary between the post-dam facies (i.e.,

260   black silt loams; Fig. 2) and the pre-dam facies (i.e., soils and fluvial sediments) was

261   identified based on colour and grain size. The validity of this visual identification has

262   been confirmed by statistical analysis on physicochemical properties of 250 samples

263   (Reinwarth et al., 2017). The distance between the facies boundary and the sediment

264   surface equals the thickness of the reservoir deposits which was ascertained with a

265   folding rule. When the boundary was not clearly identifiable, the minimum and

266 maximum sediment thickness were recorded and used separately in the calculation of

267 the volume of the reservoir deposits.

268 Errors in sediment thickness readings are mainly due to the probing with

269 hammer-driven augers (Garrison, 2016). The sediment may become compacted as the

270 auger is driven into the ground. On the opposite, friction may lead to a downward

271 displacement of sediment when the auger is removed. Additional minor errors may arise

272 from measuring inaccuracies. Effects of sediment compaction and displacement as well

273 as measuring errors are random and likely averaged out with an increasing number of

274 observations. The absolute uncertainty of mean values can be quantified with Eq. (3)

275 assuming unbiased and normally distributed random errors (e.g., Crawley, 2007).

276

$$Cl95 = \frac{\sigma \cdot t_{0.025,\ N-1}}{\sqrt{N}} \tag{3}$$

277

278 *Cl95* denotes the uncertainty of the mean value at the 95% confidence level, N is the

279 number of observations, σ is the standard deviation of all observations and $t_{0.025,\ N-1}$ is

280 the appropriate two-sided t value derived from Student's t distribution with $N - 1$

281 degrees of freedom.

282 Fig. 5 illustrates that the *Cl95* uncertainty of the mean sediment thickness,

283 obtained from all sediment thickness readings, decreases with an increasing number of

284 depth soundings. Assuming unbiased and normally distributed 2σ errors of ±1 cm,

285 ±3 cm and ±5 cm for individual readings, the *Cl95* uncertainty of the mean sediment

286 thickness drops below ±1 cm (±2.5 cm) when the number of depth soundings exceeds

287 3 (2), 11 (3) and 26 (6), respectively. It must be taken into account that errors

288
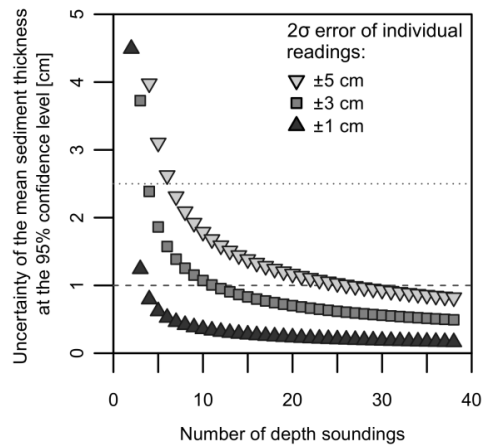
Fig. 5. The effect of unbiased and normally distributed errors in individual sediment thickness readings and the number of depth soundings on the (two-tailed) uncertainty of the determined mean sediment thickness. The uncertainty of the mean sediment thickness was calculated based on Student's t distribution and is displayed at the 95% confidence level.

are probably not perfectly unbiased and normally distributed. Hence, the uncertainty of

the mean sediment thickness was assumed to be ±2.5 cm for all reservoirs.

2.4. Determination of the water storage capacity (C) of the reservoir and the volume

of reservoir deposits (V$_S$)

In order to determine the water storage capacity (*C*) of the reservoirs and the volume of

reservoir deposits (*V$_S$*), three different digital terrain models (DTMs) were compiled for

each reservoir. The first model represents the topography of the dried-out reservoir

basin at the survey date (Fig. 4). This DTM was created from surface points surveyed

either with the RTK GNSS or the TLS. The second model represents minimum altitude

bounds for the reconstruction of the initial basin topography, and the third model the

corresponding maximum altitude bounds. Minimum (and maximum) altitude bounds

were calculated by subtracting the maximum (minimum) sediment thickness from the

altitude of the current sediment surface. The difference between the second and third

309   version of DTMs represents the uncertainty that arises from depth soundings where the

310   boundary between the pre- and post-dam facies was not clearly identifiable.

311   All DTMs are based on triangular irregular network (TIN) interpolation carried

312   out with the software ArcGIS 10.4 (Esri, 2015). For DTMs that were generated from

313   RTK GNSS data and sediment thickness readings, breaklines representing the dams and

314   other terrain features as well as reconstructed thalwegs were introduced to enhance the

315   TIN representation of the basin topography. The position of thalwegs was approximated

316   by connecting the lowest points in the reconstructed pre-dam topography of all depth

317   sounding transects. For the Newu 1 reservoir where a channel cut into the reservoir

318   deposits after the failure of the dam in 2000, the pre-erosional basin topography was

319   reconstructed. This reconstruction is based on the interpolation between terraces

320   consisting of reservoir deposits that were surveyed on both sides of the incised channel.

321   For the Hartbeesfontein, Jones-Se and Mlondozi reservoirs, DTMs were generated both

322   from the RTK GNSS and the TLS observations.

323   The DTMs were used to derive the full supply area (A_R) of the reservoirs, the

324   initial water storage capacity (C_R) and the storage capacity at the survey date (C_s). C_R

325   was determined by calculating the average of the respective minimum ($C_{R,\ min}$) and

326   maximum bounds ($C_{R,\ max}$) that were obtained from the DTMs representing the

327   maximum and minimum altitude bounds of the pre-dam topography, respectively. C_S

328   and A_R were calculated assuming a height accuracy of ±2.5 cm for the elevation of the

329   overflow spillway. For the spillways of the broken Newu 1 and Newu 2 dams, a lower

330   height accuracy of ±5 cm was assumed. The volume of the reservoir deposits (V_S) that

331   accumulated during the lifetime of the reservoir equals the difference between C_R and

332   C_S. In addition, the area that is currently covered with reservoir deposits (A_S) was

333   determined from data of the RTK GNSS survey.

334   Uncertainties in the calculation of V_S arise from the random error in the

335   determination of the mean sediment thickness (see section 2.3), whereby the mean

336   sediment thickness equals the ratio of V_S to A_S. Further uncertainty is due to the

337   difference between $C_{R, max}$ and $C_{R, min}$ that results from depth soundings for which the

338   boundary between the pre- and post-dam facies was not clearly identifiable. Following

339   Taylor (1997), the overall absolute uncertainty δV_S was calculated with Eq. (4) where

340     $\delta V_{S, ran}$ denotes the absolute random error at the 95% confidence level ($Cl95$), and

341     $\delta V_{S, boundary}$ is the absolute uncertainty arising from the identification of the facies

342   boundary.

343

$$\partial_{VS} = \sqrt{\partial V_{S, \, ran}{}^2 + \partial V_{S, \, boundary}{}^2} \qquad (4)$$

344

345   Depending on the posting of the depth soundings, additional errors may be introduced

346   by the TIN interpolation (Heritage et al., 2009). However, in this study, the posting of

347   depth soundings is rather low (i.e., high resolution) and comparable to (i.e., 0.7 to

348   1.7 times) the posting of RTK GNSS survey points (Table 2). For the Hartbeesfontein,

349   Jones-Se and Mlondozi reservoirs, where RTK GNNS and TLS survey data are both

350   available, the $Cl95$ intervals of C_S values obtained from the RTK GNSS-based and

351   TLS-based DTMs are all overlapping. Hence, the effect of interpolation errors on

352   V_S values is assumed to be negligible. In this study, the random uncertainty $\delta V_{S, \, ran}$ is the

353   major source of uncertainty contributing to δV_S as it is 1 to >10 times higher than the

354   uncertainty range $\delta V_{S, \, boundary}$ for all investigated reservoirs. Since $\delta V_{S, \, ran}$ values

355   correspond to the 95% confidence level, δV_S can be likewise interpreted as a $Cl95$

356   interval.

357

2.5. Determination of the dry bulk density (dBD)

358

359 Samples for the determination of the dry bulk density (*dBD*) of the reservoir deposits

360 were gathered from the sediment surface (0 to 0.05 m) at various locations across the

361 reservoir basin using stainless steel core rings (100 cm^3; Ø: 50 mm). Up to three profiles

362 per reservoir were established to examine *dBD* variations in the vertical dimension.

363 Vertical sampling (up to 2.7 m) was conducted in central positions close to the dam and

364 in the middle part of the reservoir basin. Subsurface samples were recovered

365 alternatively with core rings or a liner sampler (0.3 m; Ø: 50 mm) using a sampling kit

366 with extension rods (Eijkelkamp®). In the laboratory, liners were sub-sampled and the

367 height of the aliquots (ca. 50 mm) was measured to determine the sample volume. Core

368 ring and liner samples were weighed and oven-dried at 105 °C for at least 24 h after

369 which no further weight reduction was recorded. The *dBD* was calculated by dividing

370 the dry sample mass through the bulk sediment volume. In addition, the water content

371 of the samples (in wt. %) was ascertained and is reported relative to the wet mass.

372 The determination of the *dBD* was found to be more difficult for dry surfaces

373 with abundant desiccation cracks. The cracks result from swelling and shrinkage of fine

374 reservoir deposits with changing water content (Stewart et al., 2016) and are particularly

375 prominent in areas with very fine deposits close to the dam. Driving core rings and

376 liners into these surfaces frequently led to disruption of the sampled material, rendering

377 *dBD* determination from these samples unreliable (Grossmann and Reinsch, 2002).

378 Consequently, core ring and liner samples containing disrupted material were discarded.

379 Instead, clod samples (0 to <0.15 m) were gathered to obtain *dBD* values from cracked

380 surfaces. Following Burt and Soil Survey Staff (2014), three clods were collected within

381 a circumference of 1 m to determine the average *dBD* for each sample location. Clods

382 were reduced to about fist-size using hammer, chisel and spatula. Clod samples were

383   oven-dried to ascertain the dry mass. Following Baade et al. (2012), the volume was

384   determined by submerging the clods in oil and recording the volume displacement. A

385   fluid with a high viscosity was chosen to prevent intrusion of liquid into clods.

386   However, as the clods were not sealed (cf. Brasher et al., 1966), some oil intruded into

387   pores and along cracks. Thus, clods were weighed prior to and after immersion.

388   Immediately after the immersion, oil was allowed to drip off and the clod surface was

389   thoroughly dried with paper towel. Hence, the weight difference can be attributed to

390   intruded oil. The determined clod volume was corrected based on the determined mass

391   increase and the density of the oil (mean $\pm$ $Cl95$: 0.91 ± 0.02 g cm^{-3}) which was

392   ascertained from three independent measurements. The clod method typically results in

393   0.1 g cm^{-3} (Van Remortel and Shields, 1993) to 0.15 g cm^{-3} (Pires et al., 2011) higher

394   dBD values than sampling with core rings, because the clod method does not fully

395   account for the volume of macro pores and cracks. Thus, dBD values obtained from

396   clods were diminished by 0.1 g cm^{-3}, following Baade et al. (2012).

397   Neither sampling with core rings nor the clod method account for the volume of

398   large (up to 8 cm wide) desiccation cracks (Fig. 6). This leads to an overestimation of

399   dBD values where desiccation cracks are prominent. Thus, the volume fraction of

400   desiccation cracks on the bulk sediment was investigated. Rectangular reference areas

401   $(1 \times 1$ m$)$ of cracked sediment surfaces were marked with folding rulers. Hand-held

402   nadir photos were taken from about 1.5 m above ground and the mean depth of the

403   cracks in the reference area was determined. Nadir photos were ortho-rectified and areas

404   representing sediment columns and cracks were mapped to quantify the area percentage

405   of cracks at the surface. The mean depth and mean area percentage of cracks were

406   calculated from ten sample locations in total. Correction factors were compiled

407   assuming v-shaped desiccation cracks (Cummins and Potter, 1967; Baade et al., 2012),

408   i.e., correction factors equal one minus the proportion of cracks on the sediment surface

409   and increase linearly towards one with increasing sampling depth until the mean depth

410   of the cracks is reached. The mapping of desiccation cracks revealed a mean area

411   percentage and a mean depth ($\pm Cl95$) of 29 $\pm$ 6 % and 19 $\pm$ 3 cm with maximum values

412   of up to 45% and 35 cm, respectively (Fig. 6). This results in correction factors of 0.75

413   (or 0.86) for a mean sampling depth of 2.5 cm (10 cm). Corrected *dBD* values were

414   obtained by multiplying correction factors and uncorrected *dBD* values. Mean *dBD*

415   values with *Cl95* uncertainties as well as coefficients of variation (*CV*) were calculated

416   separately for the investigated reservoirs. In addition, these statistics were calculated

417   from all site-specific means. No *dBD* data is available for the N'tswiriri reservoir for

418   which the mean *dBD* value of the nearby N'wanitsana reservoir was adopted.

419
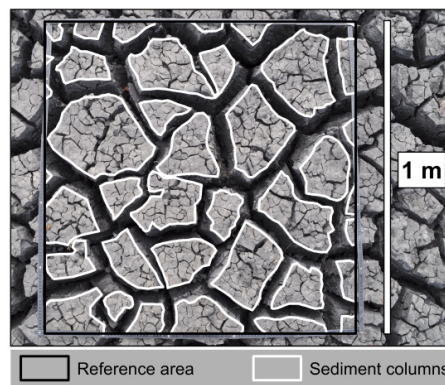
420

421   **Fig. 6.** A heavily cracked sediment surface. Mapping reveals that up to 35 cm deep v-shaped
422   desiccation cracks make up 45 % of the reference area.
423

424   **2.6. Duration of sediment accumulation (T_R)**

425   The period of time (T_R) during which the reservoir deposits were accumulated starts

426   with the year of dam construction (T_C) and ends with the year of surveying or dam

427   decommissioning (T_S). T_C has been reported for most investigated reservoirs by Pienaar

428   (1985) and Kloppers and Bornman (2005) as shown in Table 3. Since T_S is known, this

429   implies a low uncertainty of ±1 year for most T_R values. Unfortunately, T_C is not exactly

430   known for the Mazithi, Kumana and N'watimhiri reservoirs. A small dam next to the

431   present-day Mazithi dam was already established in the 1930s (Pienaar, 1985), but

432   aerial images (NGI, 2016) show that the Mazithi reservoir did not exist in its current

433   configuration prior to 1944. The completion of the present-day Mazithi and Kumana

434   dams was most probably associated to the establishment of a tar road that leads over

435   both dam crests. Another tar road is situated on the crest of the N'watimhiri dam. The

436   first tar roads within the KNP were established in 1961 (Freitag-Ronaldson and

437

438   **Table 3** Characteristics of reservoirs and reservoir catchments: year of dam construction (T_C;
439   according to Pienaar (1985) and Kloppers and Bornman (2005), year of a dam failure (if
440   applicable), year of surveying or decommissioning (T_S), effective time of sediment
441   accumulation (T_R) with maximum uncertainties, current status of the investigated reservoirs,
442   i.e., either decommissioned (De) or active (Ac), trap efficiency (TE) estimates with uncertainties
443   at the 95% confidence level (Reinwarth et al., 2018), catchment size (A) with 2σ uncertainties
444   (modified after Baade and Schmullius, 2015) and estimated sediment delivery ratio (SDR) with
445   uncertainties at the 95% confidence level (based on USDA-SCS, 1983).

Reservoir	T_C	Failure	T_S	T_R [years]	Status	TE [%]	A [km²]	SDR
Hartbeesfontein	1950	–	2015	65 ± 1	Ac	70 ± 8	4.2 ± 0.1	0.30 ± 0.10
Marheya	1970	–	2014	44 ± 1	Ac	71 ± 8	27.4 ± 0.8	0.20 ± 0.10
Lugmag	1957	2012	2012	55 ± 1	De	40 ± 10	47.4 ± 1.3	0.20 ± 0.10
Mazithi	1961[1]	–	2016	49 ± 8	Ac	60 ± 15	19.9 ± 0.6	0.25 ± 0.10
N'tswiriri	1960	–	2016	56 ± 1	Ac	50 ± 10	5.5 ± 0.2	0.30 ± 0.10
Jones-Se	1957	–	2015	58 ± 1	Ac	56 ± 9	6.2 ± 0.2	0.30 ± 0.10
Silolweni	1969	–	2008	39 ± 1	De	72 ± 6	13.3 ± 0.4	0.25 ± 0.10
N'wanetsana	1960	–	2014	54 ± 1	De	50 ± 10	3.3 ± 0.1	0.35 ± 0.15
Mlondozi	1951	–	2016	65 ± 1	Ac	25 ± 10	104.2 ± 2.9	0.15 ± 0.05
Newu 1	1971	2000	2004	31 ± 2	De	80 ± 15	20.4 ± 0.6	0.25 ± 0.10
Newu 2	1971	–	2014	43 ± 1	De	91 ± 8	0.6 ± 0.1	0.45 ± 0.15
Nhlanganzwani	1956	–	2007	51 ± 1	De	83 ± 8	16.5 ± 0.5	0.25 ± 0.10
Mpanamana	1958	1968, 1971	2016	52 ± 8	Ac	70 ± 10	10.0 ± 0.3	0.25 ± 0.10
Kumana	1961[1]	–	2015	48 ± 7	Ac	90 ± 8	6.6 ± 0.2	0.30 ± 0.10
N'watimhiri	1961[1]	–	2015	46 ± 9	Ac	89 ± 8	6.3 ± 0.2	0.30 ± 0.10

446   1) The construction of the first tar roads in the KNP in 1961 represents a maximum age for the Mazithi,
447   Kumana and N'watimhiri reservoirs. A minimum age was derived from aerial images.

448

449   Foxcroft, 2003) which is interpreted as a maximum age for the three reservoirs. A

450   minimum age can be derived from aerial images (NGI, 2016) indicating that the Mazithi

451   and Kumana reservoirs were installed prior to 1974, while the N'watimhiri reservoir was

452   built before 1978. Adopting the mean value of minimum and maximum ages results in

453   T_R values of 49 ± 8, 48 ± 7 and 46 ± 9 years for the Mazithi, Kumana and N'watimhiri

454   reservoirs, respectively. For the Mpanamana reservoir that was established in 1958, it is

455   unknown how much reservoir deposits were removed due to dam failures prior to 1971.

456   This results in an uncertainty of ±8 years for the T_R value. Likewise, an uncertainty of

457   ±2 years was adopted for the Newu 1 reservoir, since it is unclear whether the backward

458   incision of the channel started as a consequence of the dam failure in 2000 or only after

459   the decommissioning in 2004. Hence, the relative uncertainty of T_R values (ε_{TR}) ranges

460   from ±2% to ±20% among the investigated reservoirs.

461

462   **2.7. Estimation of the sediment trap efficiency (TE)**

463   The sediment trap efficiency (*TE*) of the reservoirs has been estimated with a modelling

464   framework described in detail by Reinwarth et al. (2018). This framework takes into

465   account that the reservoirs spill only during infrequent runoff events when the water

466   storage capacity is exhausted, while a *TE* of 100% can be assumed for extended periods

467   without spillage. In the absence of runoff records, catchment runoff was simulated with

468   the daily time-step Pitman rainfall-runoff model (Pitman, 1976). The relationship

469   between water and sediment discharge was modelled based on sediment rating curves.

470   Nine scenarios were established to cope with uncertainties that arise from hydrological

471   modelling and assumptions concerning sediment rating curves (for details, see

472   Reinwarth et al., 2018). The mean *TE* was calculated from all nine scenarios and ranges

473   from 25% to >90% among the reservoirs (Table 3). The relative *Cl95* uncertainty (ε_{TE})

474   of the mean *TE* varies between ±8% and ±37%.

475

476   **2.8. Determination of the catchment size (A)**

477   The catchment area of the reservoirs (Fig. 1b, c) was ascertained separately from six

478   different digital elevation models (DEMs) using the software ArcHydro Tools (Esri

479   Water Resources Team, 2014). Baade and Schmullius (2015) delineated the catchments

480   based on the 0.4 (~12 m), 1 (~30 m) and 3 arc-second (~90 m) versions of the

481   TanDEM-X Intermediate DEM (IDEM; Bräutigam et al., 2014) and the void-filled

482   1 arc-second (SRTM1GL, USGS EROS, 2015) and 3 arc-second versions (SRTM4.1,

483   Jarvis et al., 2008) of the Shuttle Radar Topography Mission (SRTM) DEM. In

484   addition, the catchment size was determined from the 1 arc-second version of the final

485   TanDEM-X DEM (Zink et al., 2016) that became available in April 2017. For each

486   reservoir, the mean catchment size (*A*) and the corresponding 2σ deviation were derived

487   from all six DEMs (Table 3). The mean relative 2σ deviation (ε_A) amounts to ±3% and

488   was adopted as a general uncertainty estimate for catchment size in this study.

489

490   **2.9. Estimation of the sediment delivery ratio (SDR)**

491   The majority of worldwide observations on the mobilization and transport of sediments

492   in river catchments $<10^4$ km^2 points to a decreasing sediment delivery ratio (*SDR*) with

493   increasing catchment size (*A*) (de Vente et al., 2007). Many authors have argued for an

494   exponential relationship (Eq. 5) with empirically fitted coefficients κ_1, κ_2, and κ_3 (e.g.,

495   Auerswald, 1989).

$$SDR = \kappa_3 + \kappa_1 \cdot A^{\kappa_2} \tag{5}$$

496

497 The prediction of the *SDR* with Eq. (5) represents a black-box concept (Walling, 1983),

498 since influencing factors such as rainfall conditions, contributions from different

499 sediment sources, sediment and hydrologic connectivity in catchments and

500 characteristics of the eroded material (Klaghofer et al., 1992; Lu et al., 2006; Wohl et

501 al., 2017) are not taken into account. It is therefore expectable that relationships

502 between *SDR* and *A* are variable (Fryirs, 2013).

503 Table 4 shows values for the coefficients κ_1, κ_2, and κ_3, derived from data

504 presented by USDA-SCS (1983), from which minimum, maximum, and best estimates

505 for *SDR* values can be calculated based on Eq. (5). Best estimates according to

506 USDA-SCS (1983) were adopted in this study and the respective uncertainty was

507 calculated at the 95% confidence level (*Cl95*). For this, a normal distributed deviation

508 of *SDR* values from best estimates was assumed. Minimum and maximum estimates

509 were interpreted as 3σ bounds (i.e., 99.7% of *SDR* values fall in between). Based on

510 these assumptions, *Cl95* intervals were calculated from equidistant percentiles (i.e.,

511 0.1%, 17%, 33%, 50%, 67%, 83%, and 99.9%). Accordingly, best estimates for *SDR*

512 values range from 0.15 to 0.45 for the study sites (Table 3) with relative uncertainties

513 (ε_{SDR}) varying from ±35% to ±42% (Fig. 7).

514

515 **Table 4** Values for the parameters κ_1, κ_2 and κ_3 in Eq. (5) for the estimation of the sediment
516 delivery ratio based on catchment size according to USDA-SCS (1983).

	κ_1	κ_2	κ_3	Unit of A
Minimum estimate	0.103	-0.299	0.005	mi^2
Best estimate	0.644	-0.096	-0.302	mi^2
Maximum estimate	1.902	-0.048	-1.331	mi^2

517 Note: 1 mi^2 equals 2.59 km^2

518
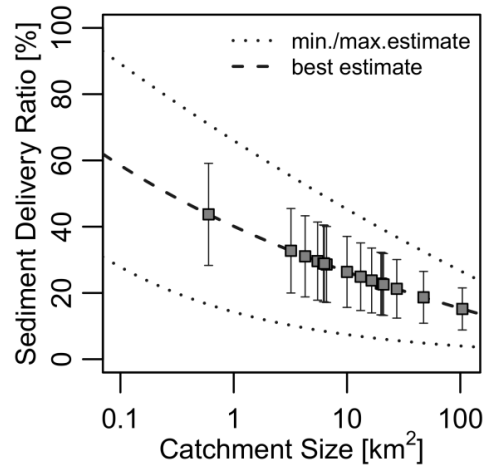
Fig. 7. Relationship between catchment size and sediment delivery ratio (SDR) according to USDA-SCS (1983) (see Eq. 5 and Table 4) and SDR estimates for all reservoir catchments. Error bars depict uncertainties at the 95% confidence level.

2.10. Assessment of uncertainty propagation and fractional uncertainty contributions

The mean area-specific sediment yield (*SSY*) of the reservoir catchments and a best estimate for catchment-wide average rates of erosion by water (*E*) were calculated with Equations (1) and (2). In addition, an estimate for minimum catchment-wide rates of erosion by water (E_{min}) was calculated with Eq. (6) from the mass of sediment trapped in the reservoirs.

$$E_{min} = \frac{V_S \cdot dBD}{T_R \cdot A} \tag{6}$$

Accordingly, E_{min} does not account for eroded material that is released to downstream reaches when the reservoir spills (i.e., the reservoir trap efficiency, *TE*) and sediment that is temporarily stored in the catchment (i.e., the sediment delivery ratio, *SDR*).

The propagation of uncertainties was quantified following Taylor (1997). Accordingly, the relative uncertainty ε_{SSY} of *SSY* values results from the propagation of

538   relative uncertainties in the determined volume (ε_{VS}) and dry bulk density (ε_{dBD}) of the

539   reservoir deposits, the period of time during which the reservoir deposits were

540   accumulated (ε_{TR}), the catchment size (ε_A) and the trap efficiency (ε_{TE}) as shown in

541   Eq. (7).

542

$$\varepsilon_{SSY} = \sqrt{\varepsilon_{VS}{}^2 + \varepsilon_{dBD}{}^2 + \varepsilon_{TR}{}^2 + \varepsilon_A{}^2 + \varepsilon_{TE}{}^2} \qquad (7)$$

543

544   The relative uncertainties ε_{VS}, ε_{dBD} and ε_{TE} represent uncertainties at the 95%

545   confidence level (*Cl95*) and ε_A is a mean 2σ deviation where 95% of all values are

546   expected to fall within the error margins when normally distributed errors are assumed.

547   The uncertainty ε_{TR} is a maximum uncertainty, but, in general, low compared to other

548   uncertainties. Hence, the resulting ε_{SSY} value can be interpreted as a 95% confidence

549   interval. The fractional uncertainty contribution ($FUC_{X, SSY}$) of individual factors X (i.e.,

550   T_R, V_S, *dBD*, A and *TE*) to the overall uncertainty inherent in *SSY* values was quantified

551   with Eq. (8).

552

$$FUC_{X, SSY} = \frac{\varepsilon_X{}^2}{\varepsilon_{SSY}{}^2} \qquad (8)$$

553

554   The relative uncertainty of best estimates for catchment-wide average erosion rates (ε_E)

555   and the fractional uncertainty contribution ($FUC_{SDR, E}$) of the relative uncertainty of the

556   sediment delivery ratio (ε_{SDR}) to ε_E were quantified analogously with the Equations (9)

557   and (10), respectively.

558

$$\varepsilon_E = \sqrt{\varepsilon_{SSY}{}^2 + \varepsilon_{SDR}{}^2} \tag{9}$$

$$FUC_{SDR,\,E} = \frac{\varepsilon_{SDR}{}^2}{\varepsilon_E{}^2} \tag{10}$$

559

560   Since ε_{SDR} is expressed at the 95% confidence level, ε_E can be likewise interpreted as a

561   relative *Cl95* uncertainty. The relative uncertainty of E_{min} values (ε_{Emin}) was calculated

562   with Eq. (7), whereby ε_{TE} was set to zero.

563   The mean of relative uncertainties and fractional uncertainty contributions

564   obtained from all studies was determined and is reported together with the respective

565   *Cl95* interval (Eq. 3). For *SSY*, *E* and E_{min} values, the mean and median were both

566   calculated to facilitate comparison with published values from related studies. The

567   boundaries of asymmetric *Cl95* intervals for median values were derived with the

568   adjusted percentile bootstrap method from Davison and Hinkley (1997, p. 203f.). The

569   calculations were performed with the R software package 'boot' (Canty and Ripley,

570   2017) based on 10,000 ordinary bootstrap replicates. The high number of replicates

571   ensures reproducible results.

572

573   **3. Results and interpretation**

574   **3.1. Water storage capacity (C) and volume of reservoir deposits (V_S)**

575   The analysis of survey data reveals full supply areas (A_R) varying from 0.6 to 16.0 ha

576   for the investigated reservoirs (Table 5). The present-day water storage capacity (C_S) is

577   lowest for the N'wanetsana reservoir ($3,700 \pm 100$ m^3) and highest for the Newu 1

578   reservoir ($312,400 \pm 4,200$ m^3). Relative uncertainties of C_S values are low, ranging

579   from ±1% to ±4%. Moreover, RTK GNSS and TLS data for the Hartbeesfontein, Jones-

580 Se and Mlondozi reservoirs result in C_S values that differ by ≤3% and show overlapping

581 uncertainty intervals.

582 Reservoir deposits show a 'wedge-shaped' distribution (Morris and Fan, 1998) in

583 all investigated reservoirs, i.e., the sediment thickness is highest close to the dam and

584 decreases steadily towards the reservoir inlet and the shorelines. This is illustrated in

585 Fig. 8 for the Jones-Se reservoir where the sediment thickness reaches 2.4 m close to the

586

587 **Table 5** Water storage capacity, volume of reservoir deposits and silting ratio for all
588 investigated reservoirs.

Reservoir	Survey	Reservoir basin			Reservoir deposits			Silting ratio	
		A_R	C_S	C_R	A_S	V_S	V_S/A_S	A_S/A_R	V_S/C_R
		[ha]	[10^3 m^3]	[10^3 m^3]	[ha]	[10^3 m^3]	[m]	[%]	[%]
Hartbeesfontein	RTK GNSS	3.0	30.1 ± 0.8	39.9 ± 0.8	1.2	9.8 ± 0.4	0.79	41	25
	TLS	2.8	31.1 ± 0.7	41.3 ± 0.8				44	24
Marheya	RTK GNSS	6.8	100.6 ± 1.7	106.9 ± 1.9	2.4	6.3 ± 0.7	0.26	36	6
Lugmag	RTK GNSS	12.0	143.0 ± 3.0	156.7 ± 3.1	2.6	13.8 ± 0.7	0.54	21	9
Mazithi	TLS	5.0	50.1 ± 1.2	57.2 ± 1.4	1.2	7.1 ± 0.5	0.57	25	12
N'tswiriri	TLS	1.0	9.9 ± 0.2	11.6 ± 0.2	0.3	1.7 ± 0.1	0.67	27	15
Jones-Se	RTK GNSS	2.3	24.3 ± 0.6	27.5 ± 0.7	0.6	3.1 ± 0.3	0.54	25	11
	TLS	2.4	23.7 ± 0.7	26.8 ± 0.8				24	12
Silolweni	RTK GNSS	11.2	144.9 ± 2.8	162.3 ± 3.1	4.2	17.4 ± 1.4	0.41	37	11
N'wanetsana	RTK GNSS	0.6	3.7 ± 0.1	5.1 ± 0.2	0.3	1.3 ± 0.1	0.46	52	26
Mlondozi	RTK GNSS	9.3	106.9 ± 2.3	140.8 ± 2.2	5.1	33.9 ± 1.3	0.66	55	24
	TLS	9.8	108.6 ± 1.7	142.6 ± 2.7				52	24
Newu 1	RTK GNSS	8.5	312.4 ± 4.2	349.4 ± 4.4	4.2	37.1 ± 1.2	0.88	50	11
Newu 2	RTK GNSS	2.8	35.0 ± 1.4	35.9 ± 1.4	0.2	0.9 ± 0.1	0.36	9	2
Nhlanganzwani	RTK GNSS	16.0	256.6 ± 4.0	279.4 ± 4.1	3.7	22.9 ± 1.0	0.62	23	8
Mpanamana	TLS	7.9	72.7 ± 2.0	101.2 ± 2.1	2.9	28.5 ± 0.7	1.00	36	28
Kumana	TLS	11.1	140.7 ± 2.8	145.5 ± 2.8	1.1	4.8 ± 0.4	0.43	10	3
N'watimhiri	TLS	4.1	66.2 ± 1.0	67.5 ± 1.0	0.4	1.3 ± 0.2	0.30	10	2

589 Note: full supply area (A_R), current water storage capacity (C_S), initial water storage capacity
590 (C_R), area covered by reservoir deposits (A_S), volume of reservoir deposits (V_S), mean sediment
591 thickness (V_S/A_S), area-related silting ratio (A_S/A_R) and volume-related silting ratio (V_S/C_R).

592

593
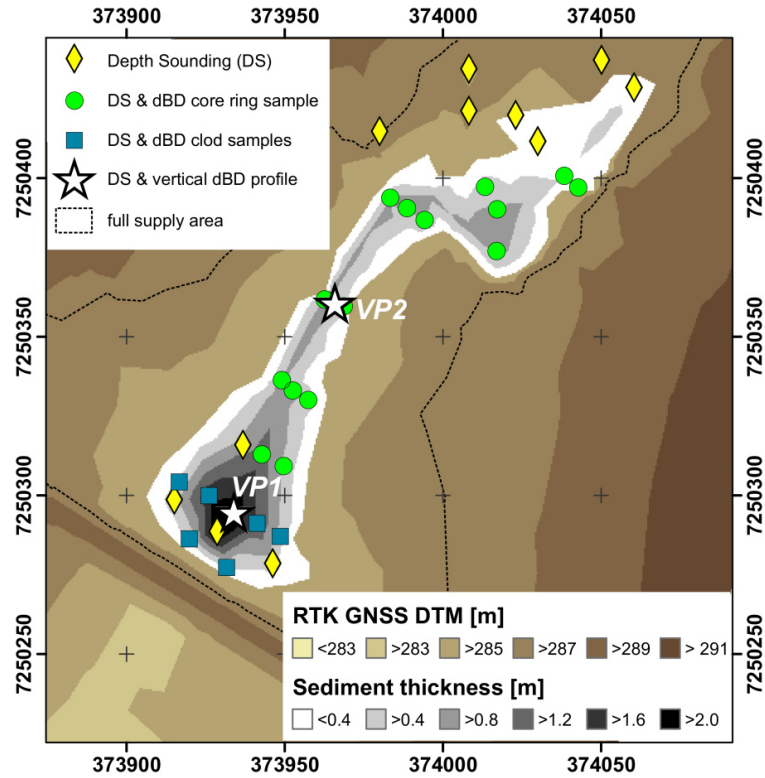
Fig. 8. Digital Terrain Model (DTM) of the central part of the Jones-Se reservoir basin obtained from TIN interpolation of RTK GNSS survey points, variations in the thickness of reservoir deposits derived from depth soundings (DS), and sample locations of surface samples (core ring and clod) and vertical sample profiles (VP1 and VP2) for the determination of the dry bulk density (dBD). Coordinates (in meters) refer to the UTM projection, Zone 36, WGS 84 Datum. Heights are shown in meters above the WGS 84 ellipsoid.

dam. Here, the area being covered with reservoir deposits (A_S) encompasses 0.6 ha which is 25% of the full supply area. For all other reservoirs, A_S ranges from 0.2 to 5.1 ha with A_S/A_R ratios of 9% to 55%. The volume of the reservoir deposits (V_S) varies from 900 to 37,100 m^3 which implies a low mean sediment thickness (V_S/A_S) of 0.26 to 1.00 m. The reconstructed initial water storage capacity (C_R) ranges from 5,100 m^3 to 349,400 m^3 and the silting ratio (V_S/C_R) indicates that 2% to 28% of the initial storage capacity has been lost by reservoir siltation. Relative uncertainties in the determination of V_S range from ±3% to ±16%.

612 **3.2. Variability of the dry bulk density (dBD)**

613 The dry bulk density (*dBD*) of the reservoir deposits shows little evidence for

614 systematic variations with sediment depth, but some scattering is recognizable in *dBD*

615 values that were obtained from surface samples. This is exemplified for the Jones-Se

616 reservoir in Fig. 9. The majority of samples taken from >50 cm depth, including the

617 vertical profiles VP1 and VP2 (see Fig. 8), give almost identical *dBD* values of 1.1 to

618 1.3 g cm^{-3} (Fig. 9a). The *dBD* of samples from ≤50 cm depth ranges from 0.9 to

619 1.5 g cm^{-3}. At the day of sampling, the water content was nearly constant (ca. 30 wt. %)

620 in >50 cm depth, and decreased from about 50 cm depth towards the sediment surface

621 (Fig. 9b).

622

623
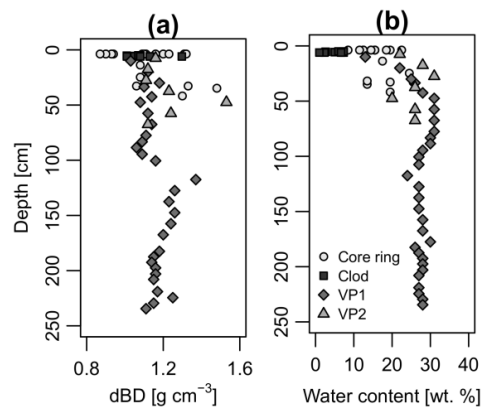
624 **Fig. 9.** Variability of the (a) dry bulk density and (b) water content of core ring and clod samples
625 gathered from reservoir deposits in the Jones-Se reservoir. The vertical sample profiles VP1
626 and VP2 (see Fig. 8) are highlighted.

627

628 Clod samples from the surface reveal a water content of <10 wt.%, while the

629 water content of core ring samples is ≥10 wt.%. This elucidates that the core ring

630 method frequently leads to disruption of sediment with a water content <10 wt.%.

631 Following the corrections for desiccation cracks and the intrusion of oil in the volume

632 determination for clods (see section 2.5), there is no significant offset between *dBD*

633 values obtained from core ring and clod samples. The coefficient of variation for *dBD*

634   values obtained from all samples is 10% and the mean *dBD* value (±*Cl95*) for the Jones-

635   Se reservoir amounts to 1.2 ± 0.1 g cm^{-3}.

636   For all other reservoirs, the mean *dBD* ranges from 0.6 to 1.5 g cm^{-3}. Site-

637   specific standard deviations (σ_{dBD}) vary between 0.10 and 0.26 g cm^{-3} (Table 6) which

638   leads to coefficients of variation (CV_{dBD}) of 8% to 22%. The *Cl95* intervals of most site-

639   specific mean *dBD* values overlap with the *Cl95* interval of the overall average of all

640   site-specific mean *dBD* values of 1.13 ± 0.12 g cm^{-3} (Fig. 10). The only exceptions are

641   the site-specific mean *dBD* values of the Mpanamana (0.63 ± 0.11 g cm^{-3}) and Kumana

642   reservoirs (1.41 ± 0.07 g cm^{-3}). Relative uncertainties (ε_{dBD}) of site-specific mean *dBD*

643   values range from 3% to 17%.

644

645   **Table 6** Dry bulk density (dBD) of reservoir deposits: number of samples (N), mean values with
646   uncertainties at the 95% confidence level (Cl95), standard deviation (σ_{dBD}) and coefficient of
647   variation (CV_{dBD}) for the investigated reservoirs (N = 14).

Reservoir	N	Mean ± Cl95 [g cm^3]	σ_{dBD} [g cm^3]	CV_{dBD} [%]
Hartbeesfontein	58	1.08 ± 0.06	0.22	20
Marheya	18	1.13 ± 0.10	0.20	18
Lugmag	46	1.15 ± 0.08	0.25	22
Mazithi	6	1.22 ± 0.10	0.10	8
Jones-Se	64	1.16 ± 0.03	0.12	10
Silolweni	68	1.32 ± 0.05	0.19	14
N'wanetsana	29	1.20 ± 0.06	0.14	12
Mlondozi	8	0.94 ± 0.12	0.14	15
Newu 1	45	1.09 ± 0.06	0.21	19
Newu 2	9	1.43 ± 0.20	0.26	18
Nhlanganzwani	72	1.06 ± 0.05	0.20	19
Mpanamana	6	0.63 ± 0.11	0.10	16
Kumana	29	1.41 ± 0.07	0.18	13
N'watimhiri	31	1.00 ± 0.08	0.21	21
All sites	14	1.13 ± 0.11	0.18	16

648
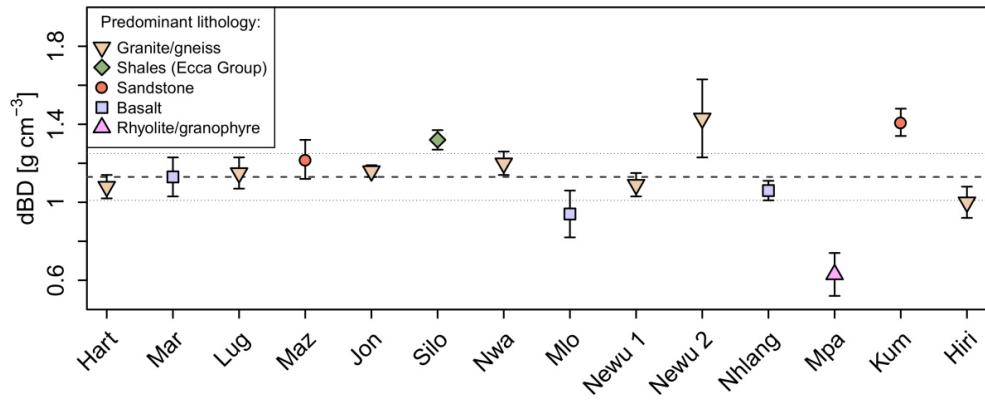
Fig. 10. Mean dry bulk density (dBD) of reservoir deposits with uncertainties at the 95% confidence level and predominant catchment lithology. The horizontal dashed line depicts the average of all site-specific mean dBD values (N = 14) and the corresponding 95% confidence uncertainty bounds.

3.3. Minimum catchment-wide rates of erosion by water (E_{min}), mean area-specific sediment yield (SSY), and best estimates for catchment-wide average rates of erosion by water (E)

Minimum catchment-wide rates of erosion by water (E_{min}) determined from the mass of the reservoir deposits range from 4 to 64 t km^{-2} yr^{-1} with a mean of 20 ± 10 t km^{-2} yr^{-1} and median of 10 [5, 35] t km^{-2} yr^{-1} (*Cl95*) for all study sites. Relative uncertainties of E_{min} values (ε_{Emin}) vary between ±5% and ±23% reflecting mainly the uncertainty of the volume and dry bulk density determination. However, E_{min} values do not account for the reservoir trap efficiency and sediment delivery ratio being considered in area-specific sediment yield (*SSY*) and catchment-wide average rates of erosion by water (*E*).

SSY varies from 5 to 80 t km^{-2} yr^{-1} (Table 7) with an overall mean (and median) of 30 ± 10 t km^{-2} yr^{-1} (20 [15, 50] t km^{-2} yr^{-1}). Relative uncertainties (ε_{SSY}) range from ±12% to ±40% and are therefore much lower than the variability of *SSY* values among the individual catchments. This variability may be partially attributable to differing catchment properties (Fig. 11). *SSY* values correlate highly significant (Pearson's

671 **Table 7** Minimum catchment-wide rates of erosion by water (E_{min}), mean area-specific
672 sediment yield (SSY, corrected for TE), and best estimates (E, corrected for TE and SDR) for
673 catchment-wide average rates of erosion by water for all study sites with relative uncertainties
674 (ε_{Emin}, ε_{SSY}, and ε_E) expressed at the 95% confidence level.

Reservoir	E_{min} [t km^{-2} yr^{-1}]	ε_{Emin} [%]	SSY [t km^{-2} yr^{-1}]	ε_{SSY} [%]	E [t km^{-2} yr^{-1}]	ε_E [%]
Hartbeesfontein	39 ± 3	7	55 ± 8	14	175 ± 75	42
Marheya	6 ± 1	10	8 ± 2	19	40 ± 20	46
Lugmag	6 ± 1	8	15 ± 4	28	80 ± 40	51
Mazithi	9 ± 2	18	15 ± 5	30	65 ± 35	51
N'tswiriri	7 ± 1	6	14 ± 3	24	45 ± 20	46
Jones-Se	10 ± 1	5	18 ± 4	20	60 ± 30	45
Silolweni	44 ± 3	6	62 ± 8	13	245 ± 105	43
N'wanetsana	9 ± 1	7	18 ± 4	22	55 ± 25	45
Mlondozi	5 ± 1	13	17 ± 7	40	115 ± 65	58
Newu 1	64 ± 6	9	80 ± 20	21	360 ± 170	47
Newu 2	49 ± 7	15	55 ± 10	19	125 ± 50	40
Nhlanganzwani	29 ± 2	6	35 ± 4	12	145 ± 65	43
Mpanamana	35 ± 8	23	50 ± 10	27	190 ± 95	49
Kumana	21 ± 3	15	24 ± 5	20	85 ± 35	45
N'watimhiri	4 ± 1	21	5 ± 1	28	15 ± 10	49
Mean	*20 ± 10*	*11*	*30 ± 10*	*21*	*120 ± 50*	*46*
Median	*10 [5, 35]*	*9*	*20 [15, 50]*	*21*	*85 [55, 145]*	*45*

675

676 R = 0.71; p < 0.01) with mean annual precipitation (*MAP*). The correlation coefficient

677 increases to R = 0.92 (p < 0.001) when the Hartbeesfontein and Silolweni catchments

678 are excluded. Moreover, a weakly significant correlation (R = 0.45; p < 0.10) exists

679 between *SSY* values and the mean slope inclination (*Slope*). This correlation is highly

680 significant (R = 0.68; p < 0.01) when the Hartbeesfontein and Silolweni catchments are

681 excluded. *MAP* and *Slope* values covary which is evident in a significant correlation

682 coefficient of R = 0.58 (p < 0.03).

683   The Hartbeesfontein and Silolweni catchments, revealing outlying values in the

684 *SSY* to *MAP* and *SSY* to *Slope* relationships, show by far the highest area percentage of

685 bare surfaces (*BareSurf* ≥ 1.5%). *SSY* and *BareSurf* values show a weakly significant

686 correlation (R = 0.44; p = 0.10), but this relationship becomes insignificant (R = 0.22;

687 p = 0.5) when the Hartbeesfontein and Silolweni catchments are excluded. Gullied

688   catchments (i.e., the Hartbeesfontein, Silolweni and Newu 1 catchments) show the

689   highest *SSY* values (≥ 55 t km^{-2} yr^{-1}) among the study sites. *SSY* values and catchment

690   size (*A*) exhibit a negative, but insignificant correlation (R = -0.22; p = 0.4). No

691   significant correlation was found between *SSY* values and the mean fractional woody

692   cover (*WCOV*; R = 0.29; p = 0.3) and the area percentage of roads (*Roads;* R = -0.19;

693   p = 0.5). Moreover, there is no obvious relationship between *SSY* values and the

694   predominant catchment lithology.

695
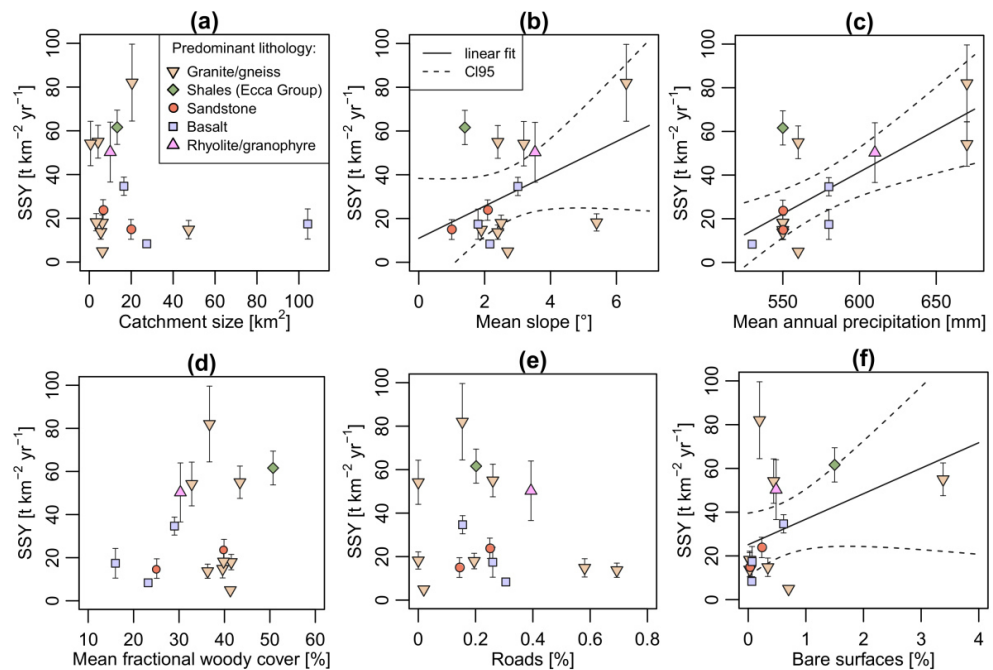
696
697   **Fig. 11.** Relationships between area-specific sediment yield (SSY) values and (a) catchment size,
698   (b) mean slope inclination, (c) mean annual precipitation, (d) mean fractional woody cover, (e)
699   area percentage of roads, and (f) area percentage of bare surfaces. Error bars depict
700   95% confidence intervals. For significant relationships (p ≤ 0.10), linear fits are depicted
701   together with uncertainty bounds corresponding to the 95% confidence level (CI95).

702

703   Best estimates for catchment-wide average rates of erosion by water (*E*) are

704   ≥ 15 t km^{-2} yr^{-1} and ≤ 190 t km^{-2} yr^{-1} (Fig. 12)   except   for   the   gullied   Silolweni

705   (245 ± 105 t km^{-2} yr^{-1}) and Newu 1 catchments (360 ± 170 t km^{-2} yr^{-1}). A comparatively

706   high   value   was   also   determined   for   the   Hartbeesfontein   catchment

707   (175 ± 75 t km^{-2} yr^{-1}), thus, highlighting the potential role of gully erosion in elevating E

708   values. The overall mean and median E value for all study sites amounts to

709   120 ± 50 t km^{-2} yr^{-1} and 85 [55, 145] t km^{-2} yr^{-1} (*Cl95*), respectively (Table 7).

710   Excluding gullied catchments results in a mean (and median) E value of

711   85 ± 30 t km^{-2} yr^{-1} (70 [45, 115] t km^{-2} yr^{-1}). Relative uncertainties of E values (ε_E)

712   range from ±40% to ±58% and are, thus, on average more than three times higher than

713   ε_{SSY} values. This leads to overlapping uncertainty intervals for most catchment-specific

714   E values and impedes the analysis of correlations between catchment properties and

715   average erosion rates.

716
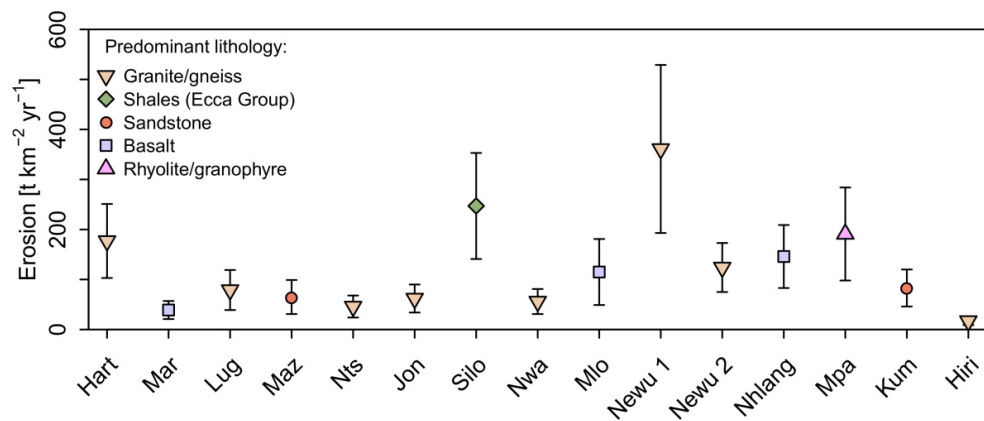
718 **Fig. 12.** Best estimates for catchment-wide average rates of erosion by water for catchments
719 of all investigated reservoirs. Error bars depict uncertainties at the 95% confidence level.
720

721 **3.4. Uncertainty propagation and fractional uncertainty contribution**

722   Table 8 provides an overview on the relative uncertainty (ε_X) and fractional uncertainty

723   contribution ($FUC_{X, SSY}$) of individual factors (X) to the overall uncertainty inherent in

724   SSY values. $FUC_{VS, SSY}$ values are ≤39% at all study sites and amount to 11% on average.

725    $FUC_{dBD, SSY}$ values reveal a similar average of 14%, whereby the rather high $FUC_{dBD, SSY}$

726   values for the Newu 2 (56%) and Mpanamana reservoirs (40%) can be attributed to the

727

728 **Table 8** Relative uncertainty (ε_X) of individual factors (X) and their fractional uncertainty
729 contribution ($FUC_{X,\,SSY}$ and $FUC_{X,\,E}$) to the overall uncertainty inherent in area-specific sediment
730 yield (SSY) and best estimates for catchment-wide average rates of erosion by water (E).

Reservoir	ε_{VS} [%]	ε_{dBD} [%]	ε_{TR} [%]	ε_{TE} [%]	ε_{A} [%]	ε_{SDR} [%]	$FUC_{VS,\,SSY}$ [%]	$FUC_{dBD,\,SSY}$ [%]	$FUC_{TR,\,SSY}$ [%]	$FUC_{TE,\,SSY}$ [%]	$FUC_{A,\,SSY}$ [%]	$FUC_{SDR,\,E}$ [%]
Hartbeesfontein	4	6	2	11	3	39	8	17	1	70	4	89
Marheya	12	9	2	11	3	42	38	22	1	36	2	83
Lugmag	5	7	2	27	3	42	4	6	<1	89	1	69
Mazithi	8	8	16	23	3	41	6	7	28	58	1	64
N'tswiriri	4	5	2	23	3	40	2	4	1	91	1	74
Jones-Se	11	3	2	16	3	40	30	2	1	65	2	80
Silolweni	8	4	3	8	3	41	39	9	4	43	5	91
N'wanetsana	6	5	2	20	3	39	7	5	1	86	2	76
Mlondozi	4	13	2	37	3	42	1	10	<1	88	<1	53
Newu 1	3	6	6	19	3	41	2	7	9	81	2	79
Newu 2	8	14	2	9	3	35	18	56	2	22	2	78
Nhlanganzwani	4	5	2	10	3	41	12	15	3	64	5	92
Mpanamana	3	17	15	14	3	41	1	40	31	27	1	69
Kumana	9	5	15	9	3	40	20	6	52	19	2	80
N'watimhiri	16	8	20	9	3	40	33	8	48	10	1	67
Mean	*7*	*8*	*6*	*16*	*3*	*40*	*11*	*14*	*9*	*64*	*2*	*79*

731 Note: individual factors are the volume (V_S) and dry bulk density (dBD) of reservoir deposits, the period
732 of time (T_R) during which the reservoir deposits were accumulated, the reservoir trap efficiency (TE), the
733 catchment size (A) and the sediment delivery ratio (SDR)

734

735 small number of *dBD* samples (N < 10) collected at these sites. Uncertainties regarding

736 the period of time during which the reservoir deposits were accumulated ($FUC_{TR,\,SSY}$)

737 contribute ≤4% to the uncertainty of *SSY* values when the year of dam construction is

738 documented, but reach up to 52% otherwise. The contribution of uncertainties in the

739 estimation of the trap efficiency ($FUC_{TE,\,SSY}$) ranges from 10% to 91% with a mean of

740 64%. Hence, the *TE* estimation contributes on average more than four times more

741 uncertainty to *SSY* values than all other factors (Fig. 13). The fractional uncertainty

742 contribution arising from the delineation of the catchment area ($FUC_{A,\,SSY}$) is ≤5% and

743 therefore unimportant. The uncertainty of *E* values is mainly due to uncertain sediment

744 delivery ratios (*SDR*) which is reflected in $FUC_{SDR,\,E}$ values ranging from 53% to 92%

745 with a mean of 79% (Table 8). Low relative uncertainties of E_{min} values are clearly

746   attributable to the fact that these values are independent of the *TE* and *SDR* estimation

747   and provide evidence for the high precision of the fieldwork.

748

749
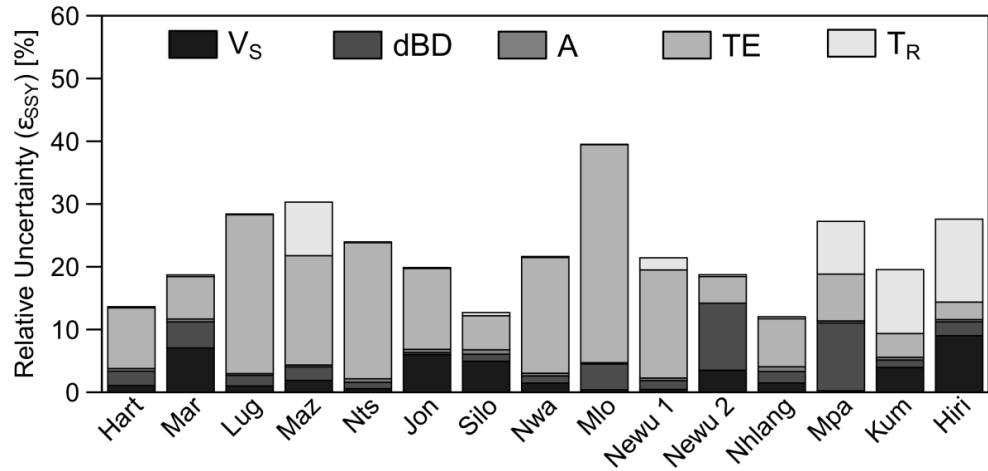
750   **Fig. 13.** Relative uncertainty (ε_{SSY}) in area-specific sediment yield (SSY) values at the
751   95% confidence level and representation of fractional uncertainty contributions arising from
752   the determination of the volume (V_S) and dry bulk density (dBD) of the reservoir deposits, the
753   catchment size (A), the trap efficiency (TE) and the operation time of the reservoirs (T_R) during
754   which the mapped reservoir deposits were accumulated.

755

756   ## 4. Discussion

757   **4.1. Low fractional uncertainty arising from the determination of the volume of**

758   **reservoir deposits (V_S)**

759   The results show that uncertainties in the determination of the volume of the reservoir

760   deposits (V_S) are rather insignificant provided that reservoir siltation surveys are carried

761   out with a sufficiently high resolution. In this study, the mean fractional uncertainty

762   contribution ($FUC_{VS, SSY}$) amounts to 11% with respect to the area-specific sediment

763   yield (*SSY*) for all catchments. The mean contribution to the uncertainty of catchment-

764   wide average erosion rates (*E*) is 2%.

765   Information about the impact of the survey resolution can be gained from the

766   comparison with V_S values that were established within the course of a preparatory

767   reconnaissance survey carried out in 2008 (Baade et al., 2012). At that time, V_S values

768   were determined for Silolweni, Mlondozi, Nhlanganzwani and Mpanamana reservoirs

769   based on sediment thickness measurements and plan views of the reservoir basins that

770   were derived from satellite images (Quickbird) available at Google Earth. The shape of

771   the sedimentary infill was approximated by means of pyramid frustums and prisms with

772   vertical trapezoidal cross sections and assuming a steadily decreasing sediment

773   thickness with increasing distance from the dam (for details, see Baade et al., 2012).

774   The method was developed at the Silolweni reservoir where nine depth soundings were

775   performed along two transects one of which ran parallel to the dam and the other one

776   followed the long axis of the reservoir. At the Mlondozi, Nhlanganzwani and

777   Mpanamana reservoirs, the sediment thickness was determined only at a single location.

778   The comparison between results from the reconnaissance survey and the current

779   study (Table 9) reveals V_S values with overlapping 95% confidence intervals for the

780   Silolweni and Nhlanganzwani reservoirs that were decommissioned in 2008 and 2007,

781   respectively. For the Mlondozi reservoir, the reconnaissance survey indicated a

782   sediment thickness of 2.0 m close to the dam resulting in a 8,000 m^3 (24%) lower V_S

783   value than in the current study. A staff gauge mounted at the Mlondozi dam shows that

784   the sediment thickness increased by about 0.4 m from 2008 until 2016 as sedimentation

785   continued (cf. Reinwarth et al., 2018). Using a maximum sediment thickness of 2.4 m,

786   the method from Baade et al. (2012) results in a V_S value of $31 \pm 5 \times 10^3$ m^3 which is

787   consistent to $34 \pm 1 \times 10^3$ m^3 ascertained in the current study. For the Mpanamana

788   reservoir, the reconnaissance survey gave a V_S value of $8 \pm 2 \times 10^3$ m^3 based on a

789   minimum sediment thickness of 1.0 m close to the dam, because the depth sounding did

790   not reach the base of the reservoir deposits. The survey in 2016 revealed a maximum

791

792 **Table 9** Comparison of the volume (V_S) and dry bulk density (dBD) of reservoir deposits and
793 associated uncertainties at the 95% confidence level determined by Baade et al. (2012) with
794 results from this study. Note the varying number of depth soundings (N_{DS}) and dry bulk density
795 measurements (N_{dBD}).

Reservoir	Baade et al. (2012)						This study					
	N_{DS}	V_S [10^3 m^3]	ε_{VS} [%]	N_{dBD}	dBD [g cm^{-3}]	ε_{dBD} [%]	N_{DS}	V_S [10^3 m^3]	ε_{VS} [%]	N_{dBD}	dBD [g cm^{-3}]	ε_{dBD} [%]
Silolweni	9	15 ± 3	20	10	1.8 ± 0.1	6	59	17 ± 1	8	68	1.3 ± 0.1	4
Mlondozi	1	26 ± 4[1]	15	11	1.6 ± 0.1	6	65	34 ± 1[1]	4	8	0.9 ± 0.1	13
Nhlanganzwani	1	24 ± 7	30	5	1.7 ± 0.1	6	56	23 ± 1	4	72	1.1 ± 0.1	5
Mpanamana	1	8 ± 2[1,2]	25	n.a.[3]	n.a.[3]	n.a.[3]	56	28 ± 1[1]	3	6	0.6 ± 0.1	17

796 1) Sedimentation continued after the reconnaissance survey carried out by Baade et al. (2012).
797 2) The depth sounding did not reach the base of the reservoir deposits.
798 3) A mean dBD value of 1.7 ± 0.1 g cm^{-3} was assumed for the Mpanamana reservoir.
799

800 sediment thickness of 3.4 m close to the dam. Using this value in combination with the

801 method from Baade et al. (2012) results in a V_S value of $27 \pm 7 \times 10^3$ m^3 which is

802 likewise in good agreement with $28 \pm 1 \times 10^3$ m^3 determined in the current study.

803 These results show that reliable V_S values can be achieved based on very limited

804 data when reasonable assumptions about the geometry of the sedimentary infill can be

805 made. Such assumptions can be underpinned when the river cross section below the

806 dam, the minimum height of the sediment surface in the reservoir basin, and the height

807 of the reservoir inlet are surveyed (e.g., Castillo et al., 2007). Relative uncertainties

808 reported by Baade et al. (2012) vary between ±15% and ±30% at the 95% confidence

809 level (*Cl95*). This is comparable to average errors of 7% to 28% that were determined

810 by Ramos-Diez et al. (2017) for various methods permitting the calculation of V_S when

811 no or only few sediment thickness readings are available. Accepting a relative

812 uncertainty ε_{VS} of ±15% (or ±30%) and mean uncertainties of other individual factors in

813 Eq. (7) as shown in Table 8 would result in a 4% (15%) higher ε_{SSY} value that would

814 then amount to ±24% (±36%). At the same time, the ε_E value would rise by 2% (9%)

815 which is a small effect.

816

817 **4.2. Low fractional uncertainty arising from the determination of the**

818 **dry bulk density (dBD)**

819 The site-specific mean dBD values determined in this study are in an expectable range.

820 According to Annandale (1987), the dBD of 50 years old reservoir deposits is typically

821 >1.10 and <1.35 g cm^{-3}. Into the latter range fall 11 out of 14 investigated reservoirs

822 when $Cl95$ intervals are taken into account (Table 6). The $Cl95$ uncertainty of the site-

823 specific mean dry bulk density (dBD) depends on the intra-site variability of dBD values

824 and the number of dBD measurements (N_{dBD}). The intra-site variability that can be

825 recognized from surface samples (Fig. 9) is probably mainly due to variations in

826 sediment texture and porosity (Morris and Fan, 1998). Variations in vertical dimension

827 are rather low which is in contrast to other reservoir siltation studies where sediment

828 compaction led to increasing dBD values with increasing sediment depth (e.g., Lane and

829 Koelzer, 1943; Rausch and Heinemann, 1984). For the investigated reservoirs, the effect

830 of sediment compaction is presumably small due to the rather low thickness of the

831 reservoir deposits ($\leq$ 3 m).

832 The standard deviation (σ_{dBD}) of dBD values ranges from 0.10 to 0.26 g cm^{-3}

833 among the reservoirs which leads to coefficients of variation (CV_{dBD}) between 8% and

834 22% (Table 6). This is comparable to CV_{dBD} values of 4% to 40% reported by

835 Verstraeten and Poesen (2001) for 13 small flood retention ponds in Belgium. For σ_{dBD}

836 values of 0.1, 0.2 and 0.3 g cm^{-3}, the absolute uncertainty (δ_{dBD}) of the mean dBD is

837 <0.1 g cm^{-3} at the 95% confidence level ($Cl95$) when N_{dBD} is $\geq$7, $\geq$18 and $\geq$38,

838 respectively (Fig. 14). In this study, the absolute uncertainty (δ_{dBD}) of the mean dBD is

839 <0.1 g cm^{-3} for all reservoirs where $\geq$20 samples were collected. Including (and

840
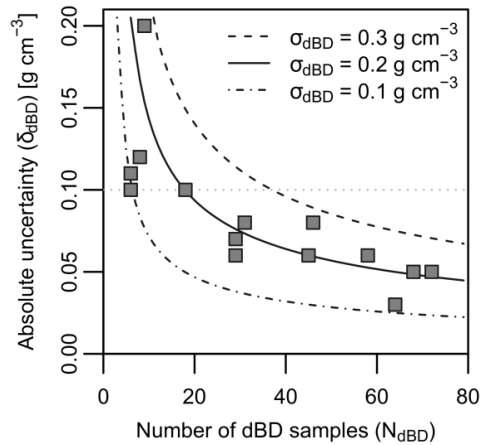
Fig. 14. Relationship between the number of dBD samples (N_{dBD}) collected at individual study sites and the absolute uncertainty of site-specific mean dBD values expressed at the 95% confidence level. Curves depicting the relationship for dBD values with a standard deviation (σ_{dBD}) of 0.1, 0.2 and 0.3 g cm^{-3} are presented.

excluding) study sites with <20 *dBD* samples results in a mean relative uncertainty (ε_{dBD}) of ±8% (±5%) and a mean fractional uncertainty contribution ($FUC_{dBD, SSY}$) of 14% (8%). With respect to *E* values, the mean fractional uncertainty contribution is 3% (1%).

The calculation of *Cl95* uncertainties (Eq. 3) relies on the assumption of unbiased and normally-distributed random errors of individual measurements, but does not account for systematic offsets. Comparing data from Baade et al. (2012) and the current study reveals 0.5 to 0.7 g cm^{-3} (40% to 80%) higher *dBD* values for the reconnaissance survey (Table 9). This discrepancy cannot be explained by the respective *Cl95* intervals, but points to methodological differences. In the reconnaissance survey, site-specific mean *dBD* values were ascertained from unsealed clod samples that were collected from side walls of excavation pits. Afterwards, the *dBD* determination followed the workflow for clod samples described in section 2.5, but *dBD* values were not corrected for intruding oil.

861   The problem of fluid intrusion that occurs when the clods are submerged to

862   ascertain the clod volume has been previously described (Burt and Soil Survey Staff,

863   2014, p. 108) and may be circumvented by sealing the clods with semi-permeable

864   plastic lacquer (Brasher et al., 1966). Results from this study suggest that uncorrected

865   *dBD* values of initially dry unsealed clod samples (water content < 10 wt. %) are on

866   average about 0.2 g cm^{-3} higher than corrected values. The usage of a fluid with low

867   viscosity and a correction for fluid intrusion are therefore recommended for *dBD*

868   determinations with unsealed clods. An additional problem may arise for moist clod

869   samples (water content ≥10 wt. %), since oven-drying prior to the volume determination

870   may lead to sediment shrinkage. For a sample with a *dBD* of 1.2 g cm^{-3}, a volume

871   reduction of 20% (i.e., about the mean area percentage of desiccation cracks on dry

872   surfaces) results in an overestimation of 0.3 g cm^{-3} (25%). Although the clod volume

873   can be determined prior to oven-drying when the clods are sealed (for details, see

874   Grossman and Reinsch, 2002), the core ring method appears to be preferable for moist

875   sediment. On the opposite, the clod method is recommended to ascertain *dBD* values of

876   dry sediment, in particular when the core ring method fails due to sediment disruption.

877   Following the correction for intruding oil and desiccation cracks, *dBD* values

878   derived from core ring and clod samples are in good agreement (Fig. 9). Even if it is

879   assumed that a mean ε_{dBD} value of ±8% underestimates the overall uncertainty in *dBD*

880   values by a factor of 2 (or 4) due to methodological issues, the mean relative uncertainty

881   of area-specific sediment yield values (ε_{SSY}) would increase by only 4% (17%) leading

882   to a mean ε_{SSY} value of ±25% (±37%). The increase in the mean relative uncertainty of

883   catchment-wide average erosion rates (ε_E) would amount to 2% (10%) which is a small

884   effect compared to uncertainties arising from other potential error sources.

885

4.3. Major fractional uncertainty arising from the estimation of the sediment trap efficiency (TE)

Estimates for the mean sediment trap efficiency (TE) show a mean relative $Cl95$ uncertainty (ε_{TE}) of ±16% which imposes a mean fractional uncertainty contribution ($FUC_{TE, SSY}$) of 64%. The TE estimation is therefore the major source of uncertainty with respect to SSY values. This is not surprising as the mean TE of a reservoir depends on numerous influential factors. The model that was used for the TE estimation (Reinwarth et al., 2018) accounts for rainfall-runoff conditions, temporally variable sediment delivery from the catchment, the distance that particles must travel across the reservoir basin to reach the reservoir outlet and the frequency and magnitude of spillage events. Grain size characteristics of the delivered sediment were implicitly taken into consideration (for details, see Reinwarth et al., 2018). Other influential factors such as the mixis of the water column, currents, turbulence, and flocculation which may affect the settling velocity of sediment particles (Heinemann, 1984; Haan et al., 1994) can be partly accounted for in more sophisticated physically-based models that were developed for small ponds (≤1 ha) (e.g., Wilson and Barfield, 1985). These factors are, however, difficult to address in larger reservoirs (>1 ha) without extensive monitoring efforts.

In general, the TE estimation is more uncertain for reservoirs with low TE values (e.g., Brown, 1944; Morris and Fan, 1998). This is supported by results from this study where the Mlondozi reservoir reveals the lowest TE estimate (25 ± 10%) and the highest ε_{TE} value (±37%). Compared to this, ε_{TE} values are ≤10% for all reservoirs with a mean TE of >80%. For the reduction of uncertainties, SSY values should be, thus, preferentially assessed from reservoirs for which a high mean TE can be anticipated (Foster et al., 1990).

910   In this study, modelled *TE* estimates are in good agreement with an empirical

911   relationship (Eq. 11) that was established by Brown (1944).

912

$$TE = 100\% \cdot \left(1 - \frac{1}{1 + 0.0021 \cdot D \cdot \dfrac{C_R}{A}} \right) \qquad (11)$$

913

914   Accordingly, *TE* values can be estimated from the ratio of the reservoir's initial water

915   storage capacity (C_R) to its catchment size (*A*) and a parameter *D* that may vary between

916   0.046 and 1. For the investigated reservoirs, the highest correlation ($R^2 = 0.81$) to

917   modelled *TE* values is achieved by setting *D* to 0.17 (Fig. 15a) which results in an

918   absolute root mean square error (RMSE) of 9%. Lower and upper envelope curves

919
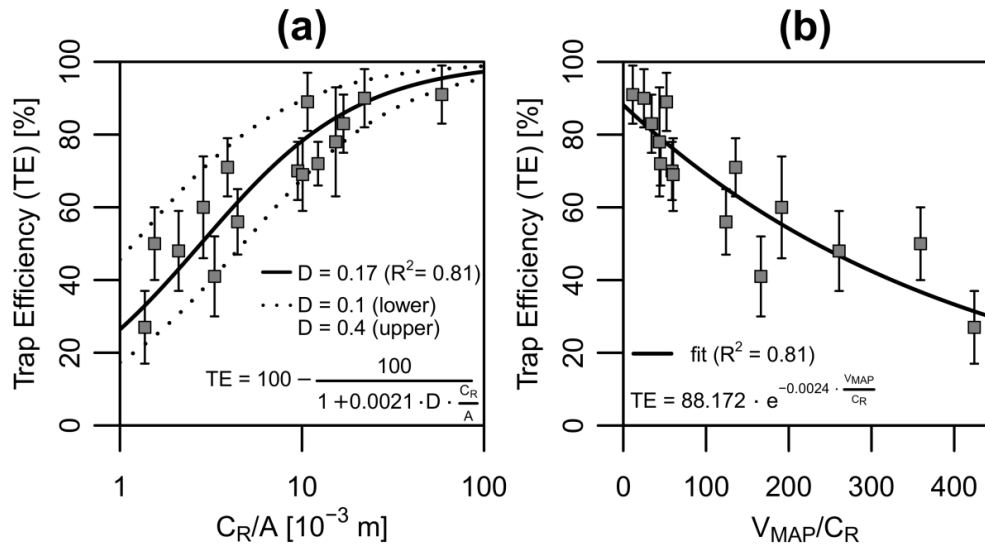
921   **Fig. 15.** Relationship between the modelled sediment trap efficiency (TE), the initial water
922   storage capacity (C_R) of the reservoirs, catchment size (A) and volume of mean annual
923   precipitation (V_{MAP}) in the reservoir catchments: (a) TE as a function of the C_R/A ratio with
924   curves corresponding to Eq. (11) from Brown (1944). The best fit ($R^2 = 0.81$) is achieved by
925   setting the parameter D to 0.17. D values of 0.1 and 0.4 represent lower and upper envelope
926   curves for the investigated reservoirs, respectively; (b) TE as function of the V_{MAP}/C_R ratio. The
927   best exponential fit ($R^2 = 0.81$) is shown. Error bars of TE estimates depict 95% confidence
928   intervals that were derived from nine modelling scenarios (for details, see Reinwarth et al.,
929   2018).

930   correspond to D values of 0.1 and 0.4, respectively. There is, moreover, a good

931   relationship between modelled TE values and the ratio of the volume of mean annual

932   precipitation (V_{MAP}) in the reservoir catchments to the initial water storage capacity (C_R)

933   of the reservoirs (Fig. 15b). Here, the best exponential fit ($R^2 = 0.81$) results in an

934   absolute RMSE of 8%.

935   These findings suggest that the relationships shown in Fig. 15 can be used to

936   estimate TE values for reservoirs in the Kruger National Park with an uncertainty

937   comparable to those obtained from modelling (Table 3). The relationship of Brown

938   (1944) appears to be rather robust considering that is was established from reservoirs in

939   the United States many of which are located in temperate climate regions. The optimal

940   D value of 0.17 derived from this study is close to the default value of 0.1 suggested by

941   Brown (1944). Using this default value would lead to an absolute RMSE of 13% which

942   is only slightly higher than the RMSE obtained for $D = 0.17$ (9%). The transferability of

943   the basic relationship between TE values and the often readily available V_{MAP}/C_R ratios

944   to reservoirs outside the study area needs further assessment since climate conditions

945   and catchment properties control the runoff regime that, in turn, exerts a strong

946   influence on TE values (Lewis et al., 2013; Reinwarth et al., 2018).

947

948   **4.4.   Major   fractional   uncertainty   arising   from   the   estimation   of   the**

949   **sediment delivery ratio (SDR)**

950   The mean relative uncertainty of best estimates for catchment-wide average rates of

951   erosion by water (E) is more than three times higher than for area-specific sediment

952   yield (SSY) values. This is clearly attributable to the uncertain estimation of the

953   sediment delivery ratio (SDR) (Fig. 7) that affects E values, but not SSY values. In this

954   study, the mean relative uncertainty of SDR values (ε_{SDR}) amounts to ±40% which

955   propagates into a mean fractional uncertainty contribution ($FUC_{SDR, E}$) of 79% with

956   respect to E values. This comparatively large uncertainty can be partially attributed to

957   the application of lumped SDR to A relationships that were developed from data

958   collected on different continents (Table 4). Establishing a regionalized relationship

959   might potentially reduce uncertainties (USDA-SCS, 1983; de Vente et al., 2007), but is

960   currently unfeasible due to the paucity of data on contemporary erosion rates for the

961   Lowveld geomorphic province. Estimating the SDR based on empirical equations

962   requires little input data, but does not capture the complex interplay of processes

963   involved in the erosion, transport and storage of sediment within the catchment (Fryirs,

964   2013). Moreover, empirical relationships fail to represent the dependency of SDR values

965   on the timescale on which SSY and E values are considered (Walling, 1983). Therefore,

966   several authors have recommended the application of sediment routing models (e.g.,

967   Klaghofer et al., 1992; Lu et al., 2006).

968   So far, no attempts have been made to model intermediate sediment storage in

969   reservoir catchments within the Kruger National Park. Models permitting a SDR

970   assessment (see Aksoy and Kavvas, 2005) typically require detailed information about

971   rainfall-runoff conditions, relief characteristics, soil properties, vegetation cover and

972   land use (e.g., Van Rompaey et al., 2001; Lu et al., 2006). The calibration and

973   validation of such models can be challenging given the difficulties to empirically assess

974   erosion rates on the catchment scale (Van Rompaey et al., 2003; Brazier, 2004). With

975   respect to the investigated reservoir catchments, further research is needed to trace

976   sediment from various sources and to quantify changes in the sediment storage. Non-

977   quantified errors in modelled SDR values can be 'significant' (Van Rompaey et al.,

978   2003), even when detailed information about the catchment is available. Assuming that

979   modelling would, for example, reduce the mean uncertainty of SDR values established

980   in this study by 25% (or 50%), the mean uncertainty of E values would decrease by

981   19% (36%). This would result in a $FUC_{SDR, E}$ value of 68% (49%) that would be then

982   still higher than the mean fractional uncertainty contribution arising from the TE

983   estimation. The SDR estimation remains therefore a major source of uncertainty and

984   challenge in erosion rate assessments based on reservoir siltation surveys.

985

986   **4.5. Unaccounted uncertainties**

987   A certain percentage of the reservoir deposits may not originate from the catchment, but

988   from other autochthonous and allochthonous sediment sources (Foster et al., 1990;

989   Verstraeten and Poesen, 2002). This may lead to an overestimation of SSY and E values

990   and, thus, induce some additional uncertainty that, so far, has not been accounted for. In

991   the investigated reservoirs, autochthonous sediment production occurs mainly due to

992   biotic processes as the presence of large mammals supports eutrophication (Oberholster

993   et al., 2009). Data from Baade et al. (2012) and additional measurements carried out

994   within the framework of this study reveal a mean total carbon (TC) content ranging

995   from 2 to 4 wt. % for reservoir deposits of the Hartbeesfontein, Marheya, Silolweni,

996   Mlondozi and Nhlanganzwani reservoirs. The ratio of the mean total organic carbon

997   (TOC) content to the mean TC content ranges from 85% to 95%. Multiplying TOC

998   concentrations with the 'Van Bemmelen factor' of 1.72 (Burt and Soil Survey Staff,

999   2014) suggests that the mean organic matter content is <6 wt. %. Since the fractional

1000   contribution of organic matter from autochthonous and allochthonous sources is

1001   unknown, an overestimation of less than $3 \pm 3\%$ can be assumed for SSY and E values.

1002   This is a small uncertainty compared to ε_{SSY} and ε_E values shown in Table 7.

1003   The wet and dry deposition of dust from the atmosphere represents an additional

1004   allochthonous sediment source (Verstraeten and Poesen, 2002). The net flux of dust into

1005 reservoirs likely increases with the mean flooded area. Hence, the sensitivity of SSY and

1006 E values increases with an increasing mean flooded area to catchment size ratio. For the

1007 study sites, total dust deposition rates are unknown, but contemporary mean rates are

1008 most probably <200 g m^{-2} yr^{-1} (DEA, 2009; Lawrence and Neff, 2009). Correcting SSY

1009 and E values based on the assumption of a uniform mean net deposition rate of

1010 100 g m^{-2} yr^{-1} (or 200 g m^{-2} yr^{-1}) on the full supply area (A_R) of the reservoir results in

1011 1 (3) t km^{-2} yr^{-1} lower SSY values and 3 (7) t km^{-2} yr^{-1} lower E values on average. This is

1012 an unimportant effect, especially as calculations based on A_R would probably lead to an

1013 overcorrection, since water levels of the investigated reservoirs are seldom at full stage

1014 (cf. Reinwarth et al., 2018).

1015 Erosion along shorelines and on nearby areas is a further potential source of

1016 uncertainty (Foster et al., 1990; Lloyd et al., 1998). At the investigated reservoirs, wave-

1017 induced erosion is likely intensified by the foraging and trampling of ungulates (e.g.,

1018 herds of buffalo and antelope) (Thrash, 1998). Volumetric core ring measurements point

1019 to a dry bulk density of about 1.5 g cm^{-3} for the eroded material. A uniform average

1020 erosion rate of 0.1 mm yr^{-1} (or 0.5 mm yr^{-1}) for the proportion of the full supply area

1021 being not covered with reservoir deposits (i.e., A_R minus A_S) would therefore lead to a

1022 maximum overestimation of SSY and E values by 1 (6) t km^{-2} yr^{-1} and 4 (19) t km^{-2} yr^{-1},

1023 respectively. Soils and sediments constituting the pre-dam facies contain coarse

1024 particles ($\leq$2 φ-units) that are nearly absent in reservoir deposits (Reinwarth et al.,

1025 2017). This might point to a minor sediment input from shorelines and adjacent areas.

1026 However, with currently available data, erosion rates within reservoir basins cannot be

1027 quantified. Appropriate data may become available in the future, when reservoir basins

1028 are resurveyed by means of high-resolution terrestrial laser scanning (TLS).

1029

1030 **4.6.   Factors governing contemporary sediment yield in the southern**

1031 **Kruger National Park**

1032 This study reveals mean area-specific sediment yield (*SSY*) values ranging from 5 to

1033 80 t km^{-2} yr^{-1} for the investigated reservoir catchments (N = 15) and observation periods

1034 of 30 to 65 years. These findings are in good agreement with *SSY* values of 10 to

1035 60 t km^{-2} yr^{-1} (N = 5) determined in the reconnaissance survey (Baade et al., 2012). The

1036 mean relative uncertainty of *SSY* values ranges from ±12% to ±40% (Table 7) and is

1037 therefore comparable to uncertainties arising from other *SSY* measuring techniques (e.g.,

1038 Phillips et al., 1999; Baade and Liese, 2002; Verstraeten and Poesen, 2002).

1039   The results indicate that *SSY* values for the investigated reservoir catchments

1040 increase with increasing mean annual precipitation (*MAP*). The correlation between *SSY*

1041 and *MAP* is high (R = 0.71; p < 0.01), although *MAP* values vary only between 530 and

1042 670 mm (Fig. 11). This might point to a higher annual rainfall erosivity for areas

1043 receiving more rainfall and is plausible as storm events contribute substantially to

1044 rainfall amounts in the Kruger National Park (Venter et al., 2003). Modelling results

1045 from Reinwarth et al. (2018) suggest, moreover, a more frequent occurrence of surface

1046 runoff for catchments with a high *MAP*, and a substantial contribution (≥65%) to the

1047 overall sediment delivery by a few (N ≤ 6) high discharge events for all investigated

1048 catchments. Higher *MAP* values leading to increased and more frequent surface runoff

1049 might enhance erosion rates as well as sediment delivery (Walling, 1983).

1050   The weakly significant correlation (R = 0.45; p < 0.10) between *SSY* values and

1051 mean slope inclination (*Slope*) is in agreement with other studies pointing to increasing

1052 erosion rates with increasing slope inclination (e.g., Glotzbach et al., 2016; Favis-

1053 Mortlock et al., in press). Taking into account the significant correlation between *MAP*

1054 and *Slope* values (R = 0.58; p < 0.03), the effects of higher rainfall amounts and steeper

1055   relief may be superimposed. More research is required to scrutinize the observed

1056   correlations and to disentangle the complex interrelationships (see Riddell et al., 2014)

1057   between rainfall characteristics and runoff generation in the KNP.

1058   Gullied catchments reveal the highest *SSY* values ($\geq$55 t km^{-2} yr^{-1}) among all

1059   study sites. Field observations show that gully heads are often located in areas with

1060   distinctively reduced vegetation cover. It is possible that these bare surfaces partly

1061   coincide with 'sodic duplex soils' (Venter et al., 2003), i.e., solonetzes with an abrupt

1062   texture change from a clayey subsoil to a loamy topsoil (Fey et al., 2010; van Zijl et al.,

1063   2016). Sodic patches in granite areas of the KNP (Khomo and Rogers, 2005) as well as

1064   duplex soils in general (e.g., van Zijl et al., 2013) were found to be vulnerable to gully

1065   erosion.

1066   Historical aerial images acquired since the 1940s (NGI, 2016) indicate that the

1067   size of bare surfaces fluctuates over time and that bare areas existed already prior to the

1068   construction of the reservoirs. Depending on the resolution and quality of historical

1069   aerial images, gullies are often not easily identified. Field observations suggest,

1070   however, that a part of the existing gully systems continued to erode in recent years.

1071   Gully systems can be furthermore expected to function as pathways along which

1072   sediment is transported towards the reservoirs (Rowntree and Foster, 2012). The

1073   potential nexus between sodic patches, duplex soils and gully formation in the KNP

1074   merits therefore further investigation.

1075

1076   **4.7. Low contemporary erosion rates in the southern Kruger National Park**

1077   Minimum catchment-wide rates of erosion by water (E_{min}) indicate that mean and

1078   median erosion rates in the southern Kruger National Park exceed 20 ± 10 t km^{-2} yr^{-1}

1079   and 10 [5, 35] t km^{-2} yr^{-1} (*Cl95*), respectively (Table 7). Best estimates (*E*) are typically

1080 $\leq$190 t km^{-2} yr^{-1}, although E values of up to 360 t km^{-2} yr^{-1} were determined for gullied

1081 catchments (N = 3). The mean (and median) E value for all study sites amounts to

1082 120 ± 50 t km^{-2} yr^{-1} (85 [55, 145] t km^{-2} yr^{-1}). If gullied catchments are excluded, the

1083 mean (and median) E value decreases to 85 ± 30 t km^{-2} yr^{-1} (70 [45, 115] t km^{-2} yr^{-1}). It

1084 must be kept in mind that erosion rates on the plot scale may differ markedly as

1085 established E values do not reflect the expectable small-scale variability of erosion rates

1086 in the catchments (e.g., Worrall et al., 2014).

1087 Relative uncertainties of E values established in this study are high ($\pm$46%), but

1088 comparable to uncertainties of soil loss estimates derived from models such as the

1089 Universal Soil Loss Equation (e.g., Gericke, 2015). Taking into account these

1090 uncertainties, the results are consistent to low E values of 2 to 75 km^{-2} yr^{-1} reported by

1091 Hoffman and Ashwell (2001, p. 85) for conservation areas within South Africa. This

1092 supports the assertion from Baade et al. (2012) that contemporary SSY and E values

1093 within the Kruger National Park are about an order of magnitude lower than in nearby

1094 areas being characterized by intensive land use (Wessels et al., 2007). Independent data

1095 on contemporary SSY and E values for small to medium-sized (<100 km^2) catchments in

1096 the Lowveld geomorphic province against which findings from this study could be

1097 compared is unfortunately still lacking.

1098

1099 **5. Conclusions**

1100 This study quantifies the mean area-specific sediment yield (SSY) and catchment-wide

1101 average rate of erosion by water (E) for 15 small to medium-sized ($\leq$100 km^2) reservoir

1102 catchments in the southern Kruger National Park and observation periods of 30 to

1103 65 years. Catchment-specific SSY values range from 5 to 80 t km^{-2} yr^{-1} with a mean (and

1104 median) of 30 ± 10 t km^{-2} yr^{-1} (20 [15, 50] t km^{-2} yr^{-1}) for all study sites. SSY values

1105 correlate highly significant with mean annual precipitation (R = 0.71; p < 0.01) and

1106 weakly significant with the mean slope inclination (R = 0.45; p < 0.10) and area

1107 percentage of bare surfaces (R = 0.44; p = 0.10) within the catchments. Best estimates

1108 for E values range from 15 to 360 t km^{-2} yr^{-1} with a mean (and median) of

1109 120 ± 50 t km^{-2} yr^{-1} (85 [55, 145] t km^{-2} yr^{-1}), whereby E values >190 t km^{-2} yr^{-1} are

1110 restricted to catchments that are affected by gully erosion. Excluding gullied catchments

1111 (N = 3) reveals a mean (and median) E value of 85 ± 30 t km^{-2} yr^{-1}

1112 (70 [45, 115] t km^{-2} yr^{-1}).

1113 A thorough error analysis points to a low mean relative uncertainty of ±21% for

1114 SSY values, while the mean relative uncertainty for E values is comparatively high

1115 amounting to ±46%. The trap efficiency (TE) estimation causes the highest fractional

1116 uncertainty contribution (64%) with respect to SSY values and the SDR estimation is by

1117 far the most important source of uncertainty (79%) in the determination of E values. By

1118 comparison, mean fractional uncertainty contributions arising from the determination of

1119 the volume (V_S) and dry bulk density (dBD) of the reservoir deposits are low, amounting

1120 together to <30% with respect to SSY values and <6% with respect to E values. Other

1121 potential sources of uncertainty are unimportant, contributing together 11% and <3% to

1122 uncertainties in SSY and E values, respectively.

1123 These results have notable implications concerning an opportune surveying and

1124 sampling strategy. Comparing the findings of this study with results from the

1125 reconnaissance survey (Baade et al., 2012) elucidates that very limited field data are

1126 sufficient to determine V_S values with an uncertainty of less than ±30%, given that valid

1127 assumptions can be made about the geometry of the sedimentary infill. When variations

1128 of dBD values (e.g., due to sediment compaction or desiccation cracks) are adequately

1129 taken into account, the mean dBD can be ascertained with a reasonably low uncertainty

1130   (i.e., less than ±8% or ±0.1 g cm^{-3} in this study), if >20 samples are collected. Increasing

1131   the surveying and sampling resolution has only a minor effect on uncertainties in *SSY*

1132   and *E* values due to the overall low fractional uncertainty contribution arising from the

1133 V_S and *dBD* determination. The highest potential to reduce uncertainties in *SSY* and *E*

1134   values obtained from reservoir siltation surveys clearly lies in an improvement of the *TE*

1135   and *SDR* estimation. Here, emerging concepts to quantify sediment and hydrologic

1136   connectivity (Wohl et al., 2017) represent a promising approach.

1137

1158

1159   References

1160   Aksoy, H., Kavvas, M.L., 2005. A review of hillslope and watershed scale erosion and
1161   sediment   transport   models.   Catena   64 (2-3),   247-271.   DOI:
1162   10.1016/j.catena.2005.08.008.

1163   Annandale, G.W., 1987. Reservoir sedimentation. Developments in Water Science 29.
1164   Elsevier: Amsterdam, The Netherlands, 221 pp.

1165   Auerswald, K., 1989. Predicting nutrient enrichment from long-term average soil loss.
1166   Soil Technology 2 (3), 271-277. DOI: 10.1016/0933-3630(89)90011-1.

1167   Baade, J., Liese, C., 2002. Accuracy of sediment yield measurements in small
1168   catchments. In: Proceedings of the IAHS Workshop 'Erosion and sediment
1169   transport measurements in rivers: technological and methodological advances',
1170   19-21 June 2002, Oslo. International Association of Hydrological Sciences
1171   (IAHS) Press: Wallingford, United Kingdom.

1172   Baade, J., Schmullius, C., 2015. Catchment properties in the Kruger National Park
1173   derived from the new TanDEM-X Intermediate Digital Elevation Model
1174   (IDEM). The International Archives of the Photogrammetry, Remote Sensing
1175   and   Spatial   Information   Sciences   XL-7/W3,   293-300.   DOI:
1176   10.5194/isprsarchives-XL-7-W3-293-2015.

1177   Baade, J., Schmullius, C., 2016. TanDEM-X IDEM precision and accuracy assessment
1178   based on a large assembly of differential GNSS measurements in the Kruger
1179   National Park, South Africa. ISPRS Journal of Photogrammetry and Remote
1180   Sensing 119, 496-508. DOI: 10.1016/j.isprsjprs.2016.05.005.

1181   Baade, J., Franz, S., Reichel, A., 2012. Reservoir siltation and sediment yield in the
1182   Kruger National Park, South Africa: a first assessment. Land Degradation &
1183   Development 23 (6), 586-600. DOI: 10.1002/ldr.2173.

1184   Balzter, H., Baade, J., Rogers, K., 2016. Validation of the TanDEM-X Intermediate
1185   Digital Elevation Model With Airborne LiDAR and Differential GNSS in
1186   Kruger National Park. IEEE Geoscience and Remote Sensing Letters 13 (2),
1187   277-281. DOI: 10.1109/LGRS.2015.2509500.

1188   Brasher, B.R., Franzmeier, D.P., Valassis, V., Davidson, S.E., 1966. Use of saran resin
1189   to coat natural soil clods for bulk density and water-retention measurements.
1190   Soil Science 101 (2), 108.

1191   Bräutigam, B., Bachmann, M., Schulze, D., Borla Tridon, D., Rizzoli, P., Martone, M.,
1192   Gonzales, C., Zink, M., Krieger, G., 2014. TanDEM-X global DEM quality
1193   status and acquisition completion. Proceedings of the IEEE International
1194   Geoscience and Remote Sensing Symposium (IGARSS), Quebec City, Canada,
1195   July 13-18, 2014. Institute of Electrical and Electronics Engineers (IEEE):
1196   Piscataway, New Jersey, USA, pp. 3390-3393. DOI:
1197   10.1109/IGARSS.2014.6947208.

1198   Brazier, R., 2004. Quantifying soil erosion by water in the UK: a review of monitoring
1199   and modelling approaches. Progress in Physical Geography 28 (3), 340-365.
1200   DOI: 10.1191/0309133304pp415ra.

1201   Brown, A.G., Carey, C., Erkens, G., Fuchs, M., Hoffmann, T., Macaire, J.-J.,
1202   Moldenhauer, K.-M., Walling, D.E., 2009. From sedimentary records to
1203   sediment budgets: multiple approaches to catchment sediment flux.
1204   Geomorphology 108, 35-47. DOI: 10.1016/j.geomorph.2008.01.021.

1205   Brown, C.B., 1944. Discussion of 'Sedimentation in Reservoirs' by B. J. Witzig.
1206   Transactions of the American Society of Civil Engineers 109, 1080-1086.

1207   Bucini, G., Hanan, B.P., Boone, R.B., Smit, I.P.J., Saatchi, S.S., Lefsky, M.A., Asner
1208   G.P., 2010. Woody fractional cover in Kruger National Park, South Africa:
1209   remote sensing-based maps and ecological insights. In: Hill, M.J., Hanan, N.P.
1210   (Eds.). Ecosystem function in savannas. Measurement and modeling at
1211   landscape to global scales. CRC Press: Boca Raton, Florida, USA, pp. 219-238.
1212   DOI: 10.1201/b10275-15.

1213 Burt, R., Soil Survey Staff, 2014. Kellogg Soil Survey Laboratory Methods Manual.
1214   Soil Survey Investigations Report 42. Version 5.0. US Department of
1215   Agriculture (USDA), Natural Conservation Service: Lincoln, Nebraska, USA,
1216   1001 pp.

1217 Bussi, G., Rodríguez-Lloveras, X, Francés, F., Benito, G., Sánchez-Moya, Y., Sopeña,
1218   A., 2013. Sediment yield model implementation based on check dam infill
1219   stratigraphy in a semiarid Mediterranean catchment. Hydrology and Earth
1220   System Sciences 17, 3339-3354. DOI: 10.5194/hess-17-3339-2013.

1221 Canty, A., Ripley, B., 2017. boot: Bootstrap R (S-Plus) Functions. R package version
1222   1.3-20. <https://cran.r-project.org/web/packages/boot/index.html> accessed
1223   05 January 2018.

1224 Castillo, V.M., Mosch, W.M., Conesa García, C., Barberá, G.G., Navarro Cano, J.A.,
1225   López-Bermúdez, F., 2007. Effectiveness and geomorphological impacts of
1226   check dams for soil erosion control in a semiarid Mediterranean catchment: El
1227   Cárcavo (Murcia, Spain). Catena 70 (3), 416-427. DOI:
1228   10.1016/j.catena.2006.11.009.

1229 Chadwick, O.A., Roering, J.J., Heimsath, A.M., Levick, S.R., Asner, G.P., Khomo, L.,
1230   2013. Shaping post-orogenic landscapes by climate and chemical weathering.
1231   Geology 41 (11), 1171-1174. DOI: 10.1130/G34721.1.

1232 Crawley, M.J., 2007. The R book. Wiley & Sons: Chichester, United Kingdom, 950 pp.

1233 Cummins, W.A., Potter, H.R., 1967. Rate of sedimentation in Cropston Reservoir,
1234   Charnwood Forest, Leicestershire. The Mercian Geologist 2 (1), 31-39.

1235 Davison, A.C., Hinkley, D.V., 1997. Bootstrap methods and their Application.
1236   Cambridge Series in Statistical and Probabilistic Mathematics. Cambridge
1237   University Press: Cambridge, United Kingdom, 582 pp. DOI:
1238   10.1017/CBO9780511802843.

1239 DEA, 2009. State of Air Report 2005. A report on the state of the air in South Africa.
1240   Department of Environmental Affairs (DEA): Pretoria, South Africa, 218 pp.

de Vente, J., Poesen, J., Arabkhedri, M., Verstraeten, G., 2007. The sediment delivery problem revisited. Progress in Physical Geography 31 (2), 155-178. DOI: 10.1177/0309133307076485.

Díaz, V., Mongil, J., Navarro, J., 2014. Topographical surveying for improved assessment of sediment retention in check dams applied to a Mediterranean badlands restoration site (Central Spain). Journal of Soils and Sediments 14 (12), 2045-2056. DOI: 10.1007/s11368-014-0958-5.

Dutta, S., 2016. Soil erosion, sediment yield and sedimentation of reservoir: a review. Modeling Earth Systems and Environment 2 (123), 18 pp. DOI: 10.1007/s40808-016-0182-y.

Esri, 2015. ArcGIS Desktop: Release 10.4. Environmental Systems Research Institute (ESRI): Redlands, California, USA.

Esri Water Resources Team, 2014. Arc Hydro Overview Document #1. Environmental Systems Research Institute, Inc. (ESRI): Redlands, California, USA.

Evans, M., Church, M., 2000. A method for error analysis of sediment yields derived from estimates of lacustrine sediment accumulation. Earth Surface Processes and Landforms 25 (11), 1257-1267. DOI: 10.1002/1096-9837(200010)25:11<1257::AID-ESP136>3.0.CO;2-K.

FAO, 2014. World reference base for soil resources 2014. International soil classification system for naming soils and creating legends for soil maps. World Soil Resources Reports 106. Food and Agriculture Organization (FAO) of the United Nations: Rome, Italy, 181 pp.

Favis-Mortlock, D., Boardman, J., Foster, I., Greenwood, P., in press. 'Local gradient' and between-site variability of erosion rate on badlands in the Karoo, South Africa. Earth Surface Processes and Landforms. DOI: 10.1002/esp.4293.

Fey, M., Hughes, J., Lambrechts, J., Dohse, T., 2010. The soil groups: distribution, properties, classification, genesis and use. In: Fey, M. (Ed.). Soils of South Africa. Their distribution, properties, classification, genesis, use and environmental significance. Cambridge University Press: Cambridge, United Kingdom, pp. 17-147.

1271   Foster, I.D.L., Walling, D.E., 1994. Using reservoir deposits to reconstruct changing
1272   sediment yields and sources in the catchments of the Old Mill Reservoir, South
1273   Devon, UK, over the past 50 years. Hydrological Sciences Journal 39 (4), 347-
1274   368. DOI: 10.1080/02626669409492755.

1275   Foster, I.D.L., Dearing, J.A., Grew, R., Orend, K., 1990. The sedimentary data base: an
1276   appraisal of lake and reservoir sediment based studies of sediment yield. In:
1277   Walling, D.E., Yair, A., Berkowicz, S. (Eds.). Erosion, Transport and Deposition
1278   Processes (Proceedings of the Jerusalem Workshop, March-April 1987). IAHS
1279   Publications 189. International Association of Hydrological Sciences (IAHS)
1280   Press: Wallingford, United Kingdom, pp. 19-43.

1281   Freitag-Ronaldson, S., Foxcroft, L.C., 2003. Anthropogenic influences at the ecosystem
1282   level. In: Du Toit, J.T., Rogers, K.H., Biggs, H.C. (Eds.). The Kruger
1283   experience. Ecology and management of savanna heterogeneity. Island Press:
1284   Washington D.C., pp. 391-421.

1285   Freitag-Ronaldson, S., Kalwa, R.H., Badenhorst, J.C., Erasmus, J.P., Venter, F.J., Nel,
1286   F.J., 2003. Wilderness, wilderness quality management, and recreational
1287   opportunities zoning within Kruger National Park, South Africa. In: Watson, A.,
1288   Sproull, J. (Eds.). Science and stewardship to protect and sustain wilderness
1289   values. Seventh World Wilderness Congress symposium 2001, November 2-8,
1290   Port Elizabeth, South Africa. USDA Forest Service Proceedings RMRS-P-27.
1291   US Department of Agriculture (USDA), Forest Service, Rocky Mountain
1292   Research Station: Ogden, Utah, USA, pp. 39-49.

1293   Fryirs, K., 2013. (Dis)Connectivity in catchment sediment cascades: a fresh look at the
1294   sediment delivery problem. Earth Surface Processes and Landforms 38 (1), 30-
1295   46. DOI: 10.1002/esp.3242.

1296   Garrison, E., 2016. Techniques in Archaeological Geology. 2nd edn. Springer: Berlin,
1297   Germany, 345 pp. DOI: 10.1007/978-3-319-30232-4.

1298   Geological Survey of South Africa, 1986a. Geological Series 1:250 000. Sheet 2430
1299   Pilgrim's Rest. Government Printer: Pretoria, South Africa.

1300 Geological Survey of South Africa, 1986b. Geological Series 1:250 000. Sheet 2530
1301   Barberton. Government Printer: Pretoria, South Africa.

1302 Gericke, A., 2015. Soil loss estimation and empirical relationships for sediment delivery
1303   ratios of European river catchments. International Journal of River Basin
1304   Management 13 (2), 179-202. DOI: 10.1080/15715124.2014.1003302.

1305 Glotzbach, C., Paape, A., Baade, J., Reinwarth, B., Rowntree, K., Miller, J., 2016.
1306   Cenozoic landscape evolution of the Kruger National Park as derived from
1307   cosmogenic nuclide analyses. Terra Nova 28 (5), 316-322. DOI:
1308   10.1111/ter.12223.

1309 Glymph, L.M., 1954. Studies of sediment yields from watersheds. International
1310   Association of Hydrological Sciences (IAHS) Publication 36, 178-191.

1311 Grossmann, R.B., Reinsch, T.G., 2002. Bulk density and linear extensibility. In: Dane,
1312   J.H., Topp, G.C. (Eds.). Methods of soil analysis. Part 4. Physical Methods. Soil
1313   Science Society of America Book Series. Soil Science Society of America,
1314   Madison, Wisconsin, USA, pp. 201-228.

1315 Haan, C.T., Barfield, B.J., Hayes, J.C., 1994. Design Hydrology and Sedimentology for
1316   Small Catchments. Academic Press: San Diego, California, USA, 588 pp.

1317 Heinemann, H.G., 1981. A new sediment trap efficiency curve for small reservoirs.
1318   Journal of the American Water Resources Association 17 (5), 825-830. DOI:
1319   10.1111/j.1752-1688.1981.tb01304.x.

1320 Heinemann, H.G., 1984. Reservoir trap efficiency. In: Hadley, R.F., Walling, D.E.
1321   (Eds.). Erosion and Sediment Yield: Some Methods of Measurement and
1322   Modelling. Geo Books: Norwich, United Kingdom, pp. 201-218.

1323 Heritage, G.L., Milan, D.J., Large, A.R.G., Fuller, I.C., 2009. Influence of survey
1324   strategy and interpolation model on DEM quality. Geomorphology 112 (3-4),
1325   334-344. DOI: 10.1016/j.geomorph.2009.06.024.

1326 Hoffman, T., Ashwell, A., 2001. Nature divided. Land degradation in South Africa.
1327   University of Cape Town Press: Lansdowne, Cape Town, South Africa, 168 pp.

1328　Jarvis, A., Reuter, H.I., Nelson, A., Guevara, E., 2008. Hole-filled seamless SRTM data
1329　　　　V4. International Centre for Tropical Agriculture (CIAT).
1330　　　　<http://srtm.csi.cgiar.org> accessed 02 August 2016.

1331　Jolly, J.P., 1982. A proposed method for accurately calculating sediment yields from
1332　　　　reservoir deposition volumes. In: Walling, D.E. (Ed.). Recent developments in
1333　　　　the explanation and prediction of erosion and sediment yield (Proceedings of the
1334　　　　Exeter Symposium, July 1982). IAHS Publication 137. International Association
1335　　　　of Hydrological Sciences (IAHS) Press: Wallingford, United Kingdom, pp. 153-
1336　　　　161.

1337　Khomo, L.M., Rogers, K.H., 2005. Proposed mechanisms for the origin of sodic patches
1338　　　　in Kruger National Park, South Africa. African Journal of Ecology 43, 29-34.
1339　　　　DOI: 10.1111/j.1365-2028.2004.00532.x.

1340　Klaghofer, E., Summer, W., Villeneuve, J.P., 1992. Some remarks on the determination
1341　　　　of the sediment delivery ratio. In: Walling, D.E., Davies, T.R., Hasholt, B.
1342　　　　(Eds.). Erosion, Debris Flows and Environment in Mountain Regions
1343　　　　(Proceedings of the Chengdu Symposium, July 1992). IAHS Publications 209.
1344　　　　International Association of Hydrological Sciences (IAHS) Press: Wallingford,
1345　　　　United Kingdom, pp. 113-118.

1346　Kloppers, J.J., Bornman, H., 2005. A dictionary of Kruger National Park Place Names.
1347　　　　SA Country Life: Barberton, South Africa, 296 pp.

1348　Lane, E.W., Koelzer, V.A., 1943. Density of sediments deposited in reservoirs. A study
1349　　　　of methods used in measurement and analysis of sediment loads in streams.
1350　　　　Report No. 9. St. Paul U.S. Engineer District Sub-Office Hydraulic Laboratory,
1351　　　　University of Iowa: Iowa City, USA, 60 pp.

1352　Langbein, W.B., Schumm, S.A., 1958. Yield of sediment in relation to mean annual
1353　　　　precipitation. Eos, Transactions American Geophysical Union 39 (6), 1076-
1354　　　　1084. DOI: 10.1029/TR039i006p01076.

1355　Lawrence, C.R., Neff, J.C., 2009. The contemporary physical and chemical flux of
1356　　　　aeolian dust: a synthesis of direct measurements of dust deposition. Chemical
1357　　　　Geology 267 (1-2), 46-63. DOI: 10.1016/j.chemgeo.2009.02.005.

1358   Leica Geosystems, 2014. Leica Geo Office Vers. 8.4. Heerbrugg, Switzerland.

1359   Lewis, S.E., Bainbridge, Z.T., Kuhnert, P.M., Sherman, B.S., Henderson, B., Dougall,
1360   C., Cooper, M., Brodie, J.E., 2013. Calculating sediment trapping efficiencies
1361   for reservoirs in tropical settings: a case study from the Burdekin Falls Dam, NE
1362   Australia. Water Resources Research 49 (2), 1017-1029. DOI:
1363   10.1002/wrcr.20117.

1364   Lloyd, S.D., Bishop, P., Reinfelds, I., 1998. Shoreline erosion: a cautionary note in
1365   using small farm dams to determine catchment erosion rates. Earth Surface
1366   Processes and Landforms 23 (10), 905-912. DOI: 10.1002/(SICI)1096-
1367   9837(199810)23:10<905::AID-ESP910>3.0.CO;2-E.

1368   Lu, H., Moran, C.J., Prosser, I.P., 2006. Modelling sediment delivery ratio over the
1369   Murray Darling Basin. Environmental Modelling & Software 21 (9), 1297-1308.
1370   DOI: 10.1016/j.envsoft.2005.04.021.

1371   MacFayden, S., 2010. Identifying priority zones within protected areas. A biodiversity
1372   sensitivity-value analysis of the Kruger National Park, South Africa. Master
1373   thesis. Faculty of Earth and Life Science, Vrije Universiteit Amsterdam:
1374   Amsterdam, The Netherlands, 57 pp.

1375   MacFayden, S., Hui, C., Verburg, P.H., Van Teeffelen, A.J.A., 2016. Quantifying
1376   spatiotemporal drivers of environmental heterogeneity in Kruger National Park,
1377   South Africa. Landscape Ecology 31 (9), 2013-2029. DOI: 10.1007/s10980-016-
1378   0378-6.

1379   Morris, G.L., Fan, J., 1998. Reservoir sedimentation handbook. Design and
1380   management of dams, reservoirs, and watersheds for sustainable use. McGraw-
1381   Hill Book Co: New York, USA, 805 pp.

1382   Msadala, V., Gibson, L., Le Roux, J., Rooseboom, A., Basson, G.R., 2012. Sediment
1383   yield prediction for South Africa: 2010 edition. WRC report No. 1765/1/10.
1384   Water Research Commission (WRC): Pretoria, South Africa, 250 pp.

1385   NGI, 2016. The integrated Topographic Information System (iTIS) Portal. Chief
1386   Directorate – National Geo-spatial Information (NGI): Cape Town, South
1387   Africa. <http://itis.ngi.gov.za/itisportalinternet> accessed 29 June 2016.

1388 Oberholster, P.J., Myburgh, J.G., Govender, D., Bengis, R., Botha, A.-M., 2009.
1389   Identification of toxigenic Microcystis strains after incidents of wild animal
1390   mortalities in the Kruger National Park, South Africa. Ecotoxicology and
1391   Environmental Safety 72 (4), 1177-1182. DOI: 10.1016/j.ecoenv.2008.12.014.

1392 Oksanen, J., Sarjakoski, T., 2005. Error propagation of DEM-based surface derivatives.
1393   Computer & Geosciences 31 (8), 1015-1027. DOI: 10.1016/j.cageo.2005.02.014.

1394 Partridge, T.C., Dollar, E.S.J., Moolman, J., Dollar, L.H., 2010. The geomorphic
1395   provinces of South Africa, Lesotho and Swaziland: a physiographic subdivision
1396   for earth and environmental scientists. Transactions of the Royal Society of
1397   South Africa 65 (1), 1-47. DOI: 10.1080/00359191003652033.

1398 Petersen, R., 2012. A conceptual understanding of groundwater recharge processes and
1399   surface-water/groundwater interactions in the Kruger NP. Master thesis.
1400   University of the Western Cape: Bellville, Cape Town, South Africa.

1401 Phillips, J.M., Webb, B.W., Walling, D.E., Leeks, G.J.L., 1999. Estimating the
1402   suspended sediment loads of rivers in the LOIS study area using infrequent
1403   samples. Hydrological Processes 13 (7), 1035-1050. DOI: 10.1002/(SICI)1099-
1404   1085(199905)13:7<1035::AID-HYP788>3.0.CO;2-K.

1405 Pienaar, U.D.V., 1985. Indications of progressive desiccation of the Transvaal Lowveld
1406   over the past 100 years, and implications for the water stabilization programme
1407   in the Kruger National Park. Koedoe 28 (1), 93-165. DOI:
1408   10.4102/koedoe.v28i1.540.

1409 Pires, L.F., Rosa, J.A., Timm, L.C., 2011. Comparação de métodos de medida da
1410   densidade do solo. Acta Scientarium Agronomy 33 (1), 161-170. DOI:
1411   10.4025/actasciagron.v33i1.5507.

1412 Pitman, W.V., 1976. A mathematical model for generating daily river flows from
1413   meteorological data in South Africa. Hydrological Research Unit Report No.
1414   2/76. University of Witwatersrand: Johannesburg, South Africa.

1415 Ramos-Diez, I., Navarro-Hevia, J., San Martín Fernandez, R., Mongil-Manso, J., 2017.
1416   Final analysis of the accuracy and precision of methods to calculate the sediment

retained in check dams. Land Degradation & Development 28, 2446-2456. DOI: 10.1002/ldr.2778.

Rausch, D.L., Heinemann, H.G., 1984. Measurement of reservoir sedimentation. In: Hadley, R,F., Walling, D.E. (Eds.). Erosion and Sediment yield. Some Methods of Measurement and Modelling. Geo Nooks, Norwich, United Kingdom, pp. 179-200.

Reinwarth, B., Miller, J.K., Glotzbach, C., Rowntree, K.M., Baade, J., 2017. Applying regularized logistic regression (RLR) for the discrimination of sediment facies in reservoirs based on composite fingerprints. Journal of Soils and Sediments 17 (6), 1777-1795. DOI: 10.1007/s11368-016-1627-7.

Reinwarth, B., Riddell, E.S., Glotzbach, C., Baade, J., 2018. Estimating the sediment trap efficiency of intermittently dry reservoirs: lessons from the Kruger National Park, South Africa. Earth Surface Processes and Landforms 43 (2), 463-481. DOI: 10.1002/esp.4263.

Riddell, E.S., Nel, J., Fundisi, D., Jumbi, F., van Niekerk, A., Lorentz, S.A., 2014. Ephemeral Hydrological Processes in Savannas. WRC Report No. TT 619/14. Water Research Commission (WRC): Gezina, Pretoria, South Africa, 231 pp.

Riegl, 2017. RiScan Pro 2.5 Operating and Processing Software. Riegl Laser Measurement Systems: Horn, Austria.

Roehl, J.W., 1962. Sediment source areas, delivery ratios and influencing morphological factors. International Association of Hydrological Sciences (IAHS) Publication 59, 202-213.

Rowan, J.S., Goodwill, P., Greco, M., 1995. Temporal variability in catchment sediment yield determined from repeated bathymetric surveys: Abbeystead Reservoir, U.K. Physics and Chemistry of the Earth 20 (2), 199-206. DOI: 10.1016/0079-1946(95)00024-0.

Rowntree, K., Foster, I., 2012. A reconstruction of historical changes in sediment sources, sediment transfer and sediment yield in a small, semi-arid Karoo catchment, South Africa. In: Beylich, A.A., Zwolinski, Z. (Eds.). Hydrogeomorphological processes in catchment geoecosystems. Zeitschrift für

1447   Geomorphologie 56, Supplementary Issue 1. Gebrüder Borntraeger: Berlin,
1448   Germany, pp. 87-100. DOI: 10.1127/0372-8854/2012/S-00074.

1449   Stewart, R.D., Rupp, D.E., Abou Najm, M.R., Selker, J.S., 2016. A unified model for
1450   soil shrinkage, subsidence and cracking. Vadose Zone Journal 15 (3), 15 pp.
1451   DOI: 10.2136/vzj2015.11.0146.

1452   Taylor, J.R., 1997. An introduction to error analysis. The study of uncertainties in
1453   physical measurements. 2nd edn. University Science Books: Sausalito,
1454   California, USA, 327 pp.

1455   Thrash, I., 1998. Impact of water provision on herbaceous vegetation in Kruger
1456   National Park, South Africa. Journal of Arid Environments 38 (3), 437-450.
1457   DOI: 10.1006/jare.1997.0318.

1458   USDA-SCS, 1983. National Engineering Handbook. Section 3. United States
1459   Department of Agriculture – Soil Conservation Service (USDA-SCS):
1460   Washington D.C., USA, 226 pp.

1461   USGS EROS, 2015. Shuttle Radar Topography Mission (SRTM) 1 Arc-Second Global.
1462   United States Geological Survey's (USGS) Earth Resources Observation and
1463   Science (EROS) Center: Sioux Falls, South Dakota, USA.
1464   <https://lta.cr.usgs.gov/SRTM1Arc> accessed 21 March 2016.

1465   Vanmaercke, M., Poesen, J., Broeckx, J., Nyssen, J., 2014. Sediment yield in Africa.
1466   Earth-Science Reviews 136, 350-368. DOI: 10.1016/j.earscirev.2014.06.004.

1467   Van Remortel, R.D., Shields, D.A., 1993. Comparison of clod and core methods for
1468   determination of soil bulk density. Communications in Soil Science and Plant
1469   Analysis 24 (17-18), 2517-2528. DOI: 10.1080/00103629309368972.

1470   Van Rompaey, A.J.J., Verstraeten, G., Van Oost, K., Govers, G., Poesen, J., 2001.
1471   Modelling mean annual sediment yield using a distributed approach. Earth
1472   Surface Processes and Landforms 26 (11), 1221-1236. DOI: 10.1002/esp.275.

1473   Van Rompaey, A.J.J., Vieillefont, V., Jones, R.J.A., Montanarella, L., Verstraeten, G.,
1474   Bazzoffi, P., Dostal, T., Krasa, J., de Vente, J., Poesen, J., 2003. Validation of
1475   soil erosion estimates at European scale. European Soil Research Report No. 13.

1476   Office for Official Publications of the European Communities: Luxembourg,
1477   26 pp.

1478 Van Tol, J.J., van Zijl, G.M., Riddell, G.S., Fundisi, D., 2015. Application of
1479   hydropedological insights in hydrological modelling of the Stevenson-Hamilton
1480   Research Supersite, Kruger National Park, South Africa. Water SA 41 (4), 525-
1481   533. DOI: 10.4314/wsa.v41i4.12.

1482 van Zijl, G.M., Ellis, F., Rozanov, D.A., 2013. Emphasising the soil factor in
1483   geomorphological studies of gully erosion: a case study in Maphutseng, Lesotho.
1484   Soil   African   Geographical   Journal   95 (2),   205-216.   DOI:
1485   10.1080/03736245.2013.847803.

1486 van Zijl, G.M., Van Tol, J.J., Riddell, E.S., 2016. Digital soil mapping for hydrological
1487   modelling. In: Zhang, G.-L., Brus, D., Liu, F., Song, X.-D., Lagacherie, P.
1488   (Eds.). Digital soil mapping across paradigms, scales and boundaries. Springer
1489   Environmental Science and Engineering. Springer: Singapore, pp. 115-129.
1490   DOI: 10.1007/978-981-10-0415-5_10.

1491 Venter F.J., Scholes, R.J., Eckhardt H.C., 2003. The abiotic template and its associated
1492   vegetation pattern. In: Du Toit, J.T., Rogers, K.H., Biggs, H.C. (Eds.). The
1493   Kruger experience. Ecology and management of savanna heterogeneity. Island
1494   Press: Washington D.C., pp. 83-129.

1495 Verstraeten, G., Poesen, J., 2001. Variability of dry sediment bulk density between and
1496   within retention ponds and its impact on the calculation of sediment yields. Earth
1497   Surface Processes and Landforms 26 (4), 375-394. DOI: 10.1002/esp.186.

1498 Verstraeten, G., Poesen, J., 2002. Using sediment deposits in small ponds to quantify
1499   sediment yield from small catchments: possibilities and limitations. Earth
1500   Surface Processes and Landforms 27 (13), 1425-1439. DOI: 10.1002/esp.439.

1501 Verstraeten, G., Bazzoffi, P., Lajczak, A, Rãdoane, M., Rey, F., Poesen, J., de Vente, J.,
1502   2006. Reservoir and pond sedimentation in Europe. In: Boardman, J., Poesen, J.
1503   (Eds.). Soil erosion in Europe. Wiley & Sons: Chichester, United Kingdom,
1504   pp. 757-774. DOI: 10.1002/0470859202.ch54.

1505 Walling, D.E., 1983. The sediment delivery problem. Journal of Hydrology 65, 209-
1506   237. DOI: 10.1016/0022-1694(83)90217-2.

1507 Wessels, K.J., Prince, S.D., Malherbe, J., Small, J., Frost, P.E., Van Zyl, D., 2007. Can
1508   human-induced land degradation be distinguished from the effects of rainfall
1509   variability? A case study in South Africa. Journal of Arid Environments 68, 271-
1510   297. DOI: 10.1016/j.jaridenv.2006.05.015.

1511 Wilson, B.N., Barfield, B.J., 1985. Modeling sediment detention ponds using reactor
1512   theory and advection-diffusion concepts. Water Resources Research 21 (4): 523-
1513   532. DOI: 10.1029/WR021i004p00523.

1514 Wohl, E., Magilligan, F.J., Rathburn, S.L., 2017. Introduction to the special issue:
1515   Connectivity in Geomorphology. Geomorphology 277, 1-5. DOI:
1516   10.1016/j.geomorph.2016.11.005.

1517 Worrall, F., Burt, T.P., Howden, N.J.K., Hancock, G.R., 2014. Variation in suspended
1518   sediment yield across the UK – a failure of the concept and interpretation of the
1519   sediment delivery ratio. Journal of Hydrology 519, Part B, 1985-1996. DOI:
1520   10.1016/j.jhydrol.2014.09.066.

1521 Zambatis, N., 2006. Average monthly and seasonal temperatures and average monthly
1522   and annual rainfall of the Kruger National Park.
1523   <http://www.sanparks.org/parks/kruger/conservation/scientific/weather/rainfall/
1524   2006/temps_rainfall_averages.pdf> accessed 18 December 2017.

1525 Zink, M., Moreira, A., Bachmann, M., Bräutigam, B., Fritz, T., Hajnsek, I., Krieger, G.,
1526   Wessel, B., 2016. TanDEM-X mission status: the complete new topography of
1527   the Earth. Proceedings of the 2016 IEEE Geoscience and Remote Sensing
1528   Symposium (IGARSS), July 10-15, 2016, Beijing, China. Institute of Electrical
1529   and Electronics Engineers (IEEE): Piscataway, New Jersey, USA, pp. 317-320.
1530   DOI: 10.1109/IGARSS.2016.7729075.

Chapter 6

Discussion and Synthesis

Author: Bastian Reinwarth

6 Discussion and Synthesis

6.1 Comparison of contemporary sediment yield and erosion rates in the Lowveld geomorphic province, inside and outside the Kruger National Park

This study reveals a contemporary mean area-specific sediment yield (SSY) of 5 to 80 t km^2 yr^{-1} for 15 reservoir catchments (<110 km^2) in the Kruger National Park (KNP) and observation periods (T_R) of 30 to 65 years. SSY data for areas located likewise in the *Lowveld* geomorphic province, but outside the KNP, is available for five reservoir catchments to the west (Fig. 1a). These catchments vary in size (A) from 27 to 165 km^2 and are characterized by mean SSY values of 55 to 565 t km^2 yr^{-1} (Rooseboom et al., 1992) for observation periods (T_R) of 8 to 39 years (Tab. 1). Only one catchment (i.e., Primkop Dam) shows a SSY value that falls into the range that was determined for catchments within the KNP by this study. The other four catchments are characterized by 2 to >100 times higher SSY values.
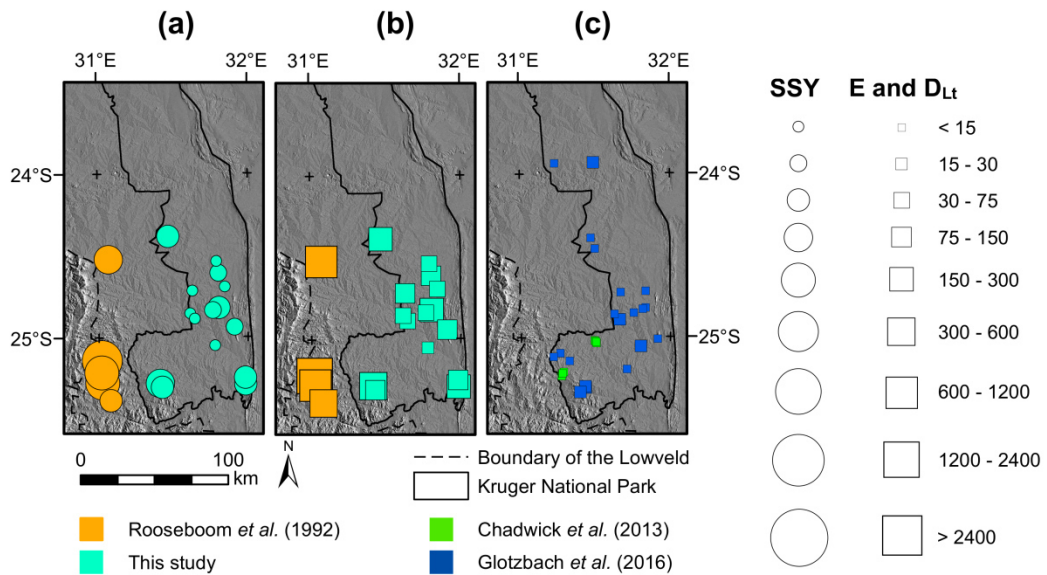
Fig. 1. Sediment yield, erosion, and denudation rates within the southern Kruger National Park and other parts of the Lowveld: (a) contemporary mean area-specific sediment yield (SSY), (b) best estimates for rates of erosion by water (E) infered from reservoir siltation surveys (Rooseboom et al., 1992, and this study), and (c) spatially averaged long-term denudation rates (D_{Lt}) determined from in-situ produced cosmogenic [10]Be in river sediment (Chadwick et al., 2013; Glotzbach et al., 2016). The hillshade representation of the relief was derived from the SRTM1GL digital elevation model (USGS EROS, 2015). The western boundary of the Lowveld geomorphic province, running along the foot of the Great Escarpment, is shown according to Partridge et al. (2010).

Tab. 1 Data for catchments of reservoirs located in the Lowveld geomorphic province, but outside the Kruger National Park (based on Rooseboom et al., 1992).

Reservoir	Long	Lat	T_R	A	MAP	SSY	SDR	E
	[° E]	[° S]	[yrs]	[km^2]	[mm]	[t km^{-2} yr^{-1}]		[t km^{-2} yr^{-1}]
Klaserie Dam	31.0708	-24.5250	19	165	630	120	0.15 ± 0.10	900 ± 400
Primkop Dam	31.0750	-25.3875	17	158	810	55	0.15 ± 0.10	400 ± 150
Longmere Dam	31.0208	-25.2792	39	27	920	250	0.20 ± 0.15	1200 ± 500
Klipkopjes Dam	31.0169	-25.2169	19	78	1020	235	0.20 ± 0.15	1400 ± 600
Da Gama Dam	31.0208	-25.1417	8	62	1140	565	0.20 ± 0.15	3200 ± 1400

Note: longitude (Long), latitude (Lat), operational lifetime of the reservoirs up to the survey date (T_R), catchment size (A), mean annual precipitation (MAP), contemporary mean area-specific sediment yield (SSY), sediment delivery ratio (SDR), best estimate for the contemporary catchment-wide average rate of erosion by water (E); MAP was interpolated using Thiessen polygons based on data provided by Pitman and Bailey (2015); SDR and E were calculated as described in chapter 5 and are reported with 95% confidence intervals.

Inside the KNP, best estimates for catchment-wide average rates of erosion by water (*E*) are typically ≤190 t km^{-2} yr^{-1} but reach of up to 360 t km^{-2} yr^{-1} for gullied catchments. Calculating sediment delivery ratios (*SDR*), as described in chapter 5 (section 2.9), leads to *E* values of 400 to 3,200 t km^2 yr^{-1} for the reservoir catchments west of the KNP (Fig. 1b). These catchments receive 630 to 1140 mm of mean annual precipitation (*MAP*; Tab. 1) which is one to two times higher than in the southern KNP. In addition, the foothills of the Great Escarpment show a higher relief energy than most areas in the southern KNP (Fig. 1). Accordingly, natural erosion rates might be elevated in the westernmost areas of the *Lowveld*. However, the results suggest that *E* values (like *SSY* values) for areas outside the KNP are typically by an order of magnitude higher than inside. This huge difference clearly points to a significant acceleration of soil erosion outside the KNP (Wentzel, 2002; Wessels et al., 2007). More research is certainly required to assess the variability of *E* values in the *Lowveld* for areas that are under continued intensive land use.

6.2 Comparison of contemporary sediment yield and rates of erosion by water with long-term denudation rates inside the Kruger National Park

Contemporary rates of erosion by water in the Kruger National Park (KNP) can be also compared against long-term denudation rates (i.e., average rates of physical erosion and chemical weathering for time spans >10^4 years) that were determined by Chadwick et al. (2013) and Glotzbach et al. (2016). In both studies, long-term average denudation

rates (D_{Lt}) were derived from in-situ produced [10]Be concentrations in quartz-bearing river sediments. Glotzbach et al. (2016) analyzed samples collected close to the tributary inlets of ten reservoirs that were also investigated in this study. This permits a direct comparison of spatially averaged D_{Lt} values with minimum estimates for contemporary catchment-wide rates of erosion by water (E_{min}), mean area-specific sediment yield (SSY), and best estimates for contemporary catchment-wide average rates of erosion by water (E) (see chapter 5 for details). To facilitate the comparison, D_{Lt} values, expressed in 10^{-6} meters per year, were converted to tonnes per square kilometre and year, assuming a mean rock density of 2.7 g cm^{-3} (Glotzbach et al., 2016).

The resulting D_{Lt} values are low, ranging from 6 to 26 t km^{-2} yr^{-1} among the reservoir catchments (Tab. 2) with a mean (and median) of 13 ± 4 t km^{-2} yr^{-1} (14 [7, 15] t km^{-2} yr^{-1}). Geochemical analysis by Chadwick et al. (2013) suggests that chemical weathering contributes on average about 50% to D_{Lt} values in the southern KNP. Accordingly, long-term average rates of physical erosion (E_{Lt}) (e.g., by wind and water) are assumed to equal $\sim 0.5 \times D_{Lt}$. This leads to a mean (and median) E_{Lt} of ~ 7 t km^{-2} yr^{-1} (~ 7 t km^{-2} yr^{-1}). Figure 2 shows pairs of D_{Lt} values and contemporary values (E_{min}, SSY, and E) for individual reservoir catchments in the KNP. The 1:1 and 1:2 lines can be used as a reference to compare contemporary rates with D_{Lt} and E_{Lt}.
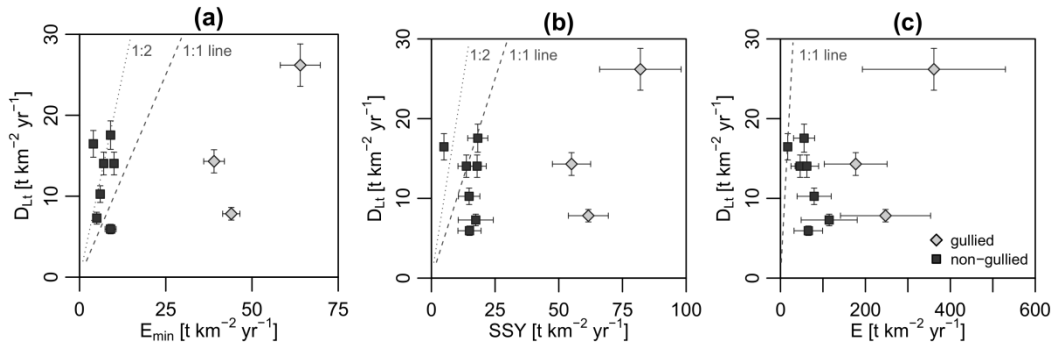
Fig. 2. Comparison between contemporary sediment yield and catchment-wide rates of erosion by water with spatially-averaged long-term denudation rates for reservoir catchments in the Kruger National Park. Long-term denudation rates (D_{Lt}) are compared against (a) contemporary minimum catchment-wide erosion rates by water (E_{min}), (b) contemporary area-specific sediment yield (SSY), and (c) best estimates for contemporary catchment-wide average erosion rates by water (E). D_{Lt} values are shown with uncertainty intervals of 10% (Glotzbach et al., 2016). Error bars of E_{min}, SSY and E values correspond to 95% confidence intervals. Dashed and dotted lines depict 1:1 and 1:2 ratios, respectively.

Tab. 2 Comparison of spatially averaged long-term average denudation rates (D_{Lt}) derived from in-situ produced cosmogenic [10]Be in river sediments (Chadwick et al., 2013; Glotzbach et al., 2016) and contemporary rates of erosion by water (this study) in the southern Kruger National Park (KNP).

Catchments	Long-term (>10^4 years) average rates			Contemporary (30 to 65 years) average rates		
	D_{Lt} [10^{-6} m yr^{-1}]	D_{Lt} [t km^{-2} yr^{-1}]	E_{Lt} [t km^{-2} yr^{-1}]	E_{min} [t km^{-2} yr^{-1}]	SSY [t km^{-2} yr^{-1}]	E [t km^{-2} yr^{-1}]
Reservoir catchments being recently affected by gully erosion for which D_{Lt} data is available (N = 3)[1)]						
Hartbeesfontein	5.3 ± 0.5	14 ± 1	~7	39 ± 3	55 ± 8	175 ± 75
Silolweni	2.9 ± 0.3	8 ± 1	~4	44 ± 3	62 ± 8	245 ± 105
Newu 1	9.7 ± 1.0	26 ± 3	~13	64 ± 6	80 ± 20	360 ± 170
Reservoir catchments without recent gully systems for which D_{Lt} data is available (N = 7)						
Lugmag	3.8 ± 0.4	10 ± 1	~5	6 ± 1	15 ± 4	80 ± 40
Mazithi	2.2 ± 0.2	6 ± 1	~3	9 ± 2	15 ± 5	65 ± 35
N'tswiriri	5.2 ± 0.5	14 ± 1	~7	7 ± 1	14 ± 3	45 ± 20
Jones-Se	5.2 ± 0.5	14 ± 1	~7	10 ± 1	18 ± 4	60 ± 30
N'wanetsana	6.5 ± 0.7	18 ± 2	~9	9 ± 1	18 ± 4	55 ± 25
Mlondozi	2.7 ± 0.3	7 ± 1	~4	5 ± 1	17 ± 7	115 ± 65
N'watimhiri	6.1 ± 0.6	16 ± 2	~8	4 ± 1	5 ± 1	15 ± 10
Mean	*5 ± 2*	*12 ± 4*	*~6*	*7 ± 2*	*14 ± 4*	*60 ± 25*
Median	*5 [2, 6]*	*14 [6, 15]*	*~7*	*7 [4, 9]*	*15 [5, 17]*	*60 [15, 65]*
All reservoir catchments for which D_{Lt} data is available (N = 10)						
Mean	*5 ± 2*	*13 ± 4*	*~7*	*20 ± 15*	*30 ± 20*	*120 ± 75*
Median	*5 [2, 6]*	*14 [7, 15]*	*~7*	*9 [5, 25]*	*20 [15, 55]*	*70 [50, 175]*
All study sites within the southern KNP (N = 32 for D_{Lt}, and N = 15 for E_{min}, SSY and E)						
Mean	*5 ± 1*	*12 ± 2*	*~6*	*20 ± 10*	*30 ± 10*	*120 ± 50*
Median	*5 [4, 5]*	*13 [10, 14]*	*~6*	*10 [5, 35]*	*20 [15, 50]*	*85 [55, 145]*

Note: long-term average denudation rate (D_{Lt}); long-term rate of physical erosion (E_{Lt}) based on the assumption of a chemical depletion fraction of ~0.5 for the southern KNP (Chadwick et al., 2013); minimum estimate for contemporary catchment-wide rates of erosion by water (E_{min}); contemporary mean area-specific sediment yield (SSY); best estimate for contemporary catchment-wide average rates of erosion by water (E). Following Glotzbach et al. (2016), an uncertainty of 10% was assumed for individual D_{Lt} values. Uncertainties of E_{min}, SSY and E values as well as uncertainties of mean and median values correspond to the 95% confidence level; 1) For gullied catchments, mean and median values are not reported as the small number of sites would induce considerable uncertainty, partly exceeding 100% at the 95% confidence level.

values, respectively. Catchments that were recently affected by gully erosion (N = 3) can be easily identified as outliers. For these catchments, *E_{min}*, *SSY* and *E* values are >2 (and >4), >3 (>6) and >12 (>24) times higher than *D_{Lt}* (and *E_{Lt}*) values, respectively. When the comparison is restricted to catchments without recent gully systems (N = 7), pairs of *E_{min}* and *D_{Lt}* values typically fall in between the 1:2 and 1:1 lines (Fig. 2a). Pairs of *SSY* and *D_{Lt}* values roughly follow the 1:1 line (Fig. 2b), while all *E* values except one (i.e., the N'watimhiri reservoir) are higher than *D_{Lt}* values (Fig. 2c). The mean and

median E value of non-gullied catchments exceeds the mean and median D_{Lt} (and E_{Lt}) value by a factor of >4 (>8). These results are in agreement with values that were derived from other sample locations in the southern KNP (Fig. 1c). Considering the mean and median for all sample locations, SSY and E values are >1.5 (and >3) and >6 (>14) times higher than D_{Lt} (and E_{Lt}) values, respectively.

In this comparison, the strongly differing temporal scales, for which average rates of denudation, erosion and sediment yield were assessed, must be kept in mind (e.g., van Blanckenburg, 2006). Differing long-term and contemporary erosion rates may be explained by above average erosion and sediment transport since the establishment of the oldest investigated reservoir in 1950 (Pienaar, 1985) which might be a stochastic effect. Variable average erosion rates on decadal scales may result from fluctuating rainfall amounts (Boardman et al., 2015). Records of mean annual precipitation (MAP) from the KNP since 1911 show alternating wet and dry spells of about five (MacFayden et al., in press) to ten years (Gertenbach, 1980) each that are possibly interlinked to the El Niño Southern Oscillation (MacFayden et al., in press) and other teleconnections (e.g., Tyson et al., 2002). At the same time, rainfall records provide no evidence for significantly different MAP values prior to and after the construction of the reservoirs (Baade et al., 2012). However, available rainfall records are too short to make precise projections on the statistical return period of high-magnitude rainfall-runoff events (e.g., Dalrymple, 1960, p. 64) that contribute substantially to erosion and sediment transport within the KNP (Heritage et al., 2014; see also chapter 4).

Low long-term average denudation rates within the study area imply a long exposure time (typically $\geq 10^5$ years) of minerals to cosmic rays (Glotzbach et al., 2016). Accordingly, denudation rates derived from cosmogenic nuclide concentrations are influenced by pre-Holocene environmental conditions. A coherent picture of environmental change in savanna biomes of southern Africa throughout the past glacial-interglacial cycles has not yet been achieved (Meadows and Quick, 2016). It is therefore unclear how well long-term average rates of denudation or physical erosion, derived from cosmogenic nuclides, reflect contemporary rates ($<10^2$ years) that would occur under pristine environmental conditions.

Contemporary erosion rates in catchments with recent gully systems are clearly higher than long-term average rates (Tab. 2), more so because [10]Be-derived values may be overrated for gullied catchments (see Glotzbach et al., 2016). Khomo and Rogers

(2005) highlighted that sodic patches, possibly associated with 'duplex soils' (i.e., solonetzes; Van Zijl et al., 2016), might play a key role in the formation of gullies within the KNP (see also chapter 5, section 4.6). Glotzbach et al. (2016, p. 318) considered gullies to reflect either a 'transient landscape response to climate change' or an 'anthropogenically induced' feature, possibly caused by an increased game number or an altered fire regime. Field observation suggest that the concentration of overland flow along management roads might partially promote gully formation. Disentangling the factors that recently led to gully erosion in the KNP would be of great interest for a sustainable management of environmental resources within the national park.

6.3 Comparison of contemporary sediment yield and erosion rates established in this study with values from other reservoir siltation studies in South Africa

Figure 3a provides an overview on the location of reservoirs within South Africa with catchments of a comparable size to those in the southern KNP (i.e., ≤ 100 km^2; N = 38) for which *SSY* and *E* values were determined (Rooseboom et al., 1992; Foster et al., 2008, 2012). Of the 23 sites located outside the KNP, twelve reservoirs are situated in a conservation estate (CE) that includes national parks, nature and biosphere reserves, and other protected environments (DEA, 2017). However, most of these reservoirs were constructed prior to the establishment of the respective CEs and some of the reservoir catchments encompass areas outside the protected zone. Hence, *SSY* values ascertained for these catchments often do not correspond to near-natural conditions.

In general, *SSY* values for reservoirs located inside CEs tend to be lower than for reservoirs outside CEs, whereby *SSY* values from the southern KNP are all lower than the overall mean *SSY* value of 140 ± 60 t km^{-2} yr^{-1} (Fig. 3b). Mean *SSY* values for catchments of reservoirs inside other CEs and outside CEs exceed the mean *SSY* value for the southern KNP by factors of four and ten, respectively (Fig. 3c). The same pattern, with lowest values for the KNP, higher values for other CEs, and highest values for areas outside CEs, applies to minimum, maximum and median *SSY* values (Tab. 3). The application of a Mann-Whitney U test (see chapter 3, section 2.6) elucidates that *SSY* values for the KNP differ significantly from *SSY* values outside CEs ($p_{MW} < 0.001$) and also from values inside CEs ($p_{MW} < 0.03$). Excluding the KNP, the difference between *SSY* values ascertained from reservoirs inside and outside CEs is barely

(a)

(b)

(c)

(d)

(e)
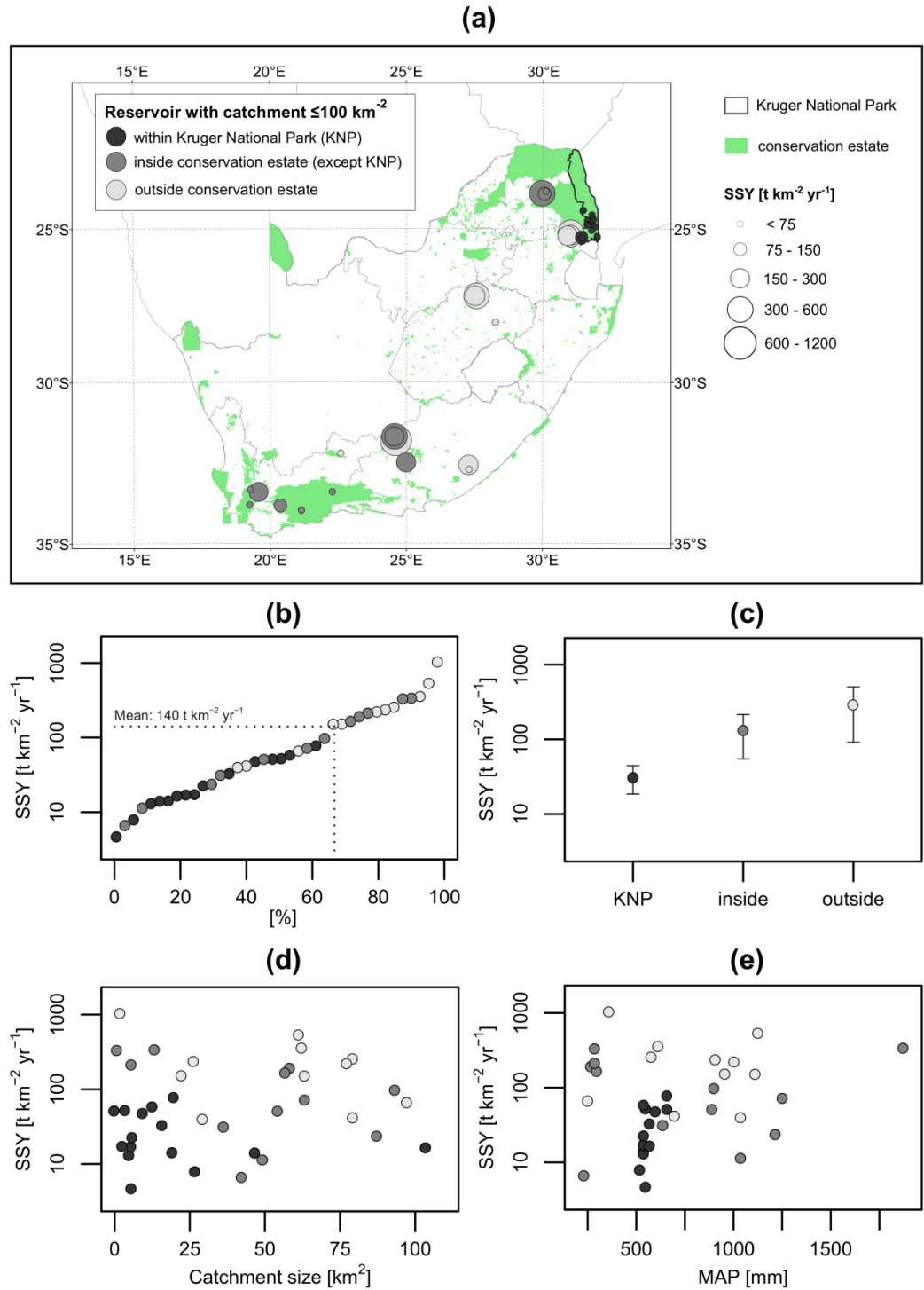
Fig. 3. Comparison of mean area-specific sediment yield (SSY) values for small catchments (≤100 km^2) of reservoirs located inside and outside conservation estates in South Africa and within the Kruger National Park: (a) overview map on the location of the reservoirs and current conservation estates (DEA, 2017); (b) cumulative distribution of SSY values (based on data from Rooseboom et al., 1992; Foster et al., 2008, 2012, and this study); (c) mean SSY values with 95% confidence intervals; (d) comparison between catchment size and SSY values; (e) comparison between mean annual precipitation (MAP; based on data from Pitman and Bailey, 2015) and SSY values.

Tab. 3 Mean area-specific sediment-yield (SSY) values and best estimates of catchment-wide average erosion by water (E) for reservoir catchments ≤100 km^2 located in the Kruger National Park (KNP), and inside and outside of conservation estates (CE; except KNP) within South Africa (based on boundaries of CEs according to DEA, 2017, and SSY data from Rooseboom et al., 1992, Foster et al., 2008, 2012, and this study).

		SSY [t km^{-2} yr^{-1}]				E [t km^{-2} yr^{-1}]			
	N	Min	Max	Mean	Median	Min	Max	Mean	Median
within KNP	15	5	80	30 ± 10	20 [15, 50]	15	360	120 ± 50	85 [55, 145]
inside CE[1)]	12	7	355	135 ± 80	90 [25, 200]	35	1500	600 ± 300	550 [150, 950]
outside CE	11	40	1100	300 ± 200	235 [45, 270]	200	3200	1400 ± 700	1200 [300, 1700]
All	*38*	*5*	*1100*	*140 ± 60*	*55 [35, 105]*	*15*	*3200*	*650 ± 250*	*250 [150, 650]*

Note: mean and median values are reported with 95% confidence intervals; 1) SSY values may not necessarily correspond to near-natural conditions, since CEs were often established after the construction of the reservoirs.

significant ($p_{MW} = 0.10$). At the same time, *SSY* values do not significantly correlate with catchment size (*A*; R = -0.06; p = 0.71) (Fig. 3d) and mean annual precipitation (*MAP*; R = 0.04; p = 0.79) (Fig. 3e).

Calculating mean and median *E* values as described in chapter 5 results in >4 and >11 times higher values for catchments of reservoirs inside recently established CEs and outside CEs, respectively, than for reservoir catchments within the southern KNP (Tab. 3). The mean (and median) *E* value for reservoir catchments outside CEs amounts to 1400 ± 700 t km^{-2} yr^{-1} (1200 [300, 1700] t km^{-2} yr^{-1}) and is in good agreement with the nation-wide average soil loss of 1260 t km^{-2} yr^{-1} (Le Roux et al., 2008; Msadala et al., 2012) predicted with a modified version of the Revised Universal Soil Loss Equation (RUSLE; Renard et al., 1991).

These results highlight that *SSY* and *E* values in the near-natural savanna landscape of the southern KNP are low compared to other areas in South Africa that are subject to a distinct human impact. Despite regional evidence for human-induced vegetation changes (Dean et al., 1995; MacPherson et al., in press) and accelerated soil erosion caused by pre-colonial pastoralists (Marker and Evers, 1976), the onset of widespread accelerated soil erosion in South Africa likely coincided with the expansion of colonial farming in the 19th century (e.g., Meadows and Asmal, 1996; Showers, 2010, 156f.; Reinwarth et al., 2013). Only little information is available regarding the magnitude by which natural erosion rates were accelerated. Compton et al. (2010) reconstructed a tenfold increase in the average sediment load of the Orange River in the late Holocene and attributed this to the man-made acceleration of soil erosion. This

study points to a similar human-induced intensification of soil erosion in areas located outside CEs in the northeast of South Africa (see section 6.1).

With respect to the catchment scale, data on contemporary erosion and sediment yield for near-natural conditions in South Africa against which results from this study could be compared is presently very scarce. In this regard, interesting insights may be gained from emerging data (DWS, 2017) obtained from recurrent reservoir siltation surveys. These data may facilitate decadal-scale assessments of *SSY* values and elucidate effects of soil protection measures and land use change outside CEs (e.g., Gebel et al., 2017), land rehabilitation and conservation inside CEs, as well as climate variability and change.

6.4 Comparison of contemporary rates of erosion by water within the Kruger National Park with previously published values for near-natural conditions and rates of tolerable soil loss in South Africa

Previous measurements that were carried out on experimental plots covered with grass and scrub (Haylett, 1960; Mathee, 1984, cit. in Hoffman and Ashwell, 2001, p. 85) or savanna vegetation (Venter, 1988) have pointed to contemporary rates of sheet and rill erosion of <75 t km^{-2} yr^{-1} for near-natural conditions in South Africa (see chapter 2.2). Excluding gullied catchments, *E* values in the southern KNP are ≤190 t km^{-2} yr^{-1} with a mean (and median) of 85 ± 30 t km^{-2} yr^{-1} (70 [45, 115] t km^{-2} yr^{-1}). Hence, catchment-specific *E* values are partly higher than values that were measured on experimental plots. Beside uncertainties related to the derivation of *E* values from reservoir siltation surveys and differing environmental conditions at the study sites, issues of scale are to be taken into consideration.

The approach of this study reveals average *E* values integrated over space and time, but does permit an assessment of spatially variable erosion rates on a scale comparable to plots (Worrall et al., 2014). At the same time, plot scale measurements may be a poor indicator for catchment-wide average erosion rates (Poesen, 2018), especially when localized sediment sources contribute substantially to the sediment flux in the catchment. With few exceptions (e.g., Haylett, 1960), plot scale studies in South Africa were undertaken for periods of <5 years. Modelling results for the southern KNP (see chapter 4) suggest that rainfall-runoff events with a return period >5 years contributed $\geq65\%$ to the overall fluvial sediment delivery over 30 to 65 years. Hence,

erosion rates likely vary by a factor of >10 among different 5 yr periods of observation. Bearing in mind these considerations, previous data on erosion rates under near-natural conditions for South Africa appear to be in accordance with results from this study.

Long-term average rates of soil formation in South Africa amount to about 10 t km^{-2} yr^{-1} (Huntley et al., 1989, cit in. Kassier and Groenewald, 1992, p. 87; Decker et al., 2011). Although rates of soil formation tend to increase with a decreasing soil thickness (Stockmann et al., 2014), a soil loss of ≥1000 t km^{-2} yr^{-1} (Russell, 1983, cit in Scott et al., 1998, p. 57; Pretorius and Cooks, 1989) is by an order of magnitude too high, if a sustainable use of soil resources in South Africa is aspired. For this, an average soil loss of <500 t km^{-2} yr^{-1} (Le Roux and Smith, 2014), and possibly distinctively less than this, is required. Interpreting E values for catchments within the southern KNP that are not affected by gully erosion as benchmarks for tolerable rates of soil loss in the *Lowveld* leads to a soil conservation management goal of ≤190 t km^{-2} yr^{-1}.

6.5 Conclusions

This study provides mean contemporary area-specific sediment yield (*SSY*) values and best estimates for catchment-wide average rates of erosion by water (*E*) for the near-natural savanna environment of the southern Kruger National Park (KNP). *SSY* and *E* values were determined by means of high-resolution reservoir siltation surveys for 15 reservoir catchments, varying in size from <1 km^2 to about 100 km^2, and observation periods of 30 to 65 years. Following Baade et al. (2012), reservoir deposits (i.e., the post-dam facies) could be distinguished from soils and sediments belonging to pre-dam facies based on colour and grain size. This field-based differentiation was verified by the physicochemical characterization of 250 samples from both facies and statistical analysis via stepwise discriminant function analysis (DFA) and regularized logistic regression (RLR). The mean relative uncertainty in the determination of the volume (*V$_S$*) and dry bulk density (*dBD*) of reservoir deposits, expressed at the 95% confidence level (*Cl95*), amounts to 7% and 8%, respectively. Together, this corresponds to a mean fractional contribution of <30% and <6% to uncertainties of *SSY* and *E* values, respectively. Hence, field and laboratory measurements are a minor source of uncertainty in this study.

Best estimates for the trap efficiency (*TE*) range from 25% to >90% among the investigated reservoirs. This is in agreement with *TE* values derived from the equation by Brown (1944). Other empirical relationships, established mainly in temperate climate regions (e.g., Heinemann, 1981), overestimate the *TE* of reservoirs in the KNP. The mean relative uncertainty in the *TE* estimation amounts to ±16% (*Cl95*). This results in a mean fractional uncertainty contribution of 64% with respect to *SSY* values. Uncertainties of *E* values arise mainly from the *SDR* estimation. The mean relative uncertainty of *SDR* values amounts to ±40% (*Cl95*) and contributes 79% to the uncertainty of *E* values. The overall mean relative uncertainty for *SSY* and *E* values amounts to ±21% and ±46% (*Cl95*), respectively.

SSY values determined in this study range from 5 to 80 t km^{-2} yr^{-1} (N = 15) and are in accordance with *SSY* values of 10 to 60 t km^{-2} yr^{-1} (N = 5) ascertained in the reconnaissance survey (Baade et al., 2012). *SSY* values correlate highly significantly with mean annual precipitation (*MAP*; R = 0.71; p < 0.01) and weakly significantly with mean slope inclination (*Slope*; R = 0.45; p < 0.10), whereby *MAP* and *Slope* covary (R = 0.58; p < 0.03). *E* values of non-gullied catchments range from 15 to 190 t km^{-2} yr^{-1} with a mean (and median) of 85 ± 30 t km^{-2} yr^{-1} (70 [45, 115] t km^{-2} yr^{-1}). Gullied catchments (N = 3) show elevated *E* values of up to 360 t km^{-2} yr^{-1}. *SSY* and *E* values of gullied catchments are still low compared to catchments outside the KNP. It cannot be decided, with the available data, whether contemporary gully erosion in the KNP is primarily driven by natural factors (e.g., climate or soil properties) or due to human impact (e.g., management roads, altered fire regime). *SSY* and *E* values appear to be highly variable on sub-decadal to decadal timescales considering that modelling results indicate a ≥65% contribution to the overall sediment delivery by a few (N ≤ 6) high-discharge events at all study sites.

Mean *SSY* and *E* values within the KNP are by an order of magnitude lower than *SSY* and *E* values from reservoir catchments located at the western boundary of the *Lowveld* (Rooseboom et al., 1992). Small catchments (≤100 km^2) of reservoirs in other regions of South Africa located outside conservation estates likewise show >10 times higher *SSY* and *E* values (ibid.; Foster et al., 2008, 2012) than reservoir catchments in the KNP. This difference can be attributed to low erosion rates in the near-natural savanna environment of the southern KNP (Baade et al., 2012) as compared to other areas where past and present anthropogenic influences such as farming activities, crop

cultivation, and other forms of land use, led to accelerated soil erosion (e.g., Boardman et al., 2012).

Results from this study are in accordance with previously published erosion rates for near-natural conditions in South Africa (see chapter 2.2) when spatially differing environmental conditions and issues of scale (i.e., spatial and temporal) are taken into account. At the same time, mean and median E values determined in this study are >4 times higher than spatially averaged long-term denudation rates (D_{Lt}) for the same catchments (Glotzbach et al., 2016). D_{Lt} values within in the KNP are, in turn, comparable to D_{Lt} values in other regions of South Africa (see chapter 2.3). Soil formation rates are possibly similar to D_{Lt} values (Huntley et al., 1989, cit. in. Kassier and Groenewald, 1992, p. 87; Decker et al., 2011) and probably not higher than E values of non-gullied catchments within the southern KNP (Stockmann et al., 2014). Thus, tolerable rates of soil loss for a sustainable use of soil resources in the *Lowveld* are ≤ 190 t km^{-2} yr^{-1}.

6.6 Open research questions and potential future research directions

This study will hopefully stimulate further research as there is a number of open questions that remain unanswered. The approach that was pursued in this study permits the assessment of spatially averaged rates of sediment yield and erosion by water. It does not allow to quantify relative contributions from localized sediment sources in the catchments. A sediment source tracing study (cf. Walling, 2013), currently undertaken at Rhodes University, Grahamstown (South Africa), might become an important step towards the assessment of erosion rates on the sub-catchment scale. Preliminary results suggest that soils originating from different lithologies can be distinguished in selected catchments using composite fingerprints consisting of magnetic (Miller, pers. comm.[1]) and geochemical properties.

A mapping of sediment sources and sinks in the catchment based on field observations and remote sensing products (e.g., high-resolution aerial imagery and digital elevation models) would help to explore sediment transport paths within the catchments (Wohl et al., 2017). Combining this information with a modelling approach (e.g., Lu et al., 2006) might reduce uncertainties regarding the estimation of sediment

---

[1] Unpublished preliminary research report by Jordan K. Miller (Rhodes University, Grahamstown) submitted to SANParks in April 2017.

delivery ratios (*SDR*). The granulometric characterization and quantification of sediments that are intermediately stored in reservoir catchments (e.g., Fuchs et al., 2011) as well as the determination of typical timescales of sediment storage (e.g., Heritage et al., 2014) might help to set-up and validate such a model. Uncertainties in the reservoir trap efficiency (*TE*) estimation can be reduced, if uncertainties in the hydrological modelling are diminished. A reduction of uncertainties is feasible on the basis of a more detailed geo-hydrological characterization of the reservoir catchments (van Zijl et al., 2016), on-site monitoring of rainfall, runoff (Riddell et al., 2014) and fluvial sediment transport, as well as the recording of water level fluctuations in reservoirs.

At the moment, it is not possible to empirically validate modelling results on the temporal variability of erosion and sediment delivery within the catchments. The reconstruction of the sediment accumulation for individual past flood events by stratigraphic analysis of reservoir deposits (e.g., Bussi et al., 2013) is likely problematic within the Kruger National Park (KNP) given intensive bioturbation caused by large mammals (e.g., hippopotamus and elephants). However, the increase in the mass of reservoir deposits after future flood events may be ascertained by repeated high-resolution surveys of reservoir basins (e.g., Rodriguez-Lloveras et al., 2015).

Furthermore, it is currently unclear whether gully erosion in the KNP is due to human impact or natural drivers (Glotzbach et al., 2016). Disentangling factors that govern gully erosion in the KNP would be of great interest in the context of previous studies which highlighted that gully erosion in South Africa may not necessarily reflect human impact (Botha et al., 1994; Lyons et al., 2013). It seems that little information is available regarding the evolution of gully systems in the KNP over time. Mapping gullies might provide information about their spatial proximity to management roads and help to elucidate the role of the fire regime and vegetation cover. A characterization of soils at places where gullies were formed might clarify a potential nexus between gully formation, sodic patches (Khomo and Rogers, 2005) and duplex soils (e.g., Van Zijl et al., 2013). Monitoring the retreat of gully heads would help to quantify the contribution of sub-surface material to the overall sediment delivery. This would be a valuable information to reduce uncertainties in the assessment of long-term average denudation rates based on cosmogenic nuclide concentrations in river sediments (cf. Glotzbach et al., 2016).

Except for a single study site in the northern KNP where cosmogenic nuclide concentrations in river sediments were determined (Chadwick et al., 2013), data on erosion rates in the KNP is only available for its southern part. There is a strong rainfall gradient from the southern KNP (mean annual precipitation, *MAP*, of 500 to 700 mm) towards the north (*MAP* of 300 to 500 mm) (MacFayden et al., in press). Given the observed correlation between mean area-specific sediment yield (*SSY*) and *MAP*, it would be interesting to extend the dataset by surveying reservoirs in the northern KNP. At the same time, it would be helpful to study areas outside the KNP, as it appears that rates of contemporary erosion and sediment yield for parts of the *Lowveld* that are under intensive land use are not yet well established.

Although the comparison of contemporary and long-term average erosion rates is not without problems (due to strongly differing timescales and the quantification of chemical weathering; cf. Riebe et al., 2003), the combined approach opens up interesting perspectives. By extending the combined analysis to other near-natural environments, it might be possible to approach the long-held research question (e.g., Murgatroyd, 1979) whether rates of denudation and soil formation under near-natural conditions in South Africa are in an approximately steady-state, or if the thickness of the soil mantle fluctuates over time as a response to climate change (e.g., within the course of glacial-interglacial cycles). Answering this question would be of great relevance as it would help to further constrain tolerable rates of soil loss permitting the conservation of soil resources in South Africa.

References

Baade, J., Franz, S., Reichel, A., 2012. Reservoir siltation and sediment yield in the Kruger National Park, South Africa: a first assessment. Land Degradation and Development 23 (6), 586-600. DOI: 10.1002/ldr.2173.

Boardman, J., Hoffman, M.T., Holmes, P.J., Wiggs, G.F.S., 2012. Soil erosion and land degradation. In: Holmes, P., Meadows, M. (Eds.). Southern African Geomorphology. Recent Trends and New Directions. Sun Press: Bloemfontein, South Africa, pp. 307-328.

Boardman, J., Favis-Mortlock, D., Foster, I., 2015. A 13-year record of erosion on badland sites in the Karoo, South Africa. Earth Surface Processes and Landforms 40 (14), 1964-1981. DOI: 10.1002/esp.3775.

Botha, G.A., Wintle, A.G., Vogel, J.C., 1994. Episodic late Quaternary palaeogully erosion in northern KwaZulu-Natal, South Africa. Catena 23, 327-340. DOI: 10.1016/0341-8162(94)90076-0.

Brown, C.B., 1944. Discussion of 'Sedimentation in Reservoirs' by B. J. Witzig. Transactions of the American Society of Civil Engineers 109, 1080-1086.

Bussi, G., Rodríguez-Lloveras, X, Francés, F., Benito, G., Sánchez-Moya, Y., Sopeña, A., 2013. Sediment yield model implementation based on check dam infill stratigraphy in a semiarid Mediterranean catchment. Hydrology and Earth System Sciences 17, 3339-3354. DOI: 10.5194/hess-17-3339-2013.

Chadwick, O.A., Roering, J.J., Heimsath, A.M., Levick, S.R., Asner, G.P., Khomo, L., 2013. Shaping post-orogenic landscapes by climate and chemical weathering. Geology 41 (11), 1171-1174. DOI: 10.1130/G34721.1.

Compton, J.S., Herbert, C.T., Hoffman, M.T., Schneider, R.R., Stuut, J.-B., 2010. A tenfold increase in the Orange River mean Holocene mud flux: implications for soil erosion in South Africa. The Holocene 20 (1), 115-122. DOI: 10.1177/0959683609348860.

Dalrymple, T., 1960. Flood-frequency analyses. Manual of Hydrology: Part 3. Flood-Flow Techniques. Geological Survey Water-Supply Paper 1543-A. Methods and practices of the Geological Survey. United States Government Printing Office: Washington D.C., USA, 80 pp.

DEA, 2017. SA Conservation Areas Data. Directorate Enterprise Geospatial Information Management, Department of Environmental Affairs (DEA): Pretoria, South Africa. <https://egis.environment.gov.za/data_egis/node/109> accessed 16 January 2018 (last modified: 10 October 2017).

Dean, W.R.J., Hoffman, M.T., Meadows, M.E., Milton, S.J., 1995. Desertification in the semi-arid Karoo, South Africa: review and reassessment. Journal of Arid Environments 30 (3), 247-264. DOI: 10.1016/S0140-1963(05)80001-1.

Decker, J.E., Niedermann, S., de Wit, M.J., 2011. Soil erosion rates in South Africa compared with cosmogenic ^{3}He-based rates of soil production. South African Journal of Geology 114 (3-4), 475-488. DOI: 10.2113/gssajg.114.3-4.475.

DWS (Department of Water and Sanitation), 2017. Water Management Areas. Reservoir sites. <https://www.dwa.gov.za/Hydrology/Verified/dwafapp2_wma/WMA01_LIMPOPO_RE SERVOIR%20SITES.doc> accessed 2 September 2017 (last modified: 28 August 2017).

Foster, I.D.L., Boardman, J., Gates, J.B., 2008. Reconstructing historical sediment yields from the infilling of farm reservoirs, Eastern Cape, South Africa. In: Schmidt, J., Cochrane, T., Phillips, C., Elliott, S., Davies, T., Basher, L. (Eds.). Sediment Dynamics in Changing Environments (Proceedings of a symposium held in Christchurch, New Zealand, December 2008). IAHS Publications 325. International Association of Hydrological Sciences (IAHS) Press: Wallingford, United Kingdom, pp. 440-447.

Foster, I.D.L., Rowntree, K.M., Boardman, J., Mighall, T.M., 2012. Changing sediment yield and sediment dynamics in the Karoo uplands, South Africa; post-European impacts. Land Degradation and Development 23 (6), 508-522. DOI: 10.1002/ldr.2180.

Fuchs, M., Will, M., Kunert, E., Kreutzer, S., Fischer, M., Reverman, R., 2011. The temporal and spatial quantification of Holocene sediment dynamics in a meso-scale catchment in

northern Bavaria, Germany. The Holocene 21 (7), 1093-1104. DOI: 10.1177/0959683611400459.

Gebel, M., Bürger, S., Wallace, M., Malherbe, H., Vogt, H., Lorz, C., 2017. Simulation of land use impacts on sediment and nutrient transfer in coastal areas of Western Cape, South Africa. Change Adaptation in Socio-Ecological Systems 3 (1), 1-17. DOI: 10.1515/cass-2017-0001.

Gertenbach, W.P.D., 1980. Rainfall patterns in the Kruger National Park. Koedoe 23 (1), 35-43. DOI: 10.4102/koedoe.v23i1.634.

Glotzbach, C., Paape, A., Baade, J., Reinwarth, B., Rowntree, K., Miller, J., 2016. Cenozoic landscape evolution of the Kruger National Park as derived from cosmogenic nuclide analyses. Terra Nova 28 (5), 316-322. DOI: 10.1111/ter.12223.

Haylett, D.G., 1960. Run-off and soil erosion studies at Pretoria. South African Journal of Agricultural Science 3 (3), 379-394.

Heinemann, H.G., 1981. A new sediment trap efficiency curve for small reservoirs. Journal of the American Water Resources Association 17 (5), 825-830. DOI: 10.1111/j.1752-1688.1981.tb01304.x.

Heritage, G., Tooth, S., Entwistle, N., Milan, D., 2014. Long-term flood controls on semi-arid river form: evidence from the Sabie and Olifants rivers, eastern South Africa. In: Xu, Y.J., Allison, M.A., Bentley, S.J., Collins, A.L., Erskine, W.D., Golosov, V., Horowitz, A.J., Stone, M. (Eds.). Sediment dynamics from the summit to the sea. IAHS Publication 367. International Association of Hydrological Sciences (IAHS) Press: Wallingford, United Kingdom, pp. 141-146. DOI: 10.5194/piahs-367-141-2015.

Hoffman, T., Ashwell, A., 2001. Nature divided. Land degradation in South Africa. University of Cape Town Press: Lansdowne, Cape Town, South Africa, 168 pp.

Huntley, B., Siegfried, R., Sunter, C., 1989. South African environments into the 21st century. Human & Rousseau: Cape Town, South Africa, 127 pp.

Kassier, W.E., Groenewald, J.A., 1992. The agricultural economy of South Africa. In: Csáki, C., Dams, T., Metzger, D., van Zyl, J. (Eds.). Agricultural restructuring in southern Africa. Papers presented at an International Symposium held at Swakopmund, Namibia, 24-27 July 1990. Association of Agricultural Economists of Namibia (AGRECONA): Windhoek, Namibia, pp. 84-100.

Khomo, L.M., Rogers, K.H., 2005. Proposed mechanisms for the origin of sodic patches in Kruger National Park, South Africa. African Journal of Ecology 43, 29-34. DOI: 10.1111/j.1365-2028.2004.00532.x.

Le Roux, J.J., Smith, H., 2014. Soil erosion in South Africa – its nature and distribution. <http://www.grainsa.co.za/soil-erosion-in-south-africa---its-nature-and-distribution> accessed 19 August 2017 (last modified: 2014-11-01).

Le Roux, J.J., Morgenthal, T.L., Malherbe, J., Pretorius, D.J., Sumner, P.D., 2008. Water erosion prediction at a national scale for South Africa. Water SA 34 (3), 305-314.

Lu, H., Moran, C.J., Prosser, I.P., 2006. Modelling sediment delivery ratio over the Murray Darling Basin. Environmental Modelling & Software 21 (9), 1297-1308. DOI: 10.1016/j.envsoft.2005.04.021.

Lyons, R., Tooth, S., Duller, G.A.T., 2013. Chronology and controls of donga (gully) formation in the upper Blood River catchment, KwaZulu-Natal, South Africa: evidence for a climatic driver of erosion. The Holocene 23 (12), 1875-1887. DOI: 10.1177/0959683613508157.

MacFayden, S., Zambatis, N., Van Teeffelen, A.J.A., Hui, C., in press. Long-term rainfall regression surfaces for the Kruger National Park, South Africa: a spatio-temporal review of patterns from 1981 to 2015. International Journal of Climatology. DOI: 10.1002/joc.5394.

MacPherson, A.J., Gillson, L., Hoffman, M.T., in press. Climatic buffering and anthropogenic degradation of a Mediterranean-type shrubland refugium at its semi-arid boundary, South Africa. The Holocene. DOI: 10.1177/0959683617735582.

Marker, M.E., Evers, T.M., 1976. Iron age settlement and soil erosion in the Eastern Transvaal, South Africa. The South African Archaeological Bulletin 31 (123/124), 153-165. DOI: 10.2307/3887737.

Mathee, J.F. la G., 1984. A primer on soil conservation. National Department of Agriculture: Pretoria, South Africa, 128 pp.

Meadows, M.E., Asmal, O., 1996. Chronology, sedimentology and geochemistry at Verlorenvlei (Western Cape Province, South Africa) as evidence of anthropogenically-induced land degradation. Zeitschrift für Geomorphologie N.F. 107 (Suppl.), 45-62.

Meadows, M.E., Quick, L.J., 2016. Terrestrial ecosystem changes in the late Quaternary. In: Knight, J., Grab, S.W. (Eds.). Quaternary environmental change in southern Africa. Physical and human dimensions. Cambridge University Press: Cambridge, United Kingdom, pp. 269-283. DOI: 10.1017/CBO9781107295483.017.

Msadala, V., Gibson, L., Le Roux, J., Rooseboom, A., Basson, G.R., 2012. Sediment yield prediction for South Africa: 2010 edition. WRC Report No. 1765/1/10. Water Research Commission (WRC): Pretoria, South Africa, 250 pp.

Murgatroyd, A.L., 1979. Geologically normal and accelerated rates of erosion in Natal. South African Journal of Science 75, 395-396.

Partridge, T.C., Dollar, E.S.J., Moolman, J., Dollar, L.H., 2010. The geomorphic provinces of South Africa, Lesotho and Swaziland: a physiographic subdivision for earth and environmental scientists. Transactions of the Royal Society of South Africa 65 (1), 1-47. DOI: 10.1080/00359191003652033.

Pienaar, U.d.V., 1985. Indications of progressive desiccation of the Transvaal Lowveld over the past 100 years, and implications for the water stabilization programme in the Kruger National Park. Koedoe 28, 93-165. DOI: 10.4102/koedoe.v28i1.540.

Pitman, B., Bailey, A., 2015. A wealth of new freely downloadable information on the water resources of South Africa, Swaziland and Lesotho. Journal of the South African Institution of Civil Engineers 23 (5), 13-18.

Pretorius, J.R., Cooks, J., 1989. Soil loss tolerance limits: an environmental management tool. GeoJournal 19 (1), 67-75.

Poesen, J., 2018. Soil erosion in the Anthropocene: research needs. Earth Surface Processes and Landforms 43 (1), 64-84. DOI: 10.1002/esp.4250.

Reinwarth, B., Franz, S., Baade, J., Haberzettl, T., Kasper, T., Daut, G., Helmschrot, J., Kirsten, K.L., Quick, L.J., Meadows, M.E., Mäusbacher, R., 2013. A 700-year record on the effects of climate and human impact on the southern Cape coast inferred from lake sediments of Eilandvlei, Wilderness Embayment, South Africa. Geografiska Annaler, Series A, Physical Geography 95, 345-360. DOI: 10.1111/geoa.12015.

Renard, K.G., Foster, G.R., Weesies, G.A., Porter, J.P., 1991. RUSLE. Revised universal loss equation. Journal of Soil and Water Conservation 46 (1), 30-33.

Riddell, E.S., Nel, J., Fundisi, D., Jumbi, F., van Niekerk, A., Lorentz, S.A., 2014. Ephemeral Hydrological Processes in Savannas. WRC Report No. TT 619/14. Water Research Commission (WRC): Gezina, Pretoria, South Africa, 231 pp.

Riebe, C.S., Kirchner, J.W., Finkel, R.C., 2003. Long-term rates of chemical weathering and physical erosion from cosmogenic nuclides and geochemical mass balance. Geochimica et Cosmochimica Acta 67 (22), 4411-4427. DOI: 10.1016/S0016-7037(03)00382-X.

Rodriguez-Lloveras, X., Bussi, G., Francés, F., Rodriguez-Caballero, E., Solé-Benet, A., Calle, M., Benito, G., 2015. Patterns of runoff and sediment production in response to land-use changes in an ungauged Mediterranean catchment. Journal of Hydrology 531 (3), 1054-1066. DOI: 10.1016/j.jhydrol.2015.11.014.

Rooseboom, A., Verster, E., Zietsman, H.L., Lotriet, H.H., 1992. The development of the new sediment yield map of southern Africa. WRC Report No. 297/2/92. Water Research Commission (WRC): Pretoria, South Africa, 117 pp.

Russell, W.B., 1983. Conservation of arable land in the USA: report on service tour, unpublished report. Department of Agriculture and Fisheries, Natal Region: Cedara, South Africa.

Scott, D.F., Versfeld, D.B., Lesch, W., 1998. Erosion and sediment yield in relation to afforestation and fire in the mountains of the Western Cape Province, South Africa. South African Geographical Journal 80 (1): 52-59. DOI: 10.1080/03736245.1998.9713644.

Showers, K.B., 2010. A history of African soil: perceptions, use and abuse. In: McNeill, J.R., Winiwarter, V. (Eds.). Soils and societies: perspectives from environmental history. White Horse Press: Isle of Harris, United Kingdom, pp. 118-176.

Stockmann, U., Minasny, B., McBratney, A.B., 2014. How fast does soil grow? Geoderma 216, 48-61. DOI: 10.1016/j.geoderma.2013.10.007.

Tyson P.D., Cooper, G.R.J., McCarthy, T.S., 2002. Millennial to multi-decadal variability in the climate of southern Africa. International Journal of Climatology 22 (9), 1105-1117. DOI: 10.1002/joc.787.

USGS EROS, 2015. Shuttle Radar Topography Mission (SRTM) 1 Arc-Second Global. United States Geological Survey's (USGS) Earth Resources Observation and Science (EROS) Center: Sioux Falls, South Dakota, USA. <https://lta.cr.usgs.gov/SRTM1Arc> accessed 21 March 2016 (last modified: January 2015).

van Zijl, G.M., Ellis, F., Rozanov, D.A., 2013. Emphasising the soil factor in geomorphological studies of gully erosion: a case study in Maphutseng, Lesotho. Soil African Geographical Journal 95 (2), 205-216. DOI: 10.1080/03736245.2013.847803.

van Zijl, G.M., Van Tol, J.J., Riddell, E.S., 2016. Digital soil mapping for hydrological modelling. In: Zhang, G.-L., Brus, D., Liu, F., Song, X.-D., Lagacherie, P. (Eds.). Digital soil mapping across paradigms, scales and boundaries. Springer Environmental Science and Engineering. Springer: Singapore, pp. 115-129. DOI: 10.1007/978-981-10-0415-5_10.

Venter, J., 1988. Soil loss and run-off in Umfolozi Game Reserve and the implications for game reserve management. Volume 1. PhD Thesis. Department of Grassland Science, Faculty of Agriculture, University of Natal: Pietermaritzburg, South Africa, 192 pp.

von Blanckenburg, F., 2006. The control mechanisms of erosion and weathering at basin scale from cosmogenic nuclides in river sediment. Earth and Planetary Science Letters 242 (3-4), 224-239. DOI: 10.1016/j.epsl.2005.11.017.

Walling, D.E., 2013. The evolution of sediment source fingerprinting investigations in fluvial systems. Journal of Soils and Sediments 13, 1658-1675. DOI: 10.1007/s11368-013-0767-2.

Wentzel, K., 2002. Determination of the overall soil erosion potential in the Nsikazi District (Mpumalanga Province, South Africa) using remote sensing and GIS. Canadian Journal of Remote Sensing 28 (2), 322-327. DOI: 10.5589/m02-013.

Wessels, K.J., Prince, S.D., Malherbe, J., Small, J., Frost, P.E., Van Zyl, D., 2007. Can human-induced land degradation be distinguished from the effects of rainfall variability? A case study in South Africa. Journal of Arid Environments 68, 271-297. DOI: 10.1016/j.jaridenv.2006.05.015.

Wohl, E., Magilligan, F.J., Rathburn, S.L., 2017. Introduction to the special issue: Connectivity in Geomorphology. Geomorphology 277, 1-5. DOI: 10.1016/j.geomorph.2016.11.005.

Worrall, F., Burt, T.P., Howden, N.J.K., Hancock, G.R., 2014. Variation in suspended sediment yield across the UK – a failure of the concept and interpretation of the sediment delivery ratio. Journal of Hydrology 519, Part B, 1985-1996. DOI: 10.1016/j.jhydrol.2014.09.066.

Appendix A

Supplementary Material to Chapter 3

Reinwarth et al.: Applying regularized logistic regression (RLR) for the discrimination of sediment facies in reservoirs based on composite fingerprints. Journal of Soils and Sediments.

Electronic Supplementary Material (Online Resource 2)

1 Introduction

In the following, the generation of synthetic dataset compilations that were used within the framework of Monte-Carlo simulations is described in detail. Three compilations containing 1000 synthetic datasets with 200 samples each were created. The first compilation contains datasets that resemble the statistical distribution of empirical data (eight sediment properties) characterizing the pre- and post-dam facies (i.e. two groups of samples). A sampling bias was simulated to examine uncertainties in variable selection and classification results arising from the limited number of samples in the empirical dataset. The second and third compilations contain datasets with differing statistical distributions that were generated based on Gaussian Density Functions (GDFs) and equal within-group covariance matrices (eCov). Datasets in the second and third compilation contain data from 8 and 15 sediment properties for two (i.e the binomial case) and five groups (i.e. the multinomial case) of samples, respectively. In each dataset 50 % of the samples from each group were included in the training set, while another 50 % were retained for validation. In binomial datasets of the first and second compilation the group-specific proportion of samples was varied randomly between 20 % and 80 %. This range includes the case of the empirical dataset (23 % samples from the pre-dam facies), while the rather comprehensive number of samples reveals a solid basis for training and validation (Brown and Tinsley 1983). In the third compilation with multinomial datasets, group-specific proportions were allowed to range randomly between 10 % to 30 %.

2 First compilation: synthetic datasets based on kernel density estimates

Datasets of the first compilation were generated based on kernel density estimates (KDEs) that were obtained from the empirical dataset using the software R (vers. 3.1.1; R Core Team 2014). KDEs were compiled separately for the pre- and post-dam facies and all investigated sediment characteristics. For each synthetic dataset, KDEs were calculated from an individual empirical data subset containing 4 and 29 samples from the pre- and post-dam facies of each reservoir, respectively. Subsets were generated via stratified random sampling (see section 2.5). Kernel density estimation was performed with Gaussian kernels and the normal reference distribution smoothing bandwidth ("nrd0") recommended by Silverman (1986, p. 48). KDEs were subsequently modified to simulate a potential sampling bias. Expectancy values (i.e. expected mean values of sample populations randomly drawn from KDEs) were allowed to vary randomly within two-tailed Cl95 intervals of mean values derived from the corresponding empirical data subset (Kraushaar et al. 2015). Coefficients of variation represented in KDEs were left unchanged. Sediment properties characterizing synthetic samples were generated by randomly drawing values from the modified KDEs. In the event of irrational sediment characteristics (negative values for P_{CAL} content, Clay&Silt$_\%$, Skeleton$_\%$, LSort, PSD$_{Dist}$ and DIP) the corresponding quantities were set to zero. Likewise, LUM was

Corresponding author: Bastian Reinwarth (bastian.reinwarth@uni-jena.de)

ensured to range between 0 and 255 and Skeleton$_\%$ was reduced accordingly, if the sum of Clay&Silt$_\%$ and Skeleton$_\%$ exceeded 100 %.

3 Second compilation: binomial synthetic datasets fulfilling multivariate normality and equal within-group covariance matrices

Datasets of the second compilation were created based on randomly generated Gaussian density functions (GDFs) and random correlation matrices. Random GDFs characterizing the value distribution of specific sediment properties in each group were generated following Sheriff et al. (2015). Random expectancy values of sediment properties were allowed to differ at maximum by a factor of 10 between the groups, while coefficients of variation determining the standard deviation of GDFs were randomly varied between 8 % and 73 %. Random 8×8 correlation matrices M_{corr} (i.e. positive definite matrices with one row and one column for each sediment property and unit diagonal) were compiled using the 'nearPD' algorithm (Higham 2002) which is implemented in the R software package 'Matrix' (Bates and Mächler 2016). Afterwards, synthetic datasets were generated following the procedure suggested by Mateo-Sanz et al. (2004). The Cholesky decomposition L_M of M_{corr} was compiled (i.e. a lower triangular matrix fulfilling $M_{corr} = L_M \, L_M^T$, where L_M^T is the transpose of L_M) and multiplied with a 8×200 matrix (8 sediment properties and 200 synthetic samples) containing numbers that were randomly drawn from the standard normal distribution. The resulting matrix consists of 8 columns (representing synthetic sediment properties) with 200 entries each (representing synthetic samples). These entries were multiplied with the standard deviation of the corresponding group-specific GDF. Afterwards, the associated mean value of the GDF was added. The resulting dataset is characterized by (approximately) normally distributed sediment properties in each group and a (nearly) equal within-group covariance (eCov) structure that is prescribed by M_{corr} (Mateo-Sanz et al. 2004). Synthetic datasets for which variable selection via stepwise DFA failed due to variable co-linearity (cf. Hill and Lewicki 2006) were replaced.

4 Third compilation: multinomial synthetic datasets fulfilling multivariate normality and equal within-group covariance matrices

Datasets of the third compilation were generated by following the workflow that was used to create datasets for the second compilation. In order to compile datasets with five groups and 15 sediment properties, five random GDFs were created for each sediment property. Random 15×15 correlation matrices were compiled. The corresponding Cholesky decompositions were multiplied with 15×200 matrices containing numbers that were randomly drawn from the standard normal distribution. All remaining calculations were performed analogously to the binomial case.

References

Bates D, Mächler M (2016) Matrix: Sparse and dense matrix classes and methods. R package version 1.2-6. http://cran.r-project.org/package=Matrix. Accessed 21 July 2016

Brown MT, Tinsley HEA (1983) Discriminant Analysis. J Leisure Res 15:290-310

Higham NJ (2002) Computing the nearest correlation matrix – a problem from finance. IMA J Numer Anal 22:329-343. doi: 10.1093/imanum/22.3.329

Hill T, Lewicki P (2006) Statistics. Methods and applications. A comprehensive reference for science, industry and data mining. StatSoft, Tulsa, 833 pp

Kraushaar S, Schumann T, Ollesch G, Schubert M, Vogel H-J, Siebert C (2015) Sediment fingerprinting in northern Jordan: element-correction factors in a carbonatic setting. J Soils Sediments 15:2155-2173. doi: 10.1007/s11368-015-1179-2

R Core Team (2014) R: a language and environment for statistical computing. R foundation for statistical computing. Vienna, Austria. http://www.R-project.org. Accessed 18 June 2014

Sheriff SC, Franks SW, Rowan JS, Fenton O, Ó'hUallacháin D (2015) Uncertainty-based assessment of tracer selection, tracer non-conservativeness and multiple solutions in sediment fingerprinting using synthetic and field data. J Soils and Sediments 15:2101-2116. doi: 10.1007/s11368-015-1123-5

Silverman BW (1986) Density estimation for statistics and data analysis. Monographs on Statistics and Applied Probability 26. Chapman & Hall, London, 175 pp

Reinwarth et al.: Applying regularized logistic regression (RLR) for the discrimination of sediment facies in reservoirs based on composite fingerprints. Journal of Soils and Sediments.

Electronic Supplementary Material (Online Resource 4)

1 Introduction

In the following, we provide a brief instruction on the use of the Online Resources 3, 5, 6, 7 and 8 which are supplied together with this pdf document. These files can be opened and run with the freely available software environment R (R Core Team 2014). The files are used to conduct binomial and multinomial regularized logistic regression (RLR) on example data (Online Resource 3) using the software package 'glmnet' (Friedman et al. 2010). We provide information on the installation of the software, explain the purpose of the R files (Online Resources 5–8) and give hints to their usage.

2 Installation of the software environment R

The R software environment is available for Windows, (Mac) OS X and Linux. The most recent release can be downloaded from the following homepage: https://cloud.r-project.org/ . Since the 'glmnet' package is subject to ongoing further development, we are confident that the package will be supported by future R versions. However, earlier releases of the software are available from the same website (https://cloud.r-project.org/). We used the 'base' installation for Windows (64-bit; version 3.1.1) and the 'glmnet' version 2.0-5. Moreover, we did not encounter any problems with the more recent version R 3.3.1. Following the installation instructions the R software can be easily installed (storage requirements: ca. 70 megabyte). The R scripts (Online Resources 5–8) may assist with the installation of the 'glmnet' package.

3 Purpose of the Online Resources 3 to 7

Online Resource 3 ('ESM_3_R_Example_Data.RData') is a workspace for the R software environment containing synthetically generated example data that are used for the illustration of binomial and multinomial RLR. The Online Resources 5 to 8 represent R scripts that can be run to perform RLR analysis on the example data. Binomial RLR (i.e. for the discrimination of 2 groups of soils and sediments) is performed with the Online Resources 5 ('ESM_5_binomial_fingerprinting.R') and 7 ('ESM_7_binomial_classification.R'). Multinomial RLR (for ≥ 3 groups) is performed with the Online Resources 6 ('ESM_6_multinomial_fingerprinting.R') and 8 ('ESM_8_multinomial_classification.R').

The Online Resources 5 and 6 are used to identify composite fingerprints and to quantify the variable importance of each sediment property involved in the analysis. Data are centred and scaled and a statistical pre-test (binomial: Mann-Whitney U-test; multinomial: Kruskal-Wallis H-test) is performed to eliminate properties that do not significantly differ between the groups. Subsequently, the RLR model is fitted based on all samples. Misclassification rates and variable importance are calculated. Properties with a variable importance > 0 represent fingerprint properties. A plot is created showing the evolution of coefficients, variable importance and cross validation derived misclassification rates with

Corresponding author: Bastian Reinwarth (bastian.reinwarth@uni-jena.de)

increasing λ (this parameter controls the strength of the regularization). A summary of the results is presented in the R console when calculations are completed. Misclassification rates derived from this procedure might overvalue the performance of the RLR model when applied to samples not involved in model training (Hastie et al. 2009).

The Online Resources 7 and 8 demonstrate the use of RLR when the performance of the model is to be validated independently from training data. Statistical pre-tests and the optimization of the RLR model are restricted to samples from the training subset and all samples (i.e. samples from the training and validation subsets) are subsequently classified. Classification involves the determination of the (posterior) probability of group membership for each sample. As above, the variable importance is compiled, but misclassification rates are calculated separately for the training and validation set. In addition, misclassification rates are assessed for single groups. R scripts are organized in consecutively numbered sections that start with three hash tags ('###'). In addition, all R scripts contain comments describing the content of the R code, which will be printed in the R console when the scripts are run.

4 Usage of the RData and R files

We recommend to save all RData (Online Resource 3) and R files (Online Resources 5–8) in the same directory (e.g., "C:\RLR\example"). Once the R software is installed, double-clicking on the R workspace (Online Resource 3) will open the R console. Alternatively, the file can be opened within R by selecting 'File' and 'Load Workspace...'. R scripts (Online Resources 5–8) can be opened by selecting 'File' and 'Open script...' (or with a text editor). The scripts are run by copying and pasting lines (or entire sections) of the script into the R console. When the script is opened within R, lines can be alternatively executed by marking them with the cursor and using the shortcut 'Ctrl' and 'R'. When functions involve multiple lines of R code, the respective lines should be run at once. In the same manner it is possible to run entire scripts.

Prior to the execution of the R code, the directory path to the R workspace (Online Resource 3) has to be set, default settings of the algorithms may be changed and the 'glmnet' package needs to be installed. This is realized by editing and running the sections 1 to 3 which are identical in all supplied R scripts. In section 1, the directory path has to be entered (i.e. the line 'Directory = "<path name>"'). The default path is "C:/RLR/example", but needs to be changed accordingly, if the R workspace (Online Resource 3) was saved in another directory. The path must be entered between double quotes. Note that R uses the slash ('/') instead of the backslash ('\') for directory paths. Afterwards, changes may be saved by clicking on the R script and selecting 'File' and 'Save'. The name of the RData file (Online Resource 3) should not be modified. Otherwise, adjustments are to made in section 4 ('Load example data') of the R scripts.

In section 2 ('Settings'), the significance level that is employed in the statistical pre-test may be changed. The default value is 0.05 for the Mann-Whitney U-test ('MW.significance.level') and Kruskal-Wallis H-test ('KW.significance.level'), respectively. Furthermore, the parameter α defining the elastic-net penalty may be set ($0 \leq \alpha \leq 1$). The default value is 'alpha_values = 1', but it is also possible to involve several values 'alpha' in the analysis. In this case a vector may be provided (e.g., 'alpha_values = c(0.5, 0.75, 1)'). Note

that vectors are defined with the R function 'c'. If various values are entered, the algorithms will eventually select the RLR model that resulted in the lowest cross validation derived misclassification rate. In addition, the number of cross validation iterations ('cv.iter') can be set. The default value is 10. Increasing this integer (e.g., 'cv.iter = 100) most probably enhances the reproducibility of the results, but leads to longer computing times.
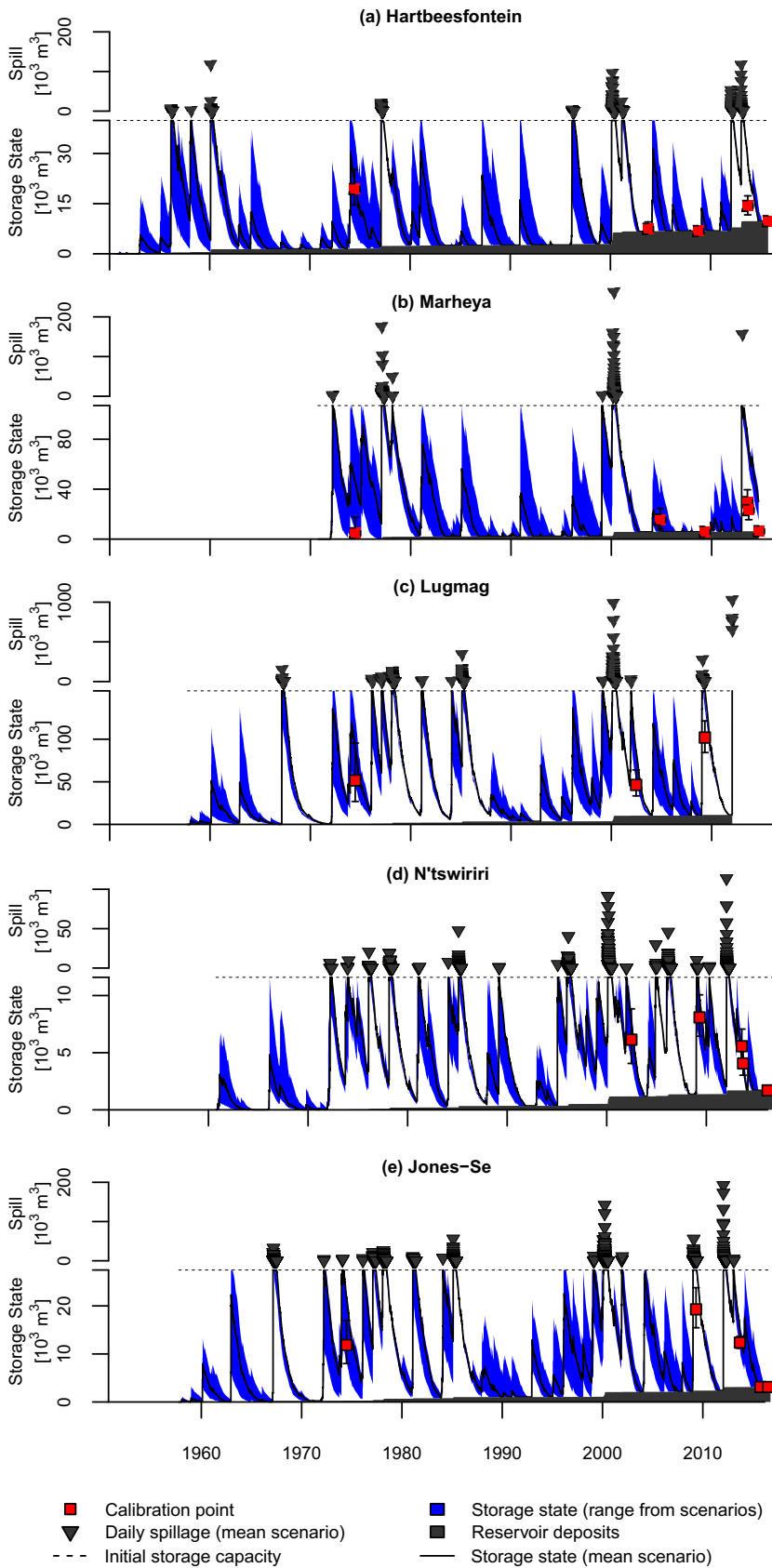
The R code in section 3 checks if the 'glmnet' package is already available. When the package is not found, installation is started automatically via the command 'install.package("glmnet")', which installs 'glmnet' and additional packages (if not yet available) that are required to run 'glmnet' (e.g., 'Matrix', 'utils', 'foreach'). An internet connection needs to be established during the installation. A 'https CRAN mirror' has to be selected from a list. The mirrors 'Germany (Münster)' and 'Australia (Melbourne)' worked fine for us, but other mirrors will most probably work just as well. Afterwards, the packages are installed automatically. Information on subsequent sections is provided with comments that will be printed in the R console when the scripts are run. The 'help' function can be useful to obtain more detailed information on specific commands. Typing 'help(require)' in the R console and pressing the 'Enter'-key will, for example, open a html file with detailed information on the 'require' function.

References

Friedman J, Hastie T, Tibshirani R (2010) Regularization paths for generalized linear models via coordinate descent. J Stat Softw 33:1-22

Hastie T, Tibshirani R, Friedman J (2009) The Elements of Statistical Learning. Data Mining, Inference, and Prediction, 2nd edn. Springer, New York, 745 pp. doi: 10.1007/978-0-387-84858-7

R Core Team (2014) R: a language and environment for statistical computing. R foundation for statistical computing. Vienna, Austria. http://www.R-project.org. Accessed 18 June 2014

Appendix B

Supplementary Material to Chapter 4

(a) Hartbeesfontein

(b) Marheya

(c) Lugmag

(d) N'tswiriri

(e) Jones−Se

■	Calibration point		■	Storage state (range from scenarios)
▼	Daily spillage (mean scenario)		■	Reservoir deposits
- - -	Initial storage capacity		—	Storage state (mean scenario)

(f) Silolweni

(g) N'wanetsana

(h) Mlondozi

(i) Nhlanganzwani

(j) Mpanamana

■ Calibration point   ■ Storage state (range from scenarios)
▼ Daily spillage (mean scenario)   ■ Reservoir deposits
- - - Initial storage capacity   —— Storage state (mean scenario)

Appendix C

Content of the Compact Disc (CD) and Author Contributions

Content of the compact disc (CD)

This doctoral thesis contains a compact disc (CD) including supplementary material for the chapters 3 and 4 (i.e., the folders 'ch3esm' and 'ch4esm'), and a digital version of this thesis. An overview on the content of the CD is provided in Tab. A1.

Tab. A1 Content of the CD attached to this thesis.

Folder	File	Description
ch3esm	ch3esm1.pdf	Screenshot of the Google Earth file 'ch3esm9.kmz' (see below)
	ch3esm2.pdf	Explanatory notes about the generation of synthetic dataset compilations used in this study
	ch3esm3.pdf	R code that can be used to create the R workspace 'ch3esm10.rdata' (see below)
	ch3esm4.pdf	Explanatory notes on the utilization of the files provided as Online Resources 5 to 8 (i.e., the files 'ch3esm10.rdata', 'ch3esm11.r', 'ch3esm12.r', 'ch3esm13.r', and 'ch3esm14.r')
	ch3esm5.pdf	pdf version of the file 'ch3esm11.r' (see below)
	ch3esm6.pdf	pdf version of the file 'ch3esm12.r' (see below)
	ch3esm7.pdf	pdf version of the file 'ch3esm13.r' (see below)
	ch3esm8.pdf	pdf version of the file 'ch3esm14.r' (see below)
	ch3esm9.kmz	GoogleEarth file containing the sample locations of the study. The number of samples, the sample type (surface or subsurface; pre-dam facies, post-dam facies, unclear or 'various' when samples from different categories were taken from varying depths) is indicated.
	ch3esm10.rdata	R workspace containing synthetically generated example data for RLR analysis
	ch3esm11.r	R script for the identification of a composite fingerprint from example data (' ch3esm10.rdata') applying binomial RLR with the R software package 'glmnet'
	ch3esm12.r	R script for the identification of a composite fingerprint from example data (ch3esm10.rdata') applying multinomial RLR with the R software package 'glmnet'
	ch3esm13.r	R script for the optimization of a regression model and subsequent classification applying binomial RLR on example data ('ch3esm10.rdata') using the software package 'glmnet'
	ch3esm14.r	R script for the optimization of a regression model and subsequent classification applying multinomial RLR on example data ('ch3esm10.rdata') using the software package 'glmnet'
ch4esm	ch4esm1.pdf	Figure showing the simulated lake level fluctuations for the investigated reservoirs (for details, see 'ch4esm3.pdf)'
	ch4esm2.pdf	Figure showing the cumulative volume sediment delivered to and deposited in the reservoirs (for details, see 'ch4esm3.pdf)
	ch4esm3.pdf	Figure captions for figures provided in 'ch4esm1.pdf' and 'ch4esm2.pdf'
digversion	dissreinwarth.pdf	digital version of this doctoral thesis

Declaration on contributions of the doctoral candidate to manuscripts included in this thesis and reprint permissions provided by the publishers

(Erklärung zu den Eigenanteilen des Promovenden an den Publikationen und Zweitpublikationsrechten)

For all publications included in this thesis, reprint permissions were provided by the publishers.

(Für alle in dieser kumulativen Dissertation verwendeten Manuskripte liegen die notwendigen Genehmigungen der Verlage vor.)

Co-authors of manuscripts included in this doctoral thesis have been informed and agree with the declaration on contributions provided below.

(Die Co-Autoren der in dieser kumulativen Dissertation verwendeten Manuskripte sind sowohl über die Nutzung, als auch über die unten angegebenen Eigenanteile informiert und stimmen dem zu.)

_____	_____	_____	_____
Name of doctoral candidate	Date	Place	Signature

I agree with the submission of this doctoral thesis in a publication-based (i.e., cumulative) form and confirm the information provided below. A justified endorsement with an indication on the scientific contribution of the doctoral candidate to the manuscripts included in this thesis will be sent to the Council of the Faculty of Chemistry and Earth Sciences.

(Ich bin mit der Abfassung der Dissertation als publikationsbasiert, d.h. kumulativ, einverstanden und bestätige die nachstehenden Angaben. Eine entsprechend begründete Befürwortung mit Angabe des wissenschaftlichen Anteils des Doktoranden an den verwendeten Publikationen werde ich parallel an den Rat der Fakultät der Chemisch-Geowissenschaftlichen Fakultät richten.)

_____	_____	_____	_____
Name of the supervisor	Date	Place	Signature

[1] **Reinwarth, B.**, Miller, J.K., Glotzbach, C., Rowntree, K.M., Baade, J., 2017. Applying regularized logistic regression (RLR) for the discrimination of sediment facies in reservoirs based on composite fingerprints. *Journal of Soils and Sediments* **17** (6), 1777-1795. DOI: 10.1007/s11368-016-1627-7.

Tab.: Author contributions to Chapter 3.

	Reinwarth	Miller	Glotzbach	Rowntree	Baade
Research proposal (funding)			X	X	X
Concept of the study	X				X
Data acquisition (field and lab work)	X	X			X
Data analysis and interpretation	X				
Writing of the manuscript	X				
Comments and suggestions to the manuscript		X	X	X	X
Suggested publication equivalent	1.0	n.a.	n.a.	n.a.	n.a.

[2] **Reinwarth, B.**, Riddell, E.S., Glotzbach, C., Baade, J., 2018. Estimating the sediment trap efficiency of intermittently dry reservoirs: lessons from the Kruger National Park, South Africa. *Earth Surface Processes and Landforms* **43** (2), 463-481. DOI: 10.1002/esp.4263.

Tab.: Author contributions to Chapter 4.

	Reinwarth	Riddell	Glotzbach	Baade
Research proposal (funding)			X	X
Concept of the study	X			X
Data acquisition (field work)	X			X
Processing of field data	X			X
Hydrological Modelling	X	X		
Writing of the manuscript	X			
Comments and suggestions to the manuscript		X	X	X
Suggested publication equivalent	1.0	n.a.	n.a.	n.a.

[3] **<u>Reinwarth, B.</u>**, Petersen, R., Baade, J., submitted. Contemporary sediment yield and erosion rates in the Kruger National Park, South Africa, and related uncertainties. Submitted to: *Geomorphology*.

Tab.: Author contributions to Chapter 5.

	Reinwarth	Petersen	Baade
Research proposal (funding)			X
Concept of the study	X		X
Data acquisition (field work)	X		X
Processing of field data	X		X
Statistical analysis and interpretation	X		
Writing of the manuscript	X		
Comments and suggestions to the manuscript		X	X
Suggested publication equivalent	1.0	n.a.	n.a.

Submitted: 07. February 2018

Manuscript ID: GEOMOR-7403

The editorial board of *Geomorphology* (Elsevier) has been informed about the inclusion of the manuscript into this doctoral thesis on 07. February 2018.

Statement of Authorship

(Selbständigkeitserklärung)

I hereby declare that I prepared this thesis independently and using the specified tools, personal messages and sources.

(Ich erkläre, dass ich die vorliegende Arbeit selbständig und unter Verwendung der angegebenen Hilfsmittel, persönlichen Mitteilungen und Quellen angefertigt habe.)

Jena, 14. February 2018   _____

Bastian Reinwarth